REGULATION OF MICAL REDOX POST-TRANSLATIONALLY-DRIVEN

F-ACTIN CYTOSKELETAL DYNAMICS

APPROVED BY SUPERVISORY COMMITTEE

Jonathan Terman, Ph.D. (Advisor)

Ryan Hibbs, Ph.D. (Chair)

Michael Rosen, Ph.D.

Ege Kavalali, Ph.D.

I dedicate this dissertation to my beautiful parents and to my beautiful country.

ACKNOWLEDGEMENTS

I would like to thank my parents, Arslan and Nesrin. I am so grateful to have such amazing parents who have always been there for me, fully supported me and believed in me. No words are enough to express their devotion to being the best of themselves as parents, their efforts and self-sacrifices, their patience for all my years in school and especially when our longing to see each other became unbearable during my years in graduate school. I love them and wish to have many more happy and healthy years with them. I would also like to thank my brother and sister for always making their little sister feel loved and cared for.

I would like to thank my mentor, Dr. Jonathan Terman. Jon always inspired me not only to be a better research scientist, but also to be a better thinker, a better learner and a better team-worker. He taught me how to think more critically and also how to accept criticism. He became a science parent for me by accepting me as I am, including my strengths and weaknesses, and by always encouraging me to become the best version of myself. I am especially grateful to him for creating the best conditions for me to do my dream research, which encompassed many different scientific areas and approaches, and combined my skills from both of my undergraduate majors (chemistry/molecular biology and genetics).

I wish the very best for all of the Terman lab members. They were great colleagues to work with and great people who are always ready to help. I would like to thank especially Ruei-Jiun, who taught me all the basic in vitro assays when starting in the lab, Chris, who showed me basic in vivo assays when starting in the lab, Shannon, who worked with me as a team to generate the in vivo data for the Mical-cofilin story, and Laura for being always there for

questions on fly genetics, but also for being a great friend and for coaching me on running, nutrition and work-life balance.

I would like to thank all the UTSW faculty, especially my committee members, Drs. Ryan Hibbs, Michael Rosen, and Ege Kavalali who were very supportive, always gave very helpful feedback and career advice and held my dissertation work to a high standard. I would like to also thank Drs. Helmut Kramer, Adrian Rothenfluh and Robin Hiesinger for supporting me when shaping my qualifying exam proposal and for also being there later for discussions in neuroscience and fly research.

I would like to thank all my great mentors throughout college and high school: Drs. Stefan Fuss and Arzu Celik, who are great mentors and have truly inspired me by being an example of how to do the best research in difficult conditions. Dr. Isil Aksan Kurnaz, who is a great mentor/PI/friend. Dr. Rana Nomak Sanyal, for the inspiration and encouragement to be a great scientist and an entrepreneur. Silke Remp, my high school biology teacher, whom I truly admired and who inspired me to start a career in science.

I cannot thank enough my beautiful friends: Gozde, who is an amazing friend, the dearest to my heart and a power source to my soul. Ece K., who is a true friend and the rock to hold on to. Yasemin and Didem, who were the friends I could have only wished to have by me in good and bad times and who made Dallas home for me. Ji Mi, who is an amazing person and an amazing soul, I hope to keep our friendship for many years. Duygu, who has such a good and sincere heart. Pavlina, who was such a joy to my life in Dallas. Paris, who I am grateful for all the music, movies, food and nerdy discussions. Ece E., who I found late but plan to hold on to for many years ahead.

REGULATION OF MICAL REDOX POST-TRANSLATIONALLY-DRIVEN F-ACTIN CYTOSKELETAL DYNAMICS

by

HUNKAR GIZEM YESILYURT

DISSERTATION

Presented to the Faculty of the Graduate School of Biomedical Sciences

The University of Texas Southwestern Medical Center at Dallas

In Partial Fulfillment of the Requirements

For the Degree of

DOCTOR OF PHILOSOPHY

The University of Texas Southwestern Medical Center at Dallas

Dallas, Texas

May, 2018

REGULATION OF MICAL REDOX POST-TRANSLATIONALLY-DRIVEN F-ACTIN CYTOSKELETAL DYNAMICS

Publication No. _____

Hunkar Gizem Yesilyurt

The University of Texas Southwestern Medical Center at Dallas, 2018

Supervising Professor: Jonathan R. Terman, PhD

The actin cytoskeleton is critical for multiple diverse cellular behaviors, including the ability of an axon to form, extend, navigate, and synapse with its target. Therefore, an important goal is to understand the mechanisms that regulate it. We have been studying one of the largest families of extracellular repulsive guidance cues, the Semaphorins, which were identified in part based on their ability to dramatically dismantle F-actin. More recently, we identified a new actin regulatory protein Mical, which directly associates with both the Semaphorin receptor Plexin and F-actin to post-translationally oxidize actin on its conserved methionine-44 and methionine-47 residues, inducing both F-actin disassembly and altered

actin polymerization. Our work has also revealed that this Mical-mediated actin regulatory process is reversible by a specific methionine sulfoxide reductase enzyme called SelR/MsrB. Thus, we have identified an unusual new actin regulatory system – which I sought for my dissertation research to focus on better understanding. I now find that each human MICAL family member, hMICAL-1-3, similar to *Drosophila* Mical, directly induces F-actin dismantling and controls F-actin-mediated cellular remodeling. Thus, the MICALs are an important phylogenetically-conserved family of catalytically-acting F-actin disassembly factors. I also investigated how this new actin regulatory system fits with classically-studied actin regulatory proteins. Employing a simple biochemical screen, I identified two proteins – cofilin and tropomyosin – that modulate Mical-mediated F-actin disassembly. Further investigation revealed that Mical synergizes with cofilin to rapidly and efficiently dismantle F-actin in a redox regulated manner and that this synergism is also necessary and sufficient for F-actin disassembly *in vivo* – for remodeling cells, wiring the nervous system, and orchestrating Semaphorin/Plexin repulsion. In contrast, I find that tropomyosin – known to decorate F-actin within specific cellular compartments and at different developmental stages – protects F-actin from Mical-mediated disassembly by stabilizing Mical-oxidized F-actin. Likewise, changing the levels of tropomyosin *in vivo* results in similar alterations to Mical-mediated F-actin/cellular remodeling suggesting a previously unknown mechanism controlling the plasticity of the actin cytoskeleton with important tissue-specific and developmental/age-related connotations. Thus, my findings provide new insights into the workings of this MICAL-mediated reversible Redox actin regulatory system including its importance to cell, developmental, and neural biology.

TABLE OF CONTENTS

PRIOR PUBLICATIONS

Hung, R. J., C. S. Spaeth, **H. G. Yesilyurt**, and J. R. Terman. 2013. 'SelR reverses Mical-mediated oxidation of actin to regulate F-actin dynamics', Nat Cell Biol, *15*: 1445-54.

Grintsevich, E. E.*****, **H. G. Yesilyurt***, S. K. Rich, R. J. Hung, J. R. Terman, and E. Reisler. 2016. 'F-actin dismantling through a redox-driven synergy between Mical and cofilin', Nat Cell Biol, *18*: 876-85. (*Co-first authors)

Grintsevich, E. E., P. Ge, M. R. Sawaya, **H. G. Yesilyurt**, J. R. Terman, Z. H. Zhou, and E. Reisler. 2017. 'Catastrophic disassembly of actin filaments via Mical-mediated oxidation', Nat Commun, *8*: 2183.

Wu, H., **H. G. Yesilyurt**, J. Yoon, and J. R. Terman. 2018. 'The MICALs are a Family of F-actin Dismantling Oxidoreductases Conserved from Drosophila to Humans', Sci Rep, *8*: 937.

LIST OF FIGURES

LIST OF DEFINITIONS

ADF – actin depolymerizing factor

CAM – cell adhesion molecule

CH – calponin homology

CRMP – collapsin response mediator protein

DAAM – disheveled-associated activator of morphogenesis

ECM – extracellular matrix

ENA/VASP – enabled/vasolidator-stimulated phosphoprotein

ERM – Ezrin, Radixin, and Moesin

F-actin – filamentous actin

FAD – flavin adenine dinucleotide

FM – flavoprotein monooxygenase

GAP – GTPase activating protein

GEF – guanine nucleotide exchange factor

GTP – guanosine triphosphate

hMICAL or hM – human MICAL

LIM – Lin11, Isl-1, and Mec-3

LIMK – LIM domain kinase

Mical – Molecule interacting with CasL

MLCK – myosin light chain kinase

MRL – Mig10/RIAM/lamellipodin

Msr – Methionine sulfoxide reductase

NADH – nicotinamide adenine dinucleotide

NADPH – nicotinamide adenine dinucleotide phosphate

NGF – nerve growth factor

PHBH – *p*-hydroxybenzoate hydroxylase

PIR – Plexin-interacting region

Plex – Plexin

Redox – oxidoreductase

ROCK – Rho kinase

SelR – Selenoprotein R

Sema – Semaphorin

SH3 – SRC Homology 3

SRF – serum response factor

Tm1 – Tropomyosin 1

Tm2 – Tropomyosin 2

CHAPTER ONE

INTRODUCTION

The actin cytoskeleton is critical for multiple diverse cellular behaviors – including those within the nervous system – and so an important research goal is to understand the factors and mechanisms that regulate its organization and function. For example, the ability of actin proteins to polymerize into filaments provides the structure and dynamics for neuronal migration, synaptogenesis, dendrite formation, axon growth and guidance, as well as other neuronal functions (Blanchoin et al. 2014; Rottner and Stradal 2011). I am particularly interested in how neurons and their axonal and dendritic processes extend, navigate, and connect within one another. These cellular events underlie the formation of a functional nervous system – and understanding them will contribute to the prevention, diagnosis and treatment of neurological diseases and injuries.

Actin cytoskeletal dynamics in cell motility and axon guidance

Motility is a primary behavior of every living cell – critical for both development and cellular maintenance, as well as underlying multiple disease processes. Motility is accomplished by polarization of a cell and dynamic rearrangements of its cytoskeletal components, orchestrating changes to cell shape, orientation, navigation, and connectivity (Rottner and Stradal 2011). These cellular changes all require the dynamic polymerization/depolymerization of actin, microtubules, and intermediate filaments as well as their ability to provide mechanical support, which generates diverse types of cellular structures (Pollard and Cooper 2009). During neural development, for example, an axon

grows by extending its tip, the growth cone, in a very dynamic fashion to reach its target. As Lowery and Van Vactor suggest (Lowery and Van Vactor 2009), this dynamic behavior can be thought of as the movement ("travel") of a 'vehicle', the growth cone, on 'roads' that are comprised of either 1) adhesive molecules on neighboring cells and axons (for example, cell adhesion molecules (CAMs); (Maness and Schachner 2007)) or 2) extracellular matrix (ECM proteins such as laminin and fibronectin; (Evans et al. 2007)), that are within the boundaries of 'guard rails' that are anti-adhesive, including repulsive surface-bound molecules like semaphorins, slits, and ephrins (Bashaw and Klein 2010). Furthermore diffusible chemotropic cues, like classical axon guidance molecules, morphogens, growth factors, and neurotransmitters (Kolodkin and Tessier-Lavigne 2011), can represent the 'road signs' that give further essential information for the trip of the axonal tip (growth cone).

The growth cone is composed of three regions that vary in size depending on their cytoskeletal organization and extracellular adhesive substrates (Dent and Gertler 2003): the peripheral (P) domain, which is comprised of filopodia and lamellipodia with long and bundled actin filaments, the central (C) domain, which is densely filled with various organelles, vesicles, and central actin bundles, as well as dynamic and bundled microtubules, and the transitional (T) domain, which is an arc-shaped region between the P and C domain that contains actomyosin contractile filaments. All these regions give the growth cone its shape and also determine its movement via their specific cytoskeletal composition. In particular, when a growing axon encounters a substrate (such as adhesive molecules on neighboring cells as mentioned above), protrusion occurs via the polymerization/elongation of actin filaments in the P domain (which drives out filopodia). Engorgement occurs as actin

in the C domain polymerizes and moves the central portion of the growth cone forward. Finally, consolidation occurs as the extending filopodia of the growth cone becomes enlarged and cylindrical, and a new segment of the axon shaft forms (Dent and Gertler 2003).

This growth/elongation happens in cycles driven by polymerization and depolymerization of actin filaments, though there is evidence that elongation (on its own and unguided) can occur for short distances in the absence of actin filaments (Marsh and Letourneau 1984). This polymerization and depolymerization of F-actin is supported by F-actin treadmilling and F-actin retrograde flow. In particular, in F-actin treadmilling, the monomeric (G-) actin gets added to the growing barbed (+)-end of filaments, which are located at the distal tip of filopodia and lamellipodia (Carlier and Shekhar 2017). Yet, at the same time, there is the F-actin retrograde flow, which is a constant flow of F-actin from the growing tip of the axon to the center. This retrograde flow is believed to occur by the pushing force of the actin on the membrane and the contractile motor protein myosin II tethered to F-actin (Medeiros, Burnette, and Forscher 2006). According to the 'molecular clutch' model that Mitchison and Kirschner first proposed (Mitchison and Kirschner 1988), the steady state balance between actin treadmilling and F-actin retrograde flow breaks when the growth cone encounters a substrate to which the F-actin can become tethered. In this way, the F-actin retrograde flow slows down and actin treadmilling becomes dominant to allow actin polymerization at leading edge to increase protrusion (Suter and Forscher 2000).

Although actin and actin regulatory proteins are thought to be the main driving force in motility/elongation, it is important to mention that microtubules are also directly involved in axon growth and guidance (Tanaka, Ho, and Kirschner 1995). There are several important

pioneering studies that indicate microtubules direct growth cone steering and respond to guidance cues (Gordon-Weeks 2004), that they get modified post-translationally to direct both axonal growth and repulsion (Lin and Forscher 1993), and that they induce growth cone turning by being directed to locally change their dynamics (Buck and Zheng 2002). Yet, it is also important to note that microtubules and their involvement in axonal elongation and navigation require the presence of and the interaction with actin (Zhou and Cohan 2004; Rodriguez et al. 2003). However, because of the scope of my dissertation, below I will focus on regulation of actin dynamics rather than microtubule dynamics.

Extracellular directors of movement including axon guidance cues

Having discussed cell motility from the specific example of the axonal growth cone, one can appreciate that any cell that migrates/elongates requires a navigation system that gathers information from the environment and then integrates the input from many signaling pathways to orchestrate directed cytoskeletal dynamics (Rottner and Stradal 2011; Lowery and Van Vactor 2009; Dent, Gupton, and Gertler 2011). In particular, axons grow and find their targets by relying on attractive and repulsive extracellular cues. For example, attractants have been described as promoting axon extension by inducing the polymerization of actin, while repellents limit extension by inducing F-actin disassembly. Classic examples of attractants and repellents are Netrins, Slits, Ephrins and Semaphorins, which although still incompletely understood, all regulate the activity of intracellular signaling proteins. Besides these classic guidance cues, morphogens, growth factors, and CAMs also play roles in attracting and repelling axons (Kolodkin and Tessier-Lavigne 2011).

Signaling proteins and actin regulators in axon guidance

Numerous intracellular signaling proteins that work downstream of extracellular guidance cues have been identified. These include well-known signaling proteins like small GTPases, as well as other broadly working signal transduction molecules like kinases, phosphatases and calcium ions. For example, Rho family GTPases are a key family of signaling proteins that direct motility of the neuronal growth cone and as well as other cells. Rho GTPases couple upstream navigational signals to cytoskeletal rearrangements, which is thought to lead to (depending on the upstream signal and whether it turns on or turns off the small GTPase) both enhanced actin polymerization for growth or disassembly and actomyosin contraction for collapse (Koh 2006; Govek, Newey, and Van Aelst 2005). Their upstream regulators include GEFs (guanine nucleotide exchange factors) and GAPs (GTPase-activating proteins), activating and inactivating them respectively (Koh 2006; Watabe-Uchida, Govek, and Van Aelst 2006). Growth cone guidance receptors can transduce their activation state by for example, recruiting other regulators such as the ephrin B3-EphA4 receptor signaling activating RacGAP α-chimerin to inhibit growth cone protrusion (Iwasato et al. 2007) . Another important feature of Rho GTPase signaling is its complexity in terms of many possible combinations of GEFs, GAPs, and GTPases and their spatial localizations that may lead to numerous and various outcomes (Lowery and Van Vactor 2009; Kurokawa et al. 2005). For instance, activation of RhoA (a Rho family GTPase related to RAC1 and CDC42) may lead to opposing outcomes such as growth cone retraction via increasing myosin II contractility (Gallo 2006) or axon outgrowth (Woo and Gomez 2006) by inhibiting the actin dynamizing/severing proteins ADF/cofilin (Wen et al. 2007).

Rho family GTPase signaling induces cytoskeletal arrangements at the leading edge of growth cone (as well as in lamellipodia and filopodia of other cells) via regulating its downstream effectors like actin binding proteins. Some of the important regulators of actin polymerization are actin nucleators, such as the Arp2/3 complex and formins, and actin polymerizing factors ENA/VASP (enabled/vasolidator-stimulated phosphoprotein). The Arp2/3 complex is activated by binding to Rho GTPases like RAC1 and CDC42, nucleating F-actin polymerization and branching (Goley and Welch 2006). Although the role of the Arp2/3 complex in promoting guidance in neuronal and nonneuronal cells has long been debated (Strasser et al. 2004), more recent evidence has helped solidify its role in growth cone protrusion and neural development (Chou and Wang 2016). Another family of actin nucleators downstream of RAC1 (Rho GTPase signaling) are formins, which also bind and stay at the barbed ends of actin filaments to promote further filament elongation (Goode and Eck 2007). The same holds truth for the ENA/VASP proteins, which antagonize capping proteins by binding to F-actin barbed ends, and also recruit other actin regulatory factors to induce polymerization (Drees and Gertler 2008). In addition, downstream effectors of Rho GTPase signaling also regulate F- actin retrograde flow and disassembly of actin at the T (transition) zone of the growth cone. For example, some of them are activated mainly by ROCK, either: 1) through MLCK (myosin light chain kinase) to induce myosin II contractility, hence actomyosin contraction and F-actin retrograde flow (Govek, Newey, and Van Aelst 2005; Zhang et al. 2003), 2) through LIMK (LIM domain kinase) to inactivate actin severing protein family member ADF/cofilin by phosphorylation to induce F-actin stabilization and growth cone protrusion (Wen et al. 2007), or 3) through ERM (ezrin-

radixin-moesin) proteins, which need to be studied further in terms of their exact function but are found to interact with guidance molecules like semaphorin 3A (Mintz et al. 2008) and to be important for neural morphogenesis (Freymuth and Fitzsimons 2017) and guidance in interaction with the L1CAM growth cone receptor (Kudumala et al. 2013).

It should also be mentioned, that I have touched here on only a few of the actin regulators affecting axon guidance and growth. More indepth discussions of F-actin motor proteins (like myosins) and F-actin severing/depolymerizing proteins (such as cofilin), as well as other effectors like other barbed-end binding proteins (such as DAAM (disheveled-associated activator of morphogenesis) and MRL ((Mig10/RIAM/lamellipodin) proteins), F-actin binding/bundling proteins (such as fascin), and monomer binding proteins (such as CAP and profilin) can be found reviewed elsewhere (Dent, Gupton, and Gertler 2011; Rottner and Stradal 2011). Yet, in all cases it is still incompletely, indeed poorly understood, how a signal goes from outside the cell to initiate a series of events that leads to growth cone extension or retraction, and results in movement in (or away from) a certain direction.

The Semaphorin-Plexin signaling pathway as a model

To better understand how guidance cues exert their effects on the cytoskeleton, we have been focusing on one of the largest families of guidance cues, the semaphorins (Semas) (Alto and Terman 2017). Indeed, our interests in employing the Semas as a model is to identify how repellents induce F-actin disassembly. In light of earliest studies (Kolodkin et al. 1992; Raper and Kapfhammer 1990; Luo, Raible, and Raper 1993), Semas were defined as axon guidance signals (Kolodkin, Matthes, and Goodman 1993). Although later studies

have identified Semas as key regulators of cell morphology and motility in many different cell types, they still remain to be one of the well-studied four canonical/classical axon guidance molecules. Further, although associated with different receptor families, Semas are best known to work through Plexin cell-surface receptors to dismantle F-actin and so we have been searching to understand how these Sema/Plexin interactions dismantle the F-actin cytoskeleton.

The MICALs: direct links between Semaphorins-Plexins and F-actin disassembly

Recently, we identified a new family of proteins called the MICALs, that directly associates with the Plexin receptor and is critical for Sema/Plexin repulsive axon guidance (Terman et al. 2002). The MICALs are a family of flavoprotein oxidoreductase (Redox) enzymes, that link their Redox catalytic domain with other well-known protein domains including a calponin homology domain and a LIM domain (**Figure 1.1a**). There is one *Mical* family gene present in invertebrates such as *Drosophila*, and three different MICAL genes present in mammals including humans (**Figure 1.1a**). While MICALs were identified as binding to the Plexin receptor, their biochemical and cellular role in Semaphorin/Plexin signaling was unknown.

Now, more recently, we have found Mical to be an F-actin disassembly factor – providing a direct link between Sema/Plexin repulsion and F-actin disassembly (Hung et al. 2010). These results identified Mical as an important new regulator of F-actin dynamics and our follow-up results using actin biochemical assays, imaging approaches, structural analysis, and the *in vivo Drosophila* model system revealed that Mical binds and disassembles F-actin

through its NADPH-dependent Redox activity. In particular, our findings revealed that Mical uses F-actin as its substrate, post-translationally oxidizing actin on its conserved Met-44 and Met-47 residues (**Figure 1.1b-c**; Hung, Pak, and Terman (2011). Interestingly, these residues sit at the junction where two subunits/monomers associate with one another in the actin filament (Sheterline, Jon, and John C. 1998; Oda et al. 2009; Murakami et al. 2010; Galkin et al. 2010; Fujii et al. 2010; Dominguez and Holmes 2011; Galkin et al. 2015; von der Ecken et al. 2015), and Mical-mediated oxidation of these residues induces F-actin disassembly and alters actin (re)polymerization (Hung, Pak, and Terman 2011; Grintsevich et al. 2017). Moreover, we have found that this Mical-mediated actin regulatory process (and Semaphorin/Plexin repulsion) is reversible by a specific methionine sulfoxide reductase enzyme called SelR/MsrB ((Hung et al. 2013) and see also (Lee et al. 2013)). Thus, we have identified a specific reversible redox actin regulatory system that controls cell and developmental biology (**Figure 1.1b**).

MICALs in development and disease

The MICAL family of proteins are ubiquitously expressed (Zhou, Gunput, et al. 2011; Vanoni, Vitali, and Zucchini 2013; Giridharan and Caplan 2014; Wilson et al. 2016; Manta and Gladyshev 2017). Although they were first known to be important for Sema/Plexin repulsion (Terman et al. 2002; Hung et al. 2010; Schmidt and Strittmatter 2007; Aggarwal et al. 2015; Hou et al. 2015), further work has revealed their importance in many cellular functions related to other classical receptor-mediated signal transduction pathways

and growth factor signaling (Grigoriev et al. 2011; Lundquist et al. 2014; Fremont et al. 2017; Yoon et al. 2017; Ashida et al. 2006).

MICALs have been found to regulate multiple cellular events in different tissues including cell morphology and positioning (Bron et al. 2007; Hung et al. 2010; Hung, Pak, and Terman 2011; Morinaka et al. 2011; Hung et al. 2013; Giridharan et al. 2012; Lee et al. 2013; Hou et al. 2015; Aggarwal et al. 2015), axon growth/guidance (Terman et al. 2002; Schmidt, Shim, and Strittmatter 2008; Hung et al. 2013; Van Battum et al. 2014; Lundquist et al. 2014), synaptogenesis/neuronal plasticity (Beuchle et al. 2007; Hung et al. 2013; Orr, Fetter, and Davis 2017), and dendritic arborization (Kirilly et al. 2009; Rumpf et al. 2014). For example, MICAL-1 was recently shown to regulate the cell surface targeting of IgCAMs (immunoglobulin superfamily cell adhesion molecules) and lamina-specific axonal targeting of hippocampal mossy fiber axons through redox-driven changes to the actin cytoskeleton (Van Battum et al. 2014). More recently, *Drosophila* Mical was shown to be essential for Sema2b-PlexB mediated regulation of presynaptic homeostatic plasticity and the redox-dependent control of presynaptic actin, hence an essential factor for the stabilization of synaptic transmission in development and adulthood (Orr, Fetter, and Davis 2017).

MICALs have also been found to be important for nonneuronal events such as muscle formation (Beuchle et al. 2007; Hung et al. 2013), cell division/cytokinesis (Liu et al. 2016; Fremont et al. 2017), exocytosis (Grigoriev et al. 2011; Bachmann-Gagescu et al. 2015), cardiovascular function (Lundquist et al. 2014; Hou et al. 2015), and cell viability (Zhou, Adolfs, et al. 2011; Ashida et al. 2006; Loria et al. 2015; Mariotti et al. 2016). For example, MICAL-3 interacts with Rab6 and Rab8 to control vesicle trafficking in exocytosis and

cytokinesis (Grigoriev et al. 2011). In another study, MICAL-2 was shown to be acting downstream of NGF (nerve growth factor) to disassemble nuclear actin in a redox dependent manner to activate SRF (serum response factor)-dependent gene transcription, which affects heart development/cardiovascular function (Lundquist et al. 2014). Furthermore, MICAL-1 has recently been shown to be recruited to cytokinetic abscission sites by the Rab35 GTPase, via a direct interaction with a flat three-helix domain found in MICAL-1 C-terminus, to induce actin depolymerization followed by recruitment of the required factor ESCRT-III and successful abscission (Fremont et al. 2017).

Importantly, altered levels of MICAL expression and polymorphisms in MICAL have been linked with different neuronal and non-neuronal pathologies. For example, they have been associated with cancer (Ashida et al. 2006; Ho et al. 2012; Loria et al. 2015; Mariotti et al. 2016; Lundquist et al. 2014; Deng et al. 2016; Shaul et al. 2014; Yoon et al. 2017; Wang et al. 2017), diabetic nephropathy (Aggarwal et al. 2015), blood brain barrier dysfunction (Hou et al. 2015), muscular dystrophy (Marotta et al. 2009), liver disease (Chambers et al. 2011), infectious susceptibility (Marbiah et al. 2014; Qin et al. 2016), skeletal anomalies (Bredrup et al. 2011), and obesity (Li et al. 2013). For instance, in recent work from my lab, MICAL activity was shown to be amplified by direct Abl tyrosine kinase-mediated phosphorylation of Mical *in vitro,* as well as by Abl-mediated growth factor signaling *in vivo,* in a process that also affects growth factor/Abl-related cancer cell behaviors (Yoon et al. 2017). Furthermore, work conducted as a part of that study revealed that knockdown of MICAL-1 decreased the size of tumors transplanted into mice (Yoon et al. 2017)

Altered levels of MICAL expression and polymorphisms in MICAL have also been associated with epilepsy (indeed, described as the causative agent behind certain forms) (Luo et al. 2011; Dazzo et al. 2018), neurological disorders (Jiang et al. 2015; Tochigi et al. 2008; Crews et al. 2012; Mychasiuk, Gibb, and Kolb 2011; Parikshak et al. 2013), aging (Aenlle et al. 2009), and neurodegenerative disease (Muller et al. 2007). For instance, MICAL-1 expression decreased from the latent stage to the chronic stage after seizures evoked in patients with intractable temporal lobe epilepsy and a pilocarpine-induced rat model, revealing its potential effect on inner pathophysiological modulation of epilepsy through altered F-actin disassembly (Luo et al. 2011). Also a more recent study revealed two variants in the MICAL-1 gene: a p.Gly150Ser substitution occurring in the enzymatically active Redox domain and a p.Ala1065fs frameshift mutation in the C-terminal domain, that causes ADLTE (Autosomal-dominant lateral temporal epilepsy) by inhibiting MICAL's redox activity and hence potentially by deregulating F-actin dynamics (Dazzo et al. 2018). Furthermore, MICAL-2 expression is induced by AICD (amyloid precursor protein intracellular domain) and its coactivator/binding protein FE65, which potentially leads to cytoskeletal changes including the destabilization of actin filaments and clumping of actin at the sites of cellular outgrowth (which are common occurrences in Alzheimer's Disease) (Muller et al. 2007). In short, all these examples show that the MICAL family of proteins are potential candidates for uncovering the aetiology and treatment of a diverse array of diseases including neurological and psychiatric ones.

Understanding how MICALs and the Reversible Redox Regulation of Actin is Modulated

In light of these findings, my dissertation research sought to further understand this Mical–SelR-mediated reversible redox actin regulatory system, its phylogenetic conservation, and how it is integrated with other more classical actin regulatory proteins to specify the organization of the actin cytoskeleton and drive cell biology. To define this interplay, I examined the ability of each of the three mammalian MICALs (MICAL-1, MICAL-2, and MICAL-3) to alter actin dynamics. My results presented in Chapter 2 of my thesis reveals that the ability of MICAL to alter actin dynamics is conserved across species, such that each of the human MICALs acts in a similar way to *Drosophila* Mical to disassemble F-actin *in vitro* and *in vivo*.

I also used a candidate-based approach to screen for interactions between Mical and other actin regulatory proteins. In particular, I initiated this "screen" by searching in the literature for proteins that were known to interact/bind on or near the site on actin where Mical acts (i.e., the Met-44 and/or Met-47 residues of actin) (**Figure 1.1c**). Based on my literature searches, I determined the following candidates: 1) Cofilin, which binds Subdomain 2 of actin at Q^{41} shifting the D-loop away from Subdomain 1 of adjacent actin protomer (Benchaar et al. 2007), 2) Troponin-I, which interacts with the Met-47 region of actin (Luo et al. 2002), 3) Tropomyosin, which binds along seven subunits of actin, including regions that might make Met-44/Met-47 more or less accessible to Mical (Perry 2001; Li et al. 2011; Memo and Marston 2013), and 4) Myosin Subfragment 1(S1), which protects actin residues Met-44-Val-45 from proteolytic attack from chymotrypsin (Fievez and Carlier

1993). Employing a biochemical screening approach using purified proteins, I present in Chapters 3 and 4, respectively, that two well-known actin regulatory proteins – cofilin and tropomyosin – modulate Mical-mediated actin regulation *in vitro* and *in vivo*. Among many other observations, my observations therefore reveal that Mical does not function in an isolated manner, but incorporates with well-known actin regulatory proteins to control cellular form and function.

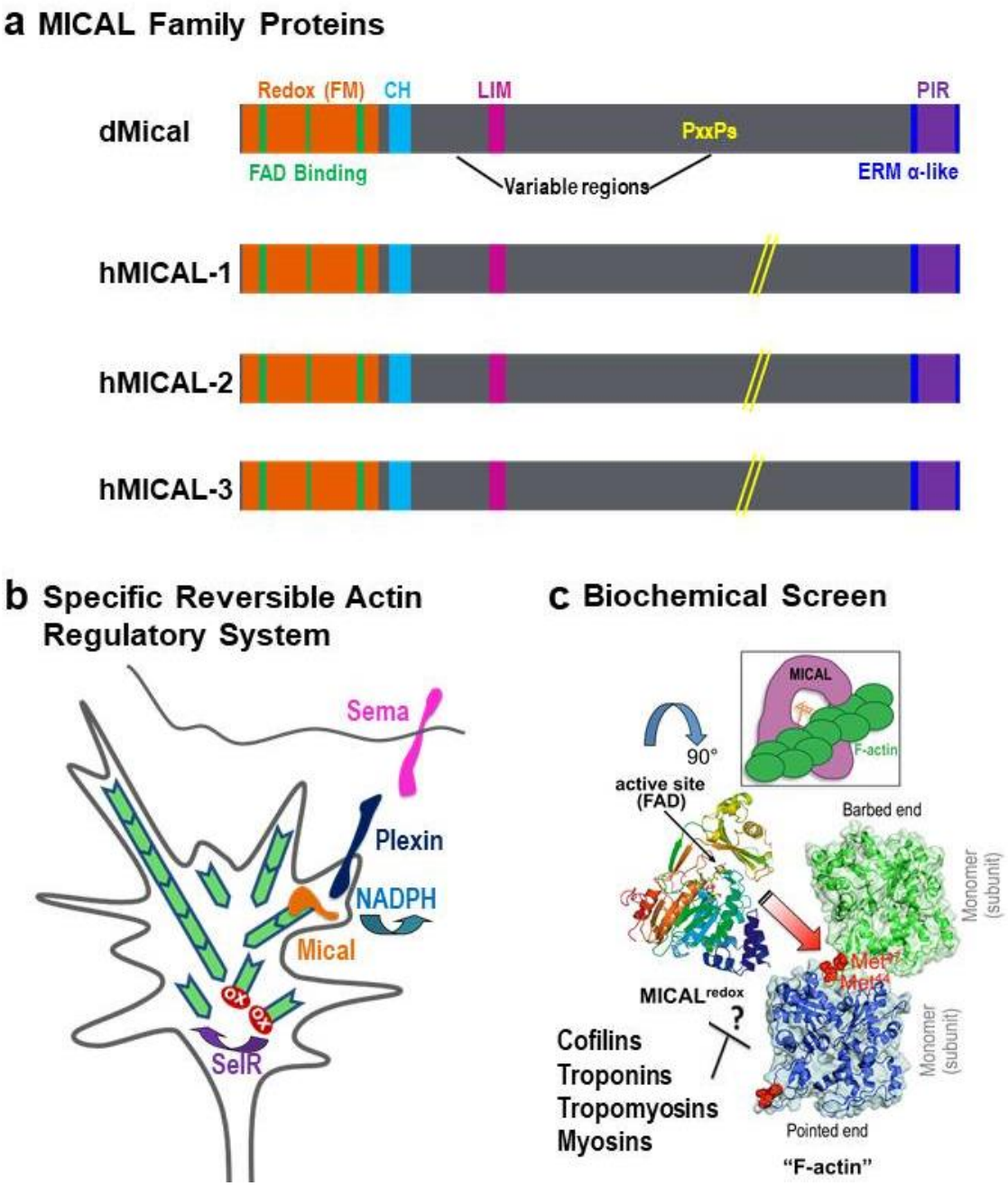

Figure 1.1. Mical and SelR proteins form a specific reversible Redox actin regulatory system.

(a) The MICAL family of proteins (dMical: Drosophila Mical, hMICAL-1-3: human MICAL 1-3) consist of multiple conserved domains/motifs: Redox (FM) (Flavoprotein monooxygenase), CH (Calponin Homology), LIM (Lin11, Isl-1, and Mec-3) domains, PxxP motifs, PIR (Plexin-interacting region), ERM (Ezrin, Radixin, Moesin) α-like domain. **(b)** Semaphorin (Sema) works through its receptor Plexin on the cell surface to dismantle F-

actin. Mical as a Plexin-interacting NADPH-dependent Redox enzyme provides a direct link between Sema/Plexin repulsion and F-actin disassembly by oxidizing (ox) specific methionine residues (Met-44 and Met-47) on F-actin (green), which dismantles F-actin. This Mical-mediated oxidation of actin is reversed by the specific methionine sulfoxide reductase enzyme called SelR (or MsrB). **(c)** Candidates for a biochemical screen for actin regulatory proteins that might interact on or near Met (M)-44, one of Mical's substrate residues on actin. Please also see **Figure 2.16**.

CHAPTER TWO

THE MICALS ARE A FAMILY OF F-ACTIN DISMANTLING OXIDOREDUCTASES CONSERVED FROM DROSOPHILA TO HUMANS

This work was previously published: Wu, H., **H. G. Yesilyurt**, J. Yoon, and J. R. Terman. 2018. 'The MICALs are a Family of F-actin Dismantling Oxidoreductases Conserved from Drosophila to Humans', Sci Rep, *8*: 937.
I designed and performed assays to determine the NADPH consumption and F-actin disassembling activities of each human MICAL family member in comparison to *Drosophila* Mical. Furthermore, I designed and performed assays to define their F-actin oxidizing activities and oxygen consumption properties. Moreover, I designed and performed experiments to look at the effects of SelR reductases on MICAL-mediated F-actin disassembly. In addition, H.W., J.Y., and J.R.T. designed/performed further *in vitro* and *in vivo* experiments and analyzed data.

Abstract

Cellular form and function – and thus normal development and physiology – are specified via proteins that control the organization and dynamic properties of the actin cytoskeleton. Using the Drosophila model, we have recently identified an unusual actin regulatory enzyme, Mical, which is directly activated by F-actin to selectively post-translationally oxidize and destabilize filaments – regulating numerous cellular behaviors. Mical proteins are also present in mammals, but their actin regulatory properties, including comparisons among different family members, remain poorly defined. We now find that each human MICAL family member, MICAL-1, MICAL-2, and MICAL-3, directly induces F-actin dismantling and controls F-actin-mediated cellular remodeling. Specifically, each human MICAL selectively associates with F-actin, which directly induces MICALs catalytic activity. We also find that each human MICAL uses an NADPH-dependent Redox activity to post-translationally oxidize actin's methionine (M) M44/M47 residues, directly dismantling filaments and limiting new polymerization. Genetic experiments also demonstrate that each

human MICAL drives F-actin disassembly in vivo, reshaping cells and their membranous extensions. Our results go on to reveal that MsrB/SelR reductase enzymes counteract each MICAL's effect on F-actin in vitro and in vivo. Collectively, our results therefore define the MICALs as an important phylogenetically-conserved family of catalytically-acting F-actin disassembly factors.

Introduction

Single actin proteins have the ability to assemble together into long chains or filaments and it is this actin polymerization that underlies cellular structure and behavior (Pollard and Cooper 2009; Fletcher and Mullins 2010). A critical goal therefore is to understand the factors that specify the organization and dynamic properties of actin. Over the years a number of proteins have been identified that directly promote actin filament (F-actin) assembly, stability, and generate branched actin networks (Pollard and Cooper 2009; Fletcher and Mullins 2010; Carlier et al. 2015). These actin regulatory proteins include some of the best studied such as bundling proteins like fascin and alpha-actinin, nucleators like formins and Arp2/3, barbed-end/pointed-end capping proteins like CapZ and tropomodulin, and actin assembly proteins like profilin (Siripala and Welch 2007a, 2007b; Blanchoin et al. 2014; Carlier et al. 2015).

In contrast to these positive effectors of actin filament assembly, the actin cytoskeleton is also regulated by proteins that negatively influence its stability and organization (Pollard and Borisy 2003; Ono 2007; Bugyi and Carlier 2010; Brieher 2013). Recently, while using genetic and biochemical assays in Drosophila we identified a new actin

disassembly protein, Mical, that directly binds F-actin and disassembles actin filaments in vitro and in vivo (Hung et al. 2010). Interestingly, our work also identified that Mical is a flavoprotein monooxygenase/hydroxylase enzyme that associates with flavin adenine dinucleotide (FAD) and uses the co-enzyme nicotinamide adenine dinucleotide phosphate (NADPH) in oxidation-reduction (redox) reactions (Terman et al. 2002; Hung, Pak, and Terman 2011). Further investigating this unusual enzyme revealed that Mical uses actin filaments as a direct substrate, selectively binding and stereospecifically oxidizing two conserved amino acids (methionine (Met) 44 and 47) within the pointed-end of actin to dismantle actin filaments and limit F-actin re-assembly (Hung, Pak, and Terman 2011). Likewise, investigations revealed that this Mical-mediated post-translational actin regulatory process is reversible by a specific methionine sulfoxide reductase enzyme called SelR/MsrB (Hung et al. 2013; Lee et al. 2013) – and that this reversible redox actin regulatory system controls multiple behaviors in different tissues including cellular remodeling, motility, process elongation, axon guidance, synaptogenesis, and muscle morphology/function (Hung et al. 2013). Mical is therefore a new type of F-actin disassembly factor, one that works through the covalent modification of actin – and one that we have also recently linked to working with important non-covalent regulators of actin such as cofilin (Grintsevich et al. 2016) and classical receptor-mediated signal transduction pathways (Yoon et al. 2017).

Mical is the sole Drosophila member of the MICAL family of proteins, which also includes three human protein family members coded for by three separate genes, *MICAL-1*, *MICAL-2*, and *MICAL-3* (**Figure 2.1a**; (Terman et al. 2002; Wilson et al. 2016)). Each member of the MICAL family of proteins contains a similar protein organization, and

includes a redox enzymatic domain, a calponin homology (CH) domain, a LIM domain, and a number of Src-homology 3 (SH3)-domain (PxxP) binding motifs (**Figure 2.1a**; (Terman et al. 2002; Wilson et al. 2016)). At the C-terminus, MICAL family proteins also contain a region that interacts with the Plexin transmembrane receptor (Terman et al. 2002; Schmidt, Shim, and Strittmatter 2008; Wilson et al. 2016), which is a receptor for one of the largest families of extracellular guidance cues, the Semaphorins (Kolodkin and Tessier-Lavigne 2011; Alto and Terman 2017). The MICAL family of proteins are ubiquitously expressed (Reviewed in (Zhou, Gunput, et al. 2011; Vanoni, Vitali, and Zucchini 2013; Giridharan and Caplan 2014; Wilson et al. 2016; Manta and Gladyshev 2017)) and they have been found to regulate multiple cellular events in different tissues including cell morphology and positioning (Bron et al. 2007; Hung et al. 2010; Hung, Pak, and Terman 2011; Morinaka et al. 2011; Hung et al. 2013; Giridharan et al. 2012; Lee et al. 2013; Hou et al. 2015; Aggarwal et al. 2015), axon growth/guidance (Terman et al. 2002; Schmidt, Shim, and Strittmatter 2008; Hung et al. 2013; Van Battum et al. 2014; Lundquist et al. 2014), synaptogenesis/neuronal plasticity (Beuchle et al. 2007; Hung et al. 2013; Orr, Fetter, and Davis 2017), dendritic arborization (Kirilly et al. 2009), muscle formation (Beuchle et al. 2007; Hung et al. 2013), cardiovascular function (Lundquist et al. 2014; Hou et al. 2015), cell division/cytokinesis (Liu et al. 2016; Fremont et al. 2017), exocytosis (Grigoriev et al. 2011; Bachmann-Gagescu et al. 2015), and cell viability (Zhou, Adolfs, et al. 2011). Likewise, altered levels of MICAL expression and polymorphisms in MICAL have been linked with different neuronal and non-neuronal pathologies including cancer (Ashida et al. 2006; Ho et al. 2012; Loria et al. 2015; Mariotti et al. 2016; Lundquist et al. 2014; Deng et al. 2016;

Shaul et al. 2014; Yoon et al. 2017; Wang et al. 2017), diabetic nephropathy (Aggarwal et al. 2015), blood brain barrier dysfunction (Hou et al. 2015), muscular dystrophy (Marotta et al. 2009), liver disease (Chambers et al. 2011), infectious susceptibility (Marbiah et al. 2014; Qin et al. 2016), epilepsy (Luo et al. 2011), neurological disorders (Jiang et al. 2015; Tochigi et al. 2008; Crews et al. 2012; Mychasiuk, Gibb, and Kolb 2011; Parikshak et al. 2013), neurodegenerative disease (Muller et al. 2007), aging (Aenlle et al. 2009), skeletal anomalies (Bredrup et al. 2011), and obesity (Li et al. 2013). Yet, Drosophila Mical remains the best-characterized MICAL family member, and the actin regulatory properties of three mammalian members of the MICAL family of proteins, including comparisons among the different family members, remain poorly defined.

Herein, we find that each of the human MICAL proteins is an F-actin disassembly enzyme. Our results reveal that human MICALs-1, 2, and 3 directly associate with actin filaments, which activate the MICALs to catalyze enzyme reactions that selectively oxidize actin. This MICAL-mediated oxidation of actin, dismantles filaments, inhibits polymerization, is counteracted by SelR/MsrB reductases, and regulates cellular remodeling in vivo. Interestingly, differences among the catalytic and F-actin regulatory activities of the MICALs also exist, including that MICAL-1, which is the most divergent of the MICALs, has a single naturally-occurring amino acid substitution that allows it to have higher basal enzymatic activity and consume NADPH more robustly in the absence of its F-actin substrate than the other MICALs. Collectively, our results define the MICALs as an important new phylogenetically-conserved family of redox-acting actin filament disassembly factors.

Results

MICAL Family Proteins are Redox Enzymes

Both Drosophila Mical and mammalian MICALs form the MICAL family of large, multidomain cytosolic proteins (**Figure 2.1a**), which direct multiple different cellular behaviors and physiological functions (e.g., (Terman et al. 2002; Beuchle et al. 2007; Bron et al. 2007; Schmidt, Shim, and Strittmatter 2008; Kirilly et al. 2009; Hung et al. 2010; Hung, Pak, and Terman 2011; Morinaka et al. 2011; Grigoriev et al. 2011; Zhou, Adolfs, et al. 2011; Hung et al. 2013; Giridharan et al. 2012; Lee et al. 2013; Van Battum et al. 2014; Lundquist et al. 2014; Hou et al. 2015; Loria et al. 2015; Aggarwal et al. 2015; Grintsevich et al. 2016; Liu et al. 2016; Fremont et al. 2017; Yoon et al. 2017)). We have recently identified Drosophila Mical as an actin filament disassembly factor (Hung et al. 2010; Hung, Pak, and Terman 2011; Hung et al. 2013) and work using purified mammalian MICAL proteins has determined that at least some of the mammalian MICALs also exhibit direct effects on actin stability (e.g., (Lee et al. 2013; Lundquist et al. 2014; Vitali et al. 2016; Fremont et al. 2017)). However, since an in-depth characterization and comparison of the different MICAL family members and their mechanisms of action is lacking, we set out to define each MICAL family member and its effects on F-actin.

Our previous results revealed that the oxidoreductase (redox) region of Drosophila Mical (**Figure 2.1a**) is sufficient to post-translationally oxidize and disassemble actin filaments (Hung et al. 2010; Hung, Pak, and Terman 2011; Hung et al. 2013), but Mical's calponin homology (CH) domain (**Figure 2.1a**) may also assist the redox region in its catalytic efficiency (Alqassim et al. 2016). Therefore, so that we could compare and contrast

the actin regulatory properties of each of the MICAL family members (and do it in the same species), we expressed and purified recombinant proteins containing the redox and CH portions of each of the three human MICALs, hMICAL^{redoxCH}-1, hMICAL^{redoxCH}-2, and hMICAL^{redoxCH}-3 (**Figure 2.2-4**). The redox regions of both invertebrate and vertebrate members of the MICAL family of proteins are highly conserved with as high as 63% identity between Drosophila and human family members (**Figure 2.5a**). Likewise, primary sequence analysis of Drosophila and human family members revealed that each of them has within their redox enzymatic domain three well-conserved amino acid motifs that are found in proteins that bind and utilize the redox enzyme co-factor flavin adenine dinucleotide (FAD) (**Figure 2.1a-b**; (Terman et al. 2002)). Experimental analysis also identified that purified human MICAL-1^{redoxCH}, MICAL-2^{redoxCH}, and MICAL-3^{redoxCH} proteins, like Drosophila Mical^{redoxCH}, are yellow in color, a distinguishing feature of flavin binding proteins (flavoproteins), and also exhibited an absorption spectra similar to flavoproteins (**Figure 2.1c-f and 2.4**). Protein denaturation studies also supported these observations, and demonstrated that recombinant Drosophila Mical and all three human MICAL proteins bind the flavin FAD non-covalently in a 1:1 MICAL:FAD stoichiometry (**Figure 2.5b-c**). Thus, each of the human MICALs, like Drosophila Mical, is an FAD binding protein.

Proteins that bind FAD typically perform oxidation-reduction reactions, so we wondered if all members of the MICAL family of proteins do the same. Primary sequence analyses revealed that MICAL family proteins are similar to a class of redox enzymes called flavoprotein monooxygenases (Terman et al. 2002), and this similarity was also observed when the redox portion of mouse MICAL-1 was crystallized, examined structurally, and

found to be most similar to the flavoprotein monooxygenase enzyme *p*-hydroxybenzoate hydroxylase (pHBH) (Nadella et al. 2005; Siebold et al. 2005; Alqassim et al. 2016). Flavoprotein monooxygenases such as pHBH utilize the pyridine nucleotide coenzyme nicotinamide adenine dinucleotide phosphate (NADPH) in their redox reactions (van Berkel and Muller 1991; Wilson et al. 2016), so we compared the redox properties of each member of the human MICAL family. Our results revealed that each mammalian MICAL family member, like Drosophila Mical, consumes NADPH (**Figure 2.1g**). Furthermore, we found that similar to Drosophila Mical, hMICAL-1, 2, and 3 are more active in the presence of NADPH than with the related pyridine nucleotide coenzyme NADH (**Figure 2.1h**). However, we also noticed differences in the redox properties among the different MICAL family members. For example, hMICAL^{redoxCH}-1 is substantially more active than the other members of the MICAL family in the absence of a substrate and consumes high levels of NADPH on its own (**Figure 2.1g**). In contrast, hMICAL^{redoxCH}-2, hMICAL^{redoxCH}-3, and Drosophila MICAL^{redoxCH} are most similar to each other with regards to NADPH consumption (**Figure 2.1g**), and most similar to PHBH, in that they each have relatively weak NADPH consumption activity on their own (i.e., in the absence of a substrate). Collectively, these results indicate that all members of MICAL family of proteins exhibit redox activity – although there are notable differences between family members in their catalytic properties.

Each Human MICAL Family Member Directly Binds and Dismantles Actin Filaments

Drosophila Mical directly binds and disassembles F-actin in an NADPH-dependent manner (Hung et al. 2010; Hung, Pak, and Terman 2011), so we wondered if each of the

human MICAL proteins also functions in a similar way. We first looked at the ability of hMICAL^{redoxCH}-1, hMICAL^{redoxCH}-2, and hMICAL^{redoxCH}-3 proteins to associate with actin filaments using actin co-sedimentation assays. Like Drosophila Mical, co-sedimentation assays revealed that all three human MICALs physically associate with F-actin (**Figure 2.6a**). Likewise, we found that these MICAL–F-actin interactions are specific, since similar to Drosophila Mical, human MICALs did not directly associate with microtubules (**Figure 2.7a**). Thus, we wondered if human MICALs affect F-actin stability. Using different actin polymerization and depolymerization assays including pyrene-actin and sedimentation analyses, we found that each of the human MICALs, similar to Drosophila Mical (Hung et al. 2010), altered actin polymerization and induced the disassembly of F-actin (**Figure 2.6b-c**). Namely, when added prior to actin polymerization, each of the MICALs induces actin polymerization to slow-down over time, which is followed by a substantial decrease in the extent of polymerization, the rapid depolymerization of F-actin, and the inability of actin to reinitiate polymer formation (**Figure 2.6b;** (Hung et al. 2010)). In a similar way, when added to polymerized actin, each of the MICALs induces the disassembly of filaments (**Figure 2.6b;** (Hung et al. 2010)). Moreover, like Drosophila Mical (Hung et al. 2010), these effects on polymerization and depolymerization were specific to F-actin, as microtubule polymerization and depolymerization dynamics were not affected by human MICALs (**Figure 2.7b**). Further analysis revealed that each of the human MICALs effects on F-actin, like Drosophila Mical (Hung et al. 2010), was more robust in the presence of NADPH versus NADH (**Figure 2.8a-b**). These results therefore reveal that each of the human MICALs

directly associates with actin filaments – inducing both F-actin disassembly and preventing normal F-actin reassembly.

Actin Filaments Serve as a Direct Substrate for Each MICAL Family Member

We next sought to examine the mechanism by which the human MICALs alter actin dynamics. Our previous results revealed that actin filaments exhibit the characteristics of a direct Mical substrate, robustly increasing the enzyme activity of Drosophila Mical (**Figure 2.9a**; (Hung et al. 2010)). Likewise, we found that the enzyme activity of each of the human MICALs, as judged by an increase in the consumption of the co-enzyme NADPH, increased in the presence of actin filaments (**Figure 2.9a**). We also had previously determined that the methionine (Met) 44 and 47 residues of actin are the sites of Drosophila Mical post-translational oxidation of actin (Hung, Pak, and Terman 2011), and that mutations to those residues makes actin resistant to Drosophila Mical (Hung, Pak, and Terman 2011). Likewise, using an antibody that specifically recognizes the Mical-oxidized Met44 residue of actin (Grintsevich et al. 2016), we found that Met44 is oxidized by human MICALs 1, 2, and 3 (**Figure 2.9b**) – and that mutating the Met44 and Met47 residues of actin prevents each of the human MICALs from disassembling F-actin (**Figure 2.9c**). Moreover, we previously determined that the methionine sulfoxide reductase enzyme SelR/MsrB specifically reverses Drosophila Mical-mediated oxidation of actin through reduction of the oxidized Met44 and Met47 residues of actin (Hung et al. 2013; Grintsevich et al. 2016) – and that this SelR/MsrB-mediated effect also restores the polymerization properties of Mical-treated actin (Hung et al. 2013; Lee et al. 2013). Thus, we wondered if each member of the MICAL

family also works in a similar way to oxidize actin and if SelR/MsrB could reverse this modification and restore the polymerization properties of human MICAL-treated actin. Indeed, we found that the methionine sulfoxide reductase enzyme SelR/MsrB restored the polymerization properties of actin that had been treated with each of the human MICALs (**Figure 2.9d**). These results therefore reveal that actin serves as a direct substrate of mammalian MICALs and that the Met44 and 47 residues are essential for the ability of each of the human MICALs to disassemble F-actin. Likewise, since SelR/MsrB enzymes specifically catalyze the reduction of the *R* isomer of methionine sulfoxide (methionine-*R*-sulfoxide) to methionine (reviewed in (Wilson et al. 2016; Manta and Gladyshev 2017)), these results also indicate that each MICAL family member oxidizes actin stereospecifically in the *R*-isomer to generate actin Met44,47-*R*-sulfoxide (actin$^{\text{Met(}R\text{)O–44,47}}$).

MICAL-1 exhibits notable differences in its activation and catalytic activity in comparison to other MICAL family members

Our results herein reveal that each member of the MICAL family of proteins uses its enzyme activity to covalently modify and disassemble F-actin, but we also noticed that MICAL-1 exhibited pronounced differences in this catalytic activity when compared to other MICAL family members. In particular, in the absence of their F-actin substrate, Drosophila Mical and human MICALs 2 and 3, consumed relatively low amounts of their essential co-enzyme NADPH (**Figures Figure 2.1g, 2.9a, 2.10a**; (Hung, Pak, and Terman 2011)). MICAL-1, in contrast, consumed high levels of NADPH in the absence of its F-actin substrate (**Figure 2.1g**, **2.9a**, **2.10a**), such that it basally (in the *absence* of F-actin) consumed

close to 100 times more NADPH per second than hMICAL-2 and 60 times more NADPH per second than Drosophila Mical (**Figure 2.10a**). Thus, MICAL-1, in contrast to other MICAL family members, is highly active in the absence of its substrate. In the class of enzymes that includes pHBH and MICALs, consumption of NADPH in the absence of a substrate leads to the production of hydrogen peroxide (H_2O_2) – since no substrates are present to directly oxidize (**Figure 2.11a**; (Hung and Terman 2011; Wilson et al. 2016)). Likewise, using several different assays to monitor H_2O_2 production in the absence of a substrate, we found that hMICAL-1 produced higher levels of H_2O_2 than other MICAL family members (**Figure 2.10b, 2.11b**). Furthermore, using an assay to monitor the usage of oxygen, we found that MICAL-1 consumed much higher levels of oxygen in the absence of a substrate in comparison to other MICALs (**Figure 2.10c**). Thus, MICAL-1 shows marked differences in its catalytic properties from other MICALs, including a robust enzymatic activity in the *absence* of its F-actin substrate.

To further investigate these differences among the MICALs we wondered what effect this MICAL-1-mediated large increase in H_2O_2 production might have on F-actin dynamics. It has been suggested that the MICALs use H_2O_2 to exert their effects (Vitali et al. 2016; Vanoni 2017). However, our previous results using multiple different approaches and those of others demonstrated that MICALs do not use the non-specific release of H_2O_2 or other diffusible oxidants to alter F-actin dynamics (Hung et al. 2010; Hung, Pak, and Terman 2011; Hung et al. 2013; Wilson et al. 2016; Fremont et al. 2017), but need to be in close proximity to F-actin, which directly activates Mical to oxidize the Met44 and Met47 residues of actin (Hung, Pak, and Terman 2011). Likewise, our results presented herein also support

these conclusions for each of the mammalian MICALs, since we observe an excessive difference in H_2O_2 production between human MICAL-1 and the other MICALs (**Figure 2.10b, 2.11b**), but not a corresponding increase in MICAL-1's effects on F-actin dynamics (**Figure 2.6b-c**). Similarly, we found that raising the levels of MICAL-1 (from 300nM to 900nM) increased H_2O_2 production but decreased F-actin alterations (**Figure 2.10d, 2.11c**), further arguing against a role for the diffusible release of H_2O_2 or other oxidants in MICAL-mediated F-actin alterations. Indeed, since hMICAL-2, hMICAL-3 and Drosophila Mical, which have a low basal NADPH consumption rate, increased their effects on F-actin dynamics in a concentration-dependent manner (**Figure 2.10e**, **2.11d**; (Hung et al. 2010)), our results argue that MICAL-1 exhibits such rapid consumption of NADPH in the absence of its F-actin substrate that NADPH (and not H_2O_2 [which is present in high quantities in the MICAL-1 reaction; **Figure 2.10b, 2.11b**]) becomes limiting in allowing MICAL-1 to modify F-actin. Thus, our results indicate that the release of H_2O_2 plays no role in MICAL-1 mediated F-actin disassembly.

To further test the role of H_2O_2 in MICAL-mediated F-actin disassembly, we made use of MICAL-1's high level of basal activity and designed one additional experiment in which we incubated MICAL-1 with NADPH either before (pre) or after (post) the addition of F-actin (**Figure 2.10f**). We reasoned that if H_2O_2 is the means by which MICAL-1 induces F-actin disassembly, there would be no difference in F-actin disassembly between these conditions. However, our results revealed that MICAL-1 no longer disassembles F-actin when it is incubated with NADPH prior to the addition of F-actin (**Figure 2.10g**) – supporting that even though MICAL-1 produces high levels of H_2O_2 in this pre-reaction

condition (i.e., without its F-actin substrate [**Figure 2.10f**]), H_2O_2 has no effect on F-actin disassembly (**Figure 2.10g**). MICAL-1, therefore, because of its high-rate of basal activity uses-up NADPH prior to the addition of F-actin, such that it can no longer use NADPH in its reaction to modify actin. Drosophila Mical, in contrast, which has a low rate of basal NADPH consumption (**Figure 2.1g, 2.9a, 2.10a**), retains NADPH levels in the absence of its F-actin substrate, and exhibited similar effects on F-actin disassembly in each condition (**Figure 2.10h**). Indeed, when we added more NADPH into the MICAL-1 pre-reaction condition tube (**Figure 2.11e**), MICAL-1 now proceeded to induce F-actin disassembly (**Figure 2.11f**). Thus, the general release of H_2O_2 is not the means by which MICAL-1 or any of the MICALs post-translationally oxidize and regulate F-actin disassembly. These results therefore further support our previous results with Drosophila Mical (Hung et al. 2010; Hung, Pak, and Terman 2011; Hung et al. 2013) and those above that the MICALs need to be in close proximity to F-actin, which directly activates the MICALs to oxidize the Met44 and 47 residues of actin.

MICAL-1 exhibits a single amino acid alteration that produces high levels of catalytic activity in the absence of its F-actin substrate

Since MICAL-1, unlike other MICAL family members (and MICAL-class enzymes like pHBH), has a high level of enzymatic activity in the absence of a substrate, we wondered what molecular variation(s) might be underlying this difference. Interestingly, comparing the sequences for the different MICALs revealed that the critical aspartate (D) amino acid residue in the DG motif of the flavin adenine dinucleotide (FAD) binding motif was instead

an alanine (A) residue in MICAL-1 (**Figure 2.1b**). The DG motif (also called the Conserved Motif; (Eppink, Schreuder, and Van Berkel 1997)) is critical for binding the pyrophosphate moiety of FAD (reviewed in (Hung and Terman 2011)), and so this "naturally-occurring" MICAL-1-specific substitution of a nonpolar alanine residue for the charged aspartate residue would be predicted to alter the positioning and flexibility of the FAD. This "naturally-occurring" MICAL-1-specific substitution might also enable MICAL-1 to be more catalytically active in the absence of its F-actin substrate than other MICALs. To test this hypothesis, we used site-directed mutagenesis to convert the alanine residue within the DG motif of MICAL-1 to an aspartate residue and thereby generated a MICAL-1 protein similar to the other MICAL family members (MICAL-1^{DG}; **Figure 2.12a, 2.13**). Our initial analysis of this MICAL-1^{DG} protein revealed that it was similar to wild-type MICAL-1 (and other MICAL family members) – yellow in color (**Figure 2.13**) and displaying the enzymatic features and absorption spectra of MICAL-class enzymes (**Figure 2.12b and 10b-c**). Yet, strikingly, we also found that making this DG substitution decreased MICAL-1's basal consumption of NADPH by close to 12-fold (1200%) per second (**Figure 2.12c**) – enabling MICAL-1^{DG} to consume much lower levels of oxygen and generate far less H_2O_2 than wild-type MICAL-1 (**Figure 2.10b-c**). However, making this DG substitution did not decrease MICAL-1's actin regulatory properties – since we observed that MICAL-1^{DG} still bound actin filaments (**Figure 2.6a**), was activated by F-actin (**Figure 2.12d**), oxidized actin's Met44 residue (**Figure 2.9b**), and had robust and specific effects on both actin polymerization and depolymerization (**Figure 2.6c, 2.12e, 2.7a-b**). Furthermore, these MICAL-1^{DG} effects on F-actin dynamics were dependent on the Met44 and Met47 residues

of actin and could be counteracted by SelR (**Figure 2.9c, 2.12f**). Therefore, despite the large differences in H_2O_2 production between MICAL-1^{DG} and wild-type MICAL-1, we did not observe any widespread differences in their actin regulatory abilities (**Figure 2.6c, 2.12e**). Indeed, our results revealed that MICAL-1^{DG} became more efficient than MICAL-1 at altering actin dynamics (**Figure 2.14**) **–** because it now had a lower basal level of NADPH consumption and generated less H_2O_2. Thus, these results further support that the MICALs do not use general H_2O_2 production to exert their effects on actin dynamics. Furthermore, these results also indicate that the aspartate (D) to alanine (A) substitution that occurs "naturally" in MICAL-1 underlie differences in basal activity and H_2O_2 production between MICAL-1 and the other MICAL family members.

Mammalian MICALs Regulate F-actin Disassembly and Cellular Remodeling In Vivo

Our biochemical experiments reveal that each member of the MICAL family of proteins functions to directly induce actin disassembly. We conducted these experiments using purified proteins in vitro so we wondered if each MICAL family member could also exert similar effects on F-actin organization in vivo. Bristle cells in the model organism Drosophila have long-provided a high-resolution single cell system for characterizing F-actin alterations in vivo (**Figure 2.15a**; (Sutherland and Witke 1999; Tilney and DeRosier 2005; Hung and Terman 2011)) – and our previous results revealed that Drosophila Mical induces F-actin disassembly in a redox-dependent manner to remodel these cells (Hung et al. 2010; Hung, Pak, and Terman 2011; Hung et al. 2013). We therefore turned to this model system to determine if each member of the MICAL family has a similar ability – and tested this by

generating transgenic flies expressing human MICALs corresponding to the exact protein construct we used in vitro, hMICAL-1^{redoxCH}, hMICAL-2^{redoxCH}, and hMICAL-3^{redoxCH}. Notably, expressing each of the human MICALs in developing bristle cells using the bristle-specific driver (*B11-GAL4*) resulted in widespread and dramatic effects to actin organization and cellular morphology. The normally bundled and parallel-arranged F-actin (**Figure 2.15a, left and middle**) that gives rise to a long slightly-curved bristle process (**Figure 2.15b, right**) was significantly altered by expressing MICALs 1, 2 or 3 within them (**Figure 2.15b-f**). Specifically, MICALs-1, 2, and 3 were each sufficient to decrease the presence of actin filaments in extending bristle processes (**Figure 2.15b-e, and compare to Figure 2.15a**) and resulted in substantial remodeling of bristle cells to generate numerous abnormal bends and branches (**Figure 2.15b-d)**. Furthermore, SelR, but not an enzyme dead version of SelR (SelR^{C124S}), rescued the F-actin and morphological defects induced by MICALs-1, 2, and 3 (**Figure 2.15f**), indicating that each of the human MICALs uses its redox activity to alter actin dynamics and cellular remodeling in vivo. Thus, as we observed in vitro using purified proteins, each of the human MICALs exerts specific negative effects on F-actin organization in vivo – effects that significantly remodel cells.

Discussion

Dynamic assembly and disassembly of the actin cytoskeleton allows cells to perform the functions necessary for normal development and physiology. Yet, while we have a considerable understanding of how actin filaments are assembled in cells, our understanding of how such filaments are disassembled remains highly incomplete (Rottner and Stradal

2011; Brieher 2013; Miyoshi and Watanabe 2013). Here, we provide an instrumental piece in the understanding of how filaments are disassembled, by characterizing a family of actin disassembly enzymes conserved from invertebrates to humans. In particular, members of the MICAL family of proteins, which includes one family member in invertebrates and three members in vertebrates including humans, are broadly expressed and have recently emerged because of their crucial role in directing numerous actin-based cellular events in vivo (reviewed in (Zhou, Gunput, et al. 2011; Vanoni, Vitali, and Zucchini 2013; Giridharan and Caplan 2014; Wilson et al. 2016; Manta and Gladyshev 2017)). Using the sole Drosophila member of the MICAL family as a model, we have uncovered that Mical is an F-actin dismantling protein that uses a new enzymatic oxygen-based signaling mechanism to both disassemble actin filaments and limit their reassembly (Hung et al. 2010; Hung, Pak, and Terman 2011; Hung et al. 2013). Now, we have worked out conditions to purify each of the human MICALs and find that each member of the MICAL family of proteins directly associates with and dismantles actin filaments. These MICAL-mediated effects occur via the ability of actin filaments to directly activate the enzymatic activity of MICAL family members – such that each of the MICAL family enzymes then post-translationally oxidizes actin subunits to destabilize filaments and decrease actin polymerization. Our results also demonstrate that these effects occur both in vitro with purified proteins and in cellular contexts in vivo – and thereby identify the MICALs as a phylogenetically-conserved family of F-actin dismantling enzymes with important in vivo implications for actin regulation because of their broad expression in multiple different tissues.

Our results also identify unique biochemical attributes that define the MICAL family of enzymes. In particular, we find that each MICAL family member binds FAD, is enzymatically active, and behaves catalytically in a generally similar manner – including using NADPH as a co-enzyme, which the MICALs prefer over the related (unphosphorylated) pyridine nucleotide co-enzyme NADH. Likewise, we find that actin filaments activate the catalytic activity of each member of the MICAL family of proteins and serve as a substrate for each MICAL. Furthermore, we find that each of the MICALs uses the same mechanism to accomplish its dismantling effects on actin filaments: the stereospecific oxidation of specific methionine residues within the D-loop portion of actin subunits – effects that are reversed by SelR/MsrB family methionine sulfoxide reductases. Thus, each MICAL family member is selective in its effects – such that it has a specific protein substrate that activates it, particular amino acid residues that it specifically modifies within that substrate, and a stereospecificity in how it modifies its amino acid substrate residues. These attributes, therefore, distinguish MICAL family enzymes from other physiologically-relevant redox enzymes characterized to date such as NADPH oxidases and nitric oxide synthases, which have different mechanisms of activation and action, as well as broader specificity both with regards to protein substrates and the amino acids that are modified within those substrates.

Our results also elucidate that a characteristic feature of each of the MICALs is that actin is their oxygen-acceptor substrate – and that specific binding of the polymeric form of this substrate (i.e., actin filaments) triggers MICALs consumption of NADPH to oxidize individual actin subunits. Thus, from both a structural perspective (Terman et al. 2002;

Siebold et al. 2005; Nadella et al. 2005; Alqassim et al. 2016), and in the way that binding of the oxygen-acceptor substrate accelerates consumption of the NADPH co-enzyme, MICALs are most similar to flavoprotein monooxygenase enzymes. However, to the best of our knowledge MICAL enzymes are the first known class of flavoprotein monooxygenases for which a protein substrate has been identified. Our results therefore raise the possibility that other (or perhaps all) flavoprotein monooxygenases have protein substrates that are awaiting identification. Moreover, it is unknown if the MICALs have other substrates, but our results herein reveal that a substrate for the MICALs should be defined based solely on its ability to both 1) activate MICAL and 2) be modified by MICALs enzymatic activity (i.e., as we have found for actin filaments). Such a definition will thus serve to differentiate a *bona fide* substrate from a protein that is simply spuriously modified by the ability of MICALs and other flavoprotein monooxygenases to produce non-selective diffusible oxidants (i.e., hydrogen peroxide) in the course of their reaction in vitro.

Our results also reveal that like other monooxygenases, the production of hydrogen peroxide (i.e., the loss of reducing equivalents in the absence of a substrate) is actively suppressed by MICAL family enzymes. However, there is some production of hydrogen peroxide, particularly in the case of MICAL-1, with its naturally-occurring single amino acid substitution that we have defined in the critical DG conserved motif of the MICAL enzymatic region. Thus, while our results herein, coupled with previous observations (Hung et al. 2010; Hung, Pak, and Terman 2011; Hung et al. 2013; Fremont et al. 2017) demonstrate that hydrogen peroxide production and MICAL-mediated F-actin disassembly are not linked together (see also **Figure 2.16**), it is interesting to consider that MICAL may

use hydrogen peroxide in physiological contexts to exert effects on other proteins. In any case, the effects that the MICALs may have using hydrogen peroxide are likely to be on cysteine residues, since hydrogen peroxide is a poor oxidizer of methionine residues (Kim, Weiss, and Levine 2014; Manta and Gladyshev 2017). Indeed, the oxidation of cysteine residues via hydrogen peroxide has been reported as a means through which MICAL-1 modifies the CRMP protein (Morinaka et al. 2011). It should also be considered that in contrast to our work herein using truncated/active forms of MICAL, full-length MICALs (including MICAL-1) are kept in an inactive state (i.e., without NADPH activity/hydrogen peroxide production) (Schmidt, Shim, and Strittmatter 2008; Hung et al. 2010; Giridharan et al. 2012; Vitali et al. 2016; Fremont et al. 2017). Thus, any hydrogen peroxide production by MICALs is likely to be tightly controlled in the cell to modify proteins in the vicinity of F-actin. Future work will aim to further elucidate the mechanistic details of these unusual and important enzymes, including the means by which the MICALs gain access to and oxidize Met44 and Met47 within filaments (**Figure 2.16**).

In summary, we have identified a family of actin regulatory proteins conserved from invertebrates to humans that use actin filaments as their enzymatic substrate – employing their unusual catalytic mechanism to covalently modify and induce the dismantling of actin filaments. These findings therefore uncover a new class of broadly-expressed negative regulators of actin stability and thereby elucidate new mechanisms underlying actin disassembly. In particular, the assembly of actin filaments is favored within cellular contexts, making it critical to understand how targeted and rapid F-actin disassembly is occurring (Rottner and Stradal 2011; Brieher 2013; Miyoshi and Watanabe 2013). In a similar way,

specific cell-cell signaling ligands including repellents such as ephrins, slits, semaphorins, myelin-associated inhibitors, and Wnts trigger the rapid disassembly of F-actin networks in multiple tissues (Bashaw and Klein 2010; Kolodkin and Tessier-Lavigne 2011; Hung and Terman 2011), but their direct effectors are still poorly understood. Our results shed light on both of these phenomena, since MICALs are heavily alternatively spliced – with different forms being targeted to specific regions of cells and organelles, as well as working both together and independently from specific repellent cues (reviewed in (Zhou, Gunput, et al. 2011; Vanoni, Vitali, and Zucchini 2013; Giridharan and Caplan 2014; Wilson et al. 2016; Manta and Gladyshev 2017)). Indeed, a model is emerging that the MICALs are maintained in an inactive conformation in the cell and are locally activated upon binding to other proteins such as the Semaphorin repellent receptor Plexin and small GTPases like Rab35 (**Figure 2.16**; (Terman et al. 2002; Schmidt, Shim, and Strittmatter 2008; Hung et al. 2010; Giridharan et al. 2012; Vitali et al. 2016; Fremont et al. 2017)). Moreover, because of the MICALs ability to covalently modify actin, the MICALs differentiate themselves from other actin disassembly proteins characterized to date because they not only rapidly dismantle F-actin, but they also generate post-translationally modified actin that has aberrant assembly properties. Given that the MICALs are widely expressed in multiple different tissues, that they have the ability to synergize with ubiquitous actin regulatory proteins and signaling pathways, and that they (and their substrate residues on actin) have been tied to different pathologies, our results bring a new understanding to how targeted and rapid F-actin disassembly occurs in cells.

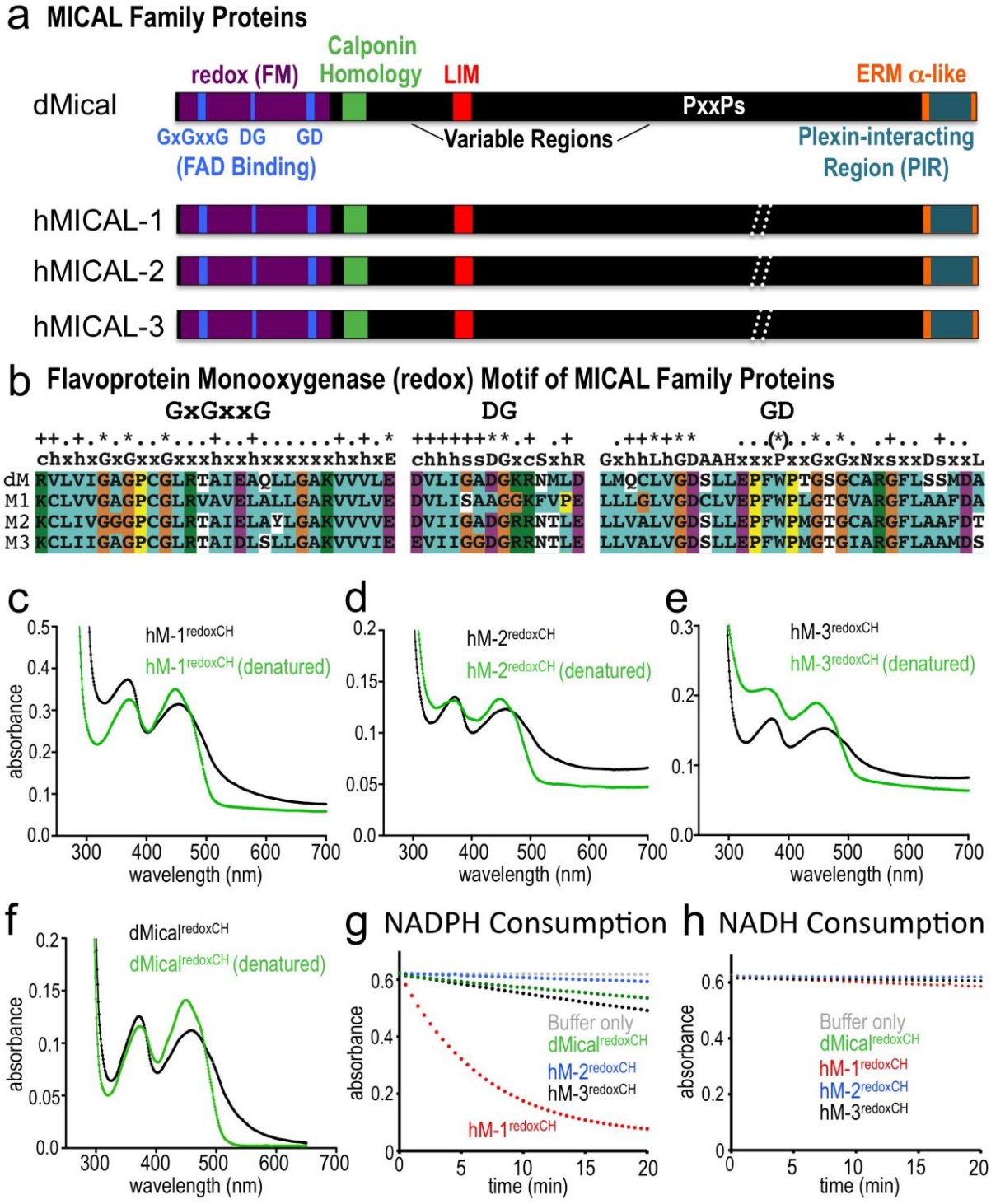
a MICAL Family Proteins
Calponin
redox (FM)
Homology
LIM
ERM α-like
dMical
PxxPs
GxGxxG DG GD
(FAD Binding)
Variable Regions
Plexin-interacting
Region (PIR)
hMICAL-1
hMICAL-2
hMICAL-3
b Flavoprotein Monooxygenase (redox) Motif of MICAL Family Proteins
GxGxxG
DG
GD
dM
M1
M2
M3
c
d
e
hM-1redoxCH
hM-1redoxCH (denatured)
hM-2redoxCH
hM-2redoxCH (denatured)
hM-3redoxCH
hM-3redoxCH (denatured)
absorbance
wavelength (nm)
f
dMicalredoxCH
dMicalredoxCH (denatured)
g NADPH Consumption
h NADH Consumption
Buffer only
dMicalredoxCH
hM-2redoxCH
hM-3redoxCH
hM-1redoxCH
time (min)

Figure 2.1. Each human MICAL family member (MICAL-1, MICAL-2, and MICAL-3) is a flavoenzyme that consumes NADPH.

(a) Although variable in length (depicted with the white dashed lines), each of the human (h) MICAL protein family members contain the same core domains as Drosophila (d) Mical including a flavoprotein monooxygenase (FM) domain (also called the redox or MO domain), a single calponin homology domain, and a single LIM domain. Multiple different splice forms of the MICALs have also been identified – some without the C terminus – as detailed in a recent review (Hung and Terman 2011). **(b)** Amino acid sequence alignments show that each of the human MICALs (M1, M2, M3), similar to Drosophila Mical (dM), contains three sequence motifs that define them as flavoprotein monooxygenases (Wierenga, Terpstra, and Hol 1986; Eggink et al. 1990; Eppink, Schreuder, and Van Berkel 1997). Each MICAL contains an exact match with each of the 11 residues of the ADP binding region of FAD binding proteins (GxGxxG motif; (Wierenga, Terpstra, and Hol 1986)), where (+) indicates that MICALs match the consensus, (*) indicates that MICALs match the highly important conserved residues, and (.) indicates the conserved spacing of these residues within these motifs. The MICALs also have well-conserved FAD Fingerprint 2 (GD) and DG motifs, which are additional distinguishing features of flavoprotein monooxygenases (Eggink et al. 1990; Eppink, Schreuder, and Van Berkel 1997). Note, however, that MICAL-1 has a "naturally" occurring substitution of an alanine residue instead of the important aspartate residue in the DG motif. light blue=hydrophobic and cysteine residues, purple = acids, green = bases, yellow = proline, and orange = glycine. The proline ((*)) in the FAD fingerprint 2 is also likely to be conserved. **(c-f)** Each of the human MICALs binds FAD. The isoalloxazine ring system within flavins generates the yellow/orange color of FAD and FMN and is also responsible for light absorption in the UV and visible spectral range such that the oxidized form of FAD has two peaks at ~360nm and ~450nm (Chapman and Reid 1999). Likewise, each of the purified human MICAL proteins, similar to Drosophila Mical (Wu, Hung, and Terman 2016), has a UV-visible light absorption spectra with peaks at ~360nm and ~450nm (black lines) – and denaturation of the MICAL proteins releases FAD, which underlies this absorption spectra (green line). Note also that the flavin is shielded to some extent from absorbing light by the protein backbone of each of the MICAL proteins (e.g., compare the absorbance levels and wavelength of the black and green lines). [MICAL]=20µM. **(g-h)** Each of the human MICALs consume the co-enzyme NADPH **(g)**, preferring it over the related pyridine nucleotide coenzyme NADH **(h)**, as observed by measuring the change in absorbance at 340nm (NADPH and NADH absorb light at 340nm, while the products of the conversion/consumption, NADP+ and NAD+, do not). Buffer only is the buffer used to store the MICAL proteins. [MICAL]=600nM, [NADPH]=100µM, [NADH]=100µM. *(Performed by HW).*

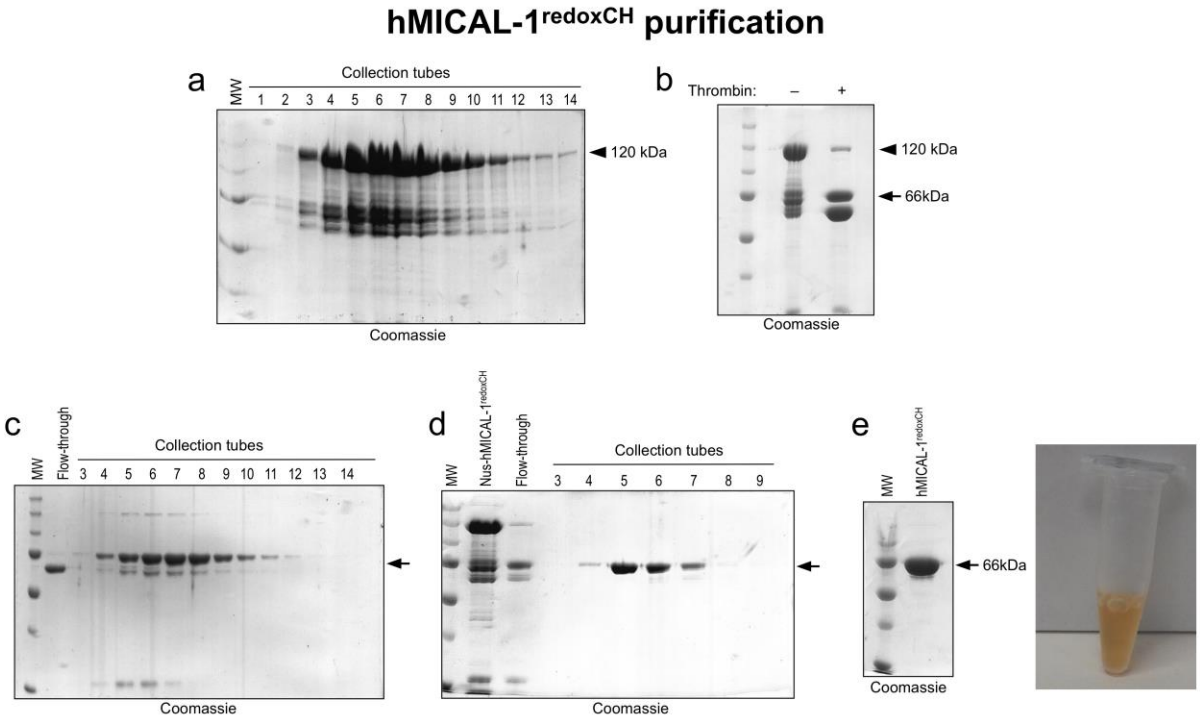

Figure 2.2. Purification and characterization of human MICAL-1^{redoxCH} protein.

(a-e) Coomassie stained gels are shown and the arrows point to the recombinant human (h) MICAL-1^{redoxCH} protein in all gels. MW in kDa. **(a)** A cDNA encoding hMICAL-1^{redoxCH} was inserted into a His-tag containing bacterial expression vector, transformed into bacteria, and following the appropriate growth conditions, lysates were loaded on a Nickel (Ni)-NTA affinity column to enrich for the Nus/His-tagged hMICAL-1^{redoxCH} (arrowhead). **(b)** Following elution from the Ni-NTA column, the enriched Nus/His-tagged hMICAL-1^{redoxCH} protein (arrowhead, 120 kDa) was digested (+) with a thrombin protease to cleave-off the Nus tag. The smaller size of the digested human MICAL-1^{redoxCH} (without the Nus tag) can be seen (arrow, 66 kDa). **(c)** The digested (+) sample from (b) was then loaded again on a Ni-NTA column to separate hMICAL-1^{redoxCH} from the Nus tag. Fractions within collection tubes 3-12 were combined. **(d)** Ion-exchange chromatography was then used to remove contaminating proteins since hMICAL-1^{redoxCH} can bind with a MonoS column (arrow). Samples within collection tubes 5-7 were then combined and concentrated **(e)** and analyzed on a gel to determine the purity of the human MICAL-1^{redoxCH} protein (arrow). The purified hMICAL-1^{redoxCH} is also shown in a transparent microcentrifuge tube, where its yellowish color is readily observed. Unprocessed original scans of gels/blots are shown in Figure 2.17. *(Performed by HW).*

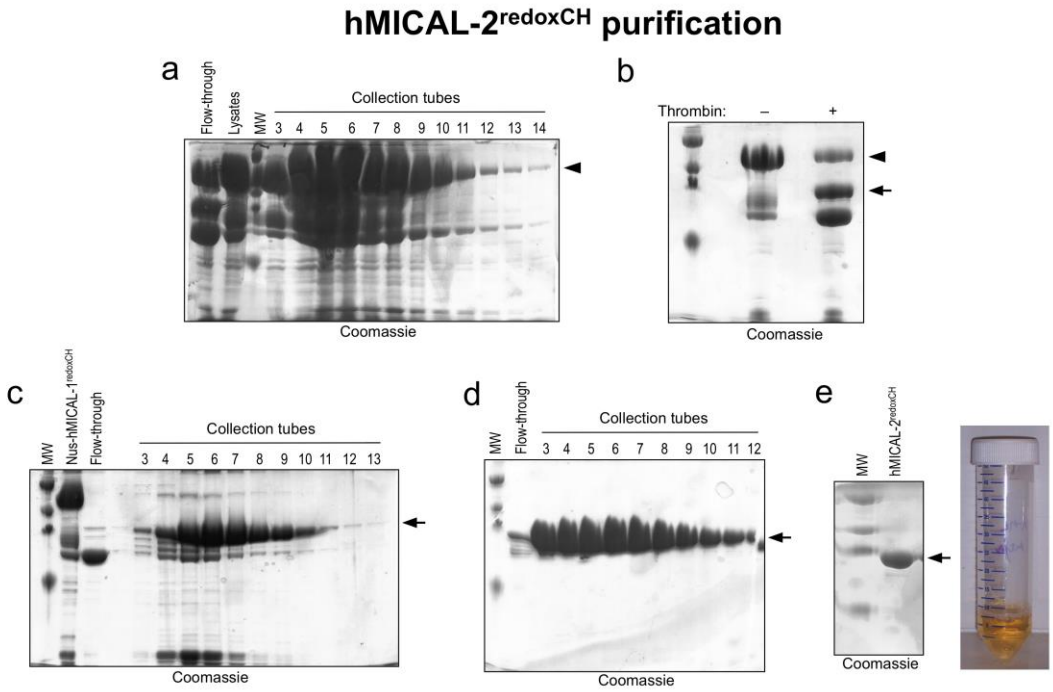

Figure 2.3. Purification and characterization of human MICAL-2redoxCH protein.

(a-e) Coomassie stained gels are shown and the arrows point to the recombinant hMICAL-2^{redoxCH} protein in all gels. MW in kDa. **(a)** A cDNA encoding hMICAL-2^{redoxCH} was inserted into a His-tag containing bacterial expression vector, transformed into bacteria, and following the appropriate growth conditions, lysates were loaded on a Ni-NTA affinity column to enrich for the Nus/His-tagged hMICAL-2^{redoxCH} (arrowhead). **(b)** Ni^{2+}-NTA affinity purified Nus-tagged hMICAL-2^{redoxCH} protein from samples in (a) were combined and subjected to thrombin digestion (+) to remove the Nus tag. A Coomassie-stained band corresponding in size to the cleaved hMICAL-2^{redoxCH} protein was observed following thrombin digestion (arrow), while the uncleaved Nus-tagged hMICAL-2^{redoxCH} protein is readily seen in the absence of thrombin (arrowhead). **(c)** Samples containing cleaved hMICAL-2^{redoxCH} protein were subjected to Ni^{2+}-NTA affinity chromatography to remove the Nus-tag and thrombin. hMICAL-2^{redoxCH} protein (arrow) was eluted with 250 mM imidazole and fractions within collection tubes 3-13 were combined for the next step. **(d)** As seen after SDS-PAGE/Coomassie-staining, cation ion exchange chromatography was used to separate hMICAL-2^{redoxCH} protein (arrow) from contaminating proteins, including chaperonins. **(e)** Samples from collection tubes 3-12 (from d) were concentrated and the purity of the hMICAL-2^{redoxCH} is shown after SDS-PAGE and Coomassie staining (arrow). The purified hMICAL-2^{redoxCH} is also shown in a transparent tube, where its yellowish color is readily observed. Unprocessed original scans of gels/blots are shown in Figure 2.17. *(Performed by HW).*

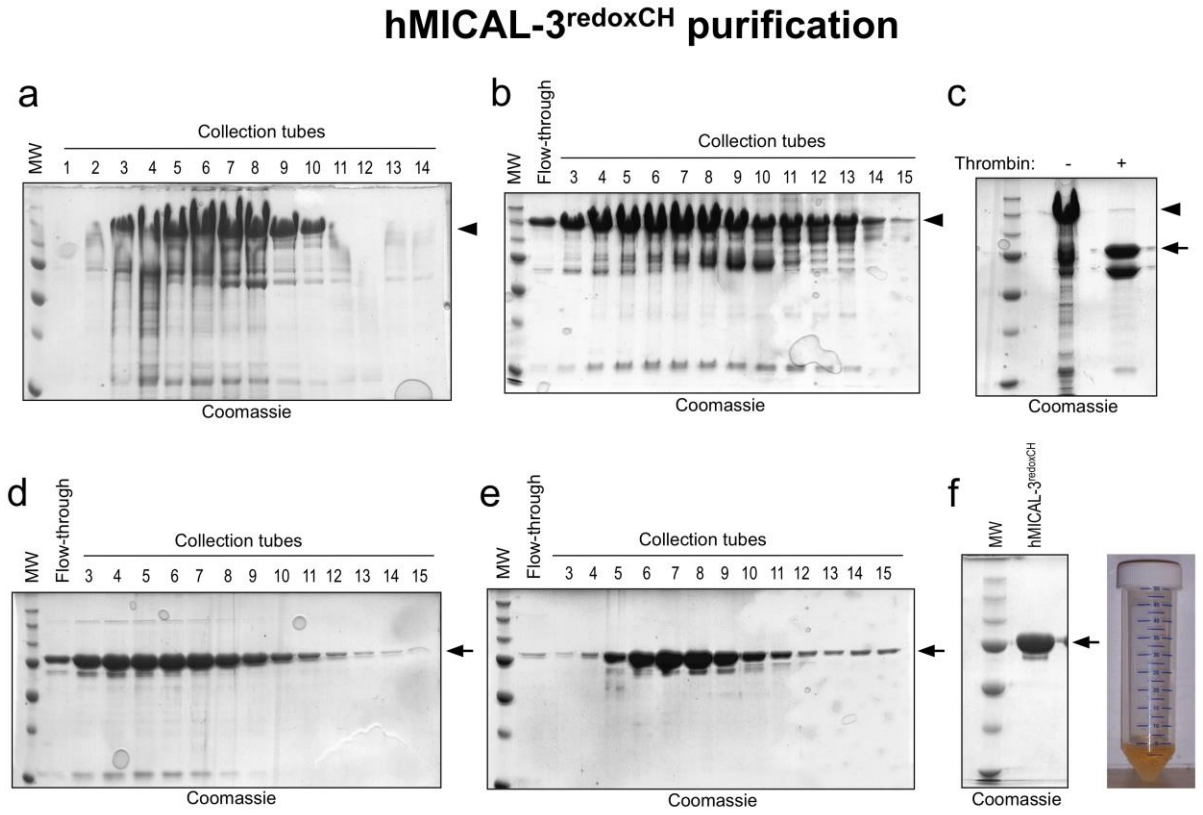

Figure 2.4. Purification and characterization of recombinant human MICAL-3^{redoxCH} protein.

(a-f) Coomassie stained gels are shown and the arrows point to the recombinant hMICAL-3^{redoxCH} protein in all gels. MW in kDa. (**a**) A cDNA encoding hMICAL-3^{redoxCH} was inserted into a His-tag containing bacterial expression vector, transformed into bacteria, and following the appropriate growth conditions, lysates were loaded on a Ni-NTA affinity column to enrich for the Nus/His-tagged hMICAL-3^{redoxCH} protein (arrowhead). **(b)** After desalting, samples were loaded on a MonoQ column to enrich for the Nus/His-tagged hMICAL-3^{redoxCH} (arrowhead). **(c)** Samples in collection tubes 3-9 (from b) were desalted and then digested with thrombin. A Coomassie-stained band corresponding in size to the uncleaved Nus-tagged hMICAL-3^{redoxCH} protein is readily seen in the absence of thrombin (arrowhead), while cleaved hMICAL-3^{redoxCH} protein is observed following thrombin digestion (arrow). **(d-e)** Ni^{2+}-NTA affinity chromatography (d) was used again to remove the Nus-tag and thrombin, after which the contents of collection tubes 3-15 were combined and subjected to cation ion exchange chromatography (e) to further separate hMICAL-3^{redoxCH} protein (arrow) from contaminating proteins. **(f)** The contents of sample tubes 4 through 15 (from e) were combined, concentrated, and analyzed on a gel to determine the purity of the hMICAL-3^{redoxCH} protein (arrow). The purified hMICAL-3^{redoxCH} is also shown in a

transparent tube, where its yellowish color is readily observed. Unprocessed original scans of gels/blots are shown in Figure 2.17. *(Performed by HW).*

a Identity/Similarity of the Redox Region of MICAL Family Proteins

	dMical^{redox}	hMICAL-1^{redox}	hMICAL-2^{redox}	hMICAL-3^{redox}
dMical^{redox} (469aa)				
hMICAL-1^{redox} (470aa)	54%(I) 70%(S)			
hMICAL-2^{redox} (473aa)	62%(I) 74%(S)	59%(I) 72%(S)		
hMICAL-3^{redox} (473aa)	63% (I) 76% (S)	60%(I) 75%(S)	81% (I) 91% (S)	

b Flavin-binding Characteristics of MICAL Family Proteins

	Supe (after Boiling)	**Pellet (after Boiling)**	***Flavin – Protein Binding***	**Peak at 446nm or 450nm?**	***FMN or FAD?***
dMical	yellow	white	*Non-covalent*	450nm	*FAD*
hMICAL-1	yellow	white	*Non-covalent*	450nm	*FAD*
hMICAL-2	yellow	white	*Non-covalent*	450nm	*FAD*
hMICAL-3	yellow	white	*Non-covalent*	450nm	*FAD*
hMICAL-1 DG	yellow	white	*Non-covalent*	450nm	*FAD*

c FAD Stoichiometry (Bound FAD) of MICAL Family Proteins

	Bound FAD (%)
dMical	97.03
hMICAL-1	99.73
hMICAL-2	95.31
hMICAL-3	99.76
hMICAL-1 DG	79.90

Figure 2.5. The redox region and flavin binding characteristics of MICAL family proteins.

Essential experimental procedures for defining a flavin-containing enzyme are 1) the recognition of the presence of a flavin co-factor, 2) the identification of the flavin co-factor, and 3) the determination of the stoichiometry of the bound flavin co-factor (Aliverti, Curti, and Vanoni 1999; Chapman and Reid 1999). Therefore, we set out to characterize each member of the MICAL family in this regard (see also **Figure 2.1c-f**). **(a)** The length, identity (I), and similarity (S) of the amino acid (aa) sequences coding for the redox portion of Drosophila (d) Mical and each of the human (h) MICALs. **(b)** Heat-induced denaturation of each the MICAL proteins using standard approaches (Aliverti, Curti, and Vanoni 1999) was used to determine the each purified MICAL family protein bound FAD non-covalently. In particular, following heat-induced denaturation of each of the MICAL proteins and centrifugation, the supernatant (Supe) and not the pellet was yellow, indicating that the flavin is bound non-covalently (i.e., the flavin was released when the protein was unfolded by heat treatment/denaturation, showing that it was not covalently linked to the MICALs). The absorbance spectrum of the released flavin exhibited a peak at 450 nm, which is characteristic of FAD. FMN exhibits a peak at 446 nm. These results indicate that each of the MICALs, including hMICAL-1^{DG} (see **Figure 2.13**), binds FAD non-covalently. [MICALs]=20µM. **(c)** Our results also revealed a 1:1 stoichiometry of the bound FAD cofactor to each of the MICAL family members. Characterization of the absorption spectra of MICAL proteins (see **Figure 2.1c-f**) also allows the amount of the purified MICAL that is bound to FAD to be determined (see Materials and Methods and (Wu, Hung, and Terman 2016)). Note that the MICAL-1^{DG} protein generated more protein in the Apo form (without FAD) than the other MICALs, indicating that it is functional but less able to bind and incorporate FAD when this amino acid change is introduced into it. *(Performed by HW and JRT).*

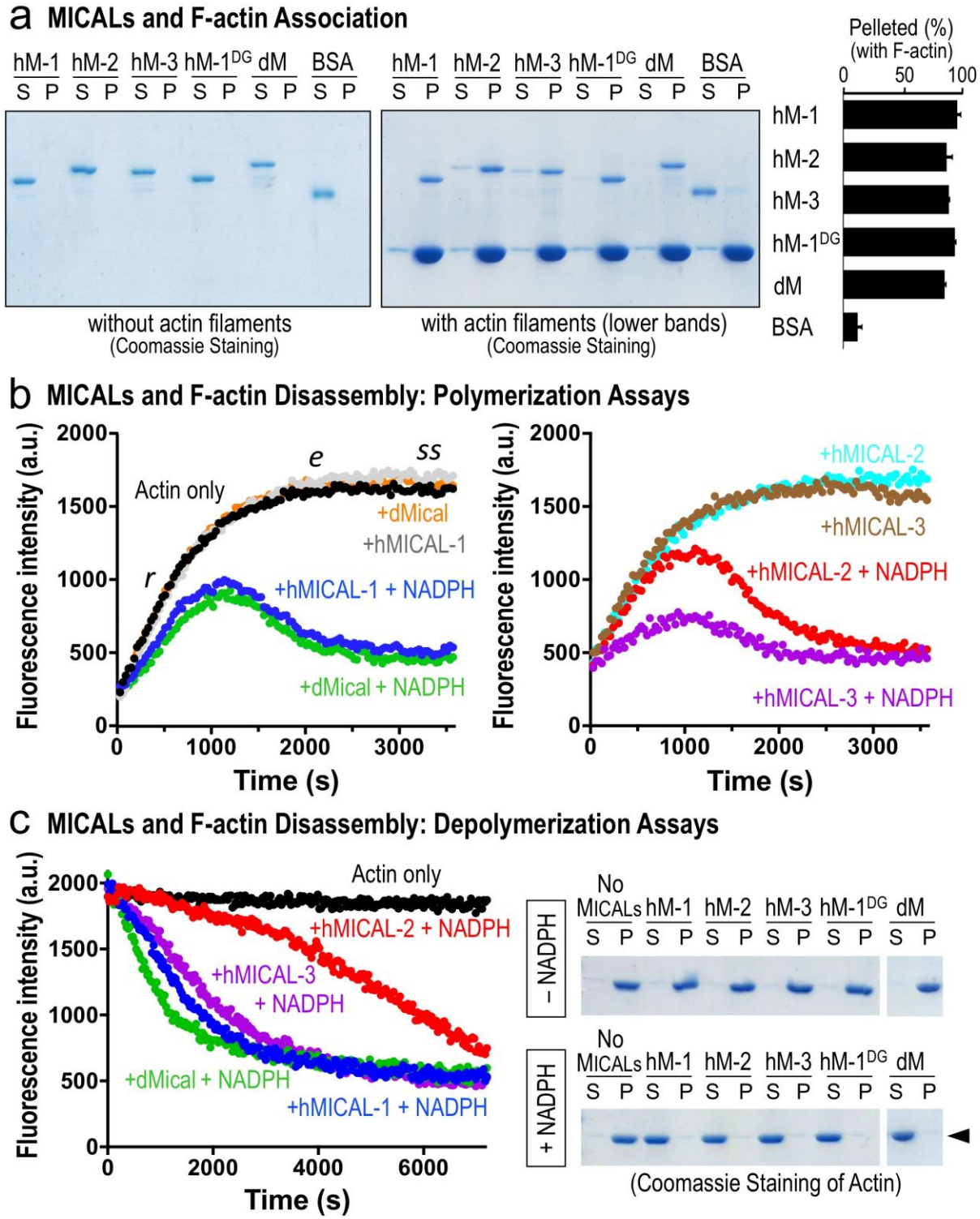

Figure 2.6. Each human MICAL family member directly binds and disassembles actin filaments.

(a) Each of the purified human MICAL^{redoxCH} proteins, hMICAL-1 (hM-1), hMICAL-2 (hM-2), hMICAL-3 (hM-3), and hMICAL-1 DG (hM-1^{DG}), like Drosophila Mical^{redoxCH} (dM), associates with F-actin as revealed by actin co-sedimentation/pelleting assays in which Coomassie blue stained gels are shown. Notice that after high-speed centrifugation, each of the purified MICALs is present in the soluble (S) fraction (left gel). In the presence of purified actin filaments, however, each of the MICALs is present in the pellet (P) fraction (right gel). The percentage (± the standard error of the mean (SEM)) of different MICAL proteins in the pelleted fraction following incubation with purified F-actin was quantified by densitometry (n = 3). Bovine serum albumin (BSA) was used as a control and was predominantly found in the S fraction. [MICALs]=600nM, [BSA]=600nM, [actin]=2.3µM. *(Performed by HW).* **(b-c)** Each of the human MICALs alters actin polymerization and depolymerization. Pyrene-labeled actin was used to monitor both the polymerization and depolymerization of actin using standard approaches, where the fluorescence intensity (a.u. (arbitrary units)) of the pyrene-labeled actin polymer is substantially higher than the pyrene-labeled actin monomer. Each of the MICALs and the reaction conditions are color-coded here and in Figures 3-5. *(Performed independently by HGY and HW).* **(b)** Standard pyrene-actin polymerization assay. No filaments are present at Time=0, when MICALs are added to actin and polymerization is induced. As can be observed by following the characteristic increase in fluorescence intensity over time, the addition of each of the purified human MICALs (in the presence of their co-enzyme NADPH) decreases the rate (*r*), extent (*e*), and steady-state level (*ss*) of actin polymerization (as compared to an actin only control, black dots; or MICAL only (no NADPH) + actin controls; or NADPH only + actin controls (not shown; see (Hung et al. 2010))). Notably, MICAL (NADPH) induces actin polymerization to slow-down over time, which is followed by a substantial decrease in the extent of polymerization, the rapid depolymerization of F-actin, and the inability of actin to reinitiate polymer formation. Thus, because each of the MICALs act on F-actin (Hung et al. 2010; Hung et al. 2013) (and herein), our data in the polymerization assays are consistent with a model in which as the actin begins to polymerize, the MICALs oxidize individual subunits of the polymer, which disassembles the polymerizing actin. This slows polymerization – and also creates fewer and fewer unoxidized monomers that can be used for polymerization. [MICAL-1]=300nM, [dMical and MICALs-2, 3]=600nM, [NADPH]=100µM, [Actin]=1.15µM. **(c)** Purified human MICALs +/– NADPH was added to actin that was polymerized and kept in buffer conditions that favored polymerization (as can be seen with the steady-state fluorescence intensity level of the actin only control (black dots); or actin with each of the MICALs without NADPH (not shown; see (Hung et al. 2010))). The addition of each of the human MICALs (in the presence of NADPH) induces actin depolymerization (decreasing fluorescence intensity that can be followed over time in the pyrene actin depolymerization assay (left)). [MICAL-1]=300nM, [dMical and MICALs-2, 3]=600nM, [NADPH]=100µM, [Actin]=1.15µM. The extent of this MICAL (NADPH)-dependent actin depolymerization is also observed when MICAL-treated F-actin was subjected to high-speed centrifugation to differentiate F-actin (P) from G-actin (S). As can be observed in these Coomassie stained gels, each of the human MICALs (in the presence of NADPH) substantially increases the ratio of G-actin to F-actin (arrowhead). [MICAL-

1]=300nM, [dMical and MICALs-2, 3]=600nM, [NADPH]=100µM, [Actin]=1.15µM. Unprocessed original scans of gels are shown in Figure 2.17.

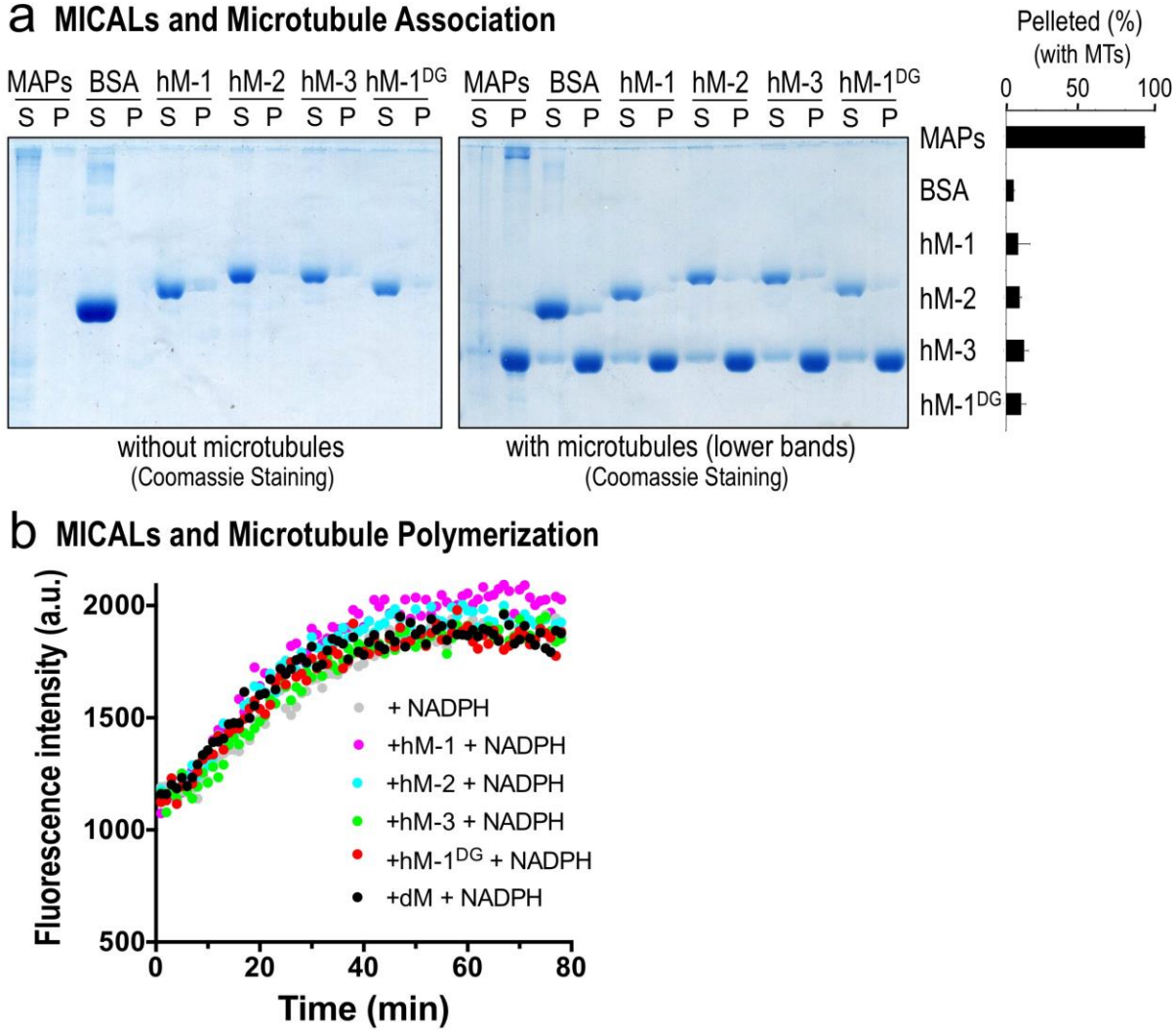

Figure 2.7. Purified human MICAL^{redoxCH} proteins show little to no association with microtubules and do not alter tubulin polymerization dynamics.

(a) Images of Coomassie blue stained gels are shown. Co-sedimentation analysis was used to examine the association between MICALs and microtubules. Notice that after high-speed centrifugation, each of the purified human MICAL^{redoxCH} proteins, hMICAL-1 (hM-1), hMICAL-2 (hM-2), hMICAL-3 (hM-3), and human MICAL-1 DG (hM-1^{DG}), like Drosophila Mical^{redoxCH} (dM) (Hung et al. 2010), is present in the soluble (S) fraction (left gel). Similarly, in the presence of microtubules, the majority of the purified MICAL proteins (and a negative control, BSA) are present in the soluble (S) fraction (right gel). Notice, however, that microtubule associated proteins (MAPs), known microtubule binding proteins

that were used as a positive control, change their distribution from the soluble fraction to pellet fraction in the presence of microtubules. These results indicate that purifed human MICAL^{redoxCH} proteins have little to no association with microtubules. The percentage ($\pm$ the standard error of the mean (SEM)) of different purified MICAL proteins in the pelleted fraction following incubation with microtubules (MTs) was quantified by densitometry ($n \geq 2$). [MICALs]=1µM, [BSA]= 2.2µM, [MAPs]= 0.64µM, [tubulin]=0.5mg/ml. **(b)** The effect of MICALs on tubulin polymerization was examined. A fluorescence-based tubulin polymerization assay was employed using standard approaches, where the fluorescence intensity (a.u. (arbitrary units)) of microtubules is substantially higher than tubulin monomers. Drosophila Mical^{redoxCH} (dM), each of the purified human MICAL^{redoxCH} proteins, hMICAL-1 (hM-1), hMICAL-2 (hM-2), hMICAL-3 (hM-3), and human MICAL-1 DG (hM-1^{DG}), and/or NADPH were added in the tubulin solution and polymerization was initiated by increasing the temperature from 4°C to 37°C. There is no appreciable difference between tubulin polymerization alone (+NADPH) and tubulin polymerization in the presence of the human MICALs with NADPH. [MICALs]=600nM, [NADPH]=100µM, [tubulin]=2mg/ml. Unprocessed original scans of gels are shown in Figure 2.17. *(Performed by HW).*

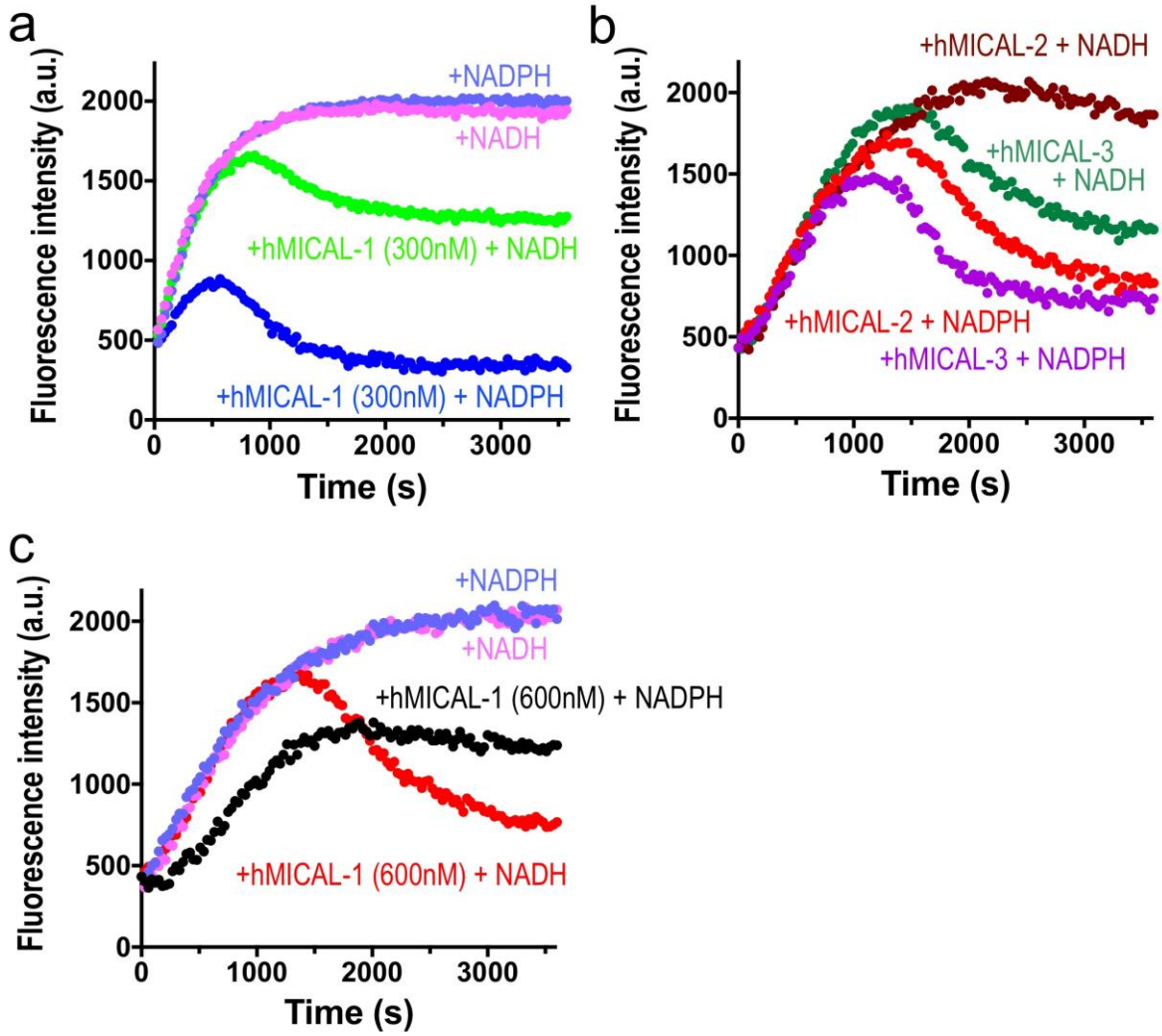

Figure 2.8. Further characterization of human MICALs effects on F-actin dynamics.

(a-b) hMICAL-1 **(a)** and hMICAL-2 and hMICAL-3 **(b)** alter the rate and extent of both actin polymerization and depolymerization more effectively in the presence of NADPH (100µM NADPH) than with the related pyridine nucleotide coenzyme NADH (100µM NADH). [Actin] = 1.15µM, [MICAL-1]=300 nM, [MICALs-2, 3]=600 nM. **(c)** However, note that NADH can allow higher concentrations of MICAL-1 to more effectively alter F-actin dynamics, since MICAL-1 does not as rapidly consume NADH (see **Figure 2.1g-h**), and thus can employ it for its oxidation reaction to modify actin. [Actin] = 1.15µM, [NADH]=100µM, [NADPH]=100µM, [MICAL-1]=600nM. *(Performed by HW).*

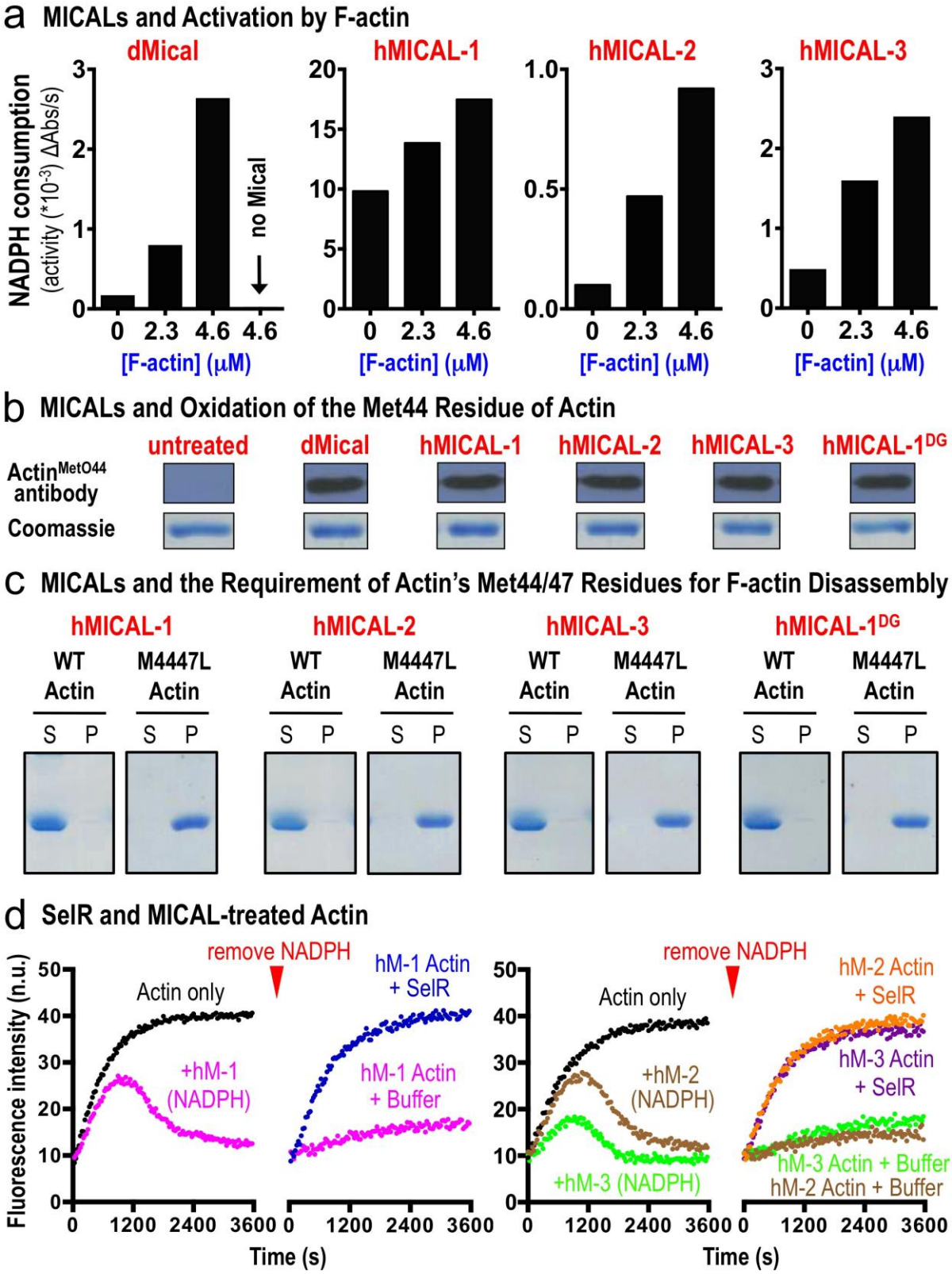
a MICALs and Activation by F-actin
dMical
hMICAL-1
hMICAL-2
hMICAL-3
NADPH consumption
(activity (*10-3) ΔAbs/s)
no Mical
0 2.3 4.6 4.6
0 2.3 4.6
[F-actin] (μM)
b MICALs and Oxidation of the Met44 Residue of Actin
untreated
dMical
hMICAL-1
hMICAL-2
hMICAL-3
hMICAL-1DG
ActinMetO44 antibody
Coomassie
c MICALs and the Requirement of Actin's Met44/47 Residues for F-actin Disassembly
hMICAL-1
hMICAL-2
hMICAL-3
hMICAL-1DG
WT Actin
M4447L Actin
S P
d SelR and MICAL-treated Actin
remove NADPH
Actin only
+hM-1 (NADPH)
hM-1 Actin + SelR
hM-1 Actin + Buffer
+hM-2 (NADPH)
+hM-3 (NADPH)
hM-2 Actin + SelR
hM-3 Actin + SelR
hM-3 Actin + Buffer
hM-2 Actin + Buffer
Fluorescence intensity (n.u.)
Time (s)

Figure 2.9. Each human MICAL family member is activated by actin filaments, oxidizing the Met44 residue of actin to induce F-actin disassembly.

(a) The enzymatic activity of each of the human (h) MICALs, similar to Drosophila (d) Mical, notably increases in the presence of F-actin. Enzyme activity was determined by consumption (conversion of NADPH to $NADP^{+}$) of MICAL's co-enzyme NADPH, which was monitored by recording the light absorbance at 340nm wavelength/time. [MICALs]=600nM; [NADPH]=200µM. **(b)** Each of the human MICALs oxidizes the Met44 residue of actin, as determined using an antibody that specifically recognizes Mical-oxidized actin ($actin^{MetO44}$; (Grintsevich et al. 2016)). Similar amounts of actin (lower panel) are present in all experiments. Note, as described in the methods, actin was polymerized to generate F-actin and 600 nM of each of the human MICALs and 200-300 µM of NADPH were added to 1.15µM of F-actin at room temperature for 2 hours. **(c)** Each of the human MICALs requires actin's Met44 and Met47 residues to disassemble F-actin. Drosophila Mical oxidizes the Met44 and Met47 residues of actin (Hung, Pak, and Terman 2011) and so we substituted as previously described a chemically related leucine residue for the methionine 44 and 47 residues in actin (M4447L) (Hung, Pak, and Terman 2011) to determine if each of the human MICALs also requires these residues to disassemble F-actin. Sedimentation assays reveal that each of the human MICALs robustly disassembles filaments composed of wild-type (WT) actin but not M4447L actin. [Actin]=1.15µM; [MICALs-1, 1^{DG}, 2, and 3]=600nM; [NADPH]=200-300µM. **(d)** The stereospecific methionine sulfoxide reductase SelR/MsrB restores the polymerization properties of actin treated with each of the human MICALs. Pyrene-actin assays, where the fluorescence is higher in the polymerized state, reveal that SelR restores the polymerization of human MICAL-1 (hM-1), human MICAL-2 (hM-2), and human MICAL-3 (hM-3) treated actin. Buffer (buffer that SelR is stored in), n.u. (normalized units between the 2 graphs). [MICAL-1]=100nM, [dMical and MICALs-2, 3]=600nM, [NADPH]=100µM, [Actin]=1.15µM. Unprocessed original scans of gels/blots are shown in Figure 2.17. *(Performed by HGY).*

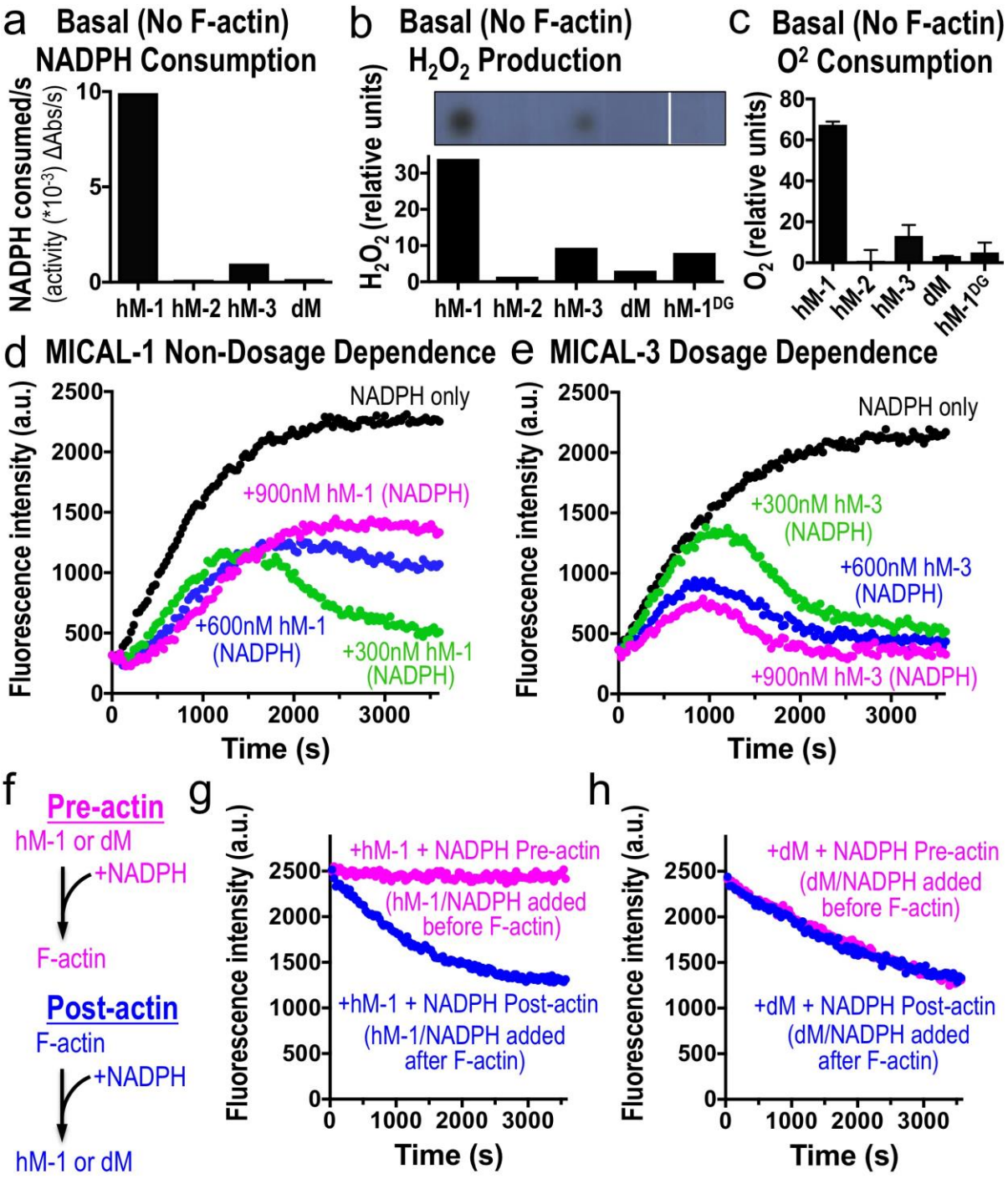

Figure 2.10. MICAL-1 exhibits notable activation and catalytic activity differences in comparison to other MICALs.

(a) The enzyme activity of human MICAL-1 (hM-1) in the absence of its substrate F-actin is substantially higher than that of the other MICALs, as judged by consumption of NADPH. In

particular, basal (in the *absence* of F-actin) NADPH consumption by MICAL-1 is close to 100 times more NADPH consumption *per second* than hMICAL-2, 60 times more NADPH consumption *per second* than Drosophila Mical, and over 10 times more NADPH consumption *per second* than hMICAL-3. [MICALs]=600nM, [NADPH]=200µM**.** *(Performed by HGY).* **(b)** hM-1 generates substantially more hydrogen peroxide (H_2O_2) than other MICALs (all assays done in the presence of NADPH and the absence of F-actin). Upper panel, chemiluminescent detection of H_2O_2 produced by MICALs, reveals significant H_2O_2 production by hM-1 in comparison to others MICALs that is quantified using a different assay, a bioluminescent assay (lower panel). Also note in both panels that hM-1^{DG} generates substantially less H_2O_2 than hM-1. [MICALs]=600nM; [NADPH]=100µM**.** *(Performed by HW).* **(c)** hM-1 consumes substantially more oxygen (O_2) than other MICALs (all assays done in the presence of NADPH and the absence of F-actin). Also note that hM-1^{DG} consumes substantially less O_2 than hM-1. [MICALs]=600nM; [NADPH]=200µM**.** *(Performed by HGY).* **(d-e)** Pyrene-actin assays reveal that hMICAL-1 *(Performed by HW).* **(d)**, unlike hMICAL-2 (**Figure 2.11d**), hMICAL-3 **(e)** and Drosophila Mical (Hung et al. 2010), exhibits decreasing effects on F-actin when higher levels of it are added to F-actin. These effects are consistent with hMICAL-1 exhibiting such rapid consumption of NADPH in the absence of its F-actin substrate that NADPH becomes limiting in allowing MICAL-1 to alter F-actin dynamics (see also main text). [Actin]=1.15µM, [NADPH]=100µM. **(f-h)** hMICAL-1 generates a high-level of basal H_2O_2, but does not use H_2O_2 to modify actin dynamics. *(Performed by HW).* **(f)** To test if MICALs use H_2O_2 to disassemble F-actin we made use of MICAL-1's high level of basal activity to produce H_2O_2 in the presence of NADPH, and added NADPH either before (pre) or after (post) the addition of F-actin. In short, we reasoned that if H_2O_2 (or another stable oxidant) was being used by MICALs to modify actin, it would not matter in which order we added F-actin to the same tube. However, if H_2O_2 (or another stable oxidant) was not being used to modify F-actin, MICAL-1 would exhaust its supply of NADPH generating H_2O_2 prior to the addition of F-actin, and would therefore have decreased effects on F-actin dynamics. **(g)** MICAL-1 no longer disassembles F-actin when it is incubated with NADPH prior to the addition of F-actin (pink), revealing it does not use H_2O_2 or another stable/generally-released oxidant to disassemble F-actin. **(h)** As a control, Drosophila Mical, which has a low rate of basal NADPH consumption (and thus retains NADPH when its F-actin substrate is not present), exhibits similar disassembly of F-actin in both the Pre- and Post- incubation conditions. [Actin]=1.15µM, [dMical and MICAL-1]=600nM, [NADPH]=100µM**.** Unprocessed original scans of blots are shown in Figure 2.17.

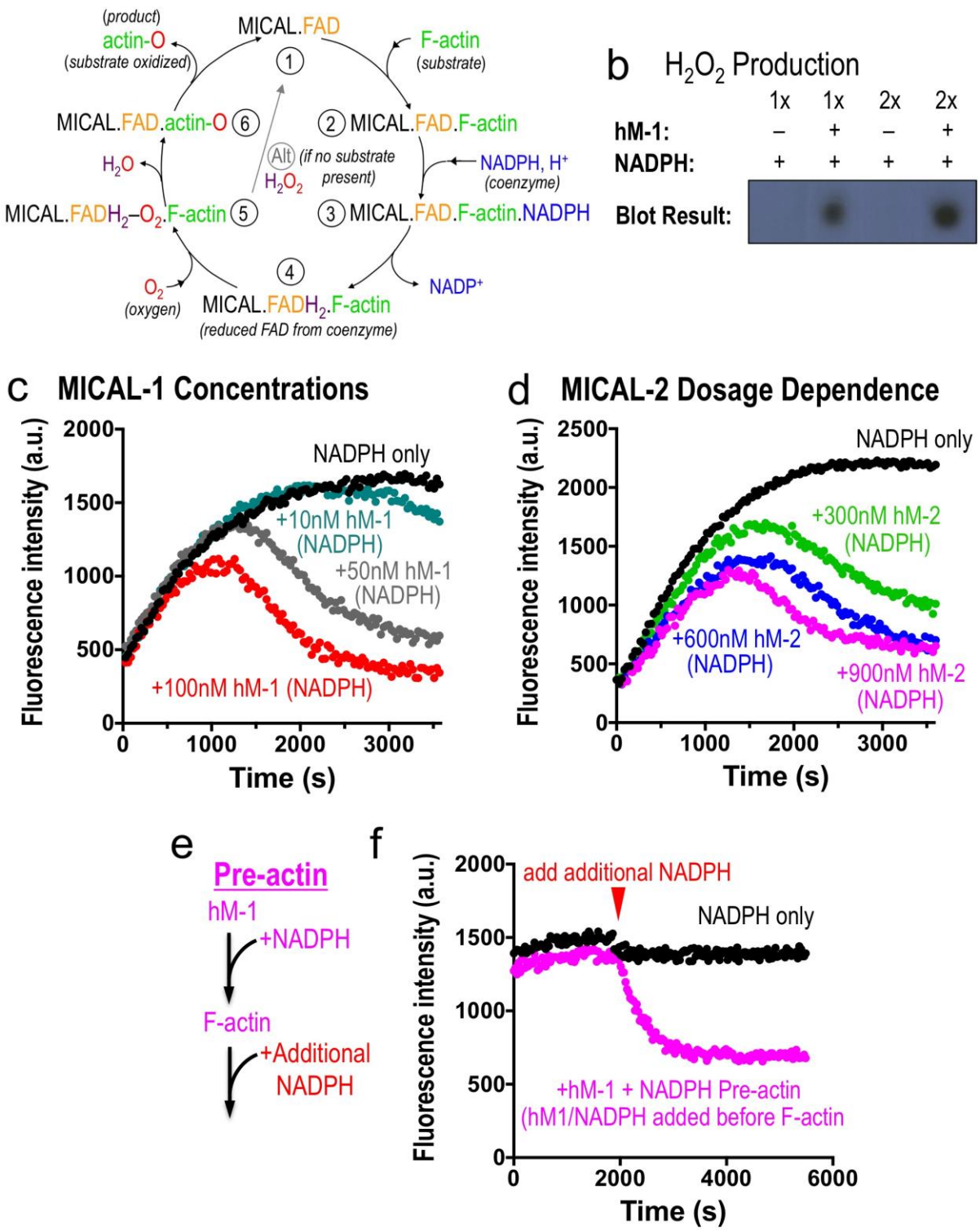
a MICAL Enzyme Reaction
(product)
actin-O
(substrate oxidized)
MICAL.FAD
F-actin
(substrate)
MICAL.FAD.actin-O
MICAL.FAD.F-actin
Alt
(if no substrate present)
H2O2
H2O
NADPH, H+
(coenzyme)
MICAL.FADH2–O2.F-actin
MICAL.FAD.F-actin.NADPH
O2
(oxygen)
MICAL.FADH2.F-actin
(reduced FAD from coenzyme)
NADP+
b H2O2 Production
1x 1x 2x 2x
hM-1: – + – +
NADPH: + + + +
Blot Result:
c MICAL-1 Concentrations
Fluorescence intensity (a.u.)
Time (s)
NADPH only
+10nM hM-1 (NADPH)
+50nM hM-1 (NADPH)
+100nM hM-1 (NADPH)
d MICAL-2 Dosage Dependence
Fluorescence intensity (a.u.)
Time (s)
NADPH only
+300nM hM-2 (NADPH)
+600nM hM-2 (NADPH)
+900nM hM-2 (NADPH)
e
Pre-actin
hM-1
+NADPH
F-actin
+Additional NADPH
f
Fluorescence intensity (a.u.)
Time (s)
add additional NADPH
NADPH only
+hM-1 + NADPH Pre-actin
(hM1/NADPH added before F-actin

Figure 2.11. MICAL-1 in comparison to other MICALs.

(a) Model of the enzyme reaction of the MICALs. MICAL (1) physically associates with its substrate F-actin (2), which triggers MICAL's conversion/consumption of its co-enzyme NADPH to NADP+ (3) and reduction of FAD (4). MICAL then uses oxygen (5), which results in oxidation of F-actin subunits on their Met44 and Met47 residues (6). When MICAL's F-actin substrate is not present, NADPH can be consumed at more limited levels (see **Figure 2.9a**; (Hung, Pak, and Terman 2011)) and H_2O_2 can be produced (Alt). **(b)** Further analysis of the generation of hydrogen peroxide by MICALs. Generation of hydrogen peroxide (H_2O_2) by human MICAL-1 **(**hM-1) as revealed by chemiluminescent detection of H_2O_2 produced by hM-1 in the presence of a substrate (luminol) and different concentrations (1x or 2x the amount) of a catalyst (horseradish peroxidase (HRP)). [MICAL-1]=600nM, [NADPH]=100µM. *(Performed by HW).* **(c)** Pyrene-actin assays reveal that at low concentrations, hMICAL-1's ability to alter actin polymerization is dosage dependent. However, with increasing higher concentrations, MICAL-1 exhibits decreasing effects on F-actin (see **Figure 2.10d**). These effects are consistent with hMICAL-1 exhibiting such rapid consumption of NADPH in the absence of its F-actin substrate that NADPH becomes limiting (as higher levels of hMICAL-1 are added to the assay) in allowing MICAL-1 to alter F-actin dynamics (see also main text). [Actin] = 1.15µM, [NADPH]=100µM. *(Performed by HW)***. (d)** hMICAL-2's ability to alter actin polymerization is dosage dependent (as observed using pyrene-actin assays). [Actin] = 1.15µM, [NADPH]=100µM. *(Performed by HW)***. (e-f)** Further analysis of hMICAL-1's effects on actin dynamics. MICAL-1 does not disassemble F-actin when it is incubated with NADPH prior to the addition of F-actin (see **Figure 2.10f-g**). These results support that MICAL-1, because of its high-rate of basal activity, consumes/uses-up NADPH prior to the addition of F-actin, such that it can no longer use NADPH in its reaction to modify actin. To further test this hypothesis, we added more NADPH (additional NADPH in e-f) into the MICAL-1 pre-reaction condition tube (f, arrowhead) (from Figure 2.8c). MICAL-1 now proceeds to modify actin and induce F-actin disassembly (f, pink). [Actin] = 1.15µM, [MICAL-1]=600nM, [NADPH]=100 µM. Unprocessed original scans of blots are shown in Figure 2.17. *(Performed independently by HGY and HW).*

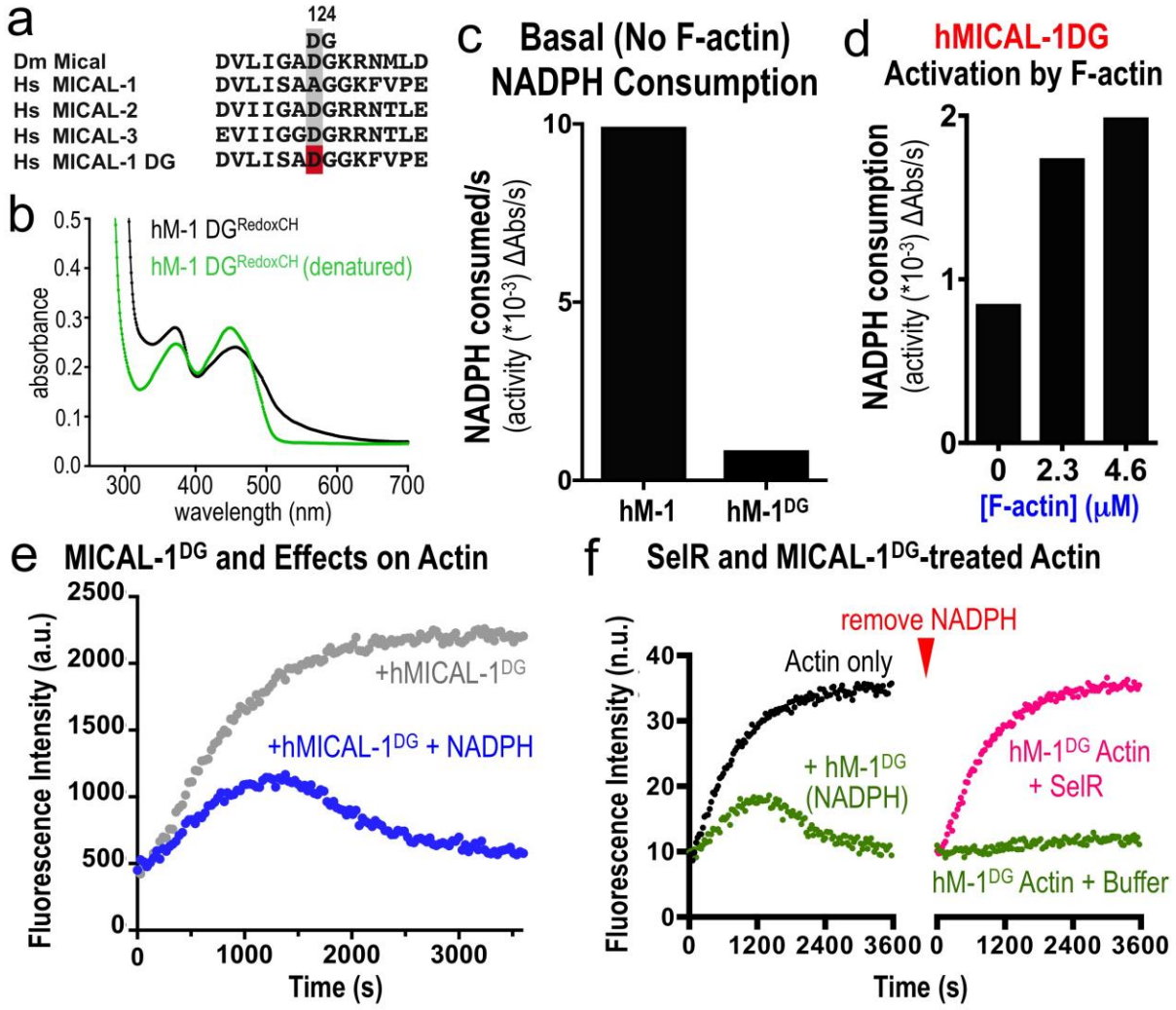

Figure 2.12. MICAL-1 exhibits a single amino acid alteration in its DG motif that produces high levels of catalytic activity in the absence of its F-actin substrate.

(a) MICAL-1 has a "naturally" occurring substitution of an alanine (A) residue instead of the important aspartate (D) residue in the DG (Conserved) motif that is present in the other MICAL family members. Using site-directed mutagenesis we converted the alanine residue within the DG motif of MICAL-1 to an aspartate residue and thereby generated a MICAL-1 protein similar to the other MICAL family members (MICAL-1^{DG}). **(b)** Purified MICAL-1^{DG} protein still exhibits the hallmarks of an FAD-binding protein. In particular, MICAL-1^{DG} maintains its UV-visible light absorption spectra (with peaks at ~360nm and ~450nm, black lines), and denaturation of the MICAL-1^{DG} releases FAD, which underlies this absorption spectra (green line). [MICAL-1^{DG}]=20μM. *(Performed by HW).* **(c)** Converting the alanine residue within the DG motif of MICAL-1 to an aspartate residue (MICAL-1^{DG}), substantially reduces (12-fold *per second*) the basal (in the absence of its F-actin substrate) enzyme activity of MICAL-1, as judged by the consumption of NADPH. [MICALs]=600nM,

[NADPH]=200µM**.** *(Performed by HGY).* (**d**) The enzymatic activity of MICAL-1^{DG}, similar to other MICALs, is notably increased in the presence of F-actin. Enzyme activity was determined by the consumption (conversion of NADPH to $NADP^{+}$) of MICAL's co-enzyme NADPH, which was monitored by recording the light absorbance at 340nm wavelength/time. [MICAL-1^{DG}]=600nM, [NADPH]=200µM. *(Performed by HGY).* **(e)** MICAL-1^{DG}, similar to unaltered MICAL-1 and other MICAL family members, induces actin polymerization to slow-down over time, which is followed by a substantial decrease in the extent of polymerization, the rapid depolymerization of F-actin, and the inability of actin to reinitiate polymer formation. [Actin]=1.15µM, [MICAL-1^{DG}]=600nM, [NADPH]=100µM. Here, as in Figure 2b, pyrene-labeled actin was used to monitor both the polymerization and depolymerization of actin using standard approaches, where the fluorescence intensity (a.u. (arbitrary units)) of the pyrene-labeled actin polymer is substantially higher than the pyrene-labeled actin monomer. *(Performed by HGY).* **(f)** Similar to unaltered MICAL-1 and other MICAL family members, the stereospecific methionine sulfoxide reductase SelR/MsrB restores the polymerization properties of actin treated with MICAL-1^{DG}. See also Figure 2.9d. Buffer (buffer that SelR is stored in), n.u. (normalized units between the 2 graphs). [Actin]=1.15µM, [MICAL-1^{DG}]=600nM, [NADPH]=100µM. *(Performed by HGY).*

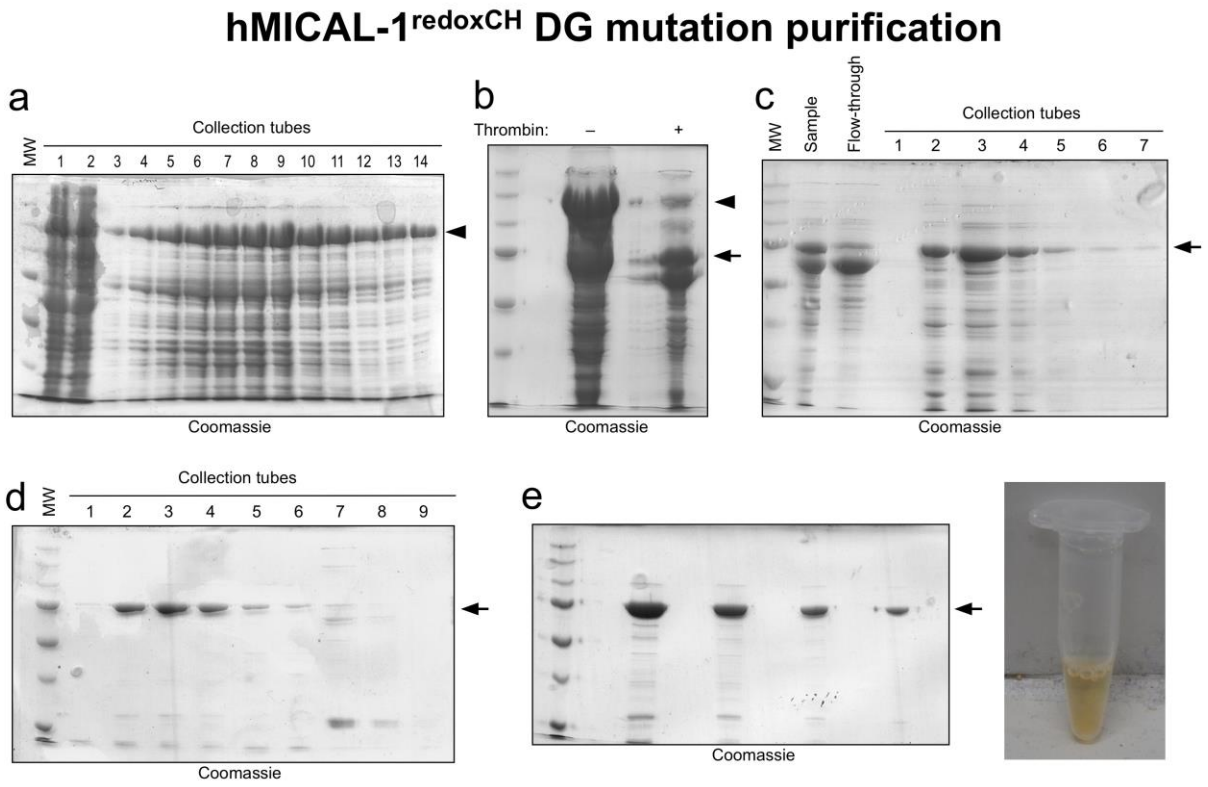

Figure 2.13. Purification and characterization of human MICAL-1^{redoxCH} DG protein (hMICAL-1^{DG}).

Compare also with the strategy used in Figure 2.2 to purify human MICAL-1^{redoxCH}. Coomassie stained gels are shown and the arrows point to the recombinant hMICAL-1^{redoxCH} DG protein in all gels. **(a)** A cDNA encoding hMICAL-1^{redoxCH} DG was inserted into a His-tag containing bacterial expression vector, transformed into bacteria, and following the appropriate growth conditions, lysates were loaded on a Ni-NTA affinity column to enrich for the Nus/His-tagged hMICAL-1^{redoxCH} DG (arrowhead). **(b)** The Nus-tagged hMICAL-1^{redoxCH} DG (arrowhead) was digested (+) with a thrombin protease to cleave-off the Nus tag. The smaller size of the digested human MICAL-1^{redoxCH} DG (without the Nus-His tag) can be seen (arrow). **(c)** The digested (+) sample from (b) was then loaded again on a Ni-NTA agarose column to remove the Nus-tag. Fractions from 2-6 were combined and used for d. **(d)** Ion-exchange chromatography was then used to remove contaminating proteins since the hMICAL-1^{redoxCH} DG can bind with the MonoQ column (arrow). Samples within collection tubes 2-6 were then combined and concentrated **(e)** and analyzed on a gel to determine the purity of the hMICAL-1^{redoxCH} DG protein. The purified hMICAL-1^{redoxCH} DG mutant is also shown in a transparent tube, where its yellowish color is readily observed. Note that the yellow color is lighter than the other MICALs (**Figures 2.2-4**), because of more protein being made without FAD bound to it (**Figure 2.5c**). *(Performed by HW).*

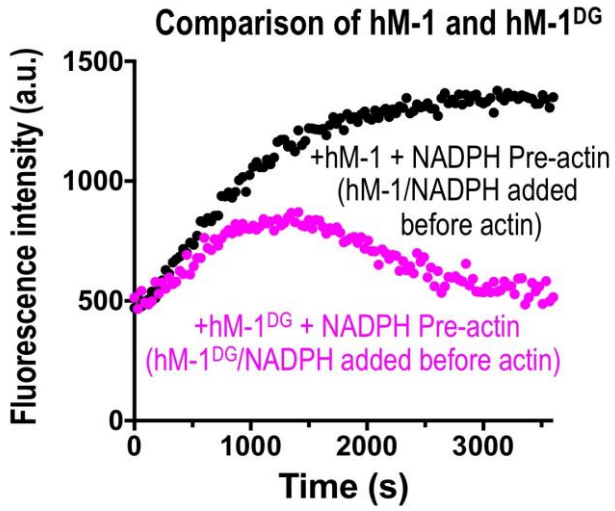

Figure 2.14. Further characterization of human MICAL-1^{DG} (hM-1^{DG}).

Using the method outlined in **Figure 2.10f**, hM-1 or hM-1^{DG} was incubated with NADPH prior to the addition of actin. Then, using a pyrene actin assembly assay as in **Figure 2.6b**, note that MICAL-1 no longer alters actin polymerization when it is incubated with NADPH prior to the addition of actin (black), whereas making the DG alteration (hM-1^{DG}) enables M-1 to alter actin polymerization. [Actin] = 1.15µM, [MICAL-1]=600nM, [NADPH]=100µM. *(Performed by HW).*

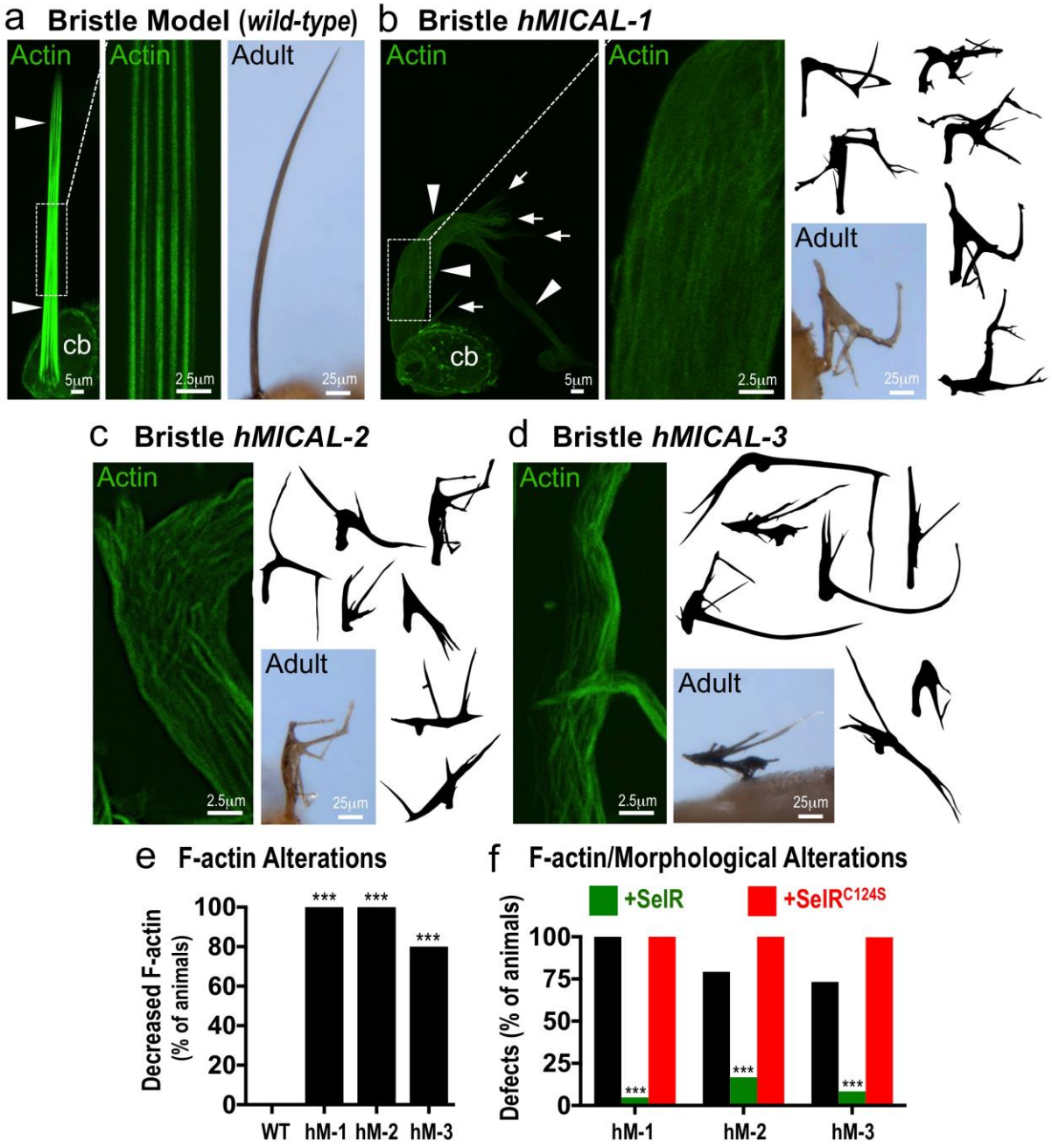

Figure 2.15. Each human MICAL family member generates F-actin disassembly and cellular remodeling in vivo.

(a) Drosophila bristle cells serve as a model for examining actin organization and cellular morphology in vivo. Bristle cells are single cells composed of a cell body (cb) and a long F-actin-rich (green) cellular extension (arrowheads). The F-actin organization (green) in the bristle process can be easily observed throughout pupal development (left and the boxed

region is shown at higher magnification in the middle), while the morphology of the single bristle cell can be observed both during development (left) and in adulthood (right). **(b)** Expression of *hMICAL-1*^{redoxCH} specifically in bristles generates alterations in F-actin organization and cellular morphology. Notice the dramatic alterations to the height, width, and shape of the bristles (arrowheads) including branches (arrows) that can be seen in developing pupae (left) and in the image and drawings of single bristles from adults (right). Notice also that a similar degree of F-actin (green) is present in patches around the periphery of the cell body (cb), but that the extent of F-actin (green) in the bristle process (arrowheads) in much less compared to the wild-type control in **(a)** – such that there is an absence of actin filaments and it is more difficult to discern F-actin/F-actin bundles. Also, note that the F-actin is no longer arrayed in linear projecting bundles (as in a), but in small filaments and bundles of filaments with no apparent organization (left and in the boxed region shown at higher magnification). **(c-d)** Similar dramatic alterations in F-actin organization and bristle morphology as observed with *hMICAL-1*^{redoxCH} **(b)** were also seen when *hMICAL-2*^{redoxCH} **(c)** and *hMICAL-3*^{redoxCH} **(d)** were specifically expressed in bristles. **(e)** Quantification of F-actin alterations following bristle expression of different human MICALs, as judged by animals that had a loss of parallel-arranged F-actin bundles. n = >10 animals/genotype. **(f)** Quantification of F-actin/morphological defects present following bristle expression of different human MICALs, or in combination with SelR or a reductase-dead form of SelR (SelR^{C124S}) (Hung et al. 2013). Note that SelR significantly rescues the F-actin/morphological alterations induced by each of the human MICALs, while SelR^{C124S} does not rescue these defects (and enhances the defects induced by *hMICAL-2*^{redoxCH} and *hMICAL-3*^{redoxCH}*). hM-1 (hMICAL-1*^{redoxCH}*), hM-2 (hMICAL-2*^{redoxCH}*), hM-3 (hMICAL-3*^{redoxCH}*).* Chi-Square Test; ***P <0.0001; n = > 10 animals/genotype. *(Performed by JY).*

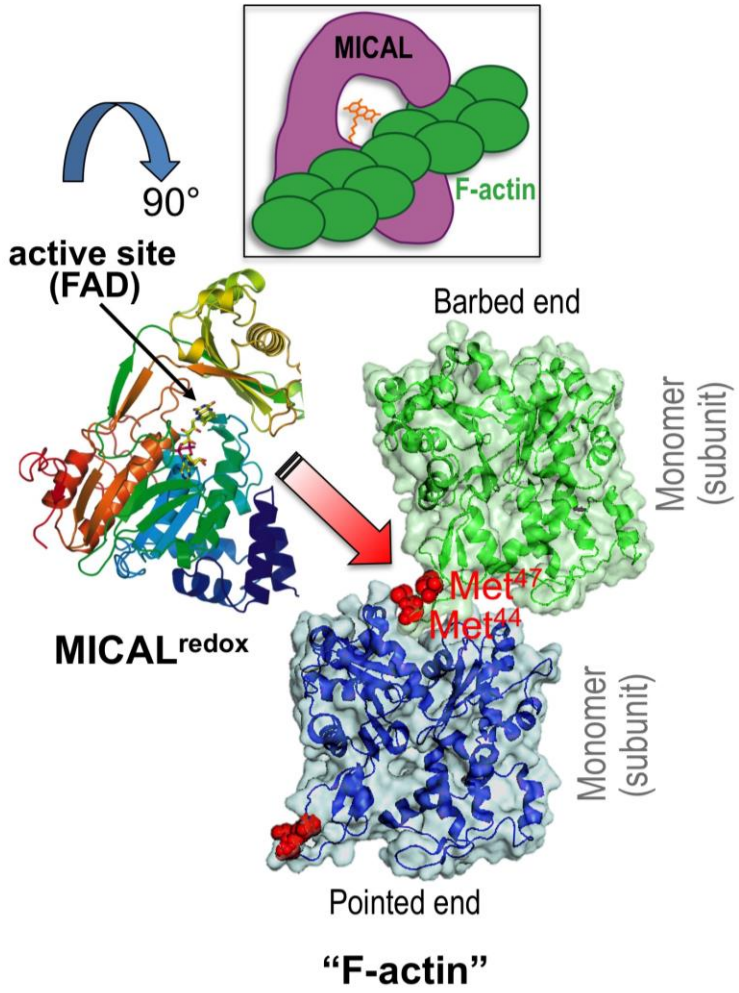

Figure 2.16. Model of the MICALs activation, regulation, and interaction with F-actin – and access to Actin's Met44 and Met47 residues within filaments.

The MICALs dismantle actin filaments by oxidizing actin subunits on their Met44 and Met47 residues. Yet, previous work from others have revealed that when actin is present in filaments, the Met44 and Met47 residues of actin are poorly accessible to diffusible solvents, including oxidants such as hydrogen peroxide (Dalle-Donne et al. 2002; Guan et al. 2003; Guan et al. 2005; Takamoto, Kamal, and Chance 2007). Therefore, these results suggest the hypothesis that MICALs do not modify F-actin through the general release of hydrogen peroxide or another diffusible oxidant. Likewise, direct experiments also support this hypothesis by revealing that hydrogen peroxide has no effects on F-actin disassembly (even when added at high millimolar concentrations), that hydrogen peroxide does not disassemble F-actin in combination with MICALs binding to F-actin, and that hydrogen peroxide scavengers do not alter MICAL-mediated actin disassembly ((Hung et al. 2010; Hung, Pak, and Terman 2011; Hung et al. 2013; Fremont et al. 2017; Hung and Terman 2011; Wilson et al. 2016); present study). Further, the general release of hydrogen peroxide or another

diffusible oxidant would not be expected to modify an amino acid stereospecifically as the MICALs do (which selectively modify actin's Met44 and Met47 residues in a single stereo-specific conformation) – and this modification as well as the MICALs effects on F-actin are selectively reversed by the methionine sulfoxide reductase SelR/MsrB ((Hung et al. 2013; Lee et al. 2013); present study). Moreover, when MICALs are separated from F-actin using a barrier/compartmentalized chamber system, MICALs do not exert effects on F-actin (Hung, Pak, and Terman 2011). Thus, all of these results indicate that the active site of the MICALs needs to gain access to the poorly accessible Met44 and Met47 residues that are buried within F-actin. A model is now emerging based on previous work and the experiments conducted herein that the MICALs are under tight regulation: both precisely localized and maintained in an inactive conformation in the cell (i.e., without O_2 consumption/NADPH activity/effects on F-actin/ hydrogen peroxide production, etc.) so as to not dismantle all F-actin structures (Schmidt, Shim, and Strittmatter 2008; Hung et al. 2010; Giridharan et al. 2012; Vitali et al. 2016; Fremont et al. 2017). MICALs are then locally activated upon binding to other proteins such as the Semaphorin repellent receptor Plexin and small GTPases like Rab35 (Terman et al. 2002; Schmidt, Shim, and Strittmatter 2008; Hung et al. 2010; Giridharan et al. 2012; Vitali et al. 2016; Fremont et al. 2017). Then, when activated, each member of the MICAL family of proteins binds to actin filaments (as illustrated in the inset). This binding to actin filaments then accelerates the enzymatic activity of each MICAL family member, allowing it to consume more NADPH. In conjunction with this activation of the MICAL enzymes, the active site (small arrow) of MICAL accesses (large arrow) the Met44 (Met^{44}) and Met47 (Met^{47}) residues within filaments. Then, the MICALs selectively oxidize both Met44 and Met47 in the *R* stereospecific pattern (generating $actin^{Met44,47\text{–}R\text{–}sulfoxide}$). In turn, because it is thought that hydrophobic interactions are critical for the binding between F-actin subunits (Holmes et al. 1990; Oda et al. 2009; Galkin et al. 2015; von der Ecken et al. 2015), this selective oxidation of (placing a charge on) Met44 and Met47 by the MICALs weakens the hydrophobic interactions between F-actin subunits – since Met44 and Met47 lie at the interface between subunits (see diagram) – and achieves controlled disassembly of filaments (Hung, Pak, and Terman 2011; Grintsevich et al. 2016; Fremont et al. 2017) (see also Ref. 24 for more detail). This disassembly of actin filaments occurs through both severing and depolymerization (Hung et al. 2010; Hung, Pak, and Terman 2011; Hung et al. 2013; Fremont et al. 2017; Grintsevich et al. 2017). PDB IDs are 2BRY, 2ZWH (Siebold et al. 2005; Nadella et al. 2005).

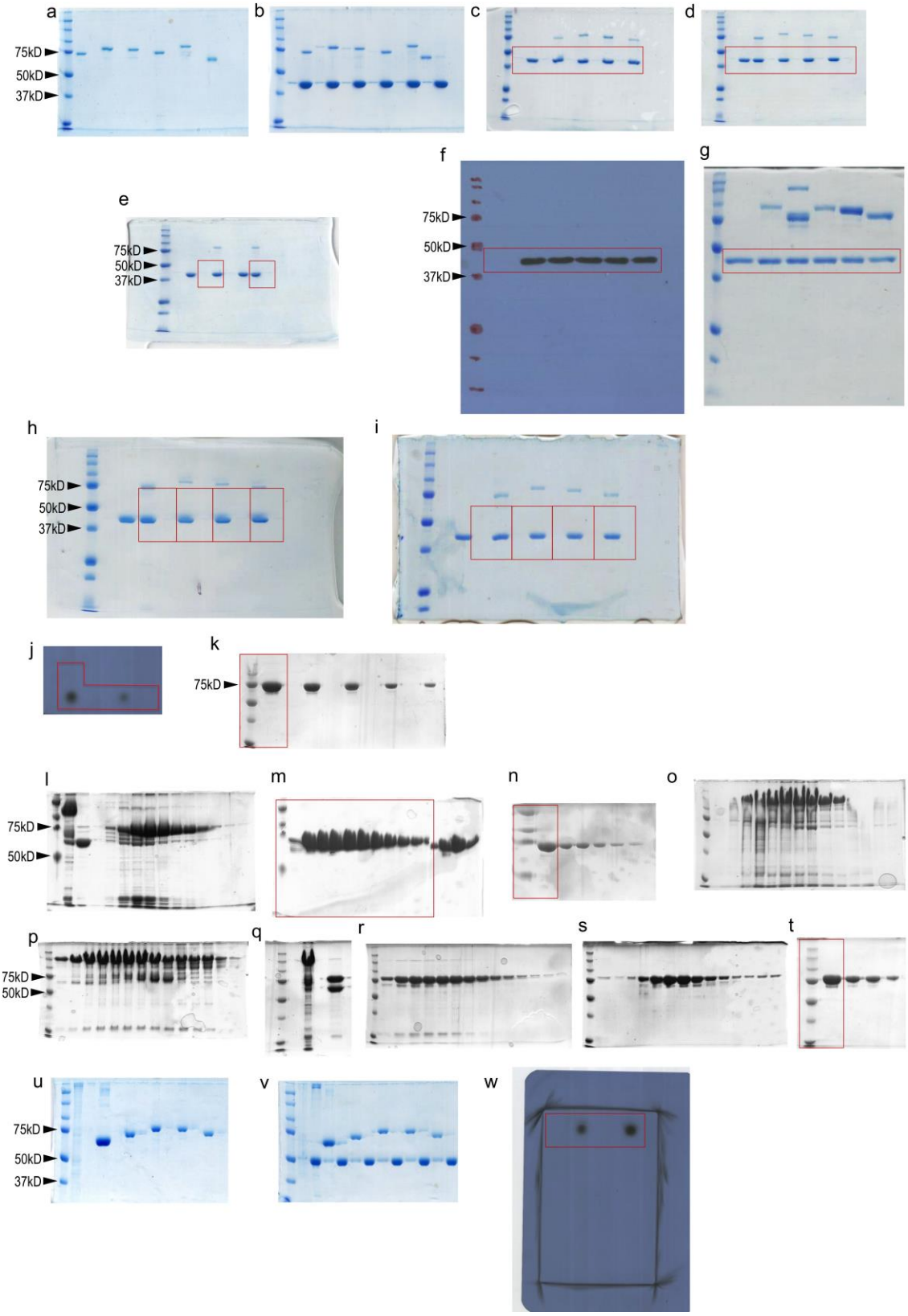
a
75kD
50kD
37kD
b
c
d
e
75kD
50kD
37kD
f
75kD
50kD
37kD
g
h
75kD
50kD
37kD
i
j
k
75kD
l
75kD
50kD
m
n
o
p
75kD
50kD
q
r
s
t
u
75kD
50kD
37kD
v
w

Figure 2.17. Uncropped Gels/Blots.

Uncropped gels/blots for Figures 2.6a Left (a), 2.6a Right (b), 2.6c Upper left (c, red box), 2.6c Lower Left (d, red box), 2.6c Upper Right and Lower Right (e, left and right red boxes, respectively), 2.9b Upper (f, red box), 2.9b Lower (g, red box), 2.9c WT actin (h, red boxes), 2.9c M2L actin (i, red boxes), 2.10b (j, red box), 2.2e (k, red box), 2.3c (l), 2.3d (m, red box), 2.3e (n, red box), 2.4a (o), 2.4b (p), 2.4c (q), 2.4d (r), 2.4e (s), 2.4f (t, red box), 2.7a Left (u), 2.7a Right (v), and 2.11b (w, red box). All other gels in Figures show the full uncropped gels.

Materials and Methods

Molecular Biology and Protein Purification

For all protein expression, plasmids were transformed into ArcticExpress bacterial competent cells (Stratagene, La Jolla, CA, USA) using general approaches (Wu, Hung, and Terman 2016). For a given plasmid, a single clone was then inoculated into a 150 ml TB culture medium (including 100 μg/ml ampicillin, 2 mM $MgSO_4$, and 20 μg/ml gentamycin) and shaken at 37°C overnight. 25 ml of overnight culture was then transferred to six 2.8 L flasks containing 1 L TB media (with 100 μg/ml ampicillin and 2 ml of Antifoam B emulsion [Sigma, A6707-500ml]). Flasks were then cultured at 30°C for ~8 hrs with shaking at 215rpm. After ~8 hrs, the temperature of the incubator was changed to 10°C and Isopropyl-β-D-thiogalactoside (IPTG) was added to each of the cultures to a final concentration of 0.5 mM, and each of the cultures were then shaken for 24 hrs. The bacteria was then collected by centrifugation at 2623 x g for 30 min and bacterial pellets were fast frozen in liquid nitrogen and stored at -80°C until use. The frozen bacterial pellets were thawed at RT and 100 ml of Lysis buffer (50 mM Tris-HCl, 500 mM NaCl, 3 mM β-mercaptoethanol, 20 mM imidazole, 1 tablet of Roche Complete® EDTA-free Protease Inhibitors Cocktail) was added to the combined pellets for a given construct and stirred until the pellet was completely dissolved. The dissolved sample was then loaded into a high-pressure homogenizer (EmulsiFlex-C5, Avestin, Inc., Ottawa, Ontario, Canada) pre-cooled for 1 hr using a refrigerated circulating bath set at 4°C, and the bacteria were broken by increasing the pressure to 40 psi. In all cases, the output pressure was within 5,000-10,000 psi and the temperature of the sample was controlled by either immersion of the machine/tubing in ice or cooling and applying water

using a re-circulating water bath. Initially, the cells were swirled during lysis to prevent cells from getting stuck in the machine and the lysis step was repeated two to three times (up to five times). As an alternative, the bacteria were lysed using a Misonix Ultrasonic Liquid Processor or similar and sonicating for 15 min at 50 amplitude, 5s on and 5s off. The bacterial sample in lysis buffer was then centrifuged at 22,000 x *g* for 2 hrs. The supernatant was transferred to a new tube and centrifuged for another 30 min at the same speed. The supernatant was then filtered with a 0.45 μm filter.

To construct human (h) MICAL-1^{redoxCH}, a portion of the human MICAL-1 cDNA coding for the redox and CH domains was PCR amplified using primers containing a 5' SalI restriction enzyme site (Forward: 5'– AGCTGTCGACggtacctctagcatggcttcacctacctccac –3') and a 3' XhoI restriction enzyme site (Reverse: 5' – AGCTctcgagtctagacttgaaggcactgt –3') and after digestion of the appropriately sized PCR product with SalI and XhoI, the fragment was inserted into the SalI and XhoI sites of the previously generated pET43.1bNG vector (Gupta, Wu, and Terman 2016). Positive clones were confirmed by digestion with SalI/XhoI and DNA sequencing. Following bacterial inoculation and preparation of the protein sample from bacteria as described above, the hMICAL-1^{redoxCH} protein was purified (see also **Figure 2.2**). In particular, a 5 ml HisTrapFF1-GE affinity column was equilibrated with Buffer Ni-A (10 mM Tris-HCl, pH8.0, 500 mM NaCl, 5% glycerol, 3 mM β-mercaptoethanol, 20 mM imidazole) and then the sample containing the hMICAL-1^{redoxCH} protein was loaded onto the column. After washing the column with >20 column volumes (CV) of Buffer Ni-A, the sample was eluted from the column using elution buffer Ni-B (10 mM Tris-HCl, pH8.0, 500 mM NaCl, 5% glycerol, 3 mM β-mercaptoethanol, 250 mM imidazole) and collected in 1 ml

aliquots. The presence of the MICAL-1^{redoxCH} protein was then examined by SDS-PAGE and tubes enriched with the hMICAL-1^{redoxCH} protein were retained and combined. The pooled protein sample was then prepared for thrombin digestion to remove the Nus solubility tag by first desalting and exchanging the buffer using a HiPrep 26/10 column (GE Healthcare Bio-Sciences Corporation, Piscataway, NJ, USA). After desalting and eluting with Desalting buffer (10 mM Tris-HCl, pH8.0, 50 mM NaCl, 5% glycerol, 1 mM DTT), the eluate was incubated with 100 µl of 10 µg/µl of the thrombin protease overnight in the cold room. After thrombin digestion, a 1ml HisTrapFF1-GE affinity column was used to remove the Nus tag using Buffer Ni-A and elution Buffer Ni-B as described above. After another desalting step in which the sample was desalted and eluted with Buffer S-A (20 mM $NaPO_4$, pH7.5, 10 mM NaCl, 5% glycerol, 1 mM DTT), the samples containing the MICAL-1^{redoxCH} protein were loaded into a MonoS column (Uno S6 column [Bio-Rad] or Mono S 5/50 GL Column [GE Healthcare]), washed with Buffer S-A (20 mM $NaPO_4$, pH7.5, 10 mM NaCl, 5% glycerol, 1 mM DTT) and eluted in 1 ml aliquots with Buffer S-B (20 mM $NaPO_4$, pH7.5, 1 M NaCl, 5% glycerol, 1 mM DTT). 10 µl from each aliquot/collection tube was then electrophoresed on an SDS-PAGE gel and those corresponding tubes containing hMICAL-1^{redoxCH} protein were combined together. Millipore Amicon Ultra centrifugal filter (Ultracel-50 kDa cutoff) was then used to reduce the volume to around 500 µl and to change the buffer to storage buffer (10 mM Tris pH8.0, 100 mM NaCl, 5% glycerol, 1 mM DTT). The protein sample was then aliquoted and fast frozen with liquid nitrogen and stored in a -80°C freezer.

To construct human MICAL-2^{redoxCH}, a portion of the human MICAL-2 cDNA encoding for the redox and CH domains was PCR amplified using primers containing a 5’ SalI restriction

enzyme site (Forward: 5'-AGCTGTCGACggtacctctagcatgggggaaaacgaggatgaga -3') and a 3' AvrII restriction enzyme site (Reverse: 5'-AGCTCCTAGGTTAGTGGTGGTGGTGGTGGTGctcgagtctagaccggaagagctcgtagaact -3') and after digestion of the appropriately sized PCR product with SalI and AvrII, the fragment was inserted into the SalI and AvrII sites of the previously generated pET43.1bNG vector as described above. Positive clones were confirmed by digestion with SalI/AvrII and DNA sequencing. Following bacterial inoculation and preparation of the protein sample from bacteria as described above, hMICAL-2^{redoxCH} protein was purified (see also **Figure 2.3**). In particular, transformation, induction, pelleting, lysis, Ni^{2+}-NTA affinity chromatography, desalting, and thrombin digestion were carried out as described for purification of hMICAL-1^{redoxCH}. The protein sample was then loaded a second time onto a 5 ml HisTrapFF1-GE affinity column and washed with Buffer Ni-A and eluted with Buffer Ni-B. The protein sample was then desalted as described for hMICAL-1^{redoxCH} and eluted with Buffer S-A, loaded onto a MonoS column, washed with Buffer S-A, and eluted with Buffer S-B. Collected samples were then processed as described for hMICAL-1^{redoxCH} and stored in a -80°C freezer.

To construct human MICAL-3^{redoxCH}, a portion of the human MICAL-3 cDNA encoding for the redox and CH domains was PCR amplified using primers containing a 5' SalI restriction enzyme site (Forward: 5'-AGCTGTCGACGGTACCTCTAGCATGGAGGAGAGGAAGCATGAG -3') and a 3' XhoI restriction enzyme site (Reverse: 5'-AGCTctcgagTCTAGACTTAAACATCTCGTAGAACTG A -3') and after digestion of the

appropriately sized PCR product with SalI and XhoI, the fragment was inserted into the SalI and XhoI sites of the previously generated pET43.1bNG vector as described above. Positive clones were confirmed by digestion with SalI/XhoI and DNA sequencing. Following bacterial inoculation and preparation of the protein sample from bacteria as described above, hMICAL-3^{redoxCH} protein was purified (see also **Figure 2.4**). In particular, to purify hMICAL-3^{redoxCH} protein, Ni^{2+}-NTA chromatography was performed as described above using a 5 ml HisTrapFF1-GE affinity column with Buffer Ni-A and Buffer Ni-B. The samples containing hMICAL-3^{redoxCH} protein was then desalted as described above using Desalting Buffer, loaded onto a MonoQ column (Mono Q 5/50GL, GE Healthcare), washed with Buffer Q-A (10 mM Tris-HCl, pH8.0, 10 mM NaCl, 5% glycerol, 1 mM DTT), and eluted with Buffer Q-B (10 mM Tris-HCl, pH8.0, 1 M NaCl, 5% glycerol, 1 mM DTT). As described above for hMICAL-2^{redoxCH} protein, the sample was then subjected to thrombin digestion, loading onto a 5 ml HisTrapFF1-GE affinity column, and desalting and purification using a MonoS column. Collected samples were then processed as described for hMICAL-1^{redoxCH} and hMICAL-2^{redoxCH} and stored in a -80°C freezer.

To construct the human MICAL-1^{redoxCH} D for A substitution (hMICAL-1^{DG}), a portion of human MICAL-1^{redoxCH} was PCR amplified using primers containing a 5' SalI restriction enzyme site (Forward: 5'-AGCTGTCGACGGTACCTCTAGCATGGCTTCACCTACCTCCAC -3') and a 3' AatII restriction enzyme site (Reverse: 5'-tgaatttgacgtccttatctcggctgATggaggtaaattcgtccctgaaggcttc -3') and inserted into the TopoTA vector (Invitrogen) using the manufacturers recommended protocol. The resulting vector/insert was then cut with the restriction enzymes AatII and

SpeI. Then, another portion of human MICAL-1^{redoxCH} was PCR amplified using a 5' primer containing an Aat II restriction enzyme site and a mutation of the AG residue of the DG motif to a DG residue (Forward Primer: 5' – tgaatttgacgtccttatctcggctgATggaggtaaattcgtccctgaaggcttc – 3') and a 3' primer containing both XhoI and Spe I restriction enzyme sites (Reverse Primer: 5'-AGCTACTAGTctcgagtctagacttgaaggcactgt -3'). The resulting PCR product was then digested with AatII and SpeI and inserted into the corresponding digested sites in the previously generated TOPO vector/insert. This newly generated MICAL-1^{redoxCH} DG cDNA was then cut out of the TopoTA vector with SalI and XhoI and inserted into the SalI and XhoI sites of the previously generated pET43.1bNG vector as described above. Positive clones were confirmed by digestion with SalI/XhoI and DNA sequencing. Following bacterial inoculation and preparation of the protein sample from bacteria as described above, MICAL-1^{redoxCH} DG protein was purified (see also **Figure 2.13**). In particular, to purify MICAL-1^{redoxCH} DG protein, identical approaches were followed to that described for hMICAL-1^{redoxCH} protein, except an anion ion exchange chromatography was used for the final purification step including a MonoQ column (Mono Q 5/50GL, GE Healthcare), Q-A buffer, and Q-B buffer to elute the sample. Collected samples were then processed as described for hMICAL-1^{redoxCH}, hMICAL-2^{redoxCH,} and hMICAL-3^{redoxCH} and stored in a -80°C freezer.

UV-visible Spectroscopy and Related Analyses

Either a NanoDrop spectrophotometer (Thermo Scientific, Wilmington, DE, USA) or fluorescence spectrophotometer (Spectra Max M2; Molecular Devices, Sunnyvale, CA, USA) was used for all assays and scanning wavelengths between 250 nm and 700 nm were used. To determine whether the flavin was bound covalently or non-covalently and whether FMN or FAD was bound, analyses of each of the MICAL proteins was done using standard approaches and heat-induced denaturation (Aliverti, Curti, and Vanoni 1999; Wu, Hung, and Terman 2016). In brief, 2 µl of purified dMical^{redoxCH}, hMICAL-1, 2 and 3^{redoxCH} and hMICAL-1 DG proteins were used for obtaining an absorbance spectrum with a NanoDrop spectrophotometer. 100 µl of purified MICAL proteins was used to monitor absorption spectra using a fluorescence spectrophotometer. 200 µl of 10 mM HEPES/NaOH, 50 mM NaCl buffer, pH7.5 was added into each tube to dilute samples. The 5 tubes with samples were incubated for 10 min at 100^{o}C. After being cooled on ice, microfuge tubes are centrifuged at 4^{o}C for 10 min at 13,000 rpm (14,500g). The supernatant was recovered and the absorbance spectrum was then recorded. The original data were then exported into Excel software (Microsoft Corp., Redmond, WA, USA) and presented using GraphPad software (La Jolla, CA, USA), to compare the difference between purified and denatured proteins.

Calculation of the percentage of FAD bound to purified MICAL proteins (i.e., the stoichiometry of FAD to MICAL proteins) was done using standard approaches (Macheroux 1999; Leferink, van den Berg, and van Berkel 2008; Wu, Hung, and Terman 2016) such that the concentration of each of the purified MICAL^{redoxCH} proteins was determined as described above by adding 2 µl to the platform of a NanoDrop spectrophotometer and measuring the

absorption at 280 nm. The concentration of FAD in the purified sample was then determined using standard approaches (Aliverti, Curti, and Vanoni 1999; Wu, Hung, and Terman 2016), by denaturing the MICAL^{redoxCH} proteins with 0.2% SDS, pelleting the denatured MICAL^{redoxCH} proteins, measuring the absorbance of the free FAD in the sample, and then using the Beer-Lambert law (Absorption at 459 nm = ε [extinction coefficient, also known as molar absorptivity] x C [concentration in M] x l [path length in cm of the cuvette in which the sample is contained]) to calculate the concentration of FAD. The concentration of FAD in the purified sample was then divided by the concentration of the MICAL^{redoxCH} proteins in the purified sample to determine the percentage (stoichiometry) of FAD bound to the purified MICAL proteins.

NADPH and NADH Consumption

NADPH and NADH (the reduced form of the coenzymes) absorb light at 340 nm, while the oxidized forms ($NADP^+$ and NAD+) do not. This difference between the oxidized and reduced forms of the coenzymes makes it straightforward to measure the conversion of one to another in enzyme assays. Thus, the enzymatic activity of Mical was monitored by the rate of NADPH or NADH oxidation, which is measured by the rate of decreasing light absorbance at 340 nm (extinction coefficient 340 = 6.2 $mM^{-1}*cm^{-1}$). 600 nM of the different MICALs to 100 μM NADPH in General Actin Buffer was used. In the absence of F-actin (**Figure 2.1g-h**), NADPH and NADH consumption was monitored and reported as described (Wu, Hung, and Terman 2016). In the presence of F-actin (**Figure 2.9a, 2.12d**), NADPH consumption was monitored and reported as described (Hung, Pak, and Terman 2011;

Grintsevich et al. 2016). In particular, the basal NADPH consumption was measured in the presence of different concentrations of F-actin for the first 3 min before adding the MICALs. The MICAL enzymatic activity was determined by subtracting the NADPH consumption after addition of the MICAL^{redoxCH} from basal NADPH consumption. The rate of NADPH consumption was determined by 10 sec intervals at the maximum rate.

MICALs and F-actin Co-sedimentation Assays

Standard approaches in multiple independent experiments ($n \geq 3$) were used for high-speed sedimentation/co-sedimentation assays ((Yin and Stossel 1979; Hung et al. 2010; Grintsevich et al. 2016; Hung, Pak, and Terman 2011); Cytoskeleton, Inc). In brief, purified non-muscle actin (85% β-actin, 15% γ-actin; Cytoskeleton, Inc.) was resuspended to 1 mg/ml in a general actin resuspension buffer (5 mM Tris-HCl pH8.0, 0.2 mM $CaCl_2$). The resuspended actin was then added to a standard actin polymerization buffer (50 mM KCl, 2 mM $MgCl_2$, and 1 mM ATP) and allowed to polymerize for 1 hour at room temperature. This generated an F-actin stock at 23μM actin. dMical^{redoxCH} protein, hMICAL^{redoxCH}-1, hMICAL^{redoxCH}-2, hMICAL^{redoxCH}-3, hMICAL^{redoxCH}-1 DG protein, or a negative control (bovine serum albumin (BSA), Cytoskeleton, Inc) were subjected to initial (clarification) high-speed centrifugation at 150,000 x g for 1 hour at 4^{o}C. Test proteins (at a final concentration of 2μM) were then added to separate tubes and incubated with either F-actin (at a final concentration of 18.4μM) or with F-actin buffer only for 30 min at room temperature. An F-actin only tube was also incubated for 30 minutes at room temperature. All test tubes were then subjected to high-speed centrifugation at 150,000 x g for 1.5 hours at

24^{o}C. Supernatants were carefully removed and added to sample buffer for loading on an SDS-PAGE gel. The pellet was resuspended in Milli-Q H_2O with pipetting, incubation on ice for 10 min, and then more pipetting before being added to sample buffer for loading on an SDS-PAGE gel. The gel was then stained with Coomassie blue using standard approaches. The intensity of each of the stained bands in the pellet and soluble fraction was then analyzed and quantified by densitometry using Image J (NIH) and the percentage of different purified proteins with F-actin in the pelleted fraction was presented. Similar approaches and as described previously for Drosophila Mical^{redoxCH} were also used for mutant actins (Hung, Pak, and Terman 2011).

Microtubule Co-sedimentation and Polymerization Assays

Tubulin was obtained from Cytoskeleton, Inc and standard approaches were used for the microtubule co-sedimentation assays ((Al-Bassam et al. 2007; Gustke et al. 1994); Cytoskeleton, Inc) and as we have previously employed for Drosophila Mical^{redoxCH} (Hung et al. 2010). In brief, microtubules were generated by polymerizing tubulin (from a 5 mg/ml tubulin stock containing 1 mM GTP; Cytoskeleton, Inc) at 35°C for 20 min in a polymerization buffer (80 mM PIPES pH 6.9, 0.5 mM EGTA, 2 mM $MgCl_2$, 7.5% glycerol). Microtubules was then diluted 10 fold in a warm buffer (35°C) containing 80mM PIPES pH 6.9, 0.5mM EGTA, 2mM $MgCl_2$, and 20µM taxol. Test proteins including hMICAL^{RredoxCH}-1, hMICAL^{redoxCH}-2, hMICAL^{redoxCH}-3, hMICAL^{redoxCH}-1 DG protein (1µM final concentration), a negative control (bovine serum albumin (BSA) [2.2µM final concentration, Cytoskeleton, Inc.]), and a positive control (microtubule associated proteins MAPs [0.64µM

final concentration; Cytoskeleton, Inc.]) were added to separate tubes and incubated with either microtubules or buffer for 30 min at room temperature. A microtubule only tube was also incubated for 30 min at room temperature. Each reaction was then subjected to high-speed centrifugation at 100,000 x g for 40 min at 24°C as described by Cytoskeleton, Inc. Supernatants were then carefully removed and added to sample buffer for loading on an SDS-PAGE gel. The pellet was resuspended in Milli-Q H_2O with pipetting before being added to sample buffer for loading on an SDS-PAGE gel. The distribution of microtubule and test proteins were visualized with Coomassie blue staining and the intensity of each of the stained bands in the pellet and soluble fraction was quantified by densitometry using Image J (NIH) and the percentage of different purified proteins with microtubules in the pelleted fraction was presented as we have previously described (Hung et al. 2010). Likewise, the effects of the hMICAL^{redoxCH} proteins on microtubule polymerization were measured using fluorescence-based standard approaches ((Bonne et al. 1985); Cytoskeleton, Inc) and as we have previously employed for Drosophila Mical^{redoxCH} (Hung et al. 2010). In brief, tubulin (bovine tubulin; Cytoskeleton, Inc.) polymerization was performed in a microtubule polymerization buffer (80 mM PIPES pH6.9, 2 mM $MgCl_2$, 0.5 mM EGTA, 15% glycerol, 1 mM GTP and 5µM fluorescent reporter (DAPI)) containing mixed tubulin (2 mg/ml final concentration), dMical^{redoxCH} protein, hMICAL^{redoxCH}-1, hMICAL^{redoxCH}-2, hMICAL^{redoxCH}-3, hMICAL^{redoxCH}-1 DG protein (0.6µM final concentration) and/or NADPH (100µM). The polymerization was initiated by raising the temperature from 4°C to 37°C. Fluorescence intensity was monitored for 1 hour at 450 nm with excitation at 360 nm by a

fluorescence spectrophotometer (Spectra max M2; Molecular Devices) with temperature control.

Actin Polymerization and Depolymerization Assays

Pyrene-actin polymerization assays were performed using standard approaches (Cooper 1992) (Cytoskeleton, Inc.) and as we have previously employed for Drosophila Mical^{redoxCH} (Hung et al. 2010; Hung, Pak, and Terman 2011; Wu, Hung, and Terman 2016; Grintsevich et al. 2016; Yoon, Hung, and Terman 2017). In brief, purified rabbit skeletal muscle actin (pyrene-labeled; Cytoskeleton, Inc) was used to monitor actin polymerization since the fluorescence intensity of the pyrene-labeled polymer is substantially higher than the pyrene-labeled monomer. G-actin (monomeric actin) was resuspended to 9.2µM in a G-actin buffer (5 mM Tris-HCl pH8.0, 0.2 mM $CaCl_2$, 0.2 mM ATP and 1 mM DTT) and incubated on ice for 1 hour. Before all the experiments, G-actin solution was centrifuged for 1 hour at 100,000 x g at 4^{o}C to remove residual actin nucleating centers. Multiple independent experiments ($n \geq 3$ by two independent researchers) were performed for each condition such that MICAL proteins, NADPH (MP Biomedicals), and/or NADH (MP Biomedicals) were then added to the actin in a 96 well plate and polymerization was initiated (Time=0) at 25^{o}C by the addition of 5 mM Tris-HCl pH 7.5, 50 mM KCl, 2 mM $MgCl_2$, 1 mM EGTA, 0.5 mM DTT, and 0.2 mM ATP (to the 96 well plate with 2-5 seconds gentle shaking using the shaking feature of the fluorescence spectrophotometer). Actin was used at a final concentration of 1.1µM. Fluorescence intensity was immediately monitored at 407 nm with

excitation at 365 nm by a fluorescence spectrophotometer (Spectra max M2; Molecular Devices).

To examine the ability of MICALs to induce depolymerization in conditions that favored polymerization (see also (Hung et al. 2010)), multiple independent experiments ($n \geq 3$ by two independent researchers) were performed similar to described previously for both pyrene-actin and non-pyrene wild-type and Actin M4447L sedimentation assays (Hung et al. 2010; Hung, Pak, and Terman 2011; Grintsevich et al. 2016; Yoon, Hung, and Terman 2017). MICAL proteins and/or NADPH were then added to the polymerized actin as described for the polymerization assays (Time=0) and depolymerization was immediately monitored by fluorescence intensity or via sedimentation as described above. In some cases, as described in the results/figures, MICAL proteins and NADPH were added together before adding them to the F-actin (pre-actin incubation) and in some cases, MICAL proteins were added to F-actin in which NADPH had already been added (post-actin incubation). In some cases, as described in the results/figures, additional NADPH was added to the F-actin/MICAL mix at a later time. Note also that these experiments were done using standard approaches and that the F-actin was not stabilized (i.e., by adding a stabilizing protein).

Analysis of MICAL-oxidized actin

Actin was polymerized to generate F-actin and 600 nM of each of the human MICALs and 200-300 µM of NADPH were added to 1.15µM F-actin at room temperature for 2 hours. The MICAL/NADPH/F-actin reaction was then stopped by adding loading buffer containing β-mercaptoethanol and boiling samples for 5 min. All samples were then

loaded into a 12% SDS-PAGE gel, transferred to PVDF membrane, blocked with 5% non-fat milk/TBST buffer for 1 hour and then incubated for 1 hour with a 1:500 dilution of the actin MetO44 antibody (Grintsevich et al. 2016).

SelR-treatment of MICAL-oxidized Actin

Purified pyrene-labeled rabbit skeletal muscle actin (Cytoskeleton, Inc.) was resuspended in G-actin buffer to 2.3µM. The resuspended actin was then polymerized with 2X polymerization buffer (1.15µM actin=final concentration) in the presence of human MICAL-1^{redoxCH}, human MICAL-2^{redoxCH}, human MICAL-3^{redoxCH}, or human MICAL-1^{redoxCH} DG and 100µM NADPH for 1 hour. The NADPH was then removed from the human MICAL-treated actin as described previously (Hung, Pak, and Terman 2011; Hung et al. 2013) (using a centrifugal filter [Amicon Ultra, Ultracel-10K, Millipore]). The human MICAL-treated actin was then either treated with SelR or the buffer the SelR was stored in (containing the 10 mM $MgCl_2$ and 20 mM DTT) for 1 hour at 37°C.

Hydrogen Peroxide Production

In one method, we used the substrate luminol and the generation of a chemiluminescence signal that we visualized on either X-ray film or a phosphoimager. In particular, luminol, when it becomes oxidized by peroxide (peroxide can be formed through a reaction of H_2O_2 with horseradish peroxidase [HRP]), results in creation of an excited state product, which then decays to a lower energy state by releasing photons of light (Heindl and Josel 2000). Therefore, to perform this reaction and to test for the ability of the different

MICALs to form H_2O_2, we added a substrate (luminal [i.e., ECL substrate]), a catalyst (HRP), and the MICALs in the presence of NADPH (which will provide H_2O_2 if they generate it). To do this, we incubated 0.6 µM of each MICAL in the presence of 200µM NADPH, HRP (the catalyst), and luminol, and then visualized the product of the reaction using either X-ray film or a phosphoimager.

As another (different) means to detect H_2O_2, we used the ROS-Glo H_2O_2 Assay Kit developed by Promega (Catalog No: G8820; (Duellman et al. 2013)), and followed the manufacturers recommended instructions. In particular, in the ROS-Glo H_2O_2 Assay Kit, a derivatized luciferin substrate is incubated with a potential H_2O_2 generating sample, and then the derivatized luciferin substrate reacts directly with H_2O_2 to generate a luciferin precursor. Addition of the ROS-Glo detection solution converts the precursor to luciferin and triggers the luciferase to produce a light signal that is proportional to the level of H_2O_2 present in the sample. Thus, the ROS-Glo H_2O_2 substrate reacts directly with H_2O_2, eliminating the need for HRP as a coupling enzyme (and thus eliminating any false detection of H_2O_2 associated with any unknown activation or inhibition of HRP by the MICALs). In particular, 60 pmol of each of the Drosophila and human MICAL^{redoxCH} proteins was diluted by General Actin Buffer to a final volume of 79 µl and transferred into a 96-well plate (Corning). 25 µM of H_2O_2 was used as the standard. Following the manufacturer's recommended protocol, the H_2O_2 substrate dilution buffer (SDB) was thawed and placed on ice. The SDB was then mixed with the manufacturer-provided H_2O_2 substrate (the derivatized luciferin substrate) just prior to use (generating the SDB-S). 20 µl of SDB-S was added into each well containing the MICALs or the H_2O_2 standard to generate a final volume of 100 µl. A control SDB-S

only well was also used. At time 0 min (reaction time: 10 min), 5 min (reaction time: 5 min), 8 min (reaction time: 2 min), 1 µl of 10mM NADPH (final concentration: 100 µM) was added into each well. 100 µl of ROS-Glo detection solution (+1 µl D-Cys and 1 µl enhancer solution/100 µl Detection solution) was added to each well. After the 96-well plate was incubated for 5 min at room temperature, the relative luminescence unit was recorded by using a plate-reading luminometer (TriStar² LB 942 Multidetection Microplate Reader, Berthold Technologies, Germany). The H_2O_2 concentration was calculated by the luminescence value of the samples, zero control and the standard sample (25 µM H_2O_2).

It should also be noted that the Amplex Red Hydrogen Peroxide/Peroxidase Assay Kit (Invitrogen) has been used in the past to determine the amount of H_2O_2 generated by MICAL-1 (Nadella et al. 2005; Schmidt, Shim, and Strittmatter 2008). We and others have determined that this Amplex Red reagent is artifactually fast and an inaccurate measure of MICAL-mediated H_2O_2 production (Zucchini et al. 2011; McDonald, Liu, and Palfey 2013). It should be noted, however, that we did see similar relative amounts of "H_2O_2" generated with this reagent (i.e., MICAL-1 generated the most reaction product and MICAL-2 generated the least) when we used this reagent to compare each of the MICALs (data not shown).

Oxygen Consumption

The electrode was prepared by adding 50% saturated KCl solution as electrolyte in the electrode well. The well was then covered with a paper spacer to provide a continuous electrolyte layer on the electrode and with an oxygen-permeable membrane on top of the

paper spacer to separate the electrolyte from the sample. Then a glass reaction vessel was placed on top of the electrode chamber and closed with a gas-tight plunger to provide an almost sealed space for the sample with a small opening on top to inject reagents. Lastly, the electrode was calibrated using dissolved oxygen in water (which provided a basal line as a sample) and then establishing a zero content of oxygen by adding an oxygen reducing agent to the water. The basal oxygen consumption was then determined by adding 200 μM of NADPH and 600 nM of each MICAL into F-actin buffer (no F-actin) (1:1 G-Buffer+2X Polymerization Buffer) in the chamber and measuring the change in the amount of oxygen dissolved in the buffer via the oxygen electrode.

Drosophila Transgenic Fly Lines

To generate hMICAL-1^{redoxCH} pUAST, the following primers were used: EcoRI-For: 5'- AGCT GAATTC atg gct tca cct acc tcc ac -3' and NotI-Rev: 5'- AGCT GCGGCCGC TTA GTG GTG GTG GTG GTG GTG ctc gag tct aga ctt gaa ggc act gtg gaa gtg -3'. Both PCR product and the pUAST vector were digested with EcoRI and NotI and the purified DNA fragments were ligated and sequenced on both strands. To generate hMICAL-2^{redoxCH} pUAST, the following primers were used: NotI- For: 5'-AGCT GCGGCCGC atg ggg gaa aac gag gat gag a -3' and NheI- Rev: 5'-AGCT gctagc TTA GTG GTG GTG GTG GTG GTG ctc gag tct aga ccg gaa gag ctc gta gaa ct -3'. Both PCR product and the pUAST vector were digested with NotI and NheI (pUAST digested with XbaI) and the purified DNA fragments were ligated. To generate hMICAL-3^{redoxCH} pUAST, the following primers were used: NotI-pUAST-For: 5'-AGCT gcggccgc atg gag gag agg aag cat ga -3' and KpnI- Rev:

5’-AGCT ggtacc TTA GTG GTG GTG GTG GTG GTG ctc gag tct aga ctt aaa cat ctc gta gaa ctg a -3’. Both PCR product and the pUAST vector were digested with NotI and KpnI and the purified DNA fragments were ligated.

In Vivo F-actin and Cellular Assays

Multiple different transgenic fly lines for each of the MICALs were generated (n>5) and transgenic fly lines of the same genotypes showed similar defects when expressed with the bristle-specific B11-GAL4 driver. Analysis of the effects on F-actin and cellular remodeling was done in vivo using the Drosophila bristle process as previously described (Hung et al. 2010; Hung et al. 2013; Grintsevich et al. 2016; Yoon et al. 2017). To visualize F-actin, Drosophila pupae were placed on double-sided tape and the dorsal surface of the pupal case was removed, allowing the pupae to be lifted from their case and immediately placed in depression-well slides and imaged. One copy of *UAS:*^{GFP}*actin* was used to visualize F-actin and imaging was done using a Zeiss LSM510 confocal microscope. Examination of bristle cell remodeling was performed on young, recently emerged adult offspring. The images and drawings of the adult bristles were done with the aid of a Zeiss Discovery M^2 Bio stereomicroscope, a motorized focus and zoom, and three-dimensional reconstruction software (Extended Focus Software; a kind gift from Bernard Lee).

Statistics and Reproducibility

For each representative protein purification, image, gel, immunoblot, graph, or in vivo experiment, the experiments were repeated at least two separate independent times and

there were no limitations in repeatability. At least two independent protein purifications and multiple independent actin biochemical experiments were performed with similar results including reproducing the effects independently from different researchers. No statistical method was used to predetermine the sample size, which was based on what is published in the field. Differences between experimental and control animal conditions were large, with little variability and so the sample size was larger than needed to ensure adequate power to detect an effect. Animal studies were based on pre-established criteria to compare against age-matched animals. Animal experiments were not randomized. Animals of the correct genotype were determined and those collected of that genotype were included as data. For genetic experiments, in which the genotype needed to be determined on the basis of different Drosophila genetic/chromosome markers, blinding was not employed. The figure legends list the sample size for each experiment. To the best of our knowledge the statistical tests are justified as appropriate.

CHAPTER THREE

F-ACTIN DISMANTLING THROUGH A REDOX-DRIVEN SYNERGY BETWEEN MICAL AND COFILIN

This work was previously published: Grintsevich, E. E.*****, **H. G. Yesilyurt***, S. K. Rich, R. J. Hung, J. R. Terman, and E. Reisler. 2016. 'F-actin dismantling through a redox-driven synergy between Mical and cofilin', Nat Cell Biol, *18*: 876-85. (*Co-first authors). I designed, performed and analyzed *in vitro* and *in vivo* experiments including the work in the screening assay and characterization (i.e., all the panels of Fig. 3.1) and the model (i.e., Fig. 3.11g). I also oversaw all aspects of the project with specific contributions listed as follows: I (along with E.E.G, R-J.H) characterized Mical-oxidized actin. R-J.H, J.R.T, and I developed the strategy and characterization of the MetO-44 and wild-type Met-44 antibodies. I developed the assays to use these antibodies to characterize cofilin's effects on Mical. I characterized the expression patterns of cofilin *in vivo* and examined all combinations of Mical and cofilin for effects on F-actin disassembly in vivo. E.E.G performed and analyzed TIRF microscopy, subtilisin proteolysis assays and experiments with Q41C and ANP-modified actin. S.K.R. defined the genetic interaction between cofilin, Mical, and Plexin. J.R.T and I performed axon guidance assays. J.R.T. performed genetic interaction analysis with SelR and Actin^{M44L}.

Abstract

Numerous cellular functions depend on actin filament (F-actin) disassembly. The best-characterized disassembly proteins, the ADF/cofilins/twinstar, sever filaments and recycle monomers to promote actin assembly. Cofilin is also a relatively weak actin disassembler, posing questions about mechanisms of cellular F-actin destabilization. Here we uncover a key link to targeted F-actin disassembly by finding that F-actin is efficiently dismantled through a post-translational-mediated synergism between cofilin and the actin-oxidizing enzyme Mical. We find that Mical-mediated oxidation of actin improves cofilin binding to filaments, where their combined effect dramatically accelerates F-actin disassembly compared to either effector alone. This synergism is also necessary and sufficient for F-actin disassembly *in vivo*, magnifying the effects of both Mical and cofilin on cellular remodeling, axon guidance, and Semaphorin/Plexin repulsion. Mical and cofilin,

therefore, form a Redox-dependent synergistic pair that promotes F-actin instability by rapidly dismantling F-actin and generating post-translationally modified actin that has altered assembly properties.

Introduction

Multiple cellular behaviors depend on the rapid assembly and disassembly of the actin filament (F-actin) cytoskeleton (Blanchoin et al. 2014). Under cellular conditions, F-actin assembly is favored (Brieher 2013; Rottner and Stradal 2011), making it critical to clarify how targeted and rapid F-actin disassembly occurs. In addition, specific extracellular cues including repellents such as ephrins, slits, semaphorins, myelin-associated inhibitors, and Wnts selectively collapse F-actin networks (Bashaw and Klein 2010; Hung and Terman 2011; Kolodkin and Tessier-Lavigne 2011), but their direct effectors are still enigmatic. The best-known F-actin disassembly proteins, the ubiquitous ADF/cofilins, sever actin filaments and recycle monomers with a net effect of promoting new actin assembly (Bernstein and Bamburg 2010; Bravo-Cordero et al. 2013; Brieher 2013; Rottner and Stradal 2011). Moreover, cofilin's relatively weak disassembly of actin (Andrianantoandro and Pollard 2006; Chin, Jansen, and Goode 2016; McCullough et al. 2011) further complicates the current understanding of cellular F-actin destabilization.

Recently, we identified an unusual class of F-actin regulatory proteins, the MICALs, which are multidomain Redox enzymes that induce F-actin disassembly via the direct post-translational oxidation of actin (Hung et al. 2010; Hung, Pak, and Terman 2011). Notably, this Mical-modified actin no longer assembles normally (Hung, Pak, and Terman 2011; Hung

et al. 2013), differentiating Mical's effects from that of other F-actin disassembly proteins (Brieher 2013; Rottner and Stradal 2011). Cellular and *in vivo* work has also revealed that MICALs are widely-expressed in different tissues (Giridharan and Caplan 2014; Hung and Terman 2011; Vanoni, Vitali, and Zucchini 2013; Wilson et al. 2016; Zhou, Gunput, et al. 2011) and control multiple cellular behaviors including motility, axon guidance, synaptogenesis, immune responses, cardiovascular integrity, muscle function, and tumorigenesis (Van Battum et al. 2014; Beuchle et al. 2007; Hou et al. 2015; Hung et al. 2013; Hung, Pak, and Terman 2011; Hung et al. 2010; Kirilly et al. 2009; Lee et al. 2013; Lundquist et al. 2014; Terman et al. 2002; Wilson et al. 2016). The MICALs have also been identified as working with different growth factors, adhesion molecules, and repulsive guidance cues to exert their effects (Aggarwal et al. 2015; Van Battum et al. 2014; Hou et al. 2015; Hung et al. 2010; Lundquist et al. 2014; Schmidt, Shim, and Strittmatter 2008; Terman et al. 2002). Yet, nothing is known of how MICALs integrate with other better-known actin regulatory proteins to direct actin cytoskeletal reorganization and cellular functions.

We now find that Mical synergizes with the ubiquitous actin regulatory protein cofilin to dramatically enhance the dismantling of actin filaments. This coupling between Mical and cofilin depends on the Redox-mediated post-translational alteration of actin. Mical oxidation of actin improves cofilin binding to filaments accelerating F-actin severing and disassembly by over an order of magnitude compared to either effector alone. This synergism also regulates F-actin disassembly *in vivo* and serves to remodel cells, wire the nervous system, and orchestrate Semaphorin/Plexin repulsive signaling. The Redox-dependent synergy between Mical and cofilin, therefore, rapidly disassembles F-actin and also generates

oxidized actin that re-assembles abnormally. This collective action has a net effect of promoting F-actin instability, revealing a previously unknown pathway of cellular F-actin disassembly.

Results

Cofilin modulates Mical Redox-mediated F-actin disassembly

Mical Redox enzymes are a new type of actin regulator – one that controls filament dynamics via the direct post-translational oxidation of actin (Hung et al. 2010; Hung, Pak, and Terman 2011). Specifically, the enzyme activity of MICALs is activated in the presence of their substrate F-actin, which triggers consumption of Mical's coenzyme NADPH and stereospecific oxidation of actin's methionine (M) 44 and M47 residues to induce F-actin disassembly (**Figure 3.1a**; (Alqassim et al. 2016; Hung et al. 2010; Hung, Pak, and Terman 2011; Hung et al. 2013; Lee et al. 2013; Lundquist et al. 2014; McDonald, Liu, and Palfey 2013; Vitali et al. 2016; Zucchini et al. 2011)). Mical's characteristic consumption of NADPH in an F-actin dependent manner has thus provided a simple biochemical test for proteins that may affect Mical's activity. We found that the well-known actin regulatory protein – cofilin (Bernstein and Bamburg 2010; Bravo-Cordero et al. 2013) – strongly suppressed the ability of F-actin to trigger Mical-mediated NADPH consumption (**Figures 3.1b-c and 3.3a**).

The ubiquitous actin depolymerizing/severing factor cofilin is known to change the conformation of the D-loop of actin (Galkin et al. 2011), which harbors Mical's substrate residues M44 and M47 (Hung, Pak, and Terman 2011). These results, coupled with the

observation that non-muscle human cofilin-1 is a relatively weak severer of F-actin (Andrianantoandro and Pollard 2006; Chin, Jansen, and Goode 2016; McCullough et al. 2011), prompted our investigation of a possible interrelation between Mical and cofilin effects on actin. In light of our NADPH consumption results (**Figure 3.1b-c**), we first wondered if cofilin affected Mical's ability to bind to its substrate F-actin. However, using co-sedimentation assays we did not observe any difference in the ability of Mical to associate with F-actin in the presence or absence of cofilin (**Figure 3.1d**). Therefore, we tested if cofilin affected Mical's ability to disassemble F-actin. Strikingly, we found that preincubation of F-actin with cofilin, which alone only minimally affects F-actin disassembly under these conditions (**Figure 3.1e**), dramatically enhanced Mical-mediated F-actin disassembly (**Figure 3.1f-g**). The rate of disassembly was greater than the combined rates with cofilin and Mical added individually (**Figure 3.1h**), which was also confirmed by co-sedimentation (**Figure 3.1i**). This cooperation was not observed in the absence of NADPH (sees **Figure 3.3b-e**), which rules out the possibility that cofilin and Mical without its NADPH coenzyme form a complex that is more efficient in F-actin dismantling than its individual components. Thus, cofilin enhances Mical-mediated actin filament disassembly and their synergistic effect requires the NADPH-dependent Redox activity of Mical.

Cofilin synergizes with Mical to accelerate F-actin disassembly

We therefore reasoned that cofilin might enhance Mical-mediated F-actin disassembly by allowing Mical to more efficiently oxidize its M44 and M47 substrate residues on actin (and thereby consume less NADPH in the process). To test for this

possibility it was important to develop an independent assay for M44/M47 actin oxidation, since NADPH consumption is not an accurate measure of Mical-mediated F-actin oxidation and occurs to some extent even in the absence of F-actin (**Figure 3.1c** and (Hung, Pak, and Terman 2011)). We found that the enzyme subtilisin, which under limited proteolysis conditions cleaves unoxidized actin between M47 and G48 (Schwyter, Phillips, and Reisler 1989), does not cleave Mical-oxidized actin under such conditions (**Figures 3.2a, 3.3f, and 3.4a-c**). Using this observation as an assay, we found that cofilin strongly decreased Mical's rate of F-actin oxidation (**Figure 3.2b**). Furthermore, generating antibodies that specifically recognized the wild-type (unoxidized) M44 residue of actin (**Figure 3.4d**) and the Mical stereospecifically oxidized M44 residue of actin (MetO-44) (**Figure 3.2c**), allowed us to confirm that cofilin does not increase the efficiency of Mical-mediated F-actin oxidation, but actually suppresses it (**Figures 3.2d and 3.4e**). Comparison of the time courses of Mical-mediated F-actin oxidation (**Figure 3.2b** and **d**) and F-actin disassembly (**Figure 3.2e**, **left**; and (Hung et al., 2011)), indicated that Mical rapidly (~ 1 min) oxidizes F-actin but it takes hundreds of seconds for Mical-oxidized actin to disassemble. Strikingly, the addition of cofilin dramatically accelerated the disassembly of Mical-oxidized actin filaments (**Figure 3.2e, right**). Thus, Mical rapidly oxidizes but only relatively slowly disassembles filaments, and cofilin markedly accelerates this disassembly. These results are also consistent with cofilin's suppressive effects on Mical-mediated NADPH consumption and actin oxidation (**Figures 3.1c and 3.2b,d**), because they reveal that Mical and cofilin combine to rapidly disassemble (i.e., deplete) F-actin – which is Mical's substrate and triggers Mical's NADPH consumption and actin oxidation activities (**Figure 3.1a**).

Mical-mediated oxidation of actin weakens the mechanical properties of filaments

To more directly monitor and quantify the effect of Mical oxidation of actin and its disassembly by cofilin, we purified Mical-oxidized actin (Materials and Methods and (Hung, Pak, and Terman 2011; Hung et al. 2013)). We found that Mical-oxidized actin forms filaments, but such filaments have altered polymerization kinetics and a critical concentration of at least an order of magnitude higher than that of unmodified actin (≥1μM) (**Figures 3.5a-e and 3.4f;** see also (Hung, Pak, and Terman 2011; Hung et al. 2013)). Specifically, purified Mical-oxidized actin did not exhibit noticeable polymerization at 1.1 μM (**Figure 3.5a;** (Hung, Pak, and Terman 2011; Hung et al. 2013)), but did polymerize to increasing levels when incubated at 2.2 μM, 3.3 μM and 4.4 μM (**Figure 3.5b-d**). However, we found that polymerization of Mical-oxidized actin proceeded after a longer nucleation phase than normal and (consistent with the higher critical concentration) reached lower plateau levels than observed for unmodified actin (**Figure 3.5b-d**). Notably, re-treating the purified Mical-oxidized actin with Mical/NADPH did not alter its polymerization properties (**Figure 3.5d**), indicating that Mical-oxidized actin is not significantly reduced during purification and storage. Thus, above its critical concentration values, Mical-oxidized actin polymerizes but with abnormal kinetics indicative of the inhibited nucleation phase.

Further analysis of purified Mical-oxidized actin revealed that it also copolymerized with unoxidized actin monomers (**Figure 3.5f;** see also Fig. S11C of (Hung, Pak, and Terman 2011)). We employed subtilisin digestion to quantify the extent of Mical-oxidized actin incorporation into such copolymers (**Figure 3.5f**). This allowed us to form and examine copolymers containing different and well-determined fractions of Mical-oxidized actin. Our

results revealed that unlike unoxidized filaments, Mical-oxidized actin filaments easily fragment upon minimal handling (gentle pipetting and mixing). Even copolymers composed of low amounts of Mical-oxidized actin (11%) had a significantly lower mechanical stability than non-oxidized actin filaments (**Figure 3.5g-h**). Therefore, Mical-oxidized actin copolymers have different mechanical properties than non-oxidized actin.

Cofilin accelerates the dismantling of Mical-oxidized actin filaments

To directly assess the effect of cofilin on the disassembly dynamics of filaments composed of Mical-oxidized actin, we polymerized purified Mical-oxidized actin and employed time-lapse TIRF microscopy. We first grew filaments composed of 100% Mical-oxidized actin from unoxidized F-actin seeds. Dramatically, such Mical-oxidized actin filaments were rapidly dismantled by the addition of cofilin within the solution exchange time (~30 s) (**Figure 3.6a, lower right**) but not upon addition of buffer (**Figure 3.6a, lower middle panel**). Under the same conditions, F-actin severing in the presence of Mical/NADPH or cofilin only was much weaker (see **Figures 3.7a and 3.6a [compare upper right to lower right]**). Thus, these results confirmed our observations using both pyrene-actin and actin sedimentation assays (**Figures 3.1e-i and 3.2e**) and demonstrated that cofilin markedly accelerates Mical-mediated F-actin disassembly.

Mical-mediated oxidation of actin increases cofilin's binding and severing of filaments

We also examined the effects of partial Mical-oxidation on cofilin-mediated F-actin disassembly by employing copolymers with known amounts of Mical-oxidized actin

incorporated. We found that even “lightly oxidized” F-actin copolymers (11% Mical-oxidized actin) accelerated cofilin severing by more than an order of magnitude (22-fold) compared to that of unmodified control F-actin (**Figures 3.6b-c**, **3.7e**, and **Supplementary Movies 1-2**). Increasing the content of the Mical-oxidized actin in the copolymers further accelerated cofilin severing and disassembly **(Supplementary Movies S3-S4, Figure 3.6a, compare upper right to lower right)**, and this effect was not cofilin isoform specific since we also observed it with yeast cofilin (**Figure 3.7b-d**). Thus, the presence of Mical-oxidized actin makes cofilin much more efficient at F-actin disassembly. Furthermore, when assisted by cofilin, partial oxidation of actin filaments by Mical is sufficient for their fast disassembly.

Additional analysis using two-color TIRF microscopy and co-sedimentation also indicated improved cofilin binding to filaments containing Mical-oxidized actin when compared to unoxidized control filaments (**Figure 3.6d-e**, **Supplementary Movies 5-6, Figures 3.8 and 3.9**). In light of the extremely rapid nature of cofilin severing of Mical-oxidized F-actin, we quantified this improved cofilin binding by employing F-actin composed of either Q41C actin (yeast) or ANP-modified (skeletal) F-actin, since they both become disassembly-resistant when cross-linked between residues 41 and 374 (**Figure 3.9**). Using this disassembly-resistant F-actin, we found that more cofilin co-sediments with filaments containing Mical-oxidized actin in comparison to unoxidized cross-linked control filaments (**Figures 3.5d-e and 3.9**) Therefore, Mical-oxidized actin increases both cofilin binding to filaments and the rate and extent of cofilin-mediated F-actin disassembly.

Cofilin modulates Mical-mediated Redox-dependent F-actin disassembly and cellular remodeling in vivo

In view of these results, we wondered if Mical and cofilin might also work together *in vivo*. Both cofilin and Mical have widespread effects on the organization of actin *in vivo* (reviewed in (Bernstein and Bamburg 2010; Bravo-Cordero et al. 2013; Giridharan and Caplan 2014; Hung and Terman 2011; Vanoni, Vitali, and Zucchini 2013; Wilson et al. 2016; Zhou, Gunput, et al. 2011)). For instance, Mical is required to shape Drosophila bristles, which are well-characterized cells (**Figure 3.10a**) that provide a high-resolution model to study actin organization and dynamics *in vivo* (Hung and Terman 2011; Sutherland and Witke 1999; Tilney and DeRosier 2005). Cofilin (which is encoded by the *twinstar* gene in Drosophila) is also required for shaping Drosophila bristles (Chen et al. 2001). Thus, we employed the bristle model to assay the interaction between Mical and cofilin *in vivo*.

Elevating the levels of Mical specifically in bristle cells results in F-actin disassembly and cellular remodeling (**Figure 3.10b**) that is dependent on Mical's Redox activity and its M44 substrate residue within actin (Hung et al. 2013; Hung, Pak, and Terman 2011; Hung et al. 2010). Notably, cofilin and Mical exhibited overlapping localization patterns within developing bristles (**Figure 3.10c**) and removing even a single copy of *cofilin* (*cofilin* heterozygous mutants) significantly suppressed the F-actin reorganization and bristle remodeling effects that are dependent on Mical (compare **Figure 3.10d** with **Figure 3.10b**; **Figures 3.10f-g and 3.12a**). Moreover, raising the levels of *cofilin* significantly enhanced Mical-mediated effects on F-actin and cellular morphology (compare **Figure 3.10e** with **Figure 3.10b**; **Figure 3.10f-g**). Further analysis revealed that cofilin's effects on Mical-

mediated F-actin reorganization *in vivo* were dependent on Mical's M44 substrate residue within actin (**Figure 3.10h**). Similarly, SelR (MsrB), which is an enzyme that reverses Mical-mediated oxidation of actin (Hung et al. 2013; Lee et al. 2013), reversed cofilin's ability to enhance Mical's effects on F-actin reorganization (**Figure 3.10h**). Thus, Mical-mediated F-actin alterations *in vivo*, as *in vitro*, are modulated by cofilin.

Mical and cofilin synergize to drive Semaphorin-Plexin repulsive signaling and axon guidance

In light of our *in vitro* and *in vivo* results demonstrating a synergistic action between Mical and cofilin, it is notable that Mical and cofilin exhibit widespread overlapping expression patterns (Van Troys et al. 2008; Wilson et al. 2016) and both mediate the effects of growth factors, adhesion molecules, and guidance cues on diverse cellular behaviors (reviewed in (Bernstein and Bamburg 2010; Bravo-Cordero et al. 2013; Giridharan and Caplan 2014; Hung and Terman 2011; Vanoni, Vitali, and Zucchini 2013; Wilson et al. 2016; Zhou, Gunput, et al. 2011)). For instance, Mical associates with Plexins, which are receptors for one of the largest families of guidance cues – the Semaphorins (Semas), and plays critical roles in Semaphorin/Plexin repulsive signaling (reviewed in (Hung and Terman 2011)). Cofilin has also been linked to Semaphorin repulsion (Aizawa et al. 2001; Bribian et al. 2014; Hu, Marton, and Goodman 2001; Hung and Terman 2011; Myster et al. 2015; Witherden et al. 2012), but its role and mechanisms of action in this regard have remained poorly understood. Since Mical-mediated bristle actin remodeling occurs in response to Semaphorin/Plexin repulsive guidance signaling (Hung et al. 2013; Hung et al. 2010), we

wondered if cofilin could also be linked with Mical in mediating Semaphorin/Plexin repulsion.

To test this hypothesis, we first employed the bristle system and our genetic experiments demonstrated that cofilin was necessary for Semaphorin/Plexin/Mical-mediated effects on cellular remodeling (**Figure 3.12b-c**). Next, we turned to *in vivo* axon guidance assays using the Drosophila model nervous system, where Semaphorins-Plexins (Sema-1a and Plexin A) serve as repulsive axon guidance cues-receptors and were first functionally linked to Mical (Terman et al. 2002). Notably, we found that *cofilin* (*tsr*) mutants exhibit axon guidance defects that are similar to loss of *Sema-1a*, *Plexin A*, and *Mical* (**Figures 3.11a-c and 3.12d**; (Terman et al. 2002; Winberg et al. 1998; Yu et al. 1998)). Furthermore, we observed transheterozygous genetic interactions between *cofilin* and *Mical* mutants (**Figure 3.11c**), indicating they function in the same signaling pathway to mediate axon guidance. Moreover, we found that increasing the levels of cofilin enhanced Sema-Plexin-Mical repulsive axon guidance, while decreasing the levels of cofilin suppressed these guidance effects (**Figure 3.11d-f**). These results further support that Mical and cofilin work together *in vivo*, as *in vitro*, and indicate that their synergistic effects are also instrumental for Semaphorin-Plexin repulsive signaling and axon guidance.

Discussion

Here we have found that Mical and cofilin function as a pair – synergizing in a Redox-dependent post-translational manner to disassemble F-actin and to control different cellular behaviors. Specifically, cofilin is a well-established actin regulatory protein and a

relatively weak severer of F-actin (Andrianantoandro and Pollard 2006; Chin, Jansen, and Goode 2016; McCullough et al. 2011). In contrast, Mical family Redox enzymes have only recently emerged downstream of Semaphorin-Plexin repellents as actin disassembly factors acting via the direct post-translational oxidation of actin (Alqassim et al. 2016; Hung et al. 2013; Hung, Pak, and Terman 2011; Hung et al. 2010; Lee et al. 2013; Lundquist et al. 2014; McDonald, Liu, and Palfey 2013; Terman et al. 2002; Vitali et al. 2016; Wilson et al. 2016; Zucchini et al. 2011). Previous work has also revealed that Mical, whose C-terminus associates with the intracellular portion of the Semaphorin transmembrane receptor plexin (Hung et al. 2010; Terman et al. 2002), binds with its N-terminal NADPH-dependent Redox domain to F-actin and selectively oxidizes actin's methionine-44 and 47 residues (**Figure 3.11g**, **left panel**; (Hung et al. 2010; Hung, Pak, and Terman 2011; Hung et al. 2013)). We propose that Mical oxidation-induced changes in filament structure and/or dynamics improve cofilin's binding to actin filaments (**Figure 3.11g**, **middle panel**). Herein, we also find that Mical-oxidized actin co-polymers have different properties than unoxidized actin filaments. It is also known that the severing of actin filaments by cofilin is related to the mechanical properties of F-actin (McCullough et al. 2011; Ngo et al. 2015; Suarez et al. 2011). Our results support the idea that Mical uses oxidation to weaken the inter-actin (inter-protomer) contacts within filaments (Hung, Pak, and Terman 2011) and these alterations dramatically speed up cofilin's ability to break/dismantle filaments (**Figure 3.11g**, **right panel**). These results, therefore, uncover a previously unknown pathway of cellular F-actin disassembly and also present an unusual type of biological synergistic interaction – one involving two different types of proteins (Mical and cofilin) and the Redox-dependent post-translational

modification of a third protein (polymerized actin).

Our results also shed new light on the mechanisms of action of both Mical and cofilin. They support a model that Mical and cofilin have been evolutionarily selected to work in tandem to ensure that even a low level of Mical activity in the presence of cofilin would facilitate F-actin disassembly, and vice versa. Moreover, unlike F-actin disassembly by cofilin, which promotes actin turnover by recirculation of monomers for polymerization (Brieher 2013; Kiuchi et al. 2007), Mical post-translationally modifies actin, decreasing its capacity for re-polymerization until the oxidation is reversed (**Figure 3.11g**, **right panel**). Thus, the Redox-driven synergy between Mical and cofilin not only rapidly disassembles F-actin but also generates post-translationally modified actin that re-assembles abnormally with a net effect of promoting F-actin instability. These results, therefore, provide important insights into how actin-based structures are rapidly and specifically dismantled in cells. Given their widespread overlapping expression patterns (reviewed in (Van Troys et al. 2008; Wilson et al. 2016)) and diverse effects on cellular behaviors (reviewed in (Bernstein and Bamburg 2010; Bravo-Cordero et al. 2013; Giridharan and Caplan 2014; Hung and Terman 2011; Vanoni, Vitali, and Zucchini 2013; Wilson et al. 2016; Zhou, Gunput, et al. 2011)), this synergistic interaction between Mical and cofilin provides the molecular framework to rapidly dismantle multiple actin-based cellular structures.

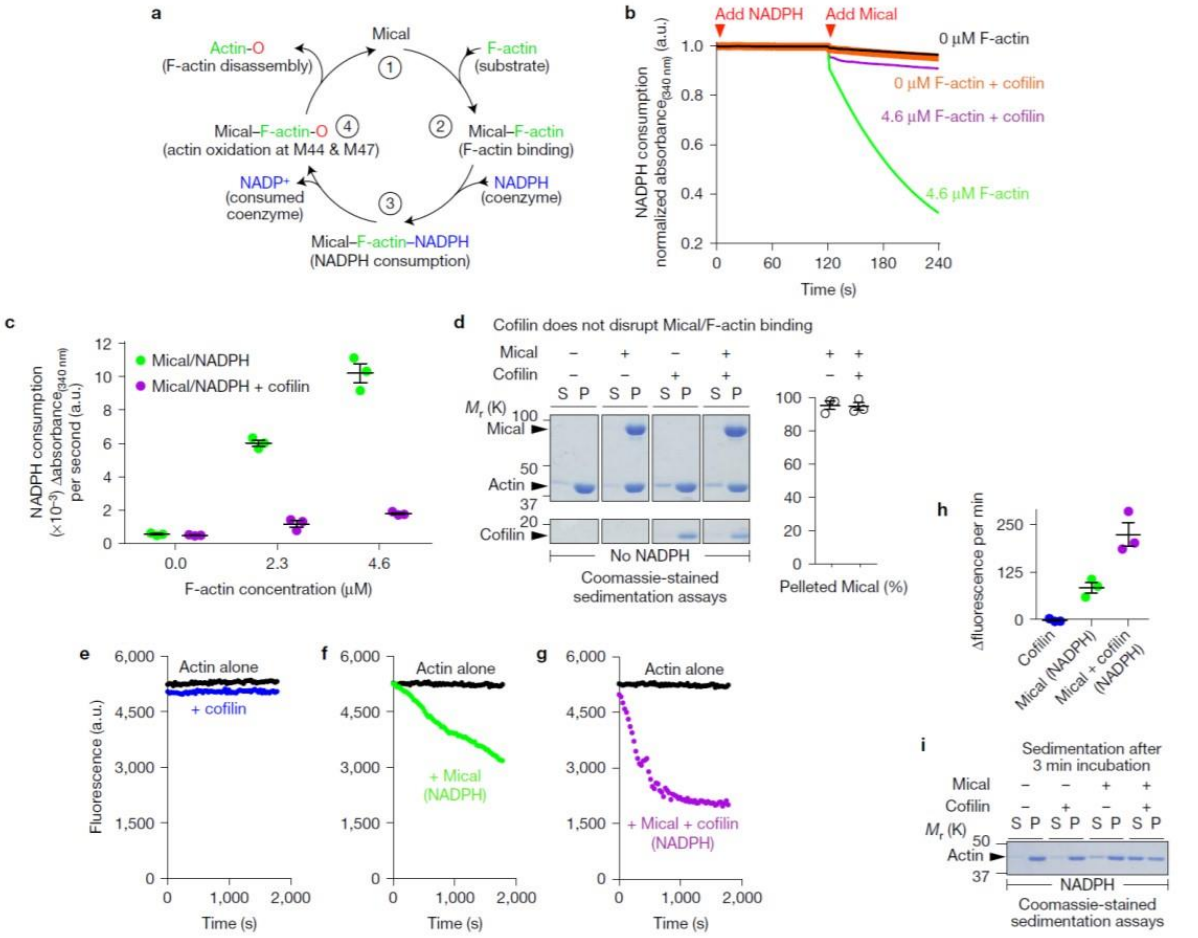

Figure 3.1. Mical/F-actin dynamics are modulated by cofilin.

(a) Mical (1) physically associates with its substrate F-actin (2), which triggers Mical's conversion/consumption of its co-enzyme NADPH to $NADP^+$ (3). Mical then oxidizes F-actin subunits on their M44 and M47 residues (4) triggering F-actin disassembly. For simplicity, the presence of molecular oxygen (O_2) and flavin adenine dinucleotide (FAD) have been excluded from this diagram. **(b-c)** Mical's enzymatic activity (as determined by conversion of NADPH to $NADP^+$, which is measured by a change in absorbance at 340 nm [NADPH Consumption]) is markedly accelerated by F-actin, but not when cofilin is present. [Mical]=600nM, [NADPH]=200µM, actin and cofilin were used at equal molar concentrations. n=3 independent experiments per condition. Mean +/- standard error of the mean (SEM). **(d)** Sedimentation/Association of Mical with F-actin is not altered by the addition of cofilin. S, soluble (G-actin); P, pellet (F-actin). [Actin]=4.6 µM; [Cofilin]=4.6 µM; [Mical]=2.4 µM. No NADPH present; n=3 independent experiments per condition. Mean +/- SEM. **(e-h)** Pyrene–actin assays, where the fluorescence (407 nm) is higher in the polymerized state. (**e**) Cofilin alone (at 1:10 mole ratio to actin) has minimal effects on F-actin disassembly (pH 6.8). **(f-h)** Mical/NADPH-mediated F-actin disassembly (**f**) is rapidly

accelerated by cofilin (at 1:10 molar ratio to actin) (**g**), resulting in a substantial increase in the change in pyrene-actin fluorescence/min (**h**). (**i**) Sedimentation of F-actin following short incubation times (3 minutes) with Mical/NADPH and/or cofilin. Sedimentation of actin shows an increase in the soluble (disassembled) actin amount following Mical/NADPH+cofilin treatment in comparison to Mical/NADPH treatment alone. For **(e-i)**, [Actin]=2.5 µM; [Cofilin]=0.25 µM; [Mical]=10 nM; [NADPH]=100 µM. n=3 independent experiments per condition. Mean +/- SEM. See also **Figure 3.13** for uncropped gels of d and i. *(Performed by HGY).*

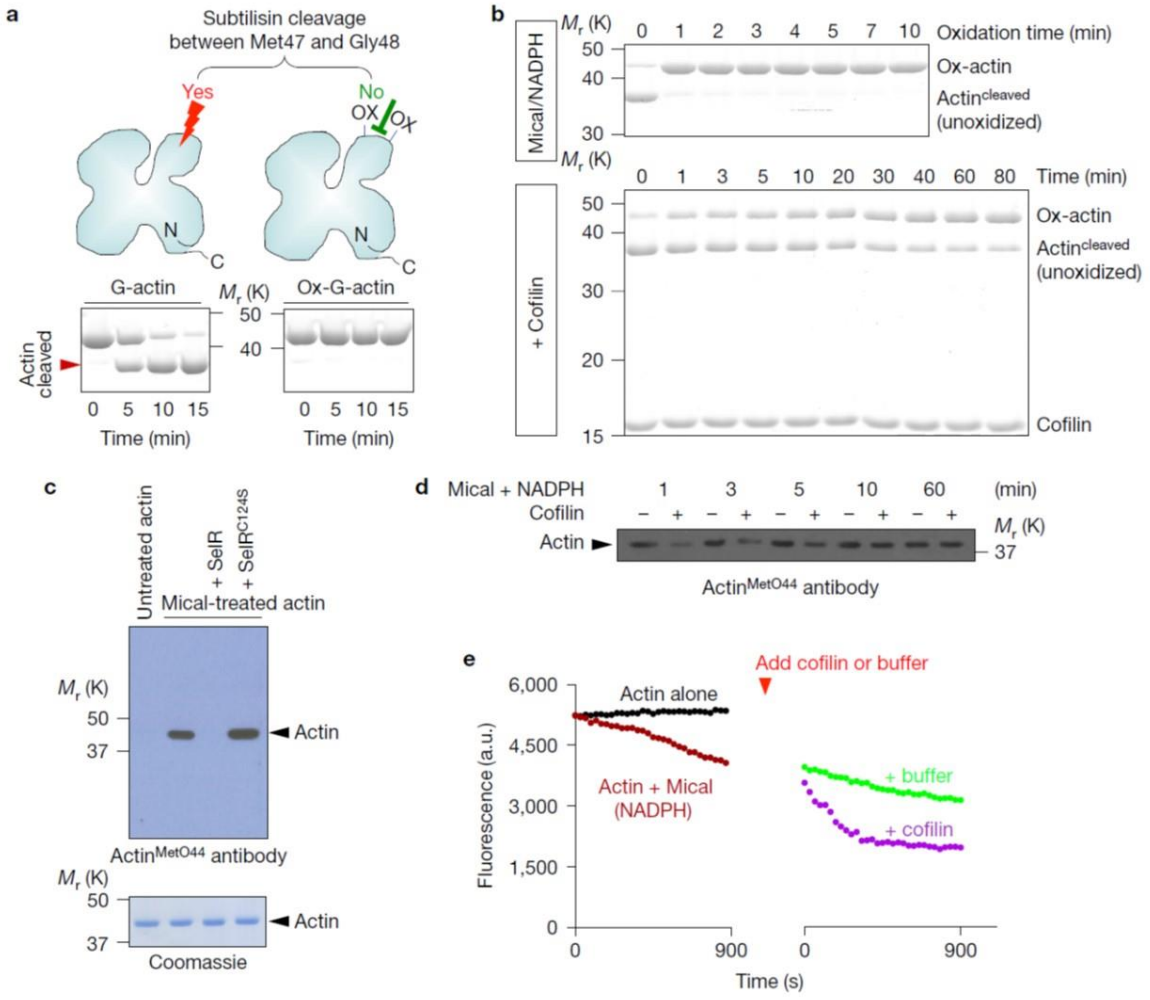

Figure 3.2. Cofilin slows F-actin oxidation by Mical but accelerates filament disassembly.

(a) Subtilisin digestion of actin to assess its oxidation by Mical. **(Top)**: Schematic representation of limited proteolysis of unmodified and Mical-oxidized actin with subtilisin. **(Bottom)**: Subtilisin cleavage occurs between residues 47 and 48 in the D-loop of actin in unmodified actin monomers (red arrowhead), but not in Mical-oxidized actin (ox-G-actin). Cleavage time (0-15 min) is indicated; n=8 preps of Mical-oxidized actin. *(Performed by EEG).* **(b)** Cofilin decreases Mical-mediated oxidation of F-actin, as assayed by limited proteolysis with subtilisin. **Top panel (Mical/NADPH)**: Mical oxidation of bare F-actin. Subtilisin cleavage of bare actin (actin^{cleaved}), which is diagnostic for unoxidized actin, was abolished within 1 min of the addition of Mical/NADPH (oxidation time) due to the accumulation of oxidized actin. **Bottom panel (+Cofilin)**: Mical oxidation of F-actin-cofilin complex (1:1 molar ratio). Significant amounts of subtilisin-cleaved actin (unoxidized actin) were detected even 30 min after the addition of Mical/NADPH indicating that cofilin strongly suppresses Mical-mediated actin oxidation. Conditions: [Actin]=3.5μM;

[Mical]=25nM; [NADPH]=100µM; [Cofilin]=3.5µM; zero time points correspond to the limited proteolysis of unoxidized (non Mical/NADPH-treated) actin using this approach. *(Performed by EEG).* **(c)** Characterization of an antibody that specifically recognizes Mical-oxidized actin (actin$^{MetO-44}$). This antibody recognizes Mical-treated actin but not untreated actin or Mical-treated actin following incubation with SelR, a reductase enzyme that reverses Mical-mediated actin oxidation (Hung et al. 2013). SelR^{C124S} is an enzymatically-dead version of SelR that does not reduce Mical-oxidized actin (Hung et al. 2013). Specifically, 2.3µM of actin (Drosophila actin 5C) was polymerized with either 600nM Mical alone (untreated actin) or 600nM Mical/100µM NADPH (Mical-treated actin) for 1 hour at room temperature. Mical-treated actin was then incubated with 2.4µM of SelR or 2.4µM of SelR^{C124S} and samples were subjected to SDS-PAGE and Western blotting with the actin$^{MetO-44}$ antibody (see also **Figure 3.4d**). Similar amounts of actin (lower panel) are present in all experiments. *(Performed by R-JH).* **(d)** Cofilin suppresses Mical-mediated oxidation of actin, as observed using the actin$^{MetO-44}$ antibody. [Actin]=1.15µM; [Cofilin]=1.15µM; [Mical]=50nM; [NADPH]=100µM. *(Performed by HGY).* **(e)** Mical induces F-actin disassembly (left), while the addition of cofilin (right) rapidly accelerates Mical/NADPH-mediated F-actin disassembly. [Actin]=2.5µM; [Cofilin]=0.25µM; [Mical]=10nM; [NADPH]=100µM. *(Performed by HGY).* See also **Figure 3.13** for uncropped gels/blots of a-d.

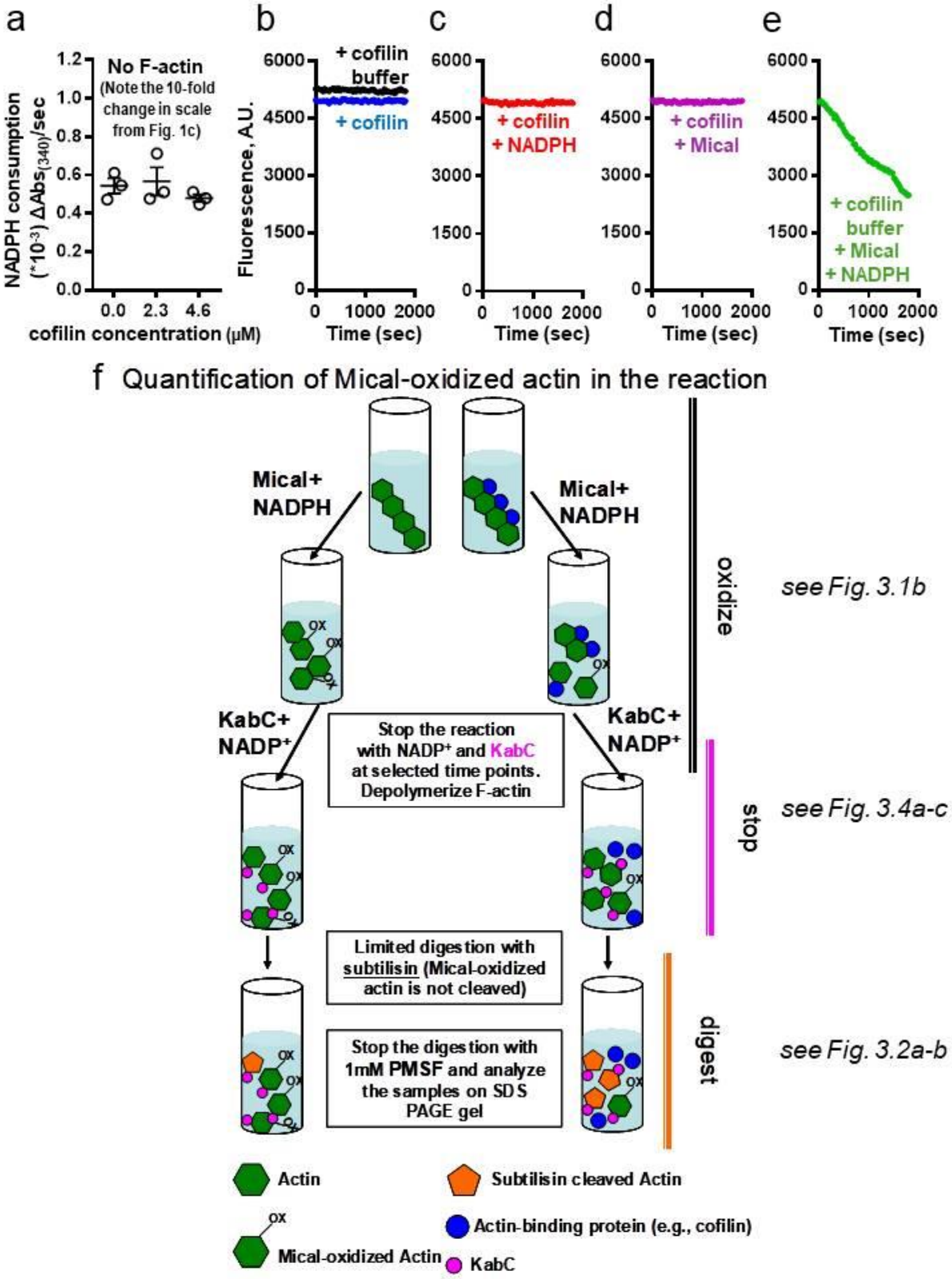
a
b
c
d
e
No F-actin
(Note the 10-fold change in scale from Fig. 1c)
NADPH consumption (*10-3) ΔAbs(340)/sec
cofilin concentration (μM)
0.0 2.3 4.6
Fluorescence, A.U.
+ cofilin buffer
+ cofilin
+ cofilin + NADPH
+ cofilin + Mical
+ cofilin buffer + Mical + NADPH
Time (sec)
f Quantification of Mical-oxidized actin in the reaction
Mical+ NADPH
Mical+ NADPH
oxidize
see Fig. 3.1b
KabC+ NADP+
KabC+ NADP+
Stop the reaction with NADP+ and KabC at selected time points. Depolymerize F-actin
stop
see Fig. 3.4a-c
Limited digestion with subtilisin (Mical-oxidized actin is not cleaved)
Stop the digestion with 1mM PMSF and analyze the samples on SDS PAGE gel
digest
see Fig. 3.2a-b
Actin
Subtilisin cleaved Actin
Mical-oxidized Actin
Actin-binding protein (e.g., cofilin)
KabC

Figure 3.3. Further characterization of the interaction of Mical and cofilin in modulating F-actin disassembly and the quantification of Mical-oxidized actin.

(a) Cofilin alone does not modify Mical's enzymatic activity, unlike Mical's substrate F-actin (**Figure 3.1b-c;** (Hung, Pak, and Terman 2011)), or cofilin in the presence of F-actin (**Figure 3.1b-c)**. Mean +/- SEM. n=3 independent experiments per condition. [Mical]=600 nM, [NADPH]=200 µM. *(Performed by HGY).* **(b-e)** Pyrene actin assays with different combinations of cofilin, Mical, NADPH, and cofilin buffer. Compare with **Figure 3.1e-i**. Note, that the enhanced effect of cofilin on Mical-mediated actin filaments disassembly is not observed in the absence of Mical's coenzyme NADPH. [Actin]=2.5 µM; [Cofilin]=0.25 µM; [Mical]=10 nM; [NADPH]=100 µM. n=3 independent experiments per condition. *(Performed by HGY).* (**f**) Limited proteolysis assay with subtilisin allows quantification of Mical-oxidized actin. This assay is based on the unique feature of Mical-oxidized actin (ox-actin) - its resistance to limited proteolysis by subtilisin that normally occurs between residues 47 and 48 on actin (Schwyter, Phillips, and Reisler 1989). F-actin and F-actin complexes with its binding partner (such as cofilin) are oxidized by Mical in the presence of NADPH. At the selected time points, oxidation is stopped with a large excess of NADP+ (product of the reaction) and the actin depolymerizing reagent Kabiramide C (KabC) (Klenchin et al. 2003). The resulting samples are subjected to limited proteolysis with subtilisin. Subtilisin A (type VIII, Bacillus licheniformis, 11.8-12 units/mg solid) was purchased from Sigma (P5380). The amount of ox-actin in the resulting samples was determined by SDS-PAGE and densitometry analysis. *(Performed by EEG).* See also **Figure 3.4a-c**.

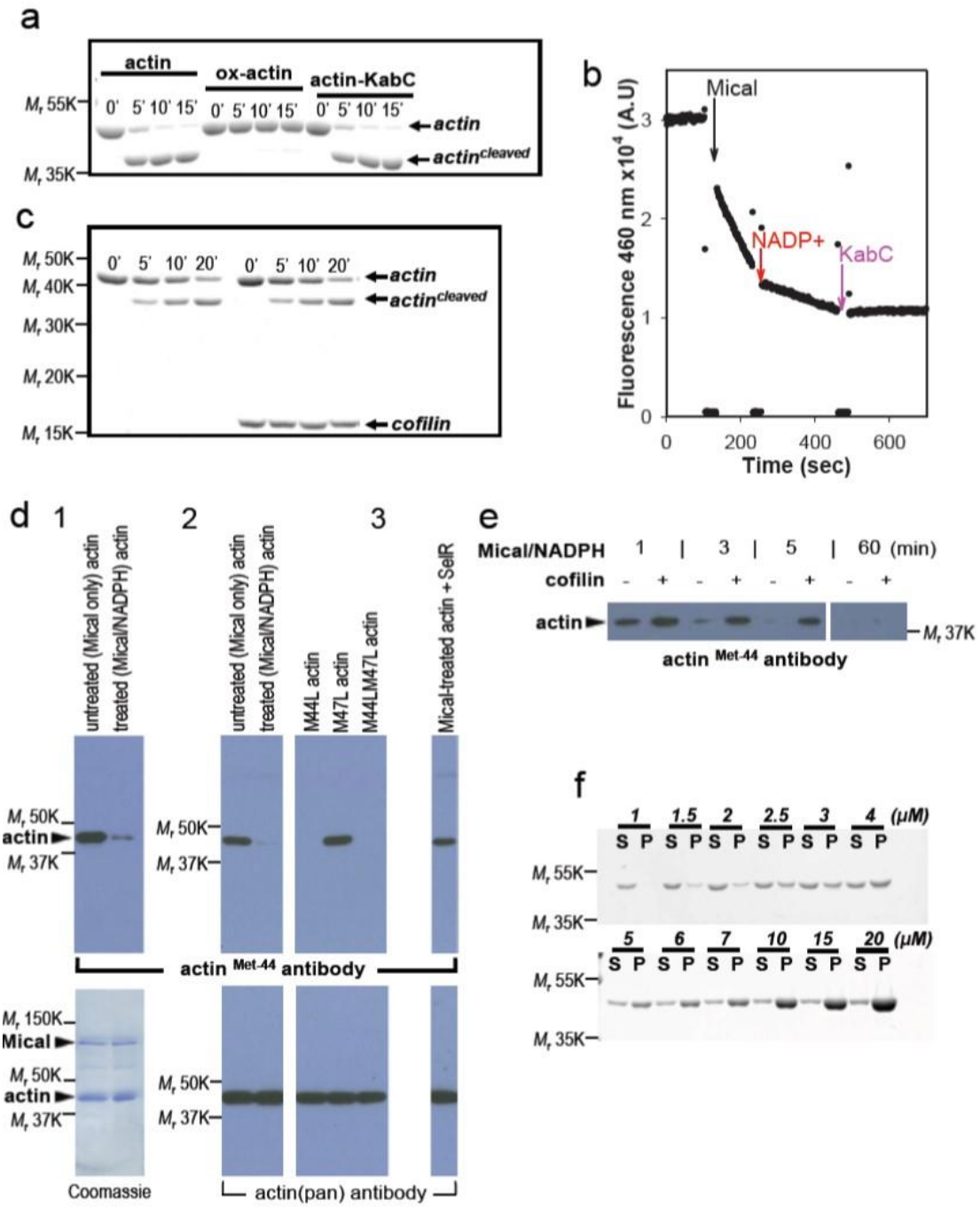

Figure 3.4. Further characterization of Mical-oxidized actin using a limited proteolysis assay with subtilisin and an antibody directed against the Met-44 residue of actin.

(**a-c**) Development of limited proteolysis-based assay for quantification of Mical-oxidized actin (see also **Figure 3.3f**). Assay was developed based on the following observations: 1) Mical oxidizes actin at residue 47 (D-loop) (Hung, Pak, and Terman 2011); 2) subtilisin

cleaves actin between residues 47 and 48 (Schwyter, Phillips, and Reisler 1989); 3) under our experimental conditions Mical oxidized actin (ox-actin) cannot be cleaved by subtilisin at position 47/48, as opposed to unmodified actin, G-actin-cofilin, and G-actin-KabC complex; 4) Mical oxidation of actin can be inhibited by a large excess of the product of the reaction (NADP+); and 5) a combination of NADP+ and the F-actin depolymerizing agent KabC (Klenchin et al., 2003) stops Mical oxidation of actin. *(Performed by EEG).* **(a)**. The small actin sequestering molecule KabC does not affect limited digestion (proteolysis) of actin by subtilisin compared to G-actin alone; *ox-actin* – Mical-oxidized G-actin; cofilin – human cofilin-1; Digestion time (in minutes) is indicated in the panel. Conditions: 2 mM Tris, pH 8, 0.2 mM $CaCl_2$, 0.2 mM ATP, 1 mM DTT; 1:1000 subtilisin:actin w/w ratio. **(b)** Mical oxidation of actin/NADPH consumption can be stopped by an excess of NADP+ (product of the reaction) in combination with KabC. NADPH consumption was followed by a decrease of its fluorescence at 460 nm (excitation wavelength was 340 nm). [F-actin] = 3.5 μM, [$NADP^+$] = 1.5 mM, [KabC] = 3.5 μM, buffer: 20 mM imidazole, pH 6.8, 50 mM KCl, 2 mM $MgCl_2$, 0.2 mM EGTA, 0.2 mM ATP, 1 mM DTT. **(c)** G-actin-cofilin complexes have the same subtilisin digestion pattern as uncomplexed G-actin; *cofilin* – human cofilin-1. [F-actin] = 3.5 μM, [cofilin] = 3.5 μM, [$NADP^+$] = 1.5 mM, [KabC] = 3.5 μM, 1:200 subtilisin:actin w/w ratio. Conditions are the same as in **(b)**. **(d-e)** Cofilin suppresses the Mical-mediated oxidation of actin, as observed using an antibody directed against the Met-44 residue of actin. **(d)** Characterization of an antibody that specifically recognizes the Met-44 residue of actin. Mical oxidizes actin on its Met-44 and Met-47 residues, but the oxidation of the Met-44 is instrumental for inducing F-actin disassembly (Hung, Pak, and Terman 2011). This Met-44 residue of actin is conserved in all actins from yeast to humans (as are almost all of the surrounding residues) (Hung, Pak, and Terman 2011). While attempting to generate antibodies to Mical-oxidized actin (using a peptide of actin residues 38-51), we identified anti-sera that preferentially recognized untreated actin from Mical-treated actin. In particular, note that the antibody (actin$^{Met\text{-}44}$ antibody) preferentially recognizes untreated (Mical only) versus treated (Mical/NADPH) actin (**d^1**, upper panel). This antibody specifically recognizes the Met-44 residue of actin since it does not recognize actin when the Met-44 residue is substituted with Leucine (M44L actin; **d^2**), but does recognize actin when the Met-47 residue is substituted with Leucine (M47L actin; **d^2**). Moreover, Mical-treated actin is recognized by the actin$^{Met\text{-}44}$ antibody following treatment with SelR (**d^3**), the reductase that reverses Mical-mediated oxidation of actin (Hung et al. 2013). Note that similar amounts of Mical (**d^1**, lower panel) and actin (**d^1-d^3**, lower panels) are present in all experiments. For western blotting, 2.3 μM of Drosophila actin (actin 5C) was polymerized with either 600 nM Mical alone (untreated [Mical only] actin) or 600 nM of Mical and 100 μM of NADPH (treated [Mical/NADPH] actin) for 1 hour at room temperature. Then, Mical-treated actin was also treated with 2.4 μM of SelR (that we had previously generated (Hung et al. 2013)) in a buffer containing 20 mM DTT and 10 mM $MgCl_2$ for 1 hour at 37°C. All samples were mixed with SDS-PAGE loading buffer, boiled for 5 min, and loaded onto a 12% SDS-PAGE. After transferring the proteins to a PVDF membrane, this membrane was blocked with 5% non-fat milk in PBST buffer for 1 hour. This membrane was then incubated with either a pan actin antibody (C4; Millipore) or actin$^{Met\text{-}44}$ antiserum for 1 hour at room temperature, and followed with standard Western blotting procedures. Other mutant actin proteins that we had

previously generated (Hung, Pak, and Terman 2011) were also employed in our experiments, including both the Mical-resistant M44L and M44LM47L actins and the M47L actin. *(Performed by R-JH).* **(e)** Cofilin suppresses the Mical-mediated oxidation of actin, as observed using this actin$^{Met\text{-}44}$ antibody (note the increased presence of actin that is recognized by this antibody in the presence of cofilin). [Actin]=1.15 μM; [Cofilin]=1.15 μM; [Mical]=50 nM; [NADPH]=100 μM. *(Performed by HGY).* (**f**) Examples of the gels used to determine the Cc of purified Mical-oxidized actin (ox-actin) are shown in **Figure 3.5e** (pH 8.0, quantified in **Figure 3.5e**, blue circles). Total concentrations of ox-actin are indicated for each sample. S – Supernatant, P – Pellet. The determined Cc was ≥1 μM, which is consistent with the data shown in **Figure 3.5a-e**. Thus, below its Cc values Mical-oxidized actin will not form filaments under polymerizing conditions. *(Performed by EEG).* See also **Figure 3.13** for uncropped gels of d-f.

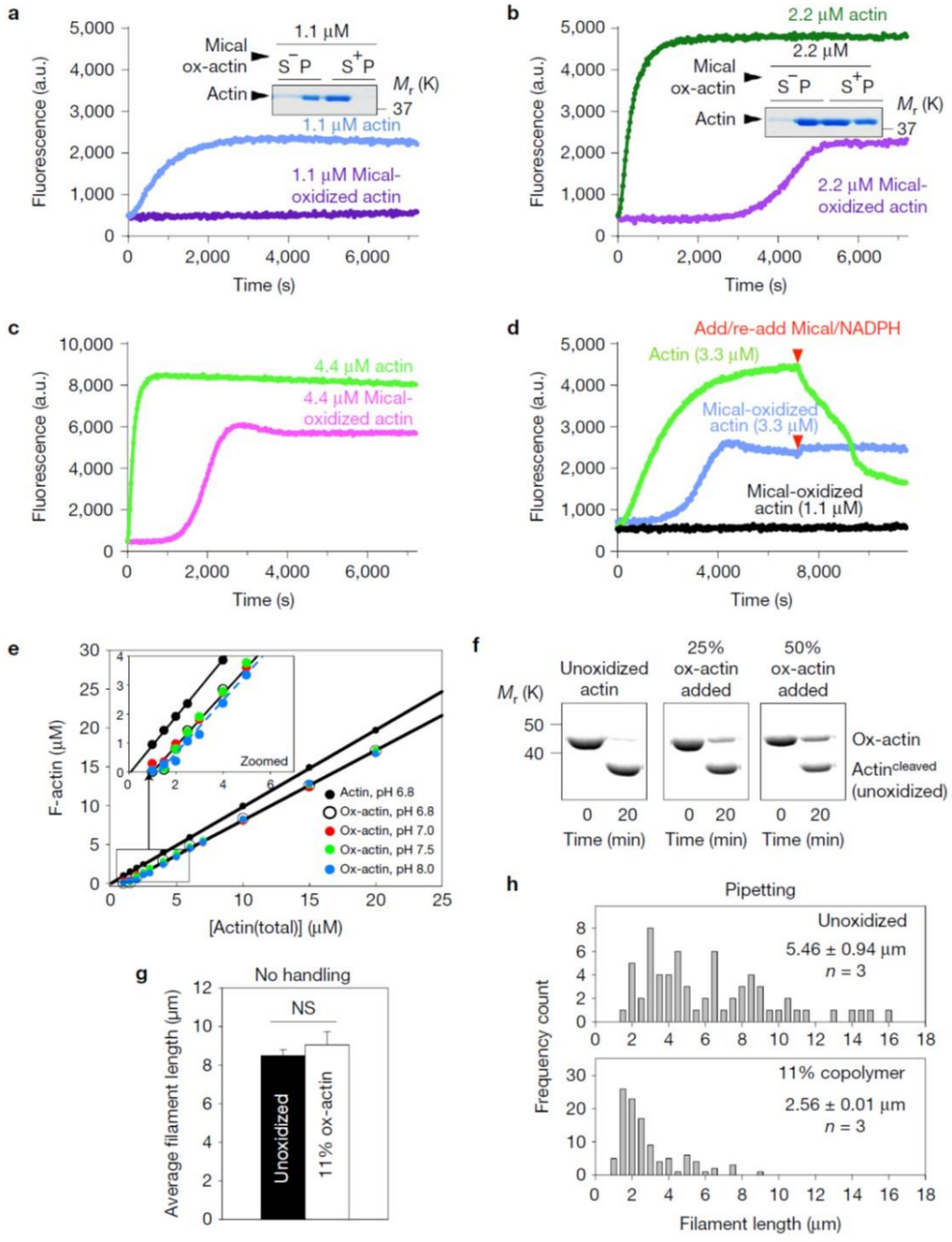

Figure 3.5. Mical-mediated oxidation of actin alters polymerization and weakens the mechanical properties of filaments.

(a-d) Purified Mical-oxidized actin can be induced to polymerize when incubated at high-enough concentrations, although with altered kinetics and extent. Pyrene-actin and

cosedimentation (insets, **a-b**) assays show that purified Mical-oxidized actin (ox-actin) does not polymerize at 1.1μM (**a**; see also (Hung, Pak, and Terman 2011; Hung et al. 2013)), but does polymerize to increasing levels when at concentrations of 2.2μM and 4.4μM (**b-c**). *(Performed by R-JH).* **(d)** Re-treating purified Mical-oxidized actin with Mical/NADPH **(**lower arrowhead**)** does not alter its polymerization state (compare with untreated actin [green curve], upper arrowhead). [Mical]=600nM; [NADPH]=100μM. Representative SDS-PAGE gels: S, soluble (G-actin); P, pellet (F-actin). *(Performed by R-JH).* **(e)** Critical concentration (Cc) of Mical-oxidized actin (ox-actin) is at least one order of magnitude higher than that of unoxidized actin. For ox-actin, intersects of linear plots of concentrations of pelleted F-actin versus total actin with the abscissa yielded a Cc value at pH 7 of 1.1μM±0.25 standard deviation (SD) (n=3 independent ox-actin preps) (red circles) and had similar values at pH 6.8-8. Unoxidized actin Cc was close to 0.1μM. Linear fits are shown for Mical-oxidized and unoxidized actin in zoomed inset. *(Performed by EEG).* **(f)** Quantification of copolymers content using the subtilisin limited proteolysis assay reveals that polymerization of actin mixtures containing unoxidized actins and 25% and 50% of Mical-oxidized actin (ox-actin) yielded copolymers with 10.8±3.2% and 27.7±1.6% ox-actin, respectively (mean+/-SD). *(Performed by EEG).* **(g-h)** Copolymers of Mical-oxidized (11%) and unoxidized actin show decreased mechanical stability compared to unmodified actin. *(Performed by EEG).* (**g**) No statistically significant differences in average length of non-oxidized versus 11% Mical-oxidized F-actin were observed when filaments were assembled in flow chambers (no mixing). n=3 independent measurements of 26-129 filaments per condition per repeat; Mean+/-SEM; NS (not significant) using Student's t-test (two-tailed). **(h)** In contrast, even minimal handling (gentle pipetting and mixing) decreases the average length of Mical-oxidized actin (11%) copolymers much more than unoxidized F-actin. Filament length distributions. Student's t-test (two-tailed). P=0.0059. Mean+/-SD. n=3 independent measurements of 69-188 unoxidized actin filaments (top panel) and 107-182 11% Mical-oxidized copolymer (bottom). See **Figure 3.13** for uncropped gels of a-b, f.

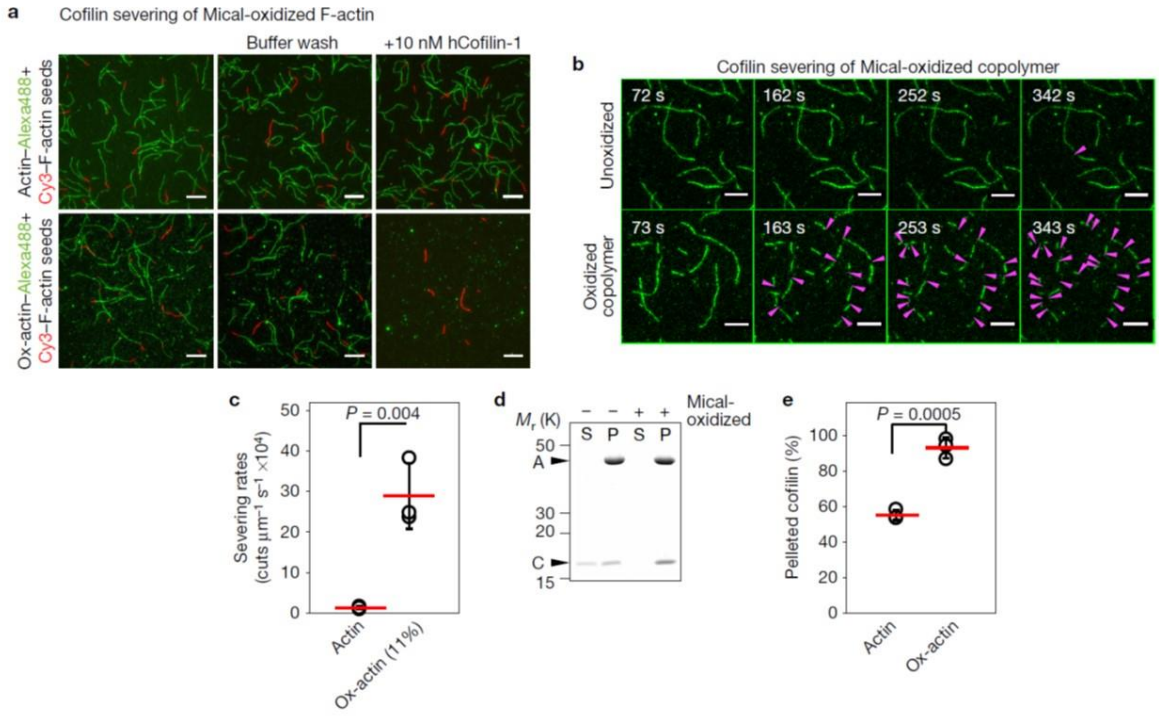

Figure 3.6. Mical oxidation of F-actin improves cofilin binding and results in accelerated filament severing.

(a) Rapid disassembly of fully oxidized actin by human cofilin. Unoxidized Cy3-F-actin seeds were introduced on the slide surface (red filaments, unoxidized) and extended with 100% Mical oxidized actin (ox-actin) labeled with Alexa488 (green stretches, oxidized). Addition of 10 nM human cofilin-1 (but not buffer) to such filaments resulted in full dismantling of Mical ox-actin stretches (green) within the mixing time (~30 sec), but unoxidized actin (red stretches) was not disassembled and stayed on the surface (**bottom panel**). No cofilin severing/fragmentation of control (unoxidized 2-colored filaments) was observed under identical conditions (**top panel**). Scale bar=10 µm. **(b-c)** Enhanced cofilin severing of Mical-oxidized actin containing filaments. (**b**) Severing events are indicated with magenta arrowheads. **Top panel**: Severing of F-actin with human cofilin-1 (100 nM) over time. **Bottom panel**: Severing of F-actin copolymers containing Mical-oxidized actin (11%) by human cofilin-1 (100 nM) over time. Scale bar=5 µm. **(c)** Quantification of cofilin severing of unoxidized F-actin and 11% Mical-oxidized (ox-actin) copolymers. Mean +/- standard deviation (SD). Number of filaments analyzed is 43-45 copolymers and 31-42 unoxidized polymers from each of 3 independent experiments (n=132 copolymers analyzed and 112 unoxidized polymers analyzed). The result of Student's t-test (two-tailed) is shown (p=0.004). **(d-e)** Improved binding of cofilin to Mical-oxidized Cu^{2+}-cross-linked Q41C F-actin, which is disassembly-resistant. (**d**) Representative SDS-PAGE gel of Mical-oxidized actin pelleted with cofilin. Before gel analysis disulfide cross-linking in Q41C actin was reversed with beta-mercaptoethanol. Actin (A). The bottom bands in the gel are cofilin (C). S, soluble (G-actin); P, pellet (F-actin). **(e)** Quantification of cofilin that co-sedimented with

unoxidized and Mical-oxidized (ox-actin) Q41C cross-linked F-actin. Mean +/- SD. n=3 independent experiments per condition. The result of Student's t-test (two-tailed) is shown (p=0.0005). *(Performed by EEG).* Also see **Figure 3.9**. See also **Figure 3.13** for uncropped gel of d.

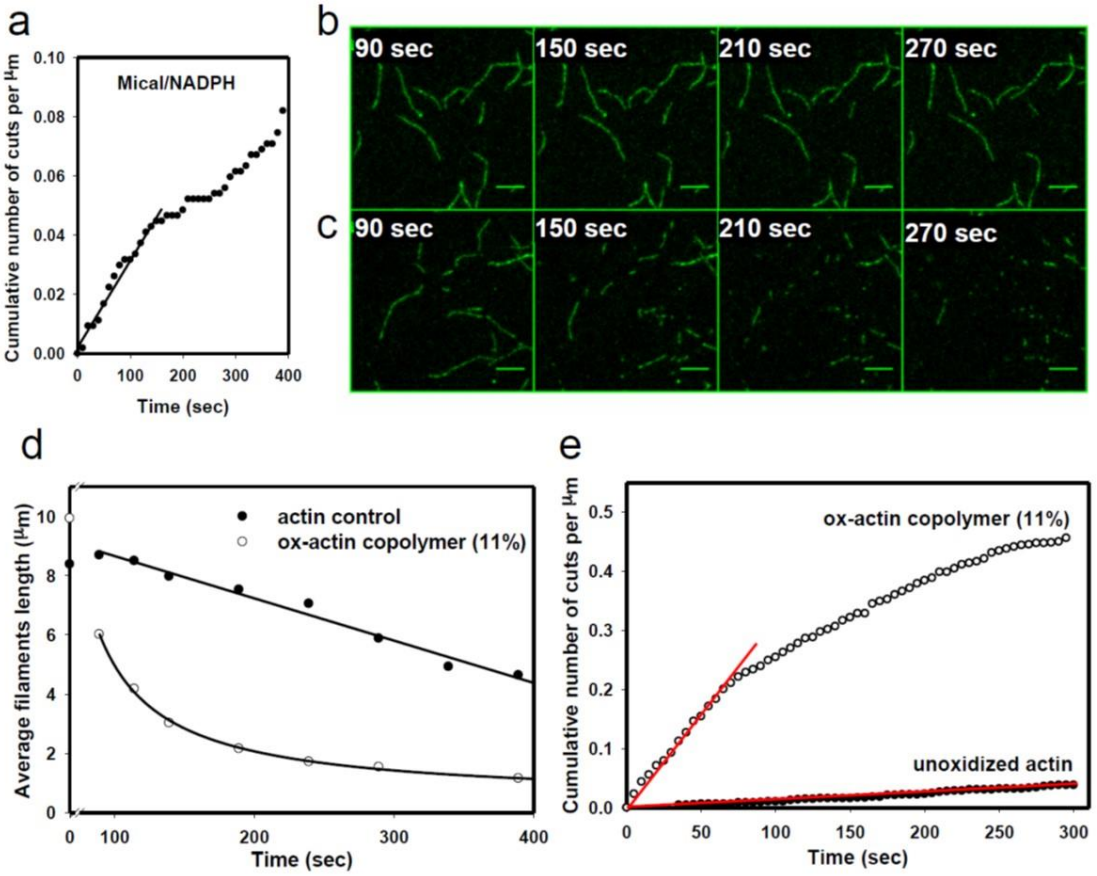

Figure 3.7. Mical oxidation of actin filaments accelerates their severing by yeast and human cofilins.

(a) Severing of actin filaments in the presence of Mical/NADPH. Average of 3 independent trials is shown (analyzing 10-13 filaments each, n=3 movies). Filaments were oxidized on-slide by addition of Mical (55 nM) and NADPH (100 μM) into the flow chamber. Filaments were allowed to oxidize for 1 min then movies were recorded. Note, that the oxidation-induced severing of F-actin by Mical can be followed for minutes (see also Ref (Hung, Pak, and Terman 2011)) as opposed to its almost instant disassembly when combined with cofilin (compare to **Figure 3.6a**). **(b-d)** Severing of unmodified F-actin **(b)** or its copolymer (11%) with Mical-oxidized actin **(c)** with yeast cofilin. Scale bar = 5 μm **(d)** Time dependant change in the average length of skeletal F-actin and 11% Mical-oxidized actin copolymers in the presence of yeast cofilin. A dramatic acceleration of severing by cofilin was observed with 11% Mical-oxidized actin copolymer **(c-d)**. This confirms that accelerated cofilin severing of 11% Mical-oxidized copolymer is not isoform specific (see **Figure 3.6b-c** for comparison). Conditions: [Actin] = 1 μM (10% Cy3-maleimide labeled), [cofilin] = 3.3 nM, pH 6.8. **(e)** Determining the rates of human cofilin-1 severing of unmodified F-actin and its copolymer with Mical ox-actin from the TIRF data (related to the **Figure 3.6c**). The plots are showing

averages of 3 independent repeats for each condition. Red solid lines correspond to the linear fits used to determine maximum cofilin severing rates in **Figure 3.6c**. Note, that in the case of the copolymers with Mical-oxidized actin, cofilin severing efficiency decreases over time (open circles). This effect is due to substantial shortening of actin filaments upon their extensive severing by cofilin within the observation time. Cofilin severs long filaments more efficiently than short filaments (McCullough et al. 2011). Since under our conditions such shortening is insignificant in the control sample (unoxidized actin), the dependence of the number of severing events per μm versus time is linear. To determine the maximum severing rates, linear parts of the traces were fitted individually for each repeat and the slopes were averaged (results are shown in **Figure 3.6c**). n=3 independent experiments per condition. Conditions: [Actin] = 1 μM (10% Cy3 labeled), [Cofilin] = 100 nM, pH 6.8. *(Performed by EEG).*

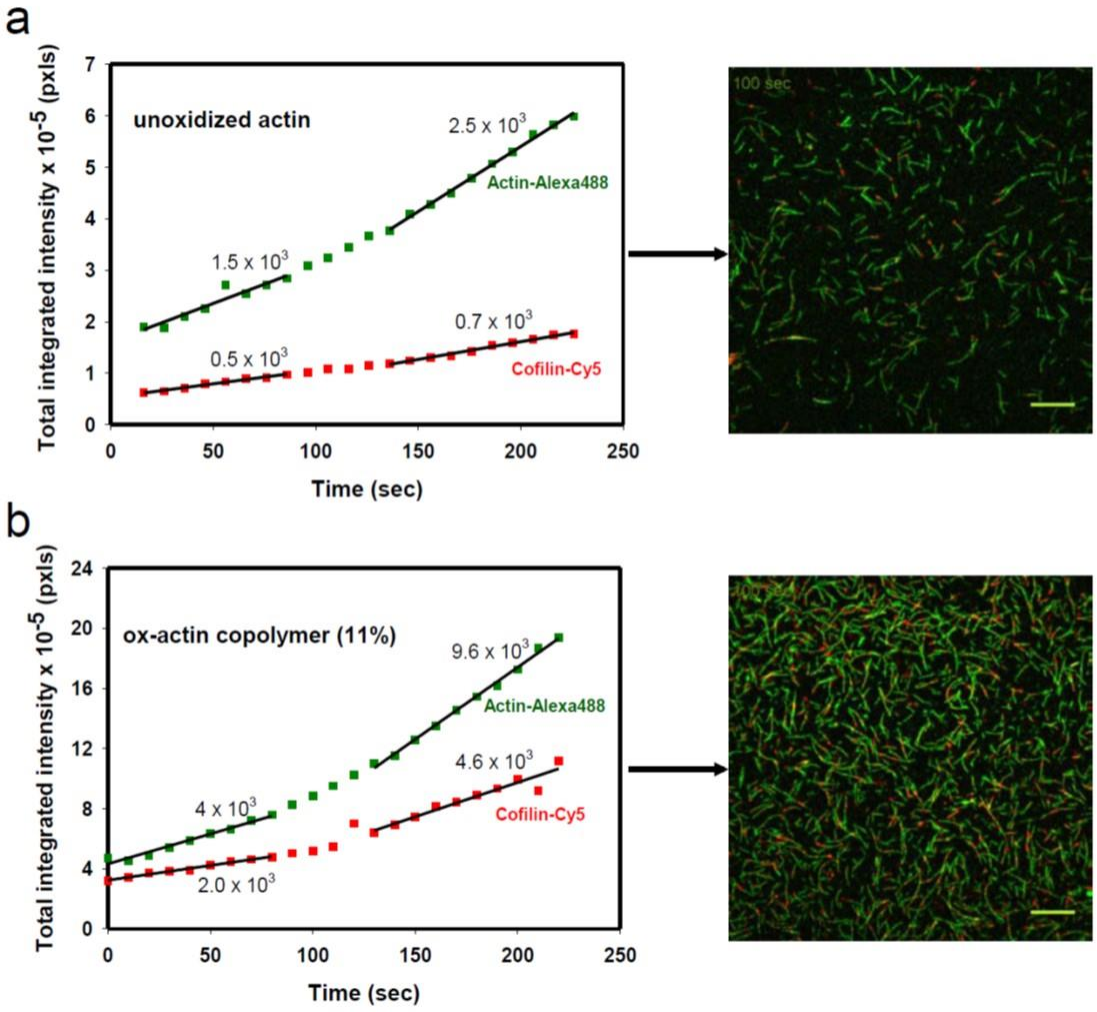

Figure 3.8. Indication of the enhanced cofilin severing and binding to actin filaments containing oxidized actin.

This figure presents analysis of the data from **Supplementary Movies 5** and **6**. [Actin] = 0.6 μM, [yeast cofilin] = 38.5 nM, pH 6.8. One time point image (at 100 sec) from the corresponding movie is shown next to each graph (Scale bar = 10 μm). After background subtraction (Rolling Ball Radius algorithm, 10 pxl), total fluorescence intensity per frame was determined in both channels (actin-Alexa488 (green) and cofilinCy5 (red)) and plotted versus time. The increase in fluorescence intensity is due to an increase in actin polymer mass (Alexa488 channel) and the mass of cofilin bound to these polymers (Cy5 channel). Note, that in both **(a)** and **(b)** the fluorescence intensity corresponding to actin and cofilin increases non-linearly within the observation time. This effect is due to the formation of new barbed ends as a result of cofilin severing activity. This tendency is more pronounced in the case of Mical-oxidized actin (ox-actin) copolymers (note the differences in the y axis scale between (**a)** and (**b)**). We determined the rates of fluorescence intensity change in both

channels for unmodified actin and its copolymer with Mical ox-actin (11%). Changes in fluorescence intensity per second (which can be approximated by linear fits within chosen windows of time) are shown for two time intervals (0-90 sec and 130-225 sec) for each channel (solid black lines). Numbers shown next to each fit correspond to their slopes. Due to undersaturating concentrations of cofilin (38.5 nM), total actin fluorescence per frame increases faster than that of cofilin. Note, that in the control population (unmodified F-actin) actin-Alexa488 fluorescence increases ~3-4 fold faster ($[1.5x10^3/0.5x10^3]=3$ or $[2.5x10^3/0.7x10^3]=3.6$) than that of cofilinCy5 **((a)**, **Supplementary Movie 5**). However, in the copolymer sample, fluorescence of actin-Alexa488 increases only ~2 fold faster ($[4.0x10^3/2.0x10^3]=2$ or $[9.6x10^3/4.6x10^3]=2.1$) than that of cofilinCy5 ((**b)**, **Supplementary Movie 6**). Thus, this decreased difference between cofilin and actin fluorescence in the Mical ox-actin copolymer sample is consistent with the presence of more cofilin associated with Mical-oxidized F-actin than with unmodified F-actin. This prompted our investigation of cofilin binding to the Mical-oxidized cross-linked F-actin (see **Figure 3.6d-e** and **Figure 3.9**). *(Performed by EEG).*

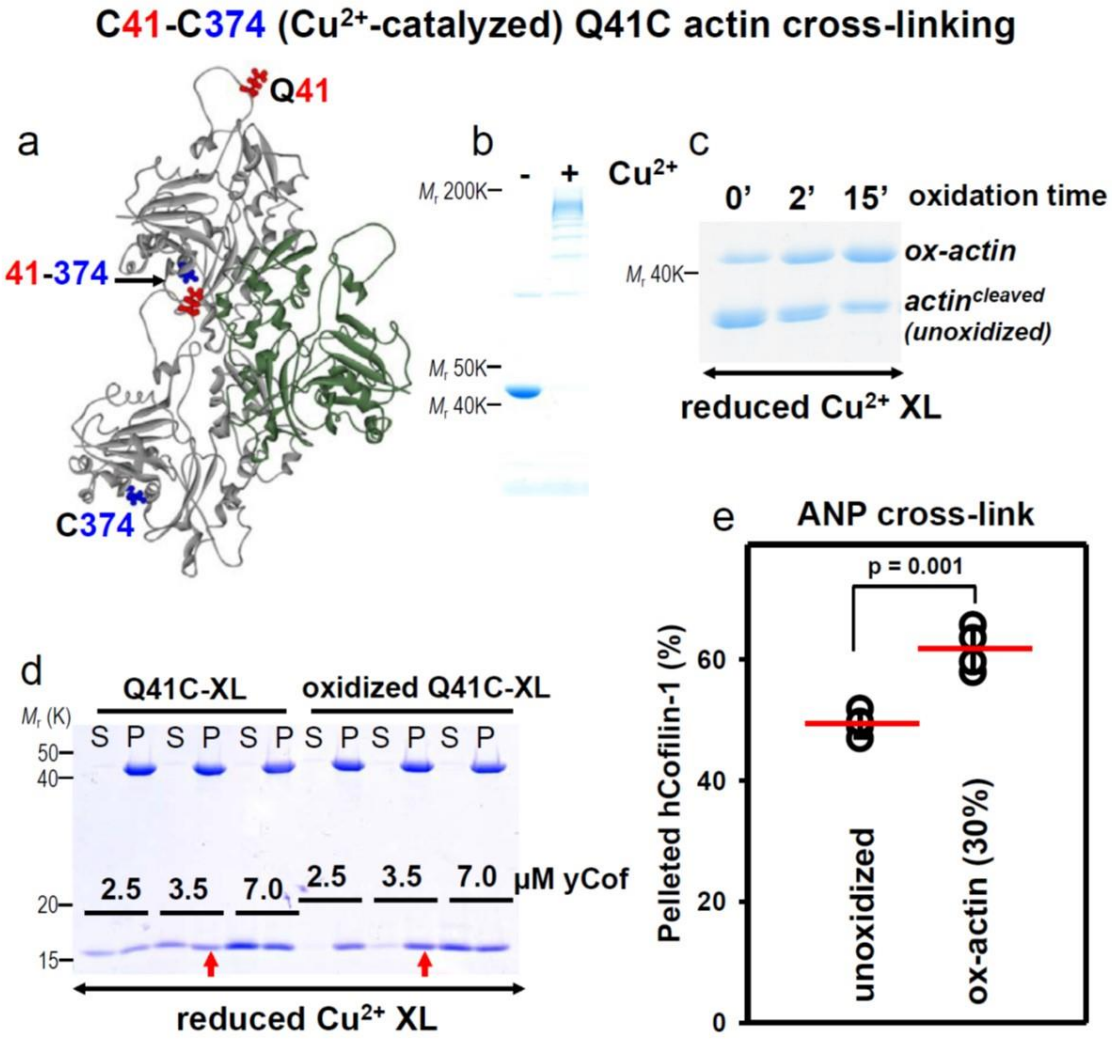

Figure 3.9. Further characterization of cofilin binding to Mical-oxidized actin.

(a-d) Enhanced cofilin binding to cross-linked Q41C F-actin after its oxidation by Mical (see also **Figure 3.6d-e**). **(a)** Positions of the cross-linked residues (41 (red) and C374 (blue)) in F-actin (PDB: 3J8A) (von der Ecken et al. 2015). Adjacent longitudinal protomers within the same actin strand are shown in grey. Actin third protomer from the opposite strand (lateral self-interacting interface) is shown in dark green. In the Q41C yeast actin mutant, residue 41 was mutated to cysteine which allows for disulfide cross-linking of this residue to native cysteine 374 on another protomer. **(b)** Representative SDS-PAGE gel under non-reducing (Coomassie stained) conditions demonstrates that Q41C actin is fully cross-linked by Cu^{2+} under our experimental conditions. Monomeric actin (left lane) is depleted upon $CuSO_4$ addition (right lane) due to the formation of higher order actin species. **(c)** Cross-linked (XL) Q41C-F-actin can be fully oxidized by Mical. Efficiency of Q41C-XL oxidation by Mical was assessed by limited proteolysis with subtilisin. To this end, Q41C F-actin cross-linking was reversed with DTT after the indicated oxidation time (to allow it to appear as monomeric

actin on the gel). Based on limited proteolysis with subtilisin, the increase in intensity of the uncleaved actin band over time reports on the progress of actin oxidation by Mical (*ox-actin*). Q41C-XL F-actin can be efficiently oxidized by Mical in the presence of NADPH (close to completion in 15 min). For cosedimentation assays with cofilin (**Figure 3.6d-e**), Mical oxidation of Q41C-XL F-actin was carried out for 1 hour at room temperature to ensure full oxidation. **(d)** Yeast cofilin binds tighter to the Mical-oxidized cross-linked Q41C F-actin (3.5 μM) than the unoxidized control. Note the absence of unbound cofilin (at 2.5 and 3.5 μM concentration) in the supernatants of its complexes with ox-actin in contrast to the complexes with unoxidized actin. Example of the SDS-PAGE gel under reducing conditions is shown (Coomassie staining). After Mical oxidation and pelleting (P) with cofilin, Q41C actin cross-linking was reversed in the presence of 2-mercaptoethanol and it now appears as a single band on the gel (compare to (**b**, right)). Note, that judging by the absence of actin in supernatants (S), complete C41-C374 cross-linking produces actin polymers that are disassembly-resistant despite their full oxidation and cofilin presence. Enhanced cofilin binding to the oxidized Q41C-XL (compared to unoxidized) was observed at three different ratios of cofilin:actin (0.7:1; 1:1; 2:1). The ratio used in **Figure 3.6d-e** (1:1) is indicated with the red arrows. (**e**) Co-sedimentation indicates improved binding of human cofilin-1 to Mical-oxidized ANP cross-linked skeletal F-actin (30% ox-actin) compared to the unoxidized ANP cross-linked F-actin. Unoxidized and Mical-oxidized ANP-cross-linked F-actin was pelleted at high speed and analysed as described in the Methods. Conditions: [ANP-cross-linked F-actin] = 3.5 μM, [Cofilin] = 3.5 μM; Buffer: 20 mM imidazole, pH 6.8, 2 mM $MgCl_2$, 0.2 mM EGTA, 150 mM KCl, 0.2 mM ATP, 0.5 mM DTT. Mean +/- SD (n=4 independent experiments per condition); the result of Student's t-test (two-tailed) is shown (p=0.001). *(Performed by EEG).* See also **Figure 3.13** for uncropped gels of b-d.

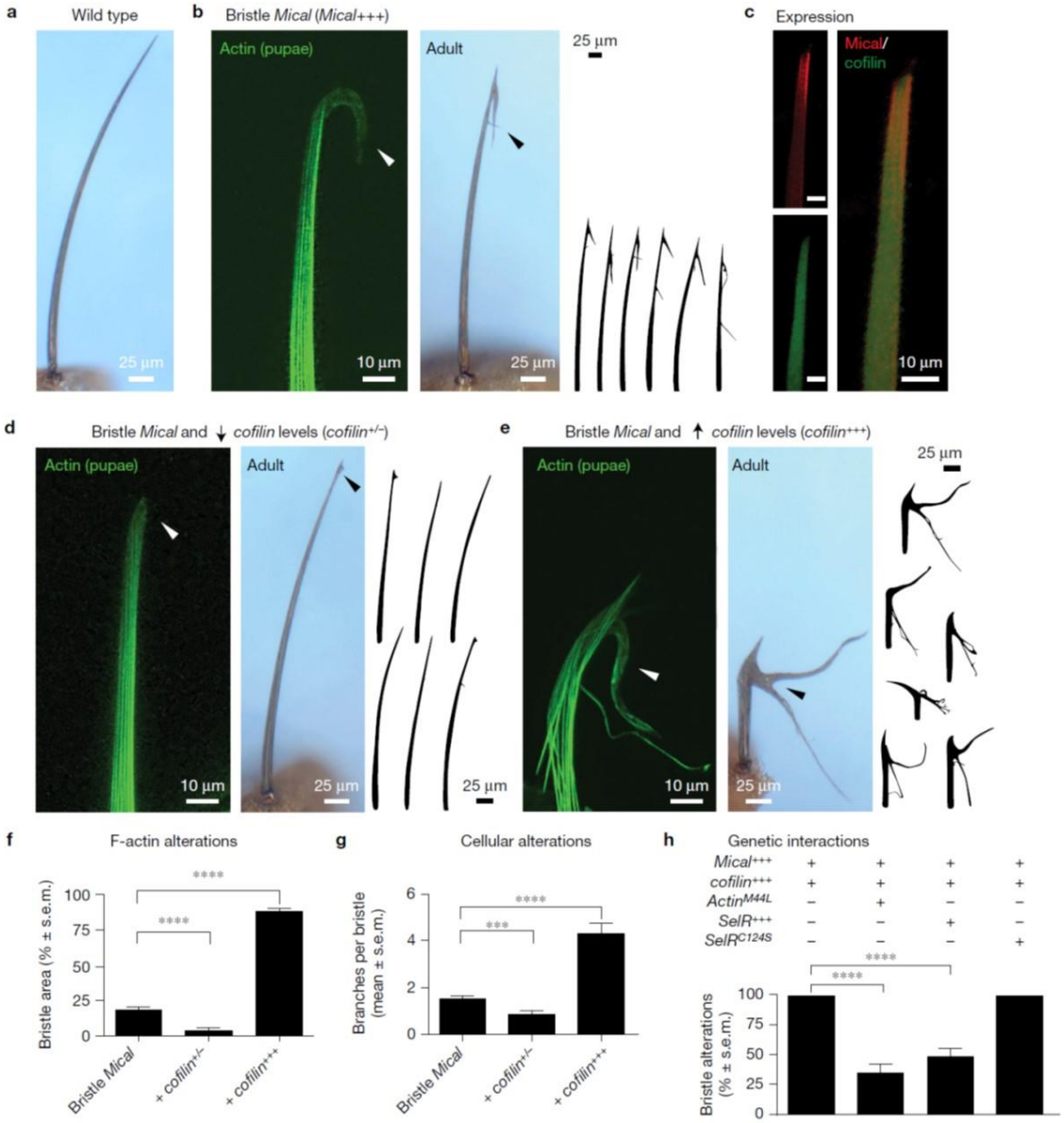

Figure 3.10. Cofilin enhances Mical-mediated F-actin alterations *in vivo*.

(a-b) Drosophila bristles are unbranched *(Performed by HGY and SKR).* (**a**) but become branched as the result of F-actin disassembly and remodeling (**b**; arrowheads and drawings) when Mical is overexpressed specifically within them (Hung et al. 2010; Hung, Pak, and Terman 2011; Hung et al. 2013). **(c)** Mical (red; see also (Hung et al. 2010)) and cofilin/twinstar (green) are both expressed in bristle processes in overlapping patterns. Note also that cofilin is more widely distributed than Mical, which shows its highest distribution at the tip of the process. Scale bars=10 µm *(Performed by HGY).* (**d**) Decreasing the levels of cofilin (*cofilin/twinstar* heterozygote genetic background [$cofilin^{+/-}$]) suppresses Mical-induced F-actin reorganization/bristle branching (arrowheads and drawings). *(Performed by*

HGY and SKR). (**e**) Increasing the levels of cofilin/twinstar (bristle specific expression of a hyperactive *cofilin*^{S3A} transgene [*cofilin+++]*, which has no bristle effects on its own) enhances Mical-induced F-actin reorganization/bristle branching (arrowhead**s**). *(Performed by HGY and SKR).* (**f-g**) Quantification of the data from b, d and e. n=20 bristle cells accessed across 20 animals per genotype, Mean +/- SEM, Student's t-test (two-tailed); ***p=0.0008, ****p<0.0001. *(Performed by HGY and SKR).* (**h**) Employing the genetic background described in (e), we find that mutating Mical's substrate residue on actin, the Met-44 residue, and expressing this mutant actin in bristles (actin^{M44L}) suppresses cofilin's effects on Mical. Likewise, expressing SelR (SelR+++), but not an enzyme dead version of SelR (SelR^{C124S}), suppresses cofilin's effects on Mical. n=40 bristle cells accessed across 10 animals per genotype. Mean +/- SEM, Student's t-test (two-tailed); ****p<0.0001. *(Performed by SKR and JRT).* All genotypes are heterozygous (*B11-GAL4/+*, *UAS:Mical/+*, *mutations/+, and/or transgenes/+*). One copy of *UAS:*^{GFP}*actin* was used when visualizing F-actin. *B11-GAL4*, *UAS:Mical*, *UAS:Actin*^{M44L}, *UAS:SelR*, *UAS:*^{GFP}*actin*, and *UAS:SelR*^{C124S} lines were as previously described (Hung et al. 2010; Hung, Pak, and Terman 2011; Hung et al. 2013). For Mical/cofilin expression analysis, we crossed *UAS:*^{mCherry}*Mical, B11-GAL4* flies to *cofilin/twinstar (tsr)* GFP-trap lines and Mical/cofilin expression and localization was imaged in pupal progeny. We used the following *cofilin* (*twinstar* [*tsr])* publicly available fly lines: *tsr*^{N121} (a loss-of-function/"knockout" adult lethal mutant due to P-element mediated imprecise excision in the *tsr* gene; (Johnson, Seppa, and Cagan 2008; Ng and Luo 2004; Ren, Charlton, and Adler 2007; Schottenfeld-Roames, Rosa, and Ghabrial 2014)) and *UAS:tsr*^{S3A} (a constitutively active *tsr* transgene; (Ng and Luo 2004; Stephan et al. 2012)). We also used the following GFP-trap *tsr* lines, all of which showed similar expression patterns: *ZCL2393*, *tsr*^{CPTI002237}, and *CC01393*.

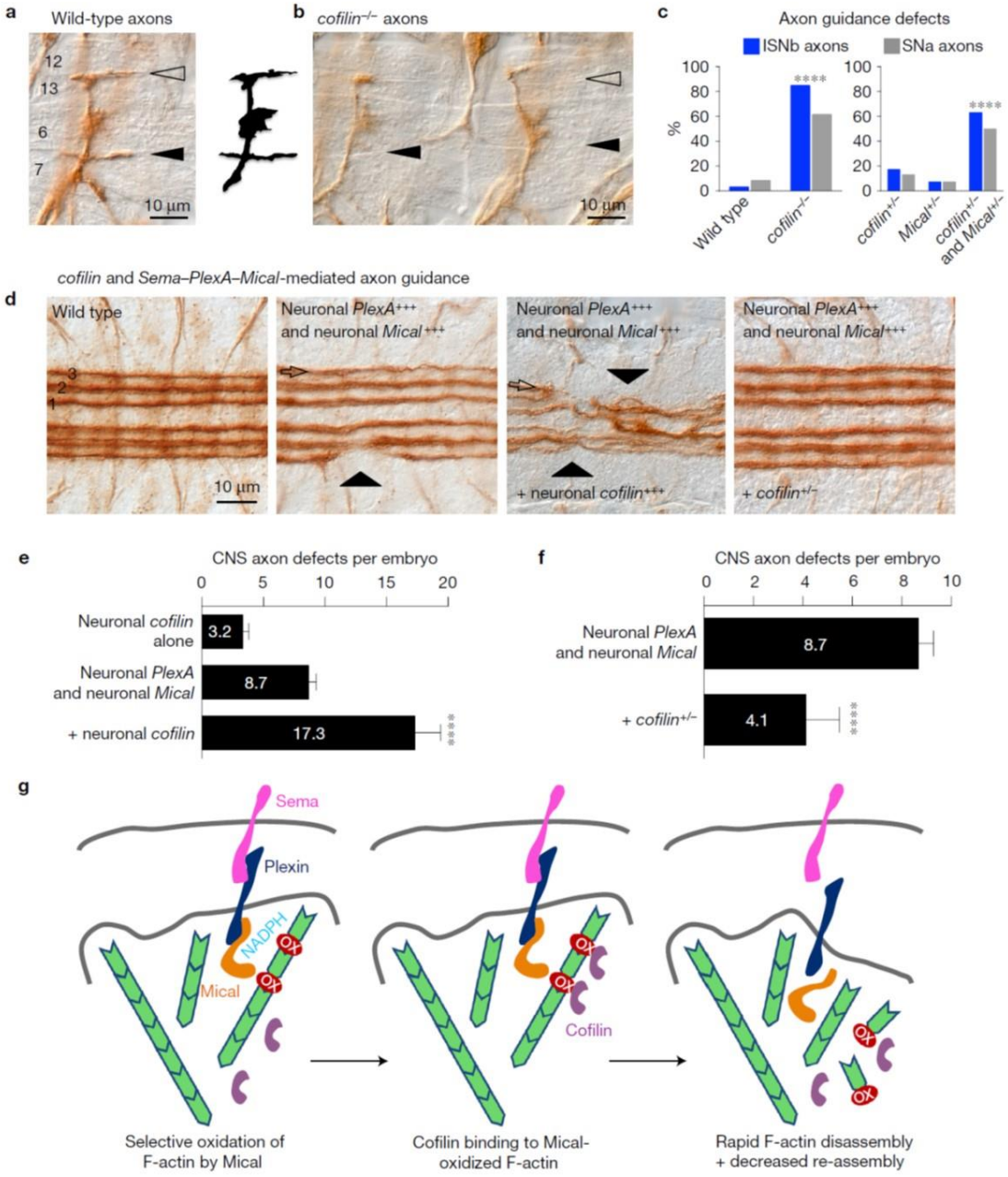

Figure 3.11. Cofilin enhances Sema-Plexin-Mical repulsive axon guidance.

(a) In *wild-type* embryos, Drosophila intersegmental nerve b (ISNb) motor axons innervate muscles 6 and 7 (filled arrowhead) and muscles 12 and 13 (open arrowhead). This normal pattern of innervation is also depicted in the drawing. **(b)** In a *cofilin* (*twinstar*) homozygous mutant embryo (*cofilin*$^{-/-}$, adult-lethal genotype), note the absence (filled arrowheads) or abnormal (open arrowhead) innervation of these muscles. **(c)** Quantification of the data from a-b, reveals that *cofilin*$^{-/-}$ mutant embryos exhibit significant ISNb axon guidance defects (left graph). Embryos with heterozygous mutations for both *cofilin* and *Mical* (*cofilin*$^{+/-}$ and

Mical$^{+/-}$) also exhibit significant ISNb guidance defects in comparison to either heterozygote alone (right graph). Examination of another motor axon pathway (segmental nerve a [SNa]) revealed similar significant differences. n=100 hemisegments assessed across 10 animals per genotype, Mean +/- SEM, Chi-Square Test; ****p<0.0001. (**d**) *Wild-type* Drosophila central nervous system (CNS) axons exhibit a characteristic organizational pattern including three longitudinal connectives (1, 2, 3) composed of bundled Fasciclin II (1D4)-positive axons. Increasing the levels of *PlexA* in combination with *Mical* in neurons (Neuronal *PlexA [PlexA+++]* and Neuronal *Mical [Mical+++]*) alters the pathfinding of these longitudinal axons (e.g., arrow, arrowhead) and creates a sensitive genetic background to quantify CNS axonal pathfinding defects including discontinuous or missing 1st, 2nd, or 3rd CNS longitudinals and/or axons crossing the midline (see also (Ayoob et al. 2004; He et al. 2009; Hung et al. 2013; Yang and Terman 2012)). Increasing the levels of cofilin (+Neuronal *cofilin [cofilin+++]*) enhances these PlexA-Mical dependent effects, while decreasing the levels of cofilin (+*cofilin+/–)* suppresses these PlexA-Mical dependent effects. Scale bar applies to all images. (**e-f**) Quantification of the data from d. n = 480 longitudinals accessed in 160 hemisegments within 10 animals per genotype, Mean +/- SEM, Student's t-test (two-tailed); ****p<0.0001. All genotypes are heterozygous (*ELAV-GAL4/+*, *UAS:*^{HA}*PlexA/+*, *UAS:Mical/+*, *mutations/+*, *and/or transgenes/+*). (**g**) A model based on our *in vitro* and *in vivo* results that Mical and cofilin form a Redox-driven synergistic pair to negatively affect the stability of the actin cytoskeleton and direct F-actin dismantling, cellular remodeling, axon guidance, and Semaphorin-Plexin repulsion. See also main text. *(Performed by JRT and HGY).*

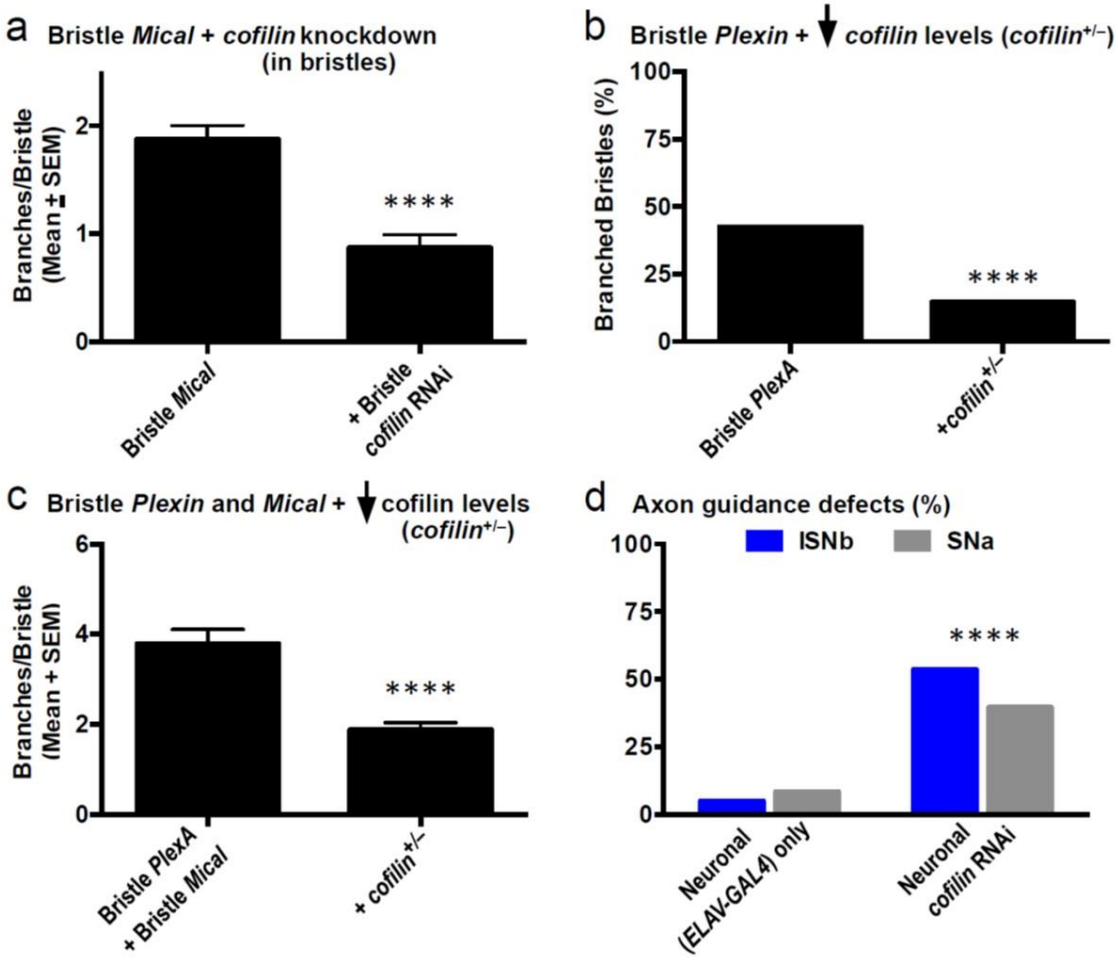

Figure 3.12. Further analysis of Cofilin's effects on Mical and Semaphorin/Plexin-mediated F-actin/cellular remodeling *in vivo*.

(a) Knockdown of cofilin specifically in bristles using an RNAi transgenic line specific for *cofilin/twinstar* suppresses Mical-induced F-actin reorganization/bristle branching. Compare with **Figure 3.10g**. Mean +/- SEM. Student's t-test (two-tailed); ****P<0.0001. n=20 animals per genotype. Replicated in at least 2 independent experiments (separate crosses) per genotype. **(b)** Increasing the levels of Plexin (Plexin A [PlexA]) in bristles generates bristle branching (Hung et al. 2010). Decreasing the levels of cofilin (*cofilin/twinstar* heterozygote genetic background) suppresses these Plexin-induced F-actin reorganization/bristle branching effects. Percent of flies with branched bristles. Chi-Square Test; ****P<0.0001. n=40 animals per genotype. Replicated in at least 2 independent experiments (separate crosses) per genotype. **(c)** Increasing the levels of both Plexin and Mical within bristles generates increased F-actin remodeling/bristle branching in a Semaphorin-dependent manner (Hung et al. 2010), and these Semaphorin/Plexin/Mical-dependent effects are suppressed by decreasing the levels of cofilin (*cofilin/twinstar* heterozygote genetic background). Mean +/- SEM, Student's t-test (two-tailed); ****P<0.0001. n=20 animals per genotype. Mean + standard error of the mean (SEM). Replicated in at least 2 independent experiments (separate

crosses) per genotype. **(d)** Knockdown of cofilin specifically in neurons using the *ELAV-GAL4* driver and an RNAi transgenic line specific for *cofilin/twinstar* generates motor axon guidance defects similar to those described in **Figure 3.11b-c**. *n*=100 hemisegments assessed in 10 animals per genotype, Chi-Square Test; **** *P*< 0.0001. *(Performed by JRT).* All genotypes in a-d are heterozygous (*B11-GAL4/+*, *ELAV-GAL4/+*, *UAS:Mical*/+, *UAS:PlexA*/+, *tsr*/+, *and/or cofilin RNAi*/+). The *twinstar* (*tsr)* RNAi knockdown lines employed were $tsr^{HMS00534}$ (obtained from the Bloomington Drosophila Stock Center) and $tsr^{KK108706}$ (obtained from the Vienna Drosophila Resource Center). The $UAS:^{HA}PlexA$ and *UAS:Mical* lines were as previously described (Hung et al. 2010; Hung, Pak, and Terman 2011; Hung et al. 2013). Other lines were as described in Figures 3.10 and 3.11.

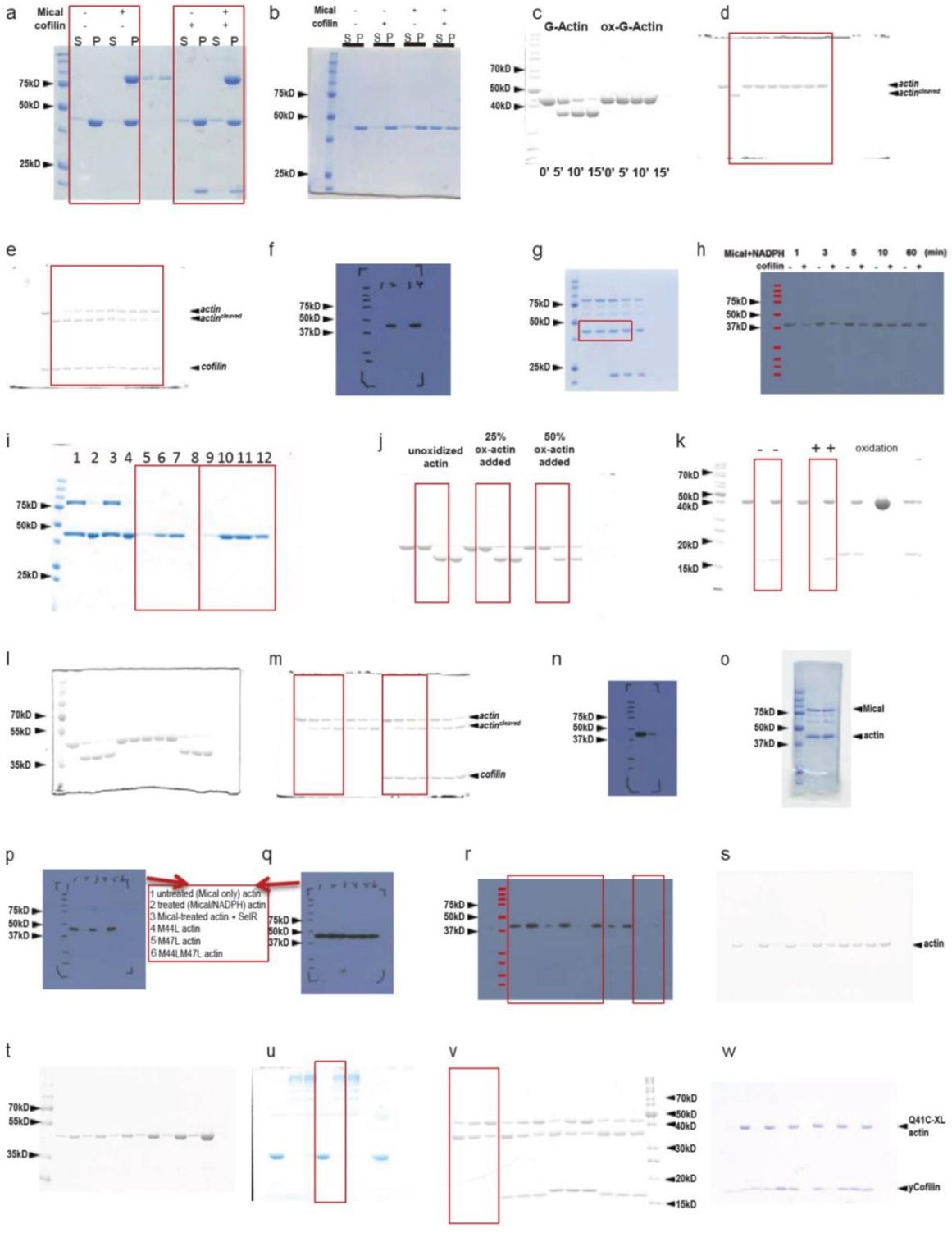

Figure 3.13. Uncropped Gels.

Uncropped gels for Figures 3.1d (a, red boxes), 3.1i (b), 3.2a (c), 3.2b[upper] (d, red boxes), 3.2b[lower] (e, red boxes), 3.2c[upper] (f), 3.2c[lower] (g, red boxes), 3.2d (h), 3.5a-b[inserts] (i, red boxes), 3.5f (j, red boxes), 3.6d (k, red boxes), 3.4a (l), 3.4c (m, red boxes), 3.4d[upper left] (n), 3.4d[lower left] (o), 3.4d[upper middle and right] (p), 3.4d[lower middle and right] (q), 3.4e (r, red boxes), 3.4f[upper] (s), 3.4f[lower] (t), 3.9b (u, red boxes), 3.9c (v, red boxes), and 3.9d (w).

Materials and Methods

Protein purification

Drosophila Mical^{redoxCH} construct (referred to as Mical in this study) (Hung et al. 2010; Wu, Hung, and Terman 2016) rabbit skeletal actin (Spudich and Watt 1971), Drosophila actin mutant M44L/M47L (Hung, Pak, and Terman 2011), yeast actin (Grintsevich et al. 2008), and human cofilin-1 (Grintsevich and Reisler 2014) were expressed and purified as previously described. Yeast cofilin was expressed and purified essentially as described (Bobkov et al. 2002). In brief, yeast cofilin expression was induced at OD_{600}=0.8 with 1mM IPTG and carried-out for 4 hours at 37°C. Cell lysate was loaded on QAE-52 column equilibrated with 20mM Tris–HCl (pH7.5 at 4°C) containing 1mM DTT, 0.2mM PMSF and cofilin was eluted with linear gradient of NaCl (0-500mM) in 5 column volumes. Cofilin containing fractions were then gel-filtered on HiLoad 16/60 Superdex 75 (Amersham Biosciences) column equilibrated with 20mM Tris–HCl (pH7.5 at 4°C), 200mM NaCl, 1mM DTT, 0.2mM PMSF. Purified cofilin was stored at -80°C.

Mical-oxidized actin purification

Rabbit skeletal G-actin was polymerized at 20μM for 1 hour at room temperature (RT) (buffer composition: 5mM Tris, 0.2mM $CaCl_2$, 0.5mM DTT, 0.2mM ATP, 2mM $MgCl_2$, 50mM KCl, pH8). Polymerized F-actin was then diluted to 2μM and supplemented with NADPH (0.4mM) and Mical 0.2μM (10:1 molar ratio, actin to Mical, unless stated otherwise). Mical-oxidation of actin was carried out for 2 hours at RT. Oxidation efficiency under chosen conditions was confirmed by mass spectrometry. After 2 hours any residual F-

actin was pelleted at 100,000g for 20 min at 4°C. Resulting supernatant containing Mical-oxidized actin (ox-actin) was dialyzed overnight into buffer G (GB_2): 2mM Tris, 0.2mM $CaCl_2$, 0.5mM DTT, 0.2mM ATP, pH 8. Actin was gel filtered using Superdex S200 16/60 column. Efficiency of oxidation was confirmed in subtilisin digestion assay (**Figure 3.4a**).

Mical-treated/oxidized pyrene actin was purified as described (Hung, Pak, and Terman 2011; Hung et al. 2013). To examine repolymerization of Mical-treated actin, the purified actin was resuspended to 2.3μM in GB_5, and polymerization was initiated with 2X polymerization buffer (10mM Tris-HCl pH 7.5, 0.1M KCl, 4mM $MgCl_2$, 2mM EGTA, 0.4mM ATP, 1mM DTT) to get a final concentration of 1.15μM actin. To further test the ability of Mical-treated actin to repolymerize, the purified actin was resuspended to 4.4μM or 8.8μM in GB_5, and polymerization was initiated as described above with 2X polymerization buffer (to yield a final concentration of actin at 2.2μM and 4.4μM, respectively). To determine whether Mical-oxidized actin might be reduced during its purification and storage, purified Mical-treated actin was polymerized (as described above), and then re-treated with 600nM of Mical and 200μM NADPH. Polymerization was monitored using either fluorescence or sedimentation assays (described below).

Critical concentration (Cc) determination

To determine the Cc, Mg-ATP-ox-actin was polymerized for 1 hour at RT by adding 10X polymerizing buffer, pH 6.8, 7.0, 7.5 or 8.0. Samples were diluted then into their corresponding 1X polymerizing buffer (pH 6.8 - 8.0), followed by 4°C overnight incubation. Supernatants and pellets were separated by ultracentrifugation (TLA100, 62K, 30 min, 4°C)

and analyzed by SDS-PAGE. Gels were stained with Coomassie Blue and densitometry was performed using Scion Image software. The intersects of these linear plots of pelleted actin ([*F-actin*]) versus total actin ([*Actin(total)*]) with the abscissa yielded Cc in μM. The following buffers were used for Cc experiments: **pH 6.8**: 20mM imidazole, pH 6.8, 2mM $MgCl_2$, 0.2mM EGTA, 50mM KCl, 0.2mM ATP, 0.5mM DTT; **pH 7.0**: 10mM Hepes, pH 7.0, 2mM $MgCl_2$, 0.4mM EGTA, 50mM KCl, 0.2mM ATP, 1mM DTT; **pH 7.5**: 5mM Tris, pH 7.5, 2mM $MgCl_2$, 0.2mM EGTA, 50mM KCl, 0.2mM ATP, 0.5mM DTT; **pH 8.0**: 10mM Tris, pH 8.0, 2mM $MgCl_2$, 50mM KCl, 1mM EGTA, 0.2mM ATP, 0.5mM DTT.

Protein labeling

Pyrene-labeled rabbit skeletal actin (RSA) (obtained from Cytoskeleton, Inc). RSA was labeled with Cy3-maleimide in thiol-free GB_5 (5mM Tris, pH 8, 0.2mM $CaCl_2$, 0.2mM ATP) using standard approach that included 1) actin polymerization with 2mM $MgCl_2$ and 50mM KCl for 30-60 min at RT; 2) labeling with Cy3 dye (1:1.5 (actin:dye) molar ratio for 2 hours on ice or overnight followed by addition of 1mM DTT; 3) pelleting (TLA110 rotor at 85,000 rpm for 20 min at 4°C); 4) depolymerization on dialysis followed by gel-filtration (Superdex S200 10/300 GL). Extent of labeling was calculated using extinction coefficient ε_{550}=130,000 $M^{-1}cm^{-1}$. Actin labeling with Alexa488-succinimidyl ester (SE) (Molecular Probes) was done essentially as described (Mahaffy and Pollard 2006) but Alexa488SE dye was added to F-actin in 3-7 fold excess (overnight, 4°C) and then carried out as described above for Cy3 actin. Actin concentration was measured by Bradford assay or by quantitative gels (Coomassie staining) employing known concentrations of unlabeled RSA as standard.

Alexa488SE-actin was used to obtain 100% oxidized labeled ox-actin (GB_2, 70:1 (actin:Mical) molar ratio, 100μM NADPH, 1 hour at RT). The resulting actin was dialyzed overnight against GB_2 then centrifuged (TLA100 rotor, 90,000 rpm, 30 min, 4°C). Oxidation was confirmed by limited proteolysis with subtilisin.

Yeast cofilin-KCK construct (for C-terminal labeling) was modified with Cy5-maleimide in buffer C: 5mM Tris, pH 7, 0.2mM $CaCl_2$, 50μM TCEP (1:1.5 (cofilin:Cy5-maleimide) molar ratio, 15 min at RT). Excess dye was removed using Zeba Desalt Spin Column (Pierce) equilibrated buffer C supplemented with 1mM DTT. Extinction coefficient of Cy5 was corrected for the solvent conditions (DMF vs [buffer C+1mM DTT]) as described (Grintsevich et al., 2010) and was estimated ε_{643}=121,420 $M^{-1}cm^{-1}$. Total concentration of labeled cofilin was measured by Bradford assay, using unlabeled WT yeast cofilin as a standard.

NADPH consumption

Different RSA concentrations (unlabeled; Cytoskeleton, Inc.) were polymerized as described (Hung, Pak, and Terman 2011). Each polymer sample (or actin buffer only) was then preincubated with cofilin (human cofilin-1; Cytoskeleton, Inc.) or cofilin buffer (10mM Tris pH 8.0, 10mM NaCl, 5% sucrose, 1% dextran, 1mM DTT) at pH of 6.8. NADPH consumption was measured essentially as described (Hung, Pak, and Terman 2011) with the decrease in the reduced form of NADPH determined from the decreased light absorption at 340 nm or alternatively (**Figure 3.4b**), by the decreased fluorescence signal at 460 nm (when excited at 340 nm).

Actin disassembly assays

Standard pyrene-actin and co-sedimentation assays using RSA (pyrene-labeled or unlabeled; Cytoskeleton, Inc.) were performed as described (Hung et al., 2010, 2011, 2013) with minor modifications to adjust sample pH. Actin in GB_5 buffer was mixed with 10X polymerization buffer (pH 6.8, 200mM Imidazole, 500mM KCl, 20mM $MgCl_2$, 2mM EGTA) to yield 10µM actin. This mixture was then incubated on ice overnight for actin polymerization and diluted the next day to 2.5µM actin. Then, each polymer sample was incubated with cofilin (or cofilin buffer), Mical (or Mical buffer), and/or NADPH, at pH of 6.8. In some cases, as described in the figures, the polymers were preincubated with cofilin (or cofilin buffer) or Mical (or Mical buffer). For pyrene-labeled actin, the fluorescence intensity was monitored immediately and over time at 407 nm (excitation at 365 nm) by a fluorescence spectrophotometer (Spectra max M2, Molecular Devices) as described (Hung, Pak, and Terman 2011). For co-sedimentation assays, the intensity of each of the stained bands in the pellet and soluble fraction was quantified by densitometry using Image J (NIH) (Hung, Pak, and Terman 2011) or Scion Image software.

Subtilisin limited proteolysis assay

Actin was polymerized at pH 6.8 for 1 hour at RT. Next, F-actin (3.5µM) was mixed with hCofilin-1 (3.5µM) or buffer (control) to form complexes. Samples were supplemented with NADPH (0.1mM). After removing unoxidized controls, reactions were started by addition of 25-50nM Mical. Aliquots of the samples were removed at selected time points

and oxidation was stopped by addition of 1.5mM NADP+ and 3.5μM of Kabiramide C (KabC, marine macrolide toxin, a kind gift from Dr. Gerard Marriott) (Klenchin et al. 2003). NADPH and KabC were also added to the control unoxidized actin/complexes. Samples were incubated overnight at 4°C for complete actin depolymerization. Then, reaction mixtures were digested with subtilisin (limited proteolysis conditions) at 1:200 subtilisin:actin w/w ratio for 20-30 min at RT. Subtilisin stock was prepared in 2mM Tris, 0.2mM $CaCl_2$ and used within 9 min. Limited digestion was started by adding 1μl of subtilisin solution to the samples (25μl) arranged in random order and stopped with PMSF (1mM). Samples were analyzed by SDS-PAGE (Coomassie stain). Densitometry analysis was performed using Scion Image software. Increased amounts of uncleaved actin reported on the accumulation of Mical-oxidized actin. After making corrections for undercleaved actin in unoxidized controls (~5-14%), the amount of Mical-oxidized actin was plotted vs oxidation time. We elected to use subtilisin:actin ratio that yields slightly undercleaved preparation in order to restrict proteolysis to a single site (47/48) on actin. We have found that a higher ratio of subtilisin to actin is needed for limited digestion of actin samples depolymerized under F-buffer conditions. For limited digestion of G-actin/G-actin-KabC in GB (pH 8) by subtilisin, we routinely used 1:1000 (w/w) ratio of subtilisin:actin.

Using this assay we quantified the amount of Mical-oxidized actin incorporated into copolymers under conditions closely mimicking those of our TIRF experiments (pH 6.8, 1μM of total actin, 30 min polymerization at RT). After polymerization, F-actin was pelleted (TLA110 rotor, 150,000g, 30 min, 4°C). Pellets were resuspended in 100μl of GB_2 and depolymerized overnight by dialysis (against GB_2), followed by a second high speed spin

(TLA100 rotor, 150,000g, 30 min, 4°C). Alternatively, samples were depolymerized by adding KabC (30μM) followed by a 3 hour dialysis against GB_2. Limited proteolysis with subtilisin was carried out at 1:1000 subtilisin:actin w/w ratio, for 15-20 min, at RT and stopped with PMSF (1mM). The resulting samples were analyzed by SDS-PAGE (Coomassie staining). The fraction of ox-actin in the sample was determined **(Figure 3.5f)** as described above.

Actin Met-44 and MetO-44 Specific Antibodies

We generated an antibody that preferentially recognized the unoxidized Met-44 residue of actin (**Figure 3.4d^{1}-d^{3}**). We also generated an antibody that specifically recognized the oxidized Met-44 residue on actin (MetO-44) (**Figure 3.2c**). These antibodies were used to observe the effect of cofilin on Mical-mediated oxidation of actin, by incubating 1.15μM F-actin for 1 hour at RT with 1.15μM cofilin or cofilin buffer only. Then, 50nM Mical and 100μM NADPH were added and the reaction was stopped at 1, 3, 5, and 10 minutes (or 1 hour) by adding loading buffer containing β-mercaptoethanol and boiling samples for 5 minutes. For Western blotting, all samples were loaded into a 12% SDS-PAGE, transferred to PVDF membrane, blocked with 5% non-fat milk/TBST buffer for 1 hour and then incubated for 1 hour with antiserum (pan actin antibody [C4; Millipore, 1:1000]; Actin Met-44 and Actin MetO-44 antibodies [1:500]).

TIRF microscopy assays

Copolymers of Mical-oxidized and unmodified actin were formed in flow chambers assembled with 25x75x1 glass slides (Fisherfinest, Premium Slides, Superfrost, 12-544-7) and 22×30-1.5 glass coverslips (Fisherbrand, 12-544-A). Coverslips were treated with polylysine PEG solution (1.25mg/ml in H_2O) for 4 min, rinsed 3 times with water and air-dried. Single flow chambers (V~30µl) were assembled using two layers of permanent double-sided Scotch tape. Before each experiment the flow chamber was treated with 2 chamber volumes (CV) of 1% Pluronic F127 solution (Sigma, P2443) (Gurel et al. 2014) for 3 min then equilibrated with 5 CV of 1xTIRF imaging buffer (20mM imidazole, 2mM $MgCl_2$, 50mM KCl, 0.2mM EGTA (pH 6.8) supplemented with 50mM DTT, 0.2mM ATP, 0.05mg/ml caseine, 20mM glucose, 0.25mg/ml glucose oxidase, 50µM catalase, 0.5% methyl cellulose). G-actin mixtures (10% Cy3b-maleimide labeled) were incubated for 3 min at RT with Mg/EGTA exchange buffer (0.1mM EGTA, 50µM $MgCl_2$) and the resulting mixture (3 CV) was introduced into the flow chamber. After 15 min of on-slide polymerization, the excess of actin monomers was removed with 1 CV of 1xTIRF imaging buffer. Since cofilin binds weaker to ADP-Pi-F-actin (compared to ADP-F-actin) (Muhlrad et al. 2006; Suarez et al. 2011), filaments were aged on the surface to allow for phosphate release. For severing experiments with yeast actin, at least 3 fields were imaged between minutes 29 and 30 to determine the average filaments length before cofilin severing. At 30 min time point from the start of actin polymerization, cofilin/buffer (2 CV) was introduced into the flow chamber and movies of severing were recorded. Copolymers containing 11% ox-actin weren't severed

upon buffer additions within the monitoring time. Images were acquired every 5 sec. Filaments were imaged using DMI6000 TIRF microscope (Leica).

Average filament length of on-slide grown ox-actin copolymers (0 and 11% oxidized) was compared to those pre-polymerized in tubes and applied to the polyK surface (related to **Figure 3.5h**). On-slide polymerization was carried out as described above. Images were collected after 16-17 min from the beginning of polymerization (immediately after the buffer wash, at 15 min of on-slide polymerization) (**Figure 3.5g**). Experiments with pre-polymerized ox-actin copolymers (0% and 11% oxidized) were performed as follows. Coverslips were treated with 1mg/ml polyK for 3 min, rinsed with mQ water and air-dried. Mg-ATP-G-actin (15% Cy3b labeled) was polymerized at 10μM by 1xKMEI6.8 buffer (20mM imidazole, 2mM $MgCl_2$, 50mM KCl, 0.2mM EGTA (pH 6.8)). F-actin samples were diluted to 8μM and mixed by pipetting up and down 2 times. The resulting mixtures were incubated 5 min at RT, followed by one step dilution into 1xKMEI6.8 buffer supplemented with 100mM DTT and 1μM phalloidin and mixing by inversion. Filaments' length was measured manually using JFilament plugin to Fiji (JFilament 2D).

Severing of fully oxidized actin by human cofilin-1 was examined as follows (related to **Figure 3.5a**). Flow chambers were assembled as described above. Untethered filaments were imaged on Pluronic F127-coated surface (Gurel et al., 2014) as described. F-actin-Cy3-maleimide (15% labeled) was polymerized in 1xKMEI6.8 buffer overnight at 4°C and used as F-actin seeds. Mical-oxidized (15% Alexa488SE) or unoxidized actin was mixed with 10nM of Cy3-F-actin seeds in 1xTIRF imaging buffer and polymerized for 20 min on slides. After 20 min, unpolymerized monomers were washed with 1xTIRF buffer. To test for

severing, 10nM of human cofilin-1 in 1xTIRF buffer was introduced into the flow chambers. Filaments fragmentation induced by Mical in the presence of NADPH was monitored under the same conditions (**Figure 3.7a**). Unoxidized filaments (15% Alexa488SE) were grown in the flow chambers then Mical (55nM)/NADPH (100μM) were introduced into the flow chamber simultaneously washing out the remaining actin monomers.

Cofilin clustering on intact filaments and copolymers with ox-actin (11%) was imaged using two-color TIRF microscopy. Actin (Alexa488-SE, 23% labeled) and yeast cofilin (Cy5-maleimide labeled) were copolymerized in flow chambers prepared as described above and imaged, unattached, on Pluronic F127-coated surface (Gurel et al. 2014). Co-polymerization was started by simultaneous addition of cofilin-Cy5 and polymerizing salts to Mg-ATP-G-actin.

Analysis of cofilin severing

Fiji (Image J) software was employed for movie processing. Background subtraction was done using rolling ball radius algorithm (routinely 10 pxls). Total filaments' length (L_0) was estimated using the first frame recorded after cofilin addition (L_0 (μm)=sum of the lengths of all filaments in frame #1). Filaments' length was measured manually using JFilament plugin to Fiji (JFilament 2D). Bundled filaments were excluded from the analysis. To quantify cofilin severing of F-actin, the number of severing events (cuts) was counted manually for each frame, starting from frame #2. Cumulative number of cuts divided by L_0 (cuts/μm) was plotted versus time. Linear segments of the obtained dependencies were used

to determine the rates of F-actin severing by cofilin (**Figure 3.7e**). Between 31 and 45 filaments were analyzed in each movie.

F-actin cross-linking

Disulfide cross-linking of Q41C yeast actin mutant was carried out as follows. DTT-free Ca-ATP-Q41C actin was polymerized by adding 0.1 volume of polymerizing buffer (20mM imidazole, 50mM KCl, 2mM $MgCl_2$) for 1 hour at RT. Disulfide cross-linking in QC-F-actin was triggered by addition of $CuSO_4$ solution (in water) to F-actin in 1:1.5 (actin:Cu) molar ratio and carried out for 1 hour at RT. Cross-linked samples were supplemented with 1mM EGTA and dialyzed against 20mM imidazole, 50mM KCl, 2mM $MgCl_2$, 1mM EGTA, 0.2mM ATP for ≥3 hours. Efficiency of cross-linking was confirmed by SDS-PAGE analysis under non-reducing conditions in the presence of NEM. Cross-linked and uncross-linked QC-F-actin and its cofilin complexes were subjected to Mical-mediated oxidation (140:1, molar ratio Actin:Mical, thiol-free Mical preparation) in the presence of 0.1mM NADPH under non-reducing (DTT-free) conditions for 1 hour at RT. Co-sedimentation with cofilin was performed as described above (TLA100 rotor, 150,000g, 30 min, 4°C).

N-(4-azido-2-nitrophenyl) putrescine (ANP) cross-linking was carried out as described (Kim et al., 2002). In brief, thiol-free skeletal G-actin was incubated with ANP (1:8, actin:ANP molar ratio) and transglutaminase (2 units per 1mg of actin) in DTT-free GB_2 (pH 8) for 2 hours at RT. Actin was centrifuged to remove any aggregates (21,000g, 10 min, 4°C) and then polymerized (20mM imidazole, pH 6.8, 50mM KCl, 2mM $MgCl_2$,

0.2mM ATP, 100μM NADPH). Mical-mediated oxidation was started with the addition of thiol-free Mical to ANP-F-actin (1:140, Mical:actin molar ratio) for 1 hour at RT. Prior to photoactivation and cross-linking, the extent of Mical-mediated oxidation was assessed by subtilisin digestion. Cross-linking (between Gln 41-Cys 374) in Mical-oxidized and unoxidized ANP-F-actin was triggered by UV exposure (20 min at RT) and stopped with 1mM DTT. Mical-oxidized and unoxidized ANP-F-actin yielded the same cross-linking patterns. Co-sedimentation with human cofilin-1 and gel analysis was performed as described above.

In vivo data

Expression analysis, F-actin organization, and bristle cell remodeling was examined and quantified as described (Hung et al. 2010; Hung et al. 2013). Embryos were collected, processed, staged, dissected, and analyzed for axon guidance defects using an antibody to Fasciclin II (1:4, 1D4 supernatant (Van Vactor et al. 1993), Developmental Studies Hybridoma Bank) as described (Huang et al. 2007; Terman et al. 2002; Yang and Terman 2012; Yu et al. 1998). Males and females of Drosophila embryos, pupae, and adults were used.

Statistics and reproducibility

For each representative image, gel, immunoblot, graph, movie, or in vivo experiment, the experiments were repeated at least two separate independent times and there were no limitations in repeatability. At least two independent protein purifications and multiple

independent actin biochemical experiments were performed with similar results including reproducing the effects in Figure 3.1b and Figure 3.1g-h independently in both of our labs using non-overlapping/independent sets of reagents. No statistical method was used to predetermine the sample size, which was based on what is published in the field. Differences between experimental and control animal conditions were large, with little variability – and so the sample size was larger than needed to ensure adequate power to detect an effect.

Animal studies were based on pre-established criteria to compare against age-matched animals. Animal experiments were not randomized. Animals of the correct genotype were determined and those collected of that genotype were included as data. For genetic experiments, in which the genotype needed to be determined based on different Drosophila genetic/chromosome markers, blinding was not employed. The figure legends list the sample size for each experiment. To the best of our knowledge the statistical tests are justified as appropriate. No cell lines were used in this study.

CHAPTER FOUR

SPATIOTEMPORAL TARGETING OF TROPOMYOSIN PROTECTS NEW ACTIN-RICH CELLULAR PROTRUSIONS FROM DISASSEMBLY

All work performed by HGY.

Abstract

Multiple cellular behaviors depend on the stability and rearrangeability of the actin cytoskeleton. The well-studied actin-binding protein tropomyosin is known to decorate actin filaments within specific cellular compartments and at different developmental stages to affect the stability of actin filaments. Tropomyosins also synergize and compete with other well-characterized actin binding proteins revealing its complex functions and interactions in regulating actin dynamics. Here we find that tropomyosin strongly modulates the ability of F-actin oxidizing protein Mical to disassemble F-actin. It holds the filaments together protecting them from Mical-mediated disassembly but not from Mical-post-translational-mediated oxidation. Moreover, Mical can bind F-actin to a lesser degree in the presence of tropomyosin. Genetic analyses also revealed that tropomyosin controls Mical-mediated F-actin alterations and cellular remodeling – such that spatiotemporal targeting of different tropomyosins protects newly built actin-rich protrusions from Mical-mediated F-actin disassembly. Thus, these competitive interactions between Mical and tropomyosin provides a means to control the dismantling of actin structures, while also allowing for the generation of new actin-based cellular structures.

Introduction

The outgrowth, shaping, and interactions of cells and their membranous extensions underlie the formation and function of multiple tissues and organ systems. These changes in motility, morphology, and connectivity are accomplished by the targeted remodeling of the actin and microtubule cytoskeletons – and extracellular cues such as attractants and repellents have long been known to control this cellular remodeling (Tessier-Lavigne and Goodman 1996; Hung and Terman 2011). Yet, how these cues specify which cytoskeletal regions – such as those present in closely adjacent portions of elongating axonal growth cones and dendritic spines – should be specifically torn down or built-up is poorly understood. In much the same way, how these specific subcellular regions quickly transition from a program of cytoskeletal disassembly to one of assembly is also unclear. Such precise control of cytoskeletal architecture is essential however for cell-cell and tissue-level communications during development and adulthood.

To try to make inroads into these and other related problems, we have been using the Drosophila model system and investigating how one of the largest families of guidance cues (Semaphorins (Semas)) exert their effects. Semas with over 20 members conserved from invertebrates to humans are best known for their inhibitory/repulsive effects on cells – working through Plexin transmembrane receptors to elicit destabilizing effects on actin filaments (F-actin) that include a loss of F-actin and the decreased ability to polymerize new F-actin (Alto and Terman 2017). Using these model system approaches we recently

identified a conserved family of flavoprotein oxidoreductase (Redox) enzymes, the MICALs, that work downstream of Semas/Plexins to directly disassemble F-actin and inhibit actin polymerization (Terman et al. 2002; Hung et al. 2010; Hung, Pak, and Terman 2011). Our results have also gone on to determine that this Mical-mediated actin regulatory process is reversible by a specific methionine sulfoxide reductase enzyme called SelR (Hung et al. 2013; Lee et al. 2013) and that this Mical/SelR actin regulatory process combines with classical actin regulatory and signaling pathways to direct multiple cellular events *in vivo* (Grintsevich et al. 2016; Fremont et al. 2017; Yoon et al. 2017; Grintsevich et al. 2017). Thus, we have focused on better understanding this new Semaphorin-Mical actin regulatory system and how actin networks are remodeled by it.

Now, in the process of conducting a biochemical screen to look for proteins that modulate Mical-mediated F-actin disassembly, we identified tropomyosin (Tm), a protein well-known to decorate actin filaments (Gunning et al. 2015; Brettle, Patel, and Fath 2016), as decreasing Mical's ability to disassemble F-actin. This tropomyosin-mediated inhibition also occurs *in vivo*, protecting specific F-actin networks from Mical-mediated remodeling. Moreover, our observations reveal that following Mical-mediated F-actin disassembly in specific subcellular regions, tropomyosin becomes enriched in these new regions, protecting actin and allowing the assembly of new F-actin structures.

Results

Tropomyosin slows Mical-mediated F-actin disassembly

Mical is a redox enzyme that induces F-actin disassembly by oxidizing actin post-translationally. In particular, Mical is activated in the presence of F-actin, which triggers the

consumption of Mical's co-enzyme NADPH and subsequently the specific oxidation of the Met-44 and Met-47 amino acid residues of actin to induce F-actin disassembly (Hung, Pak, and Terman 2011). This Mical-mediated F-actin disassembly has thus provided a simple biochemical assay to search for proteins that affect Mical's activity – including those that might work by binding on or near the site where Mical oxidizes actin. In particular, this biochemical screen employed pyrene-labeled actin, where the fluorescence is higher when actin is present in filaments, so as to gauge in real-time proteins that affect Mical-mediated F-actin disassembly (**Figure 4.1a**). Starting with pyrene-labeled F-actin, we could detect Mical's ability to disassemble its substrate F-actin in the absence of candidate proteins (**Figure 4.1a,b**). Strikingly, we found that the well-known actin stabilizing factor – tropomyosin – which on its own had no effects on F-actin disassembly (**Figure 4.1c**), significantly slowed Mical-mediated F-actin disassembly (**Figure 4.1d,e**). To further examine tropomyosin's effect on Mical-mediated F-actin disassembly, we performed sedimentation assays – where we could examine the ability of F-actin to sediment, thus indicating it is in a polymerized form (**Figure 4.1f**). Similar to our results with pyrene-actin, our sedimentation assays revealed that tropomyosin significantly slowed/decreased the ability of Mical to disassemble F-actin (**Figure 4.1f**). Therefore, our observations reveal that tropomyosin antagonizes Mical-mediated F-actin disassembly.

Tropomyosin interferes with Mical's ability to interact with F-actin

Tropomyosin is known to decorate and stabilize actin filaments by binding along seven subunits of actin (Perry 2001; Li et al. 2011; Memo and Marston 2013). Thus, we

wondered if tropomyosin might be slowing Mical's F-actin disassembling activity by interfering with Mical's ability to bind F-actin. To test for this possibility, we performed co-sedimentation assays, looking at the ability of Mical to sediment (associate) with F-actin (**Figure 4.1g**). Our results revealed that tropomyosin strongly decreased the ability of Mical to associate with F-actin (**Figure 4.1g**). Thus, tropomyosin interferes with Mical's ability to interact with F-actin, thereby slowing Mical-mediated F-actin disassembly.

Tropomyosin stabilizes Mical-oxidized actin filaments and prevents their disassembly

Mical specifically oxidizes the Met-44 and Met-47 residues of actin to induce F-actin disassembly (Hung, Pak, and Terman 2011). Therefore, to further investigate the means by which tropomyosin slows Mical-mediated F-actin disassembly, we examined the ability of Mical to oxidize its F-actin substrate. Interestingly, using an antibody that specifically recognizes the Mical-stereospecifically-oxidized Met44 residue of actin (MetO-44) (Grintsevich et al. 2016), we did not observe any differences in the ability of Mical to oxidize F-actin (**Figure 4.1h, upper**). Thus, although tropomyosin decreases the ability of Mical to associate with F-actin, the amount of Mical that associates with F-actin is sufficient to oxidize F-actin in a manner that is indistinguishable from normal.

We thus wondered why there was less Mical-mediated F-actin disassembly in the presence of tropomyosin, although the amount of Mical-mediated actin oxidation did not decrease (**Figure 4.1d-f**). To further explore this discrepancy, we looked at the amount of Mical-oxidized actin in the supernatant (i.e., G-actin) versus the pellet (i.e., F-actin). In the absence of tropomyosin, all the Mical-oxidized actin was present in the supernatant (**Figure**

4.1h, lower and please see **Figure 4.1f** for Coomassie-stained controls). However, in the presence of tropomyosin, Mical-oxidized actin was present in the pellet fraction (**Figure 4.1h, lower** and please see **Figure 4.1f** for Coomassie-stained controls). Strikingly, these results revealed that actin in the presence of tropomyosin – although oxidized by Mical – was not disassembled. Thus, tropomyosin antagonizes Mical-mediated F-actin disassembly not only by restricting Mical's binding to filaments (interaction with its Met44 substrate residue on actin), but by also holding Mical-oxidized actin together in filaments. Thus, tropomyosin prevents Mical from disassembling but not from oxidizing F-actin, and this competitive interaction depends on tropomyosin's ability to physically stabilize Mical-oxidized actin filaments (**Figure 4.1i**).

Tropomyosin controls Mical-mediated F-actin disassembly and cellular remodeling in vivo

In light of our *in vitro* results using purified proteins, we wondered if tropomyosin and Mical interact to regulate actin disassembly and cellular remodeling *in vivo*. Tropomyosin is known to decorate actin filaments with its various isoforms within specific cellular compartments and at different developmental stages (Gunning et al. 2005; Gunning, O'Neill, and Hardeman 2008). In the Drosophila model system, for example, there are two *tropomyosin* genes, *Tropomyosin 1* (*Tm1*) and *Tropomyosin 2* (*Tm2*), which give rise to 17 and 6 transcripts, respectively. The canonical cytoskeletal isoforms of Tm1, Tm1A/L (Cho et al. 2016), show 60% identity to Tm2 (**Figure 4.2a;** (Karlik and Fyrberg 1986)). Yet, the two Drosophila tropomyosins have been shown to be involved in different cellular events and expressed in different cells – Tm2 being more prominent in muscle (Karlik and Fyrberg

1986), while Tm1 is more prominent in other tissues (Basi, Boardman, and Storti 1984; Karlik, Coutu, and Fyrberg 1984; Karlik and Fyrberg 1986).

To investigate whether tropomyosin also modulates Mical-mediated F-actin dynamics *in vivo*, we turned to the high-resolution Drosophila bristle model, where stereotypical changes to F-actin are required to extend a process (**Figure 4.2b;** (Tilney and DeRosier 2005; Sutherland and Witke 1999; Hung and Terman 2011)). Moreover, raising the levels of Mical specifically in bristles induces F-actin disassembly and easily quantifiable bristle branching (**Figure 4.2c;** (Hung et al. 2010)), and thus provides a readily observable assay for in vivo effects on Mical-mediated F-actin remodeling. Examining the expression of both *Tm1* and *Tm2* revealed that *Tm1* was prominently expressed in the bristle (**Figure 4.2d**), whereas Tm2 showed no discernable bristle expression (data not shown). Moreover, removing even a single copy of *Tm1* in this system (i.e., generating *Tm1* heterozygotes), enhanced Mical-mediated F-actin reorganization and bristle remodeling (compare **Figure 4.2e** with **Figure 4.2c; Figure 4.2f, g**), whereas removing *Tm2* had no significant effect on these Mical-mediated effects (**Figure 4.2f,g**). Thus, Tm1 modulates Mical-mediated F-actin dynamics *in vivo*. Moreover, consistent with the antagonistic interaction between tropomyosin and Mical we observed *in vitro* using purified proteins, decreasing the levels of tropomyosin *in vivo* increases Mical's effects on F-actin disassembly.

Differential effects of Tropomyosins on Mical-mediated cellular remodeling in vivo

As a complementary approach to our tropomyosin loss-of-function studies described above, we next wondered if increasing the levels of tropomyosin inhibits Mical-mediated F-

actin disassembly *in vivo*. To address this, we chose a representative form of Tm1 from each of the three groups of Tm1 splice forms (Tm1L, A and I) (**Figure 4.3a**). Surprisingly, increasing Tm1 levels enhanced Mical-mediated cellular remodeling (**Figure 4.3b, d-e**). Thus, paradoxically, increasing Tm1 levels, similar to decreasing Tm1 levels, resulted in a significant enhancement of Mical-mediated cellular remodeling. Interestingly, in contrast to increasing Tm1 levels, increasing Tm2 levels significantly suppressed Mical-mediated cellular remodeling (**Figure 4.3c,** quantified in **Figure 4.3d-e**). Thus, increasing the levels of Tm1 and Tm2 resulted in opposite effects on Mical-mediated cellular remodeling (**Figure 4.3f**).

Differential subcellular targeting of Tropomyosins in response to Mical-mediated F-actin disassembly stabilizes new actin-rich protrusions

To attempt to understand the mechanisms underlying the difference between Tm1 and Tm2 effects on Mical-mediated cellular remodeling, we looked at the bristle localization of Tm1 and Tm2 when we increased their levels in bristles. Overexpression of Tm1 or Tm2 in bristles resulted in a similar non-descript localization (**Figure 4.3g**), with each of them showing a uniform distribution in the developing bristle. Strikingly, however, in combination with increasing the levels of Mical, Tm1 redistributed and showed enrichment in specific areas of the bristle (**Figure 4.3h-i**). In particular, in combination with Mical-mediated cellular remodeling, Tm1 initially became enriched at the bristle tip and then redistributed into the branch that formed as a result of Mical's actions (**Figure 4.3h-i**). In contrast to Tm1 (and including different isoforms of Tm1 (Tm1L and Tm1A)), which redistributed in

response to Mical-mediated F-actin disassembly, Tm2 did not redistribute and showed uniform localization throughout the bristle (**Figure 4.3i**). Thus, these differences in Tm1 and Tm2's redistribution into the branch provides an understanding of why increasing Tm1 but not Tm2's levels have different effects on Mical-driven cellular remodeling (**Figure 4.3b-e**). Moreover, these results, together with our *in vitro* results, indicate that tropomyosin protects actin including in newly formed branches from Mical-mediated disassembly and thereby stabilizes actin-rich cellular protrusions.

Discussion

Neuronal form and function is dictated through the dynamic actions of actin – with its ability to transition from a 43kDa monomeric state (globular (G) actin) into a linear double-stranded helical organization (filamentous (F) actin). Such linear arrays of actin can then be further transformed with the aid of various actin-regulatory proteins into higher order structures, including bundled F-actin and 3-D branched actin networks (Pollard 2016). This interplay between polymerizing actin and its organization into complicated networks drives the formation of diverse cellular structures (Pollard 2016; Blanchoin et al. 2014). Here, we have found that interactions between the well-studied actin regulatory protein tropomyosin and the F-actin disassembly protein Mical, dictate the formation and stability of F-actin networks. In particular, tropomyosin strongly inhibits Mical's ability to disassemble F-actin. This competitive interaction between Mical and tropomyosin depends on tropomyosin's ability to stabilize Mical-oxidized actin filaments. Moreover, in addition to limiting Mical's destructive effects on F-actin, tropomyosin stabilizes new actin-rich protrusions that form as

a result of Mical-mediated F-actin disassembly. Thus, Mical–tropomyosin interactions are crucial for the control of cellular morphology and behavior.

My findings also put the mechanisms of action of both Mical and tropomyosin into a broader picture. As previously noted (Chhabra and Higgs 2007; Hung and Terman 2011), for an actin-rich protrusion to form, there needs to occur a dynamic balance, namely F-actin disassembly followed by a means of formation and stabilization of the actin filaments in the newly-built protrusion. So Mical and tropomyosin represent a means to establish this balance between the dual forces of destruction and construction/maintenance. Thus, the competitive interaction I have observed between Mical and tropomyosin provides a broader and new understanding on how actin networks are dismantled and then stabilized – and suggests a mechanism to spatiotemporally remodel actin-based cellular structures (including into more complex forms). Furthermore this would give a way to weaken or protect certain actin networks, such as the ones in specific migrating cells, navigating growth cones, dendritic spines, and synaptic boutons. Moreover, as actin dynamics underlie specific cellular behaviors and events in both development and disease, this Mical–tropomyosin-mediated dismantling/stabilization effect would be positioned to control important physiological behaviors like learning and memory as well as pathological events that occur during both aging and trauma/disease.

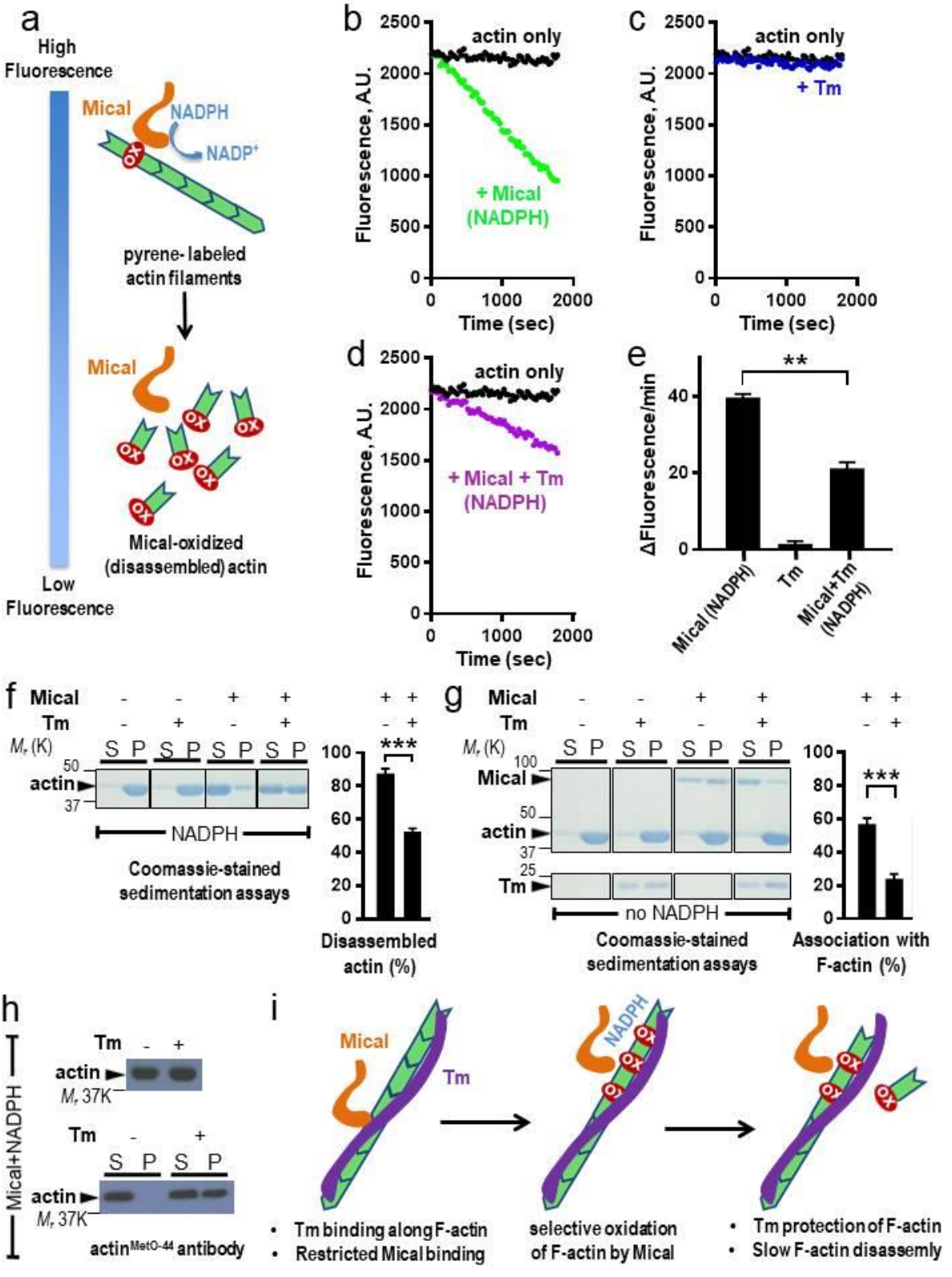
a
High Fluorescence
Mical
NADPH
NADP+
ox
pyrene-labeled actin filaments
Mical
Mical-oxidized (disassembled) actin
Low Fluorescence
b
actin only
+ Mical (NADPH)
Fluorescence, A.U.
Time (sec)
c
actin only
+ Tm
Fluorescence, A.U.
Time (sec)
d
actin only
+ Mical + Tm (NADPH)
Fluorescence, A.U.
Time (sec)
e
**
ΔFluorescence/min
Mical (NADPH)
Tm
Mical+Tm (NADPH)
f
Mical
Tm
M, (K)
S P S P S P S P
50
actin
37
NADPH
Coomassie-stained sedimentation assays
***
Disassembled actin (%)
g
Mical
Tm
M, (K)
100
Mical
50
actin
37
25
Tm
no NADPH
Coomassie-stained sedimentation assays
***
Association with F-actin (%)
h
Mical+NADPH
Tm
actin
M, 37K
Tm
S P S P
actin
M, 37K
actinMetO-44 antibody
i
Mical
Tm
NADPH
ox
• Tm binding along F-actin
• Restricted Mical binding
selective oxidation of F-actin by Mical
• Tm protection of F-actin
• Slow F-actin disassemly

Figure 4.1. Tropomyosin slows Mical-mediated F-actin disassembly by stabilizing Mical-oxidized actin.

(a-b) Mical oxidizes and disassembles F-actin using its coenzyme NADPH, where pyrene-actin fluorescence is higher in the polymerized state. **(c-e)** Tropomyosin, which alone has no effect on F-actin disassembly (c), slows Mical-mediated F-actin disassembly with a significant (2-fold) decrease in pyrene fluorescence change per minute (b, d, and e). [Actin]=2.3 µM; [Tm]=2.3 µM; [Mical]=600 nM. NADPH=100 µM; n=2 separate experiments per condition. mean +/- s.e.m., Student's t-test (two-tailed); **P=0.0095. **(f)** Tropomyosin decreases Mical-mediated F-actin disassembly, as seen by sedimentation analysis. Note the amount of pelleted actin in the presence or absence of Tm. S, soluble (G-actin); P, pellet (F-actin). [Actin]=6.25 µM; [Tm]=3 µM; [Mical]=600 nM. NADPH=100 µM; n=3 separate experiments per condition. mean +/- s.e.m., Student's t-test (two-tailed); ***P=0.0006. **(g)** Tropomyosin inhibits Mical binding to F-actin, as revealed using co-sedimentation assays and the percentage of pelleted Mical in the presence or absence of Tm. [Actin]=6.25 µM; [Tm]=3 µM; [Mical]=600 nM.; no NADPH present; n=3 separate experiments per condition. mean +/- s.e.m., Student's t-test (two-tailed); ***P=0.0003. **(h)** Tropomyosin does not decrease the total amount of Mical-mediated actin oxidation, but keeps Mical-oxidized actin as a part of F-actin. (Top) Whole samples in which the total amount of Mical-oxidized actin is determined following incubation of purified F-actin with Tm in the presence or absence of Mical. (Bottom) Following incubation of F-actin with Mical in the presence or absence of Tm, samples were centrifuged to examine both supernatant (G-actin) and pellet (F-actin). Note that there is no Mical-oxidized actin in the pellet (F-actin) in the absence of Tm, but there is in the presence of Tm. Please also see **Figure 4.1f-right** half for Coomassie stained controls). [Actin]=6.25 µM; [Tm]=3 µM; [Mical]=600 nM. NADPH=100 µM; n=2 separate experiments per condition. **(i)** A model based on our *in vitro* results indicating that tropomyosin decreases Mical-mediated F-actin disassembly by stabilizing Mical-oxidized actin filaments. See also main text.

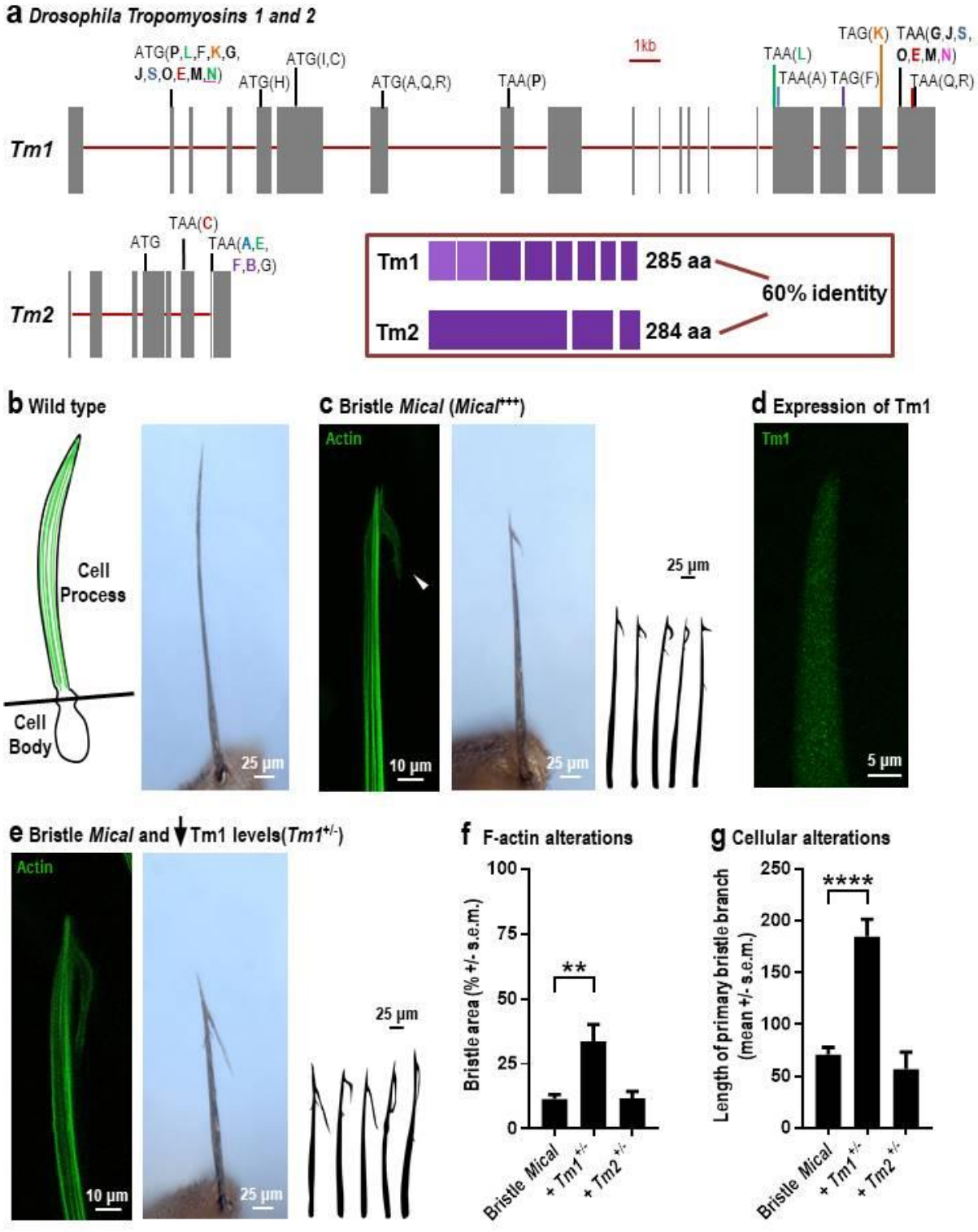
a Drosophila Tropomyosins 1 and 2
ATG(P,L,F,K,G, J,S,O,E,M,N)
ATG(H)
ATG(I,C)
ATG(A,Q,R)
TAA(P)
1kb
TAA(L)
TAA(A)
TAG(K)
TAG(F)
TAA(G,J,S, O,E,M,N)
TAA(Q,R)
Tm1
ATG
TAA(C)
TAA(A,E, F,B,G)
Tm2
Tm1
285 aa
60% identity
Tm2
284 aa
b Wild type
Cell Process
Cell Body
25 µm
c Bristle Mical (Mical+++)
Actin
10 µm
25 µm
25 µm
d Expression of Tm1
Tm1
5 µm
e Bristle Mical and Tm1 levels(Tm1+/-)
Actin
10 µm
25 µm
25 µm
f F-actin alterations
Bristle area (% +/- s.e.m.)
100
75
50
25
0
**
Bristle Mical
+ Tm1+/-
+ Tm2+/-
g Cellular alterations
Length of primary bristle branch (mean +/- s.e.m.)
250
200
150
100
50
0
****
Bristle Mical
+ Tm1+/-
+ Tm2+/-

Figure 4.2. Tropomyosin 1 counteracts Mical-mediated cellular modeling in vivo.

(a) *Drosophila* Tropomyosins 1 and 2 genomic organizations and protein models of the canonical forms. *Tm1* has a very complex gene structure with 4 start codons and 7 stop codons leading to 17 different transcripts. *Tm2* has a simpler genomic organization with one start codon and two stop codons leading to 6 mostly identical transcripts. However, the canonical Tm1 splice forms (A/L) (Cho et al. 2016) and Tm2 have similar lengths and 60% amino acid sequence identity. **(b)** *Drosophila* bristles are large cells that require actin to extend a process that is slightly curved and unbranched. **(c)** When the levels of Mical are increased specifically in bristles, F-actin disassembly occurs at the tip (arrowhead, left panel) that results in branch formation **(**middle and left panels**)**. **(d)** Tm1 is expressed in bristle cells and localizes within the bristle process. **(e)** Decreasing *Tm1* levels in the bristle (*Tm1* heterozygote genetic background ($Tm1^{+/-}$)) enhances Mical-induced F-actin alterations and lengthens Mical-induced bristle branches. **(f-g)** Quantification of data shown in **c**, **e** and with $Tm2^{+/-}$. Note, that in contrast to *Tm1*, decreasing *Tm2* levels in the bristle (*Tm2* heterozygote genetic background ($Tm2^{+/-}$)) does not have a significant effect on Mical-induced bristle phenotype. n=20 bristle cells assessed across 10 animals per genotype for **(f)** and n>100 bristle cells assessed across >100 animals per genotype for **(g)**. mean +/- s.e.m., Student's t-test (two-tailed); **P=0.0023, ****P<0.0001.All genotypes are heterozygous (*B11-GAL4/+*, *UAS:Mical*/+, and/or *mutations*/+). One copy of *UAS:*^{GFP}*actin* was used when visualizing F-actin. The *B11-GAL4*, *UAS:Mical*, and *UAS:*^{GFP}*actin* lines were as previously described (Hung et al. 2010; Hung, Pak, and Terman 2011). For Tm1 and Tm2 expression analysis, we crossed *B11-GAL4* flies to *Tm1* and *Tm2* GFP-trap lines and their expression and localization was imaged in pupal progeny. For testing Tm1 and Tm2's effect on Mical-mediated F-actin organization (imaged in pupal progeny) and cell remodeling (imaged in adult progeny), we crossed the *B11-GAL4, UAS:Mical* and *B11-GAL4, UAS:Mical, UAS:*^{GFP}*actin* line with the following lines: *FRT82B, Tm1null* fly line (a loss-of-function/"knockout" mutant due to HR or CRISPR deletion of a 135 basepair gene region that is common to all isoforms (Cho et al. 2016)) and $Tm2^{(\Delta 8\text{-}261)}$ fly line (a loss-of-function/"knockout" mutant due to CRISPR deletion of a gene region that corresponds to 254 aminoacids of the whole 284aa-long Tm2 protein (Williams et al. 2015)). We also used the following publicly available GFP-trap *Tm1* and *Tm2* lines, which showed detectable and undetectable expression in the bristle, respectively: *Tm1[KM0210]* and *Tm2[ZCL2456]*.

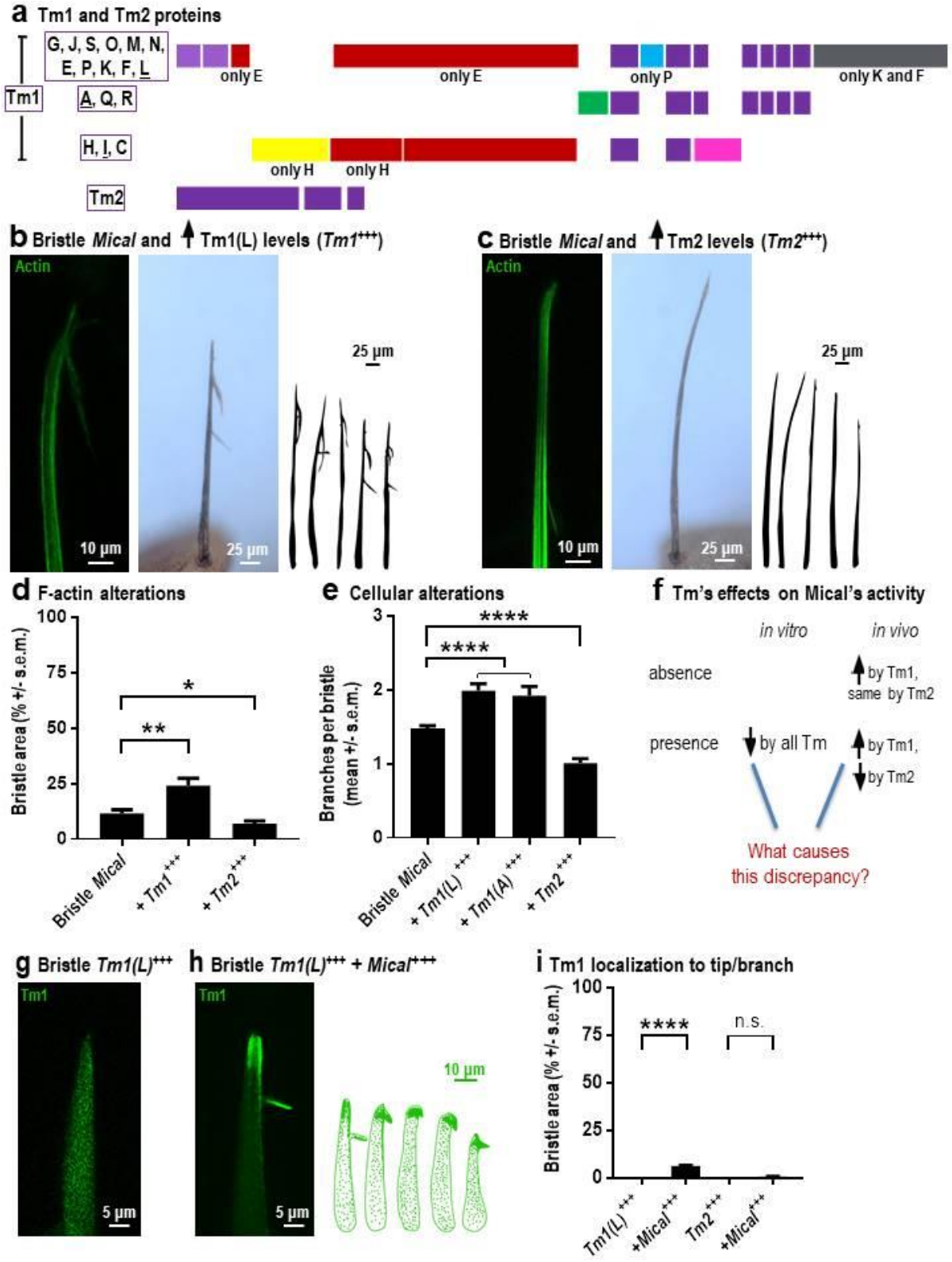
a Tm1 and Tm2 proteins
G, J, S, O, M, N, E, P, K, F, L
A, Q, R
H, I, C
Tm1
Tm2
only E
only E
only P
only K and F
only H
only H
b Bristle Mical and Tm1(L) levels (Tm1+++)
Actin
10 µm
25 µm
25 µm
c Bristle Mical and Tm2 levels (Tm2+++)
Actin
10 µm
25 µm
25 µm
d F-actin alterations
Bristle area (% +/- s.e.m.)
100
75
50
25
0
*
**
Bristle Mical
+ Tm1+++
+ Tm2+++
e Cellular alterations
Branches per bristle (mean +/- s.e.m.)
3
2
1
0
****
****
Bristle Mical
+ Tm1(L)+++
+ Tm1(A)+++
+ Tm2+++
f Tm's effects on Mical's activity
in vitro
in vivo
absence
by Tm1, same by Tm2
presence
by all Tm
by Tm1,
by Tm2
What causes this discrepancy?
g Bristle Tm1(L)+++
Tm1
5 µm
h Bristle Tm1(L)+++ + Mical+++
Tm1
5 µm
10 µm
i Tm1 localization to tip/branch
Bristle area (% +/- s.e.m.)
100
75
50
25
0
****
n.s.
Tm1(L)+++
+Mical+++
Tm2+++
+Mical+++

Figure 4.3. Tropomyosin 1 stabilizes Mical-induced F-actin protrusions.

(a) *Drosophila* Tropomyosins 1 and 2 protein models. Tm1 L/A, the canonical cytoskeletal isoforms. Tm1 I/C, the atypical isoforms. Tm2 is 60% identical to canonical Tm1 isoforms (Please also see red box in **Figure 4.2a**). **(b)** Increasing *Tm1* levels in the bristle (Shown here $Tm1L^{+++}$, not shown here but also $Tm1A^{+++}$ and $Tm1I^{+++}$) enhances Mical-induced F-actin alterations and results in more and/or longer branches. **(c)** Increasing *Tm2* levels in the bristle ($Tm2^{+++}$) suppresses Mical-induced F-actin alterations and results in fewer and/or shorter branches. **(d-e)** Quantification of data shown at **b**, **c** and additionally for $Tm1A^{+++}$. n=20 bristle cells assessed across 10 animals per genotype for **(d)** and n>100 bristle cells assessed across >100 animals per genotype for **(e)**. mean +/- s.e.m., Student's t-test (two-tailed); *P=0.0342 **P=0.0016, ****P<0.0001. **(f)** Summary of Tm's effects on Mical's activity indicates differences between Tm1's *in vitro* and *in vivo* results that should be further explored. **(g-i)** Mical-induced F-actin disassembly induces changes to the localization of Tm1, including its enrichment to the tip and newly formed branches. **(g)** Tm1 (L), on its own, is uniformly distributed throughout the bristle cell. **(h)** In the presence of Mical, Tm1 (L) shows a redistribution and enrichment to the bristle tip and out to the branches. **(i)** Quantification of Tm1 (L) and Tm2 to the tip and branch of bristles as percentage in bristle area. Note, that unlike Tm1, Tm2 does not redistribute in response to Mical. n=24 bristle cells assessed across 12 animals per genotype mean percentage +/- s.e.m., Student's t-test (two-tailed); ****P<0.0001.All genotypes are heterozygous (*B11-GAL4*/+, *UAS:Mical*/+, *UAS:Tm1*/+ and/or *UAS:Tm2*/+). One copy of $UAS:^{GFP}actin$ was used when visualizing F-actin. The *B11-GAL4*, *UAS:Mical*, and $UAS:^{GFP}actin$ lines were as previously described (Hung et al. 2010; Hung, Pak, and Terman 2011). For testing Tm1 and Tm2's effect on Mical-mediated F-actin organization (imaged in pupal progeny) and cell remodeling (imaged in adult progeny), we crossed the *B11-GAL4*, *UAS:Mical* and *B11-GAL4*, *UAS:Mical*, $UAS:^{GFP}actin$ line with the following lines: *UASt-eGFP-Tm1L*, *UASt -Tm1A-GFP*, *UASt-eGFP-Tm1I* fly lines (transgenic fly lines generated by standard transgenic insertion methods (Cho et al. 2016)) and *Tm2-cDNA.GFP* fly line (a transgenic fly line generated by standard transgenic insertion methods (Williams et al. 2015)).

Materials and Methods

Protein purification

Drosophila Mical^{redoxCH} construct (referred to as Mical in this study) (Hung et al. 2010; Wu, Hung, and Terman 2016) were expressed and purified as previously described.

Actin disassembly

Standard pyrene-actin and co-sedimentation assays using RSA (pyrene-labeled or unlabeled; Cytoskeleton, Inc.) were performed as described (Hung et al. 2010; Hung, Pak, and Terman 2011) with minor modifications. G-actin was incubated in cold G-Buffer (2mM Tris-HCl pH 7.5, 0.1mM $CaCl_2$, 1mM NaN_3, 0.5mM DTT, 0.5mM ATP) on ice for 30 min to get rid of any polymerized ends. To polymerize the actin, an actin polymerization buffer, 10X KMI buffer (0.5M KCl, 10mM $MgCl_2$, 100mM Imidazole, pH 7.5) was added to actin-G-buffer solution. The resulting solution was incubated for an hour at RT for actin polymerization. To observe tropomyosin's effect on Mical-mediated F-Actin disassembly or Mical binding to F-actin, the F-actin samples were preincubated with tropomyosin (Cdc8: pombe yeast isoform, a kind gift from Dr Matt Lord's lab in the University of Vermont) or with tropomyosin storage buffer (50mM KCl, 1mM $MgCl_2$, 1mM DTT, 10mM Imidazole) for 15 minutes. Then, Mical (600nM) or Mical storage buffer (10 mM Tris-HCl pH8.0, 100 mM NaCl, 5% glycerol, 1 mM DTT) and NADPH (100 µM) or NADPH buffer (10 mM Tris-HCl pH8.0) were added to observe F-actin depolymerization of Tm- or no-Tm-preincubated F-actin samples. The fluorescence intensity was monitored immediately and over time at 407 nm (excitation at 365 nm) by a fluorescence spectrophotometer (Spectra max M2, Molecular

Devices) as described (Hung, Pak, and Terman 2011).

For sedimentation/association assays, the samples were collected 30 minutes after Mical/NADPH (or storage buffers) addition and ultracentrifuged at 55K for an hour at RT. The supernatant and pellets were separated and loaded into an SDS-PAGE gel to be stained after by Coomassie. The intensity of each of the stained bands in the pellet and soluble fraction was quantified by densitometry using Image J (NIH) (Hung, Pak, and Terman 2011).

For detecting Mical-mediated actin oxidation, an antibody that preferentially recognized the oxidized Met-44 residue on actin (MetO-44) was used as described (Grintsevich et al. 2016). The samples were collected 30 minutes after Mical/NADPH (or storage buffers) addition. When used as a whole sample, the reaction was stopped by adding loading buffer containing β-mercaptoethanol and boiling samples for 5 minutes. Otherwise the samples were ultracentrifuged at 55K for an hour at RT and the supernatant and pellets were treated with loading buffer as above. For Western blotting, all samples were loaded into a 12% SDS-PAGE, transferred to PVDF membrane, blocked with 5% non-fat milk/TBST buffer for 1 hour and then incubated for 1 hour with antiserum (Actin MetO-44 antibodies [1:500]).

In vivo data

Expression analysis, F-actin organization, and bristle cell remodeling was examined and quantified as described (Hung et al. 2010; Hung et al. 2013; Grintsevich et al. 2016). All genotypes are heterozygous (*B11-GAL4*/+, *UAS:Mical*/+, *UAS:Tm1*/+ , *UAS:Tm2*/+ and/or *mutations*/+). For Tm1 and Tm2 expression analysis, we crossed *B11-GAL4* flies to *Tm1* and *Tm2* GFP-trap lines, respectively: *Tm1[KM0210]* and *Tm2[ZCL2456]* and their expression

and localization was imaged in pupal progeny. One copy of *UAS:^{GFP}actin* was used when visualizing F-actin. The *B11-GAL4*, *UAS:Mical*, and *UAS:^{GFP}actin* lines were used as previously described (Hung et al. 2010; Hung, Pak, and Terman 2011; Grintsevich et al. 2016). For testing Tm1 and Tm2's effect on Mical-mediated F-actin organization (imaged in pupal progeny) and cell remodeling (imaged in adult progeny), we crossed the *B11-GAL4*, *UAS:Mical* and *B11-GAL4*, *UAS:Mical, UAS:^{GFP}actin* line with the following lines: *FRT82B, Tm1null* fly line (a loss-of-function/"knockout" mutant due to HR or CRISPR deletion of a 135 basepair gene region that is common to all isoforms (Cho et al. 2016)), *UASt-eGFP-Tm1L, UASt -Tm1A-GFP, UASt-eGFP-Tm1I* fly lines (transgenic fly lines generated by standard transgenic insertion methods (Cho et al. 2016)) and *Tm2$^{(\Delta 8\text{-}261)}$* fly line (a loss-of-function/"knockout" mutant due to CRISPR deletion of a gene region that corresponds to 254 amino acids (aa) of the whole 284aa-long Tm2 protein (Williams et al. 2015)) and *Tm2-cDNA.GFP* fly line (a transgenic fly line generated by standard transgenic insertion methods (Williams et al. 2015)).

CHAPTER FIVE

SUMMARY AND CONCLUSIONS

Actin cytoskeletal dynamics is important for various cellular behaviors such as migration, synaptogenesis, dendrite formation, and axon guidance (Blanchoin et al. 2014; Rottner and Stradal 2011). As Pollard and Cooper discuss (Pollard and Cooper 2009), the main goal of actin dynamics research is to answer the 'how' rather than 'what' about the molecular mechanisms of different systems. I believe one of the most efficient approaches to achieve this type of understanding is the approach I used to conduct my dissertation research (and also used by others in the field with great effect (Bugyi et al. 2008)). Namely, of translating *in vitro* results to *in vivo* understanding, and relating physical interactions to genetic interactions.

So stemming from my main interest in how an axon grows, changes its shape and orientation, and finds its target, I wanted to focus my graduate work on how extracellular cues work to specify these functions. Specifically, I have been focusing on how the largest family of repulsive extracellular cues, Semaphorins (Semas), work through their Plexin receptors to dismantle F-actin (Alto and Terman 2017). Recently, we identified a new family of proteins called the MICALs, that directly associates with the Plexin receptor to become active and is critical for Sema/Plexin repulsive axon guidance (Terman et al. 2002). Now, more recently, we have found Mical to be an actin disassembly protein – and thereby a direct link between Sema/Plexin repulsion and F-actin dismantling (Hung et al. 2010). In particular, our findings revealed that Mical uses F-actin as its substrate and NADPH as its coenzyme, to

post-translationally oxidize actin on its conserved Met-44 and Met-47 residues (Hung, Pak, and Terman 2011). Moreover, we have found that this Mical-mediated actin regulatory process is reversible by a specific methionine sulfoxide reductase enzyme called SelR/MsrB (Hung et al. 2013; Lee et al. 2013). Thus, we have identified a specific reversible redox actin regulatory system that is crucial for Semaphorin/Plexin repulsive axon guidance (and other physiological processes in different types of cells). But we knew very little about this system, and so for my dissertation work I sought to better understand the MICALs (including comparisons among different family members), as well as if and how Mical works together with other actin regulatory proteins.

Summary of my dissertation work: Understanding how MICALs and the Reversible Redox Regulation of Actin is Regulated

Now, in the first part of my dissertation research (as presented in Chapter 2), I find that this Mical–SelR-mediated reversible redox actin regulatory system is phylogenetically conserved from *Drosophila* to humans. In particular, my work comparing the actin regulatory properties of *Drosophila* Mical with each of the three human MICALs (hMICAL-1, hMICAL-2, and hMICAL-3) revealed that, similar to *Drosophila* Mical, each human MICAL family member directly induces F-actin dismantling and controls F-actin-mediated cellular remodeling. Furthermore, I have found that each of the MICALs does this by post-translationally oxidizing actin through their NADPH-dependent Redox activity, which directly dismantles filaments and limits new actin polymerization. Moreover, I have found that MsrB/SelR reductase enzymes counteract each of the MICALs effect on F-actin *in vitro*

and *in vivo*. These results therefore reveal that the MICALs are a family of F-actin dismantling oxidoreductase enzymes conserved from *Drosophila* to humans (Wu et al. 2018).

In other lines of investigation (presented in Chapters 3 and 4, respectively), I show that two classical actin regulatory proteins – cofilin and tropomyosin – which I identified in my initial candidate-based biochemical screen, interact with Mical to regulate actin dynamics *in vitro* and Mical-mediated F-actin alterations and cellular remodeling *in vivo*. In particular (as presented in Chapter 3), cofilin, as one of the most studied actin regulatory proteins, is characterized as an actin depolymerizing factor that severs F-actin by changing the conformation of it. However, cofilin severs actin only weakly and its end result is to promote actin assembly (Andrianantoandro and Pollard 2006; McCullough et al. 2011; Chin, Jansen, and Goode 2016). Interestingly, Mical, on its own, although oxidizing actin very quickly, disassembles it more slowly. Yet, I have found that cofilin and Mical together show a synergy, which depends on the ability of Mical to posttranslationally oxidize F-actin. This Mical-mediated oxidation of F-actin leads to mechanical destabilization of filaments. Cofilin can then work more efficiently to mechanically sever them. Further analysis showed that this synergy is crucial for regulating F-actin disassembly *in vivo* – and also for remodeling cells, wiring the nervous system, and orchestrating Semaphorin/Plexin repulsion (Grintsevich et al. 2016).

On the other hand (as presented in Chapter 4), I find that tropomyosin, which is known to decorate actin filaments within specific cellular compartments and at different developmental stages (Li et al. 2011; Perry 2001; Memo and Marston 2013), protects F-actin

from Mical-mediated disassembly. My further analysis indicates that tropomyosin restricts Mical's binding to F-actin – and when Mical oxidizes tropomyosin-decorated F-actin, tropomyosin holds together these Mical-oxidized actin filaments. Thus, in contrast to cofilin, tropomyosin's competitive interplay with Mical depends on its ability to mechanically stabilize Mical-oxidized actin filaments when Mical oxidizes tropomyosin-decorated F-actin. Furthermore, this interaction is important for F-actin alterations and cellular remodeling *in vivo* with possible tissue-specific and developmental/age-related connotations.

Since Mical, cofilin and tropomyosin share widespread overlapping expression patterns and are all critical for axon guidance, synaptogenesis, dendrite morphology, as well as non-neuronal functions, my studies bring up the possibility that they might work together with other guidance cues, growth factors, and adhesion molecules. Thus, my dissertation research provides important evidence for both the synergistic interaction between Mical and cofilin and the competitive interaction between Mical and tropomyosin. My results also suggest a previously unknown set of mechanisms to remodel actin-based cellular structures and reveals a new understanding on how actin networks like the ones in typical cells, growth cones, specific dendritic spines, or synaptic boutons are stabilized or dismantled and strengthened or weakened. Also, as both assembly and disassembly of F-actin are known to be crucial for cellular behaviors and multiple events in normal development, maintenance of normal physiology, as well as in disease (Blanchoin et al. 2014; Rottner and Stradal 2011), my results may have important implications for behaviors like learning and memory, and events like aging and neurodegeneration.

Actin cytoskeletal dynamics in cell motility and axon guidance – challenges and advances

One of the most important advances in the field, which has enabled my dissertation research, has been the availability of techniques to allow researchers to monitor the function of single purified proteins (such as actin, Mical, cofilin, and tropomyosin) and quantify different aspects of their behavior over time using a variety of means (such as fluorescence, absorbance, or physical quantities). Furthermore, complementing these powerful in vitro methods with other types of approaches is critical for advancing our incomplete understanding of cell motility (Blanchoin et al. 2014). Thus, I also turned to genetic tools in the *Drosophila* model system. Utilizing tools to both increase (transgenic fly lines) or decrease (homologous recombination, small deficiencies, or CRISPR-generated mutations) the expression of the proteins has also provided a complementary means to gain a more complete picture of the mechanisms by which these proteins are acting. Moreover, the high-resolution *Drosophila* bristle cellular model has provided an '*in vivo* test tube' to study the molecular mechanisms of actin dynamics and the response of F-actin *in vivo* to increasing or decreasing the levels of particular proteins. In particular, bristle cells require actin to extend a process, and the ability to form and shape this process in a highly dynamic manner is sensitive to actin regulatory systems (Tilney and DeRosier 2005; Sutherland and Witke 1999). Finally, I was able to link both my *in vitro* findings using purified proteins and my *in vivo* observations in the bristle model to changes in axon guidance – employing both *Drosophila* motor and central nervous system axons as model systems (Terman et al. 2002; Winberg et al. 1998; Yu et al. 1998). For example, this provided a critical connection

between Mical's newly-identified interactor cofilin and Semaphorin-Plexin-Mical repulsive axon guidance (Chapter 3).

Perspectives and Future Directions

My dissertation research has thus led to a better understanding of Mical's function and has also revealed its interactions with well-known classically defined regulators of the actin cytoskeleton. However, much remains to be learned of Mical and its interactions with the actin cytoskeleton. For example, I have identified both a positive and negative regulator of Mical's function, cofilin and tropomyosin, respectively, but how the MICALs fit in with other classes of actin regulatory proteins is not known. In particular, determining if Mical interacts with actin nucleators (or other positive effectors of polymerization) is an important next step – especially given the cellular remodeling and new actin polymerization that occurs following Mical-mediated F-actin disassembly (See Chapters 2, 3, and 4). Moreover, better understanding the interaction of these different actin regulatory proteins will help in our understanding of the mechanisms of axon growth, guidance, and connectivity, including better understanding how actin-rich protrusions like axons/growth cones form.

As an axon grows and steers in a specific direction, F-actin and microtubules work both on their own as well as together to respond to environmental cues and signals (Dent and Gertler 2003). Thus, future directions should also seek to understand if and how Mical-mediated F-actin alterations are combined with changes to microtubules to drive directed axonal growth. Moreover, gaining a clearer picture of how different actin regulatory proteins combine to drive axonal growth and guidance is also an important future direction. For

example, as discussed in Chapter 1, when an axon protrudes towards an attractant cue, it is thought that actin-nucleating proteins, as well as monomer binding proteins, barbed-end capping proteins, bundling proteins, and other classes of actin regulatory proteins are there to coordinate and help actin-mediated protrusion (Dent, Gupton, and Gertler 2011). Likewise, actin severing proteins also appear to become active so that 1) more free barbed ends become available on filaments to allow for additional polymerization and 2) more free monomeric actin becomes available for treadmilling (Dent, Gupton, and Gertler 2011; Lowery and Van Vactor 2009). Cofilin is thought to play a prominent role in these events, such that its severing function dynamizes further actin polymerization (Carlier and Shekhar 2017). Yet, when an axon retracts or steers away from a certain direction, which is favored on the side of a growth cone opposite to an attractant cue or facing a repellent cue, actin severing/disassembly must occur without further immediate polymerization at the site of retraction. The synergy between Mical and cofilin I describe in Chapter 3 would allow for this type of event to occur – including resulting in Mical-oxidized actin monomers, which do not polymerize well (critical concentration increased at least an order of magnitude compared to unoxidized actin). Thus, the synergy between Mical and cofilin would allow for rapid and localized F-actin dismantling, and is a prime interaction to underlie growth cone collapse. Yet, it is reasonable that there also occurs disruption of actin barbed-end protectors and actin bundling proteins during growth cone collapse (Dent, Gupton, and Gertler 2011). How this occurs is unknown, including whether Mical may also directly regulate these events. In much the same way, previous results suggest a requirement for maintaining stabilized actin in certain areas of the growth cone during collapse (Dent and Gertler 2003). Based on my

results in Chapter 4, Tropomyosin is a good candidate to test for underlying this stability in the growth cone, as my results show it to be protective against Mical-mediated F-actin disassembly.

It will also be critical to better understand how Mical and its Redox system works to regulate actin and what this means to how actin dynamics are altered in vivo. For example, Mical oxidizes actin in a residue- and stereo-specific manner on Met-44 and Met-47 of actin (reviewed in (Wilson et al. 2016)). Yet, those residues acquire different susceptibilities to post-translational modification depending on actin's ionic state, conformation and polymerization condition (Dalle-Donne et al. 2002; Guan et al. 2003; Guan et al. 2005; Takamoto, Kamal, and Chance 2007; Hung, Pak, and Terman 2011), which might lead to altered regulation of MICAL's interactions with other actin binding proteins and even different *in vivo* disorders or disease states. Furthermore, during its enzymatic reaction, MICALs also release oxidants such as H_2O_2 (Chapter 2), which could potentially affect indirect substrates (Hung and Terman 2011). In addition, MICALs exhaust O_2 in vitro (Chapter 2), which suggests that they may decrease/exhaust oxygen levels in a localized manner in cells and thereby indirectly alter other oxygen-dependent reactions. Future work should therefore address each of these possibilities so as to gain further insight into how MICALs regulate cellular functions. Given the importance of the MICALs in normal development and physiology, and their increasing emergence in disease processes, these types of future directions are of critical biomedical importance.

BIBLIOGRAPHY

Aenlle, K. K., A. Kumar, L. Cui, T. C. Jackson, and T. C. Foster. 2009. 'Estrogen effects on cognition and hippocampal transcription in middle-aged mice', *Neurobiol Aging*, 30: 932-45.

Aggarwal, P. K., D. Veron, D. B. Thomas, D. Siegel, G. Moeckel, M. Kashgarian, and A. Tufro. 2015. 'Semaphorin3a promotes advanced diabetic nephropathy', *Diabetes*, 64: 1743-59.

Aizawa, H., S. Wakatsuki, A. Ishii, K. Moriyama, Y. Sasaki, K. Ohashi, Y. Sekine-Aizawa, A. Sehara-Fujisawa, K. Mizuno, Y. Goshima, and I. Yahara. 2001. 'Phosphorylation of cofilin by LIM-kinase is necessary for semaphorin 3A-induced growth cone collapse', *Nat Neurosci*, 4: 367-73.

Al-Bassam, J., B. Roger, S. Halpain, and R. A. Milligan. 2007. 'Analysis of the weak interactions of ADP-Unc104 and ADP-kinesin with microtubules and their inhibition by MAP2c', *Cell Motil Cytoskeleton*, 64: 377-89.

Aliverti, A., B. Curti, and M. A. Vanoni. 1999. 'Identifying and quantitating FAD and FMN in simple and in iron-sulfur-containing flavoproteins', *Methods Mol Biol*, 131: 9-23.

Alqassim, S. S., M. Urquiza, E. Borgnia, M. Nagib, L. M. Amzel, and M. A. Bianchet. 2016. 'Modulation of MICAL Monooxygenase Activity by its Calponin Homology Domain: Structural and Mechanistic Insights', *Sci Rep*, 6: 22176.

Alto, L.T., and J. R. Terman. 2017. 'Semaphorins and their Signaling Mechanisms', *Methods Mol Biol*, 1493: 1-25.

Andrianantoandro, E., and T. D. Pollard. 2006. 'Mechanism of actin filament turnover by severing and nucleation at different concentrations of ADF/cofilin', *Mol Cell*, 24: 13-23.

Ashida, S., M. Furihata, T. Katagiri, K. Tamura, Y. Anazawa, H. Yoshioka, T. Miki, T. Fujioka, T. Shuin, Y. Nakamura, and H. Nakagawa. 2006. 'Expression of novel molecules, MICAL2-PV (MICAL2 prostate cancer variants), increases with high Gleason score and prostate cancer progression', *Clin Cancer Res*, 12: 2767-73.

Ayoob, J. C., H. H. Yu, J. R. Terman, and A. L. Kolodkin. 2004. 'The Drosophila receptor guanylyl cyclase Gyc76C is required for semaphorin-1a-plexin A-mediated axonal repulsion', *J Neurosci*, 24: 6639-49.

Bachmann-Gagescu, R., M. Dona, L. Hetterschijt, E. Tonnaer, T. Peters, E. de Vrieze, D. A. Mans, S. E. van Beersum, I. G. Phelps, H. H. Arts, J. E. Keunen, M. Ueffing, R. Roepman, K. Boldt, D. Doherty, C. B. Moens, S. C. Neuhauss, H. Kremer, and E. van Wijk. 2015. 'The Ciliopathy Protein CC2D2A Associates with NINL and Functions in RAB8-MICAL3-Regulated Vesicle Trafficking', *PLoS Genet*, 11: e1005575.

Bashaw, G. J., and R. Klein. 2010. 'Signaling from axon guidance receptors', *Cold Spring Harb Perspect Biol*, 2: a001941.

Basi, G. S., M. Boardman, and R. V. Storti. 1984. 'Alternative splicing of a Drosophila tropomyosin gene generates muscle tropomyosin isoforms with different carboxy-terminal ends', *Mol Cell Biol*, 4: 2828-36.

Benchaar, S. A., Y. Xie, M. Phillips, R. R. Loo, V. E. Galkin, A. Orlova, M. Thevis, A. Muhlrad, S. C. Almo, J. A. Loo, E. H. Egelman, and E. Reisler. 2007. 'Mapping the interaction of cofilin with subdomain 2 on actin', *Biochemistry*, 46: 225-33.

Bernstein, B. W., and J. R. Bamburg. 2010. 'ADF/cofilin: a functional node in cell biology', *Trends Cell Biol*, 20: 187-95.

Beuchle, D., H. Schwarz, M. Langegger, I. Koch, and H. Aberle. 2007. 'Drosophila MICAL regulates myofilament organization and synaptic structure', *Mech Dev*, 124: 390-406.

Blanchoin, L., R. Boujemaa-Paterski, C. Sykes, and J. Plastino. 2014. 'Actin dynamics, architecture, and mechanics in cell motility', *Physiol Rev*, 94: 235-63.

Bobkov, A. A., A. Muhlrad, K. Kokabi, S. Vorobiev, S. C. Almo, and E. Reisler. 2002. 'Structural effects of cofilin on longitudinal contacts in F-actin', *J Mol Biol*, 323: 739-50.

Bonne, D., C. Heusele, C. Simon, and D. Pantaloni. 1985. '4',6-Diamidino-2-phenylindole, a fluorescent probe for tubulin and microtubules', *J Biol Chem*, 260: 2819-25.

Bravo-Cordero, J. J., M. A. Magalhaes, R. J. Eddy, L. Hodgson, and J. Condeelis. 2013. 'Functions of cofilin in cell locomotion and invasion', *Nat Rev Mol Cell Biol*, 14: 405-15.

Bredrup, C., S. Saunier, M. M. Oud, T. Fiskerstrand, A. Hoischen, D. Brackman, S. M. Leh, M. Midtbo, E. Filhol, C. Bole-Feysot, P. Nitschke, C. Gilissen, O. H. Haugen, J. S. Sanders, I. Stolte-Dijkstra, D. A. Mans, E. J. Steenbergen, B. C. Hamel, M. Matignon, R. Pfundt, C. Jeanpierre, H. Boman, E. Rodahl, J. A. Veltman, P. M. Knappskog, N. V. Knoers, R. Roepman, and H. H. Arts. 2011. 'Ciliopathies with skeletal anomalies and renal insufficiency due to mutations in the IFT-A gene WDR19', *Am J Hum Genet*, 89: 634-43.

Brettle, M., S. Patel, and T. Fath. 2016. 'Tropomyosins in the healthy and diseased nervous system', *Brain Res Bull*, 126: 311-23.

Bribian, A., S. Nocentini, F. Llorens, V. Gil, E. Mire, D. Reginensi, Y. Yoshida, F. Mann, and J. A. del Rio. 2014. 'Sema3E/PlexinD1 regulates the migration of hem-derived Cajal-Retzius cells in developing cerebral cortex', *Nat Commun*, 5: 4265.

Brieher, W. 2013. 'Mechanisms of actin disassembly', *Mol Biol Cell*, 24: 2299-302.

Bron, R., M. Vermeren, N. Kokot, W. Andrews, G. E. Little, K. J. Mitchell, and J. Cohen. 2007. 'Boundary cap cells constrain spinal motor neuron somal migration at motor exit points by a semaphorin-plexin mechanism', *Neural Dev*, 2: 21.

Buck, K. B., and J. Q. Zheng. 2002. 'Growth cone turning induced by direct local modification of microtubule dynamics', *J Neurosci*, 22: 9358-67.

Bugyi, B., and M. F. Carlier. 2010. 'Control of actin filament treadmilling in cell motility', *Annu Rev Biophys*, 39: 449-70.

Bugyi, B., C. Le Clainche, G. Romet-Lemonne, and M. F. Carlier. 2008. 'How do in vitro reconstituted actin-based motility assays provide insight into in vivo behavior?', *FEBS Lett*, 582: 2086-92.

Carlier, M. F., J. Pernier, P. Montaville, S. Shekhar, and S. Kuhn. 2015. 'Control of polarized assembly of actin filaments in cell motility', *Cell Mol Life Sci*, 72: 3051-67.

Carlier, M. F., and S. Shekhar. 2017. 'Global treadmilling coordinates actin turnover and controls the size of actin networks', *Nat Rev Mol Cell Biol*, 18: 389-401.

Chambers, J. C., W. Zhang, J. Sehmi, X. Li, M. N. Wass, P. Van der Harst, H. Holm, S. Sanna, M. Kavousi, S. E. Baumeister, L. J. Coin, G. Deng, C. Gieger, N. L. Heard-Costa, J. J. Hottenga, B. Kuhnel, V. Kumar, V. Lagou, L. Liang, J. Luan, P. M. Vidal, I. Mateo Leach, P. F. O'Reilly, J. F. Peden, N. Rahmioglu, P. Soininen, E. K. Speliotes, X. Yuan, G. Thorleifsson, B. Z. Alizadeh, L. D. Atwood, I. B. Borecki, M. J. Brown, P. Charoen, F. Cucca, D. Das, E. J. de Geus, A. L. Dixon, A. Doring, G. Ehret, G. I. Eyjolfsson, M. Farrall, N. G. Forouhi, N. Friedrich, W. Goessling, D. F. Gudbjartsson, T. B. Harris, A. L. Hartikainen, S. Heath, G. M. Hirschfield, A. Hofman, G. Homuth, E. Hypponen, H. L. Janssen, T. Johnson, A. J. Kangas, I. P. Kema, J. P. Kuhn, S. Lai, M. Lathrop, M. M. Lerch, Y. Li, T. J. Liang, J. P. Lin, R. J. Loos, N. G. Martin, M. F. Moffatt, G. W. Montgomery, P. B. Munroe, K. Musunuru, Y. Nakamura, C. J. O'Donnell, I. Olafsson, B. W. Penninx, A. Pouta, B. P. Prins, I. Prokopenko, R. Puls, A. Ruokonen, M. J. Savolainen, D. Schlessinger, J. N. Schouten, U. Seedorf, S. Sen-Chowdhry, K. A. Siminovitch, J. H. Smit, T. D. Spector, W. Tan, T. M. Teslovich, T. Tukiainen, A. G. Uitterlinden, M. M. Van der Klauw, R. S. Vasan, C. Wallace, H. Wallaschofski, H. E. Wichmann, G. Willemsen, P. Wurtz, C. Xu, L. M. Yerges-Armstrong, G. R. Abecasis, K. R. Ahmadi, D. I. Boomsma, M. Caulfield, W. O. Cookson, C. M. van Duijn, P. Froguel, K. Matsuda, M. I. McCarthy, C. Meisinger, V. Mooser, K. H. Pietilainen, G. Schumann, H. Snieder, M. J. Sternberg, R. P. Stolk, H. C. Thomas, U. Thorsteinsdottir, M. Uda, G. Waeber, N. J. Wareham, D. M. Waterworth, H. Watkins, J. B. Whitfield, J. C. Witteman, B. H. Wolffenbuttel, C. S. Fox, M. Ala-Korpela, K. Stefansson, P. Vollenweider, H. Volzke, E. E. Schadt, J. Scott, M. R. Jarvelin, P. Elliott, and J. S. Kooner. 2011. 'Genome-wide association study identifies loci influencing concentrations of liver enzymes in plasma', *Nat Genet*, 43: 1131-8.

Chapman, Stephen K. , and Graeme A. Reid (ed.)^(eds.). 1999. *Flavoprotein Protocols* (Humana Press: Totowa, NJ).

Chen, J., D. Godt, K. Gunsalus, I. Kiss, M. Goldberg, and F. A. Laski. 2001. 'Cofilin/ADF is required for cell motility during Drosophila ovary development and oogenesis', *Nat Cell Biol*, 3: 204-9.

Chhabra, E. S., and H. N. Higgs. 2007. 'The many faces of actin: matching assembly factors with cellular structures', *Nat Cell Biol*, 9: 1110-21.

Chin, S. M., S. Jansen, and B. L. Goode. 2016. 'TIRF microscopy analysis of human Cof1, Cof2, and ADF effects on actin filament severing and turnover', *J Mol Biol*, 428: 1604-16.

Cho, A., M. Kato, T. Whitwam, J. H. Kim, and D. J. Montell. 2016. 'An Atypical Tropomyosin in Drosophila with Intermediate Filament-like Properties', *Cell Rep*, 16: 928-38.

Chou, F. S., and P. S. Wang. 2016. 'The Arp2/3 complex is essential at multiple stages of neural development', *Neurogenesis (Austin)*, 3: e1261653.
Cooper, J. A. 1992. 'Actin filament assembly and organization in vitro.' in K.L. Carraway and C.A.C. Carraway (eds.), *The Cytoskeleton: A Practical Approach* (Oxford University Press: New York).
Crews, D., R. Gillette, S. V. Scarpino, M. Manikkam, M. I. Savenkova, and M. K. Skinner. 2012. 'Epigenetic transgenerational inheritance of altered stress responses', *Proc Natl Acad Sci U S A*, 109: 9143-8.
Dalle-Donne, I., R. Rossi, D. Giustarini, N. Gagliano, P. Di Simplicio, R. Colombo, and A. Milzani. 2002. 'Methionine oxidation as a major cause of the functional impairment of oxidized actin', *Free Radic Biol Med*, 32: 927-37.
Dazzo, E., K. Rehberg, R. Michelucci, D. Passarelli, C. Boniver, V. Vianello Dri, P. Striano, S. Striano, R. J. Pasterkamp, and C. Nobile. 2018. 'Mutations in MICAL-1cause autosomal-dominant lateral temporal epilepsy', *Ann Neurol*, 83: 483-93.
Deng, W., Y. Wang, L. Gu, B. Duan, J. Cui, Y. Zhang, Y. Chen, S. Sun, J. Dong, and J. Du. 2016. 'MICAL1 controls cell invasive phenotype via regulating oxidative stress in breast cancer cells', *BMC Cancer*, 16: 489.
Dent, E. W., and F. B. Gertler. 2003. 'Cytoskeletal dynamics and transport in growth cone motility and axon guidance', *Neuron*, 40: 209-27.
Dent, E. W., S. L. Gupton, and F. B. Gertler. 2011. 'The growth cone cytoskeleton in axon outgrowth and guidance', *Cold Spring Harb Perspect Biol*, 3.
Dominguez, R., and K. C. Holmes. 2011. 'Actin structure and function', *Annu Rev Biophys*, 40: 169-86.
Drees, F., and F. B. Gertler. 2008. 'Ena/VASP: proteins at the tip of the nervous system', *Curr Opin Neurobiol*, 18: 53-9.
Duellman, S., J. Shultz, G. Vidugiris, and J. Cali. 2013. 'A new luminescent assay for detection of reactive oxygen species', *Available from: http://www.promega.com/resources/pubhub/a-luminescent-assay-for-detection-of-reactive-oxygen-species/*.
Eggink, G., H. Engel, G. Vriend, P. Terpstra, and B. Witholt. 1990. 'Rubredoxin reductase of Pseudomonas oleovorans. Structural relationship to other flavoprotein oxidoreductases based on one NAD and two FAD fingerprints', *J Mol Biol*, 212: 135-42.
Eppink, M. H., H. A. Schreuder, and W. J. Van Berkel. 1997. 'Identification of a novel conserved sequence motif in flavoprotein hydroxylases with a putative dual function in FAD/NAD(P)H binding', *Protein Sci*, 6: 2454-8.
Evans, A. R., S. Euteneuer, E. Chavez, L. M. Mullen, E. E. Hui, S. N. Bhatia, and A. F. Ryan. 2007. 'Laminin and fibronectin modulate inner ear spiral ganglion neurite outgrowth in an in vitro alternate choice assay', *Dev Neurobiol*, 67: 1721-30.
Fievez, S., and M. F. Carlier. 1993. 'Conformational changes in subdomain-2 of G-actin upon polymerization into F-actin and upon binding myosin subfragment-1', *FEBS Lett*, 316: 186-90.
Fletcher, D. A., and R. D. Mullins. 2010. 'Cell mechanics and the cytoskeleton', *Nature*, 463: 485-92.

Fremont, S., H. Hammich, J. Bai, H. Wioland, K. Klinkert, M. Rocancourt, C. Kikuti, D. Stroebel, G. Romet-Lemonne, O. Pylypenko, A. Houdusse, and A. Echard. 2017. 'Oxidation of F-actin controls the terminal steps of cytokinesis', *Nat Commun*, 8: 14528.

Freymuth, P. S., and H. L. Fitzsimons. 2017. 'The ERM protein Moesin is essential for neuronal morphogenesis and long-term memory in Drosophila', *Mol Brain*, 10: 41.

Fujii, T., A. H. Iwane, T. Yanagida, and K. Namba. 2010. 'Direct visualization of secondary structures of F-actin by electron cryomicroscopy', *Nature*, 467: 724-8.

Galkin, V. E., A. Orlova, D. S. Kudryashov, A. Solodukhin, E. Reisler, G. F. Schroder, and E. H. Egelman. 2011. 'Remodeling of actin filaments by ADF/cofilin proteins', *Proc Natl Acad Sci U S A*, 108: 20568-72.

Galkin, V. E., A. Orlova, G. F. Schroder, and E. H. Egelman. 2010. 'Structural polymorphism in F-actin', *Nat Struct Mol Biol*, 17: 1318-23.

Galkin, V. E., A. Orlova, M. R. Vos, G. F. Schroder, and E. H. Egelman. 2015. 'Near-atomic resolution for one state of F-actin', *Structure*, 23: 173-82.

Gallo, G. 2006. 'RhoA-kinase coordinates F-actin organization and myosin II activity during semaphorin-3A-induced axon retraction', *J Cell Sci*, 119: 3413-23.

Giridharan, S. S., and S. Caplan. 2014. 'MICAL-Family Proteins: Complex Regulators of the Actin Cytoskeleton', *Antioxid Redox Signal*, 20: 2059-73.

Giridharan, S. S., J. L. Rohn, N. Naslavsky, and S. Caplan. 2012. 'Differential regulation of actin microfilaments by human MICAL proteins', *J Cell Sci*, 125: 614-24.

Goley, E. D., and M. D. Welch. 2006. 'The ARP2/3 complex: an actin nucleator comes of age', *Nat Rev Mol Cell Biol*, 7: 713-26.

Goode, B. L., and M. J. Eck. 2007. 'Mechanism and function of formins in the control of actin assembly', *Annu Rev Biochem*, 76: 593-627.

Gordon-Weeks, P. R. 2004. 'Microtubules and growth cone function', *J Neurobiol*, 58: 70-83.

Govek, E. E., S. E. Newey, and L. Van Aelst. 2005. 'The role of the Rho GTPases in neuronal development', *Genes Dev*, 19: 1-49.

Grigoriev, I., K. L. Yu, E. Martinez-Sanchez, A. Serra-Marques, I. Smal, E. Meijering, J. Demmers, J. Peranen, R. J. Pasterkamp, P. van der Sluijs, C. C. Hoogenraad, and A. Akhmanova. 2011. 'Rab6, Rab8, and MICAL3 Cooperate in Controlling Docking and Fusion of Exocytotic Carriers', *Curr Biol*, 21: 967-74.

Grintsevich, E. E., S. A. Benchaar, D. Warshaviak, P. Boontheung, F. Halgand, J. P. Whitelegge, K. F. Faull, R. R. Loo, D. Sept, J. A. Loo, and E. Reisler. 2008. 'Mapping the cofilin binding site on yeast G-actin by chemical cross-linking', *J Mol Biol*, 377: 395-409.

Grintsevich, E. E., P. Ge, M. R. Sawaya, H. G. Yesilyurt, J. R. Terman, Z. H. Zhou, and E. Reisler. 2017. 'Catastrophic disassembly of actin filaments via Mical-mediated oxidation', *Nat Commun*, 8: 2183.

Grintsevich, E. E., and E. Reisler. 2014. 'Drebrin inhibits cofilin-induced severing of F-actin', *Cytoskeleton (Hoboken)*, 71: 472-83.

Grintsevich, E. E., H. G. Yesilyurt, S. K. Rich, R. J. Hung, J. R. Terman, and E. Reisler. 2016. 'F-actin dismantling through a redox-driven synergy between Mical and cofilin', *Nat Cell Biol*, 18: 876-85.

Guan, J. Q., S. C. Almo, E. Reisler, and M. R. Chance. 2003. 'Structural reorganization of proteins revealed by radiolysis and mass spectrometry: G-actin solution structure is divalent cation dependent', *Biochemistry*, 42: 11992-2000.

Guan, J. Q., K. Takamoto, S. C. Almo, E. Reisler, and M. R. Chance. 2005. 'Structure and dynamics of the actin filament', *Biochemistry*, 44: 3166-75.

Gunning, P., G. O'Neill, and E. Hardeman. 2008. 'Tropomyosin-based regulation of the actin cytoskeleton in time and space', *Physiol Rev*, 88: 1-35.

Gunning, P. W., E. C. Hardeman, P. Lappalainen, and D. P. Mulvihill. 2015. 'Tropomyosin - master regulator of actin filament function in the cytoskeleton', *J Cell Sci*, 128: 2965-74.

Gunning, P. W., G. Schevzov, A. J. Kee, and E. C. Hardeman. 2005. 'Tropomyosin isoforms: divining rods for actin cytoskeleton function', *Trends Cell Biol*, 15: 333-41.

Gupta, N., H. Wu, and J. R. Terman. 2016. 'Data presenting a modified bacterial expression vector for expressing and purifying Nus solubility-tagged proteins', *Data Brief*, 8: 1227-31.

Gurel, P. S., P. Ge, E. E. Grintsevich, R. Shu, L. Blanchoin, Z. H. Zhou, E. Reisler, and H. N. Higgs. 2014. 'INF2-mediated severing through actin filament encirclement and disruption', *Curr Biol*, 24: 156-64.

Gustke, N., B. Trinczek, J. Biernat, E. M. Mandelkow, and E. Mandelkow. 1994. 'Domains of tau protein and interactions with microtubules', *Biochemistry*, 33: 9511-22.

He, H., T. Yang, J. R. Terman, and X. Zhang. 2009. 'Crystal structure of the plexin A3 intracellular region reveals an autoinhibited conformation through active site sequestration', *Proc Natl Acad Sci U S A*, 106: 15610-5.

Heindl, D., and H.-P. Josel. 2000. 'Chemiluminescent detection with horseradish peroxidase and luminol.' in C. Kessler (ed.), *Nonradioactive analysis of biomolecules* (Springer: Berlin).

Ho, J. R., E. Chapeaublanc, L. Kirkwood, R. Nicolle, S. Benhamou, T. Lebret, Y. Allory, J. Southgate, F. Radvanyi, and B. Goud. 2012. 'Deregulation of Rab and Rab effector genes in bladder cancer', *PLoS One*, 7: e39469.

Holmes, K. C., D. Popp, W. Gebhard, and W. Kabsch. 1990. 'Atomic model of the actin filament', *Nature*, 347: 44-9.

Hou, S. T., L. Nilchi, X. Li, S. Gangaraju, S. X. Jiang, A. Aylsworth, R. Monette, and J. Slinn. 2015. 'Semaphorin3A elevates vascular permeability and contributes to cerebral ischemia-induced brain damage', *Sci Rep*, 5: 7890.

Hu, H., T. F. Marton, and C. S. Goodman. 2001. 'Plexin B mediates axon guidance in Drosophila by simultaneously inhibiting active Rac and enhancing RhoA signaling', *Neuron*, 32: 39-51.

Huang, Z., U. Yazdani, K. L. Thompson-Peer, A. L. Kolodkin, and J. R. Terman. 2007. 'Crk-associated substrate (Cas) signaling protein functions with integrins to specify axon guidance during development', *Development*, 134: 2337-47.

Hung, R.-J., and J.R. Terman. 2011. 'Extracellular inhibitors, repellents, and Semaphorin/Plexin/MICAL-mediated actin filament disassembly', *Cytoskeleton*, 68: 415-33.

Hung, R. J., C. W. Pak, and J. R. Terman. 2011. 'Direct redox regulation of F-actin assembly and disassembly by Mical', *Science*, 334: 1710-3.

Hung, R. J., C. S. Spaeth, H. G. Yesilyurt, and J. R. Terman. 2013. 'SelR reverses Mical-mediated oxidation of actin to regulate F-actin dynamics', *Nat Cell Biol*, 15: 1445-54.

Hung, R. J., U. Yazdani, J. Yoon, H. Wu, T. Yang, N. Gupta, Z. Huang, W. J. van Berkel, and J. R. Terman. 2010. 'Mical links semaphorins to F-actin disassembly', *Nature*, 463: 823-7.

Iwasato, T., H. Katoh, H. Nishimaru, Y. Ishikawa, H. Inoue, Y. M. Saito, R. Ando, M. Iwama, R. Takahashi, M. Negishi, and S. Itohara. 2007. 'Rac-GAP alpha-chimerin regulates motor-circuit formation as a key mediator of EphrinB3/EphA4 forward signaling', *Cell*, 130: 742-53.

Jiang, P., J. R. Scarpa, K. Fitzpatrick, B. Losic, V. D. Gao, K. Hao, K. C. Summa, H. S. Yang, B. Zhang, R. Allada, M. H. Vitaterna, F. W. Turek, and A. Kasarskis. 2015. 'A systems approach identifies networks and genes linking sleep and stress: implications for neuropsychiatric disorders', *Cell Rep*, 11: 835-48.

Johnson, R. I., M. J. Seppa, and R. L. Cagan. 2008. 'The Drosophila CD2AP/CIN85 orthologue Cindr regulates junctions and cytoskeleton dynamics during tissue patterning', *J Cell Biol*, 180: 1191-204.

Karlik, C. C., M. D. Coutu, and E. A. Fyrberg. 1984. 'A nonsense mutation within the act88F actin gene disrupts myofibril formation in Drosophila indirect flight muscles', *Cell*, 38: 711-9.

Karlik, C. C., and E. A. Fyrberg. 1986. 'Two Drosophila melanogaster tropomyosin genes: structural and functional aspects', *Mol Cell Biol*, 6: 1965-73.

Kim, G., S. J. Weiss, and R. L. Levine. 2014. 'Methionine oxidation and reduction in proteins', *Biochim Biophys Acta*, 1840: 901-5.

Kirilly, D., Y. Gu, Y. Huang, Z. Wu, A. Bashirullah, B. C. Low, A. L. Kolodkin, H. Wang, and F. Yu. 2009. 'A genetic pathway composed of Sox14 and Mical governs severing of dendrites during pruning', *Nat Neurosci*, 12: 1497-505.

Kiuchi, T., K. Ohashi, S. Kurita, and K. Mizuno. 2007. 'Cofilin promotes stimulus-induced lamellipodium formation by generating an abundant supply of actin monomers', *J Cell Biol*, 177: 465-76.

Klenchin, V. A., J. S. Allingham, R. King, J. Tanaka, G. Marriott, and I. Rayment. 2003. 'Trisoxazole macrolide toxins mimic the binding of actin-capping proteins to actin', *Nat Struct Biol*, 10: 1058-63.

Koh, C. G. 2006. 'Rho GTPases and their regulators in neuronal functions and development', *Neurosignals*, 15: 228-37.

Kolodkin, A. L., and M. Tessier-Lavigne. 2011. 'Mechanisms and molecules of neuronal wiring: a primer', *Cold Spring Harb Perspect Biol*, 3: a001727.
Kolodkin, A.L., D. Matthes, and C.S. Goodman. 1993. 'The semaphorin genes encode a family of transmembrane and secreted growth cone guidance molecules', *Cell*, 75: 1389-99.
Kolodkin, A.L., D. Matthes, T. O'Connor, N.H. Patel, A. Admon, D. Bentley, and C.S. Goodman. 1992. 'Fasciclin IV: Sequence, expression, and function during growth cone guidance in the grasshopper embryo', *Neuron*, 9: 831-35.
Kudumala, S., J. Freund, M. Hortsch, and T. A. Godenschwege. 2013. 'Differential effects of human L1CAM mutations on complementing guidance and synaptic defects in Drosophila melanogaster', *PLoS One*, 8: e76974.
Kurokawa, K., T. Nakamura, K. Aoki, and M. Matsuda. 2005. 'Mechanism and role of localized activation of Rho-family GTPases in growth factor-stimulated fibroblasts and neuronal cells', *Biochem Soc Trans*, 33: 631-4.
Lee, B. C., Z. Peterfi, F. W. Hoffmann, R. E. Moore, A. Kaya, A. Avanesov, L. Tarrago, Y. Zhou, E. Weerapana, D. E. Fomenko, P. R. Hoffmann, and V. N. Gladyshev. 2013. 'MsrB1 and MICALs Regulate Actin Assembly and Macrophage Function via Reversible Stereoselective Methionine Oxidation', *Mol Cell*, 51: 397-404.
Leferink, N. G., W. A. van den Berg, and W. J. van Berkel. 2008. 'l-Galactono-gamma-lactone dehydrogenase from Arabidopsis thaliana, a flavoprotein involved in vitamin C biosynthesis', *FEBS J*, 275: 713-26.
Li, W. D., H. Jiao, K. Wang, C. K. Zhang, J. T. Glessner, S. F. Grant, H. Zhao, H. Hakonarson, and R. Arlen Price. 2013. 'A genome wide association study of plasma uric acid levels in obese cases and never-overweight controls', *Obesity (Silver Spring)*, 21: E490-4.
Li, X. E., L. S. Tobacman, J. Y. Mun, R. Craig, S. Fischer, and W. Lehman. 2011. 'Tropomyosin position on F-actin revealed by EM reconstruction and computational chemistry', *Biophys J*, 100: 1005-13.
Lin, C. H., and P. Forscher. 1993. 'Cytoskeletal remodeling during growth cone-target interactions', *J Cell Biol*, 121: 1369-83.
Liu, Q., F. Liu, K. L. Yu, R. Tas, I. Grigoriev, S. Remmelzwaal, A. Serra-Marques, L. C. Kapitein, A. J. Heck, and A. Akhmanova. 2016. 'MICAL3 flavoprotein monooxygenase forms a complex with centralspindlin and regulates cytokinesis', *J Biol Chem*, 291: 20617-29.
Loria, R., G. Bon, V. Perotti, E. Gallo, I. Bersani, P. Baldassari, M. Porru, C. Leonetti, S. Di Carlo, P. Visca, M. F. Brizzi, A. Anichini, R. Mortarini, and R. Falcioni. 2015. 'Sema6A and Mical1 control cell growth and survival of BRAFV600E human melanoma cells', *Oncotarget*, 6: 2779-93.
Lowery, L. A., and D. Van Vactor. 2009. 'The trip of the tip: understanding the growth cone machinery', *Nat Rev Mol Cell Biol*, 10: 332-43.
Lundquist, M. R., A. J. Storaska, T. C. Liu, S. D. Larsen, T. Evans, R. R. Neubig, and S. R. Jaffrey. 2014. 'Redox Modification of Nuclear Actin by MICAL-2 Regulates SRF Signaling', *Cell*, 156: 563-76.

Luo, J., Y. Xu, Q. Zhu, F. Zhao, Y. Zhang, X. Peng, W. Wang, and X. Wang. 2011. 'Expression pattern of Mical-1 in the temporal neocortex of patients with intractable temporal epilepsy and Pilocarpine-induced rat model', *Synapse*, 65: 1213-21.

Luo, Y., J. Leszyk, B. Li, Z. Li, J. Gergely, and T. Tao. 2002. 'Troponin-I interacts with the Met47 region of skeletal muscle actin. Implications for the mechanism of thin filament regulation by calcium', *J Mol Biol*, 316: 429-34.

Luo, Y., D. Raible, and J.A. Raper. 1993. 'Collapsin: a protein in brain that induces the collapse and paralysis of neuronal growth cones', *Cell*, 75: 217-27.

Macheroux, P. 1999. 'UV-visible spectroscopy as a tool to study flavoproteins', *Methods Mol Biol*, 131: 1-7.

Mahaffy, R. E., and T. D. Pollard. 2006. 'Kinetics of the formation and dissociation of actin filament branches mediated by Arp2/3 complex', *Biophys J*, 91: 3519-28.

Maness, P. F., and M. Schachner. 2007. 'Neural recognition molecules of the immunoglobulin superfamily: signaling transducers of axon guidance and neuronal migration', *Nat Neurosci*, 10: 19-26.

Manta, B., and V. N. Gladyshev. 2017. 'Regulated methionine oxidation by monooxygenases', *Free Radic Biol Med*, 109: 141-55.

Marbiah, M. M., A. Harvey, B. T. West, A. Louzolo, P. Banerjee, J. Alden, A. Grigoriadis, H. Hummerich, H. M. Kan, Y. Cai, G. S. Bloom, P. Jat, J. Collinge, and P. C. Klohn. 2014. 'Identification of a gene regulatory network associated with prion replication', *Embo J*, 33: 1527-47.

Mariotti, S., I. Barravecchia, C. Vindigni, A. Pucci, M. Balsamo, R. Libro, V. Senchenko, A. Dmitriev, E. Jacchetti, M. Cecchini, F. Roviello, M. Lai, V. Broccoli, M. Andreazzoli, C. M. Mazzanti, and D. Angeloni. 2016. 'MICAL2 is a novel human cancer gene controlling mesenchymal to epithelial transition involved in cancer growth and invasion', *Oncotarget*, 7: 1808-25.

Marotta, M., C. Ruiz-Roig, Y. Sarria, J. L. Peiro, F. Nunez, J. Ceron, F. Munell, and M. Roig-Quilis. 2009. 'Muscle genome-wide expression profiling during disease evolution in mdx mice', *Physiol Genomics*, 37: 119-32.

Marsh, L., and P. C. Letourneau. 1984. 'Growth of neurites without filopodial or lamellipodial activity in the presence of cytochalasin B', *J Cell Biol*, 99: 2041-7.

McCullough, B. R., E. E. Grintsevich, C. K. Chen, H. Kang, A. L. Hutchison, A. Henn, W. Cao, C. Suarez, J. L. Martiel, L. Blanchoin, E. Reisler, and E. M. De La Cruz. 2011. 'Cofilin-linked changes in actin filament flexibility promote severing', *Biophys J*, 101: 151-9.

McDonald, C. A., Y. Y. Liu, and B. A. Palfey. 2013. 'Actin stimulates reduction of the MICAL-2 monooxygenase domain', *Biochemistry*, 52: 6076-84.

Medeiros, N. A., D. T. Burnette, and P. Forscher. 2006. 'Myosin II functions in actin-bundle turnover in neuronal growth cones', *Nat Cell Biol*, 8: 215-26.

Memo, M., and S. Marston. 2013. 'Skeletal muscle myopathy mutations at the actin tropomyosin interface that cause gain- or loss-of-function', *J Muscle Res Cell Motil*, 34: 165-9.

Mintz, C. D., I. Carcea, D. G. McNickle, T. C. Dickson, Y. Ge, S. R. Salton, and D. L. Benson. 2008. 'ERM proteins regulate growth cone responses to Sema3A', *J Comp Neurol*, 510: 351-66.

Mitchison, T., and M. Kirschner. 1988. 'Cytoskeletal dynamics and nerve growth', *Neuron*, 1: 761-72.

Miyoshi, T., and N. Watanabe. 2013. 'Can filament treadmilling alone account for the F-actin turnover in lamellipodia?', *Cytoskeleton (Hoboken)*, 70: 179-90.

Morinaka, A., M. Yamada, R. Itofusa, Y. Funato, Y. Yoshimura, F. Nakamura, T. Yoshimura, K. Kaibuchi, Y. Goshima, M. Hoshino, H. Kamiguchi, and H. Miki. 2011. 'Thioredoxin Mediates Oxidation-Dependent Phosphorylation of CRMP2 and Growth Cone Collapse', *Sci Signal*, 4: ra26.

Muhlrad, A., D. Pavlov, Y. M. Peyser, and E. Reisler. 2006. 'Inorganic phosphate regulates the binding of cofilin to actin filaments', *FEBS J*, 273: 1488-96.

Muller, T., C. G. Concannon, M. W. Ward, C. M. Walsh, A. L. Tirniceriu, F. Tribl, D. Kogel, J. H. Prehn, and R. Egensperger. 2007. 'Modulation of gene expression and cytoskeletal dynamics by the amyloid precursor protein intracellular domain (AICD)', *Mol Biol Cell*, 18: 201-10.

Murakami, K., T. Yasunaga, T. Q. Noguchi, Y. Gomibuchi, K. X. Ngo, T. Q. Uyeda, and T. Wakabayashi. 2010. 'Structural basis for actin assembly, activation of ATP hydrolysis, and delayed phosphate release', *Cell*, 143: 275-87.

Mychasiuk, R., R. Gibb, and B. Kolb. 2011. 'Prenatal stress produces sexually dimorphic and regionally specific changes in gene expression in hippocampus and frontal cortex of developing rat offspring', *Dev Neurosci*, 33: 531-8.

Myster, F., L. Palmeira, O. Sorel, F. Bouillenne, E. DePauw, I. Schwartz-Cornil, A. Vanderplasschen, and B. G. Dewals. 2015. 'Viral semaphorin inhibits dendritic cell phagocytosis and migration but is not essential for gammaherpesvirus-induced lymphoproliferation in malignant catarrhal fever', *J Virol*, 89: 3630-47.

Nadella, M., M. A. Bianchet, S. B. Gabelli, J. Barrila, and L. M. Amzel. 2005. 'Structure and activity of the axon guidance protein MICAL', *Proc Natl Acad Sci U S A*, 102: 16830-5.

Ng, J., and L. Luo. 2004. 'Rho GTPases regulate axon growth through convergent and divergent signaling pathways', *Neuron*, 44: 779-93.

Ngo, K. X., N. Kodera, E. Katayama, T. Ando, and T. Q. Uyeda. 2015. 'Cofilin-induced unidirectional cooperative conformational changes in actin filaments revealed by high-speed atomic force microscopy', *Elife*, 4.

Oda, T., M. Iwasa, T. Aihara, Y. Maeda, and A. Narita. 2009. 'The nature of the globular- to fibrous-actin transition', *Nature*, 457: 441-5.

Ono, S. 2007. 'Mechanism of depolymerization and severing of actin filaments and its significance in cytoskeletal dynamics', *Int Rev Cytol*, 258: 1-82.

Orr, B. O., R. D. Fetter, and G. W. Davis. 2017. 'Retrograde semaphorin-plexin signalling drives homeostatic synaptic plasticity', *Nature*, 550: 109-13.

Parikshak, N. N., R. Luo, A. Zhang, H. Won, J. K. Lowe, V. Chandran, S. Horvath, and D. H. Geschwind. 2013. 'Integrative functional genomic analyses implicate specific molecular pathways and circuits in autism', *Cell*, 155: 1008-21.

Perry, S. V. 2001. 'Vertebrate tropomyosin: distribution, properties and function', *J Muscle Res Cell Motil*, 22: 5-49.
Pollard, T. D. 2016. 'Actin and Actin-Binding Proteins', *Cold Spring Harb Perspect Biol*, 8: pii: a018226.
Pollard, T. D., and G. G. Borisy. 2003. 'Cellular motility driven by assembly and disassembly of actin filaments', *Cell*, 112: 453-65.
Pollard, T. D., and J. A. Cooper. 2009. 'Actin, a central player in cell shape and movement', *Science*, 326: 1208-12.
Qin, X. B., W. J. Zhang, L. Zou, P. J. Huang, and B. J. Sun. 2016. 'Identification potential biomarkers in pulmonary tuberculosis and latent infection based on bioinformatics analysis', *BMC Infect Dis*, 16: 500.
Raper, J.A., and J.P. Kapfhammer. 1990. 'The enrichment of a neuronal growth cone collapsing activity from embryonic chick brain', *Neuron*, 4: 21-29.
Ren, N., J. Charlton, and P. N. Adler. 2007. 'The flare gene, which encodes the AIP1 protein of Drosophila, functions to regulate F-actin disassembly in pupal epidermal cells', *Genetics*, 176: 2223-34.
Rodriguez, O. C., A. W. Schaefer, C. A. Mandato, P. Forscher, W. M. Bement, and C. M. Waterman-Storer. 2003. 'Conserved microtubule-actin interactions in cell movement and morphogenesis', *Nat Cell Biol*, 5: 599-609.
Rottner, K., and T. E. Stradal. 2011. 'Actin dynamics and turnover in cell motility', *Curr Opin Cell Biol*, 23: 569-78.
Rumpf, S., J. A. Bagley, K. L. Thompson-Peer, S. Zhu, D. Gorczyca, R. B. Beckstead, L. Y. Jan, and Y. N. Jan. 2014. 'Drosophila Valosin-Containing Protein is required for dendrite pruning through a regulatory role in mRNA metabolism', *Proc Natl Acad Sci U S A*, 111: 7331-6.
Schmidt, E. F., S. O. Shim, and S. M. Strittmatter. 2008. 'Release of MICAL autoinhibition by semaphorin-plexin signaling promotes interaction with collapsin response mediator protein', *J Neurosci*, 28: 2287-97.
Schmidt, E. F., and S. M. Strittmatter. 2007. 'The CRMP family of proteins and their role in Sema3A signaling', *Adv Exp Med Biol*, 600: 1-11.
Schottenfeld-Roames, J., J. B. Rosa, and A. S. Ghabrial. 2014. 'Seamless tube shape is constrained by endocytosis-dependent regulation of active Moesin', *Curr Biol*, 24: 1756-64.
Schwyter, D., M. Phillips, and E. Reisler. 1989. 'Subtilisin-cleaved actin: polymerization and interaction with myosin subfragment 1', *Biochemistry*, 28: 5889-95.
Shaul, Y. D., E. Freinkman, W. C. Comb, J. R. Cantor, W. L. Tam, P. Thiru, D. Kim, N. Kanarek, M. E. Pacold, W. W. Chen, B. Bierie, R. Possemato, F. Reinhardt, R. A. Weinberg, M. B. Yaffe, and D. M. Sabatini. 2014. 'Dihydropyrimidine accumulation is required for the epithelial-mesenchymal transition', *Cell*, 158: 1094-109.
Sheterline, Peter, Clayton Jon, and Sparrow John C. 1998. *Actin* (oxford).
Siebold, C., N. Berrow, T. S. Walter, K. Harlos, R. J. Owens, D. I. Stuart, J. R. Terman, A. L. Kolodkin, R. J. Pasterkamp, and E. Y. Jones. 2005. 'High-resolution structure of the catalytic region of MICAL (molecule interacting with CasL), a

multidomain flavoenzyme-signaling molecule', *Proc Natl Acad Sci U S A*, 102: 16836-41.

Siripala, A. D., and M. D. Welch. 2007a. 'SnapShot: actin regulators I', *Cell*, 128: 626.

———. 2007b. 'SnapShot: actin regulators II', *Cell*, 128: 1014.

Spudich, J. A., and S. Watt. 1971. 'The regulation of rabbit skeletal muscle contraction. I. Biochemical studies of the interaction of the tropomyosin-troponin complex with actin and the proteolytic fragments of myosin', *J Biol Chem*, 246: 4866-71.

Stephan, D., N. Sanchez-Soriano, L. F. Loschek, R. Gerhards, S. Gutmann, Z. Storchova, A. Prokop, and I. C. Kadow. 2012. 'Drosophila Psidin regulates olfactory neuron number and axon targeting through two distinct molecular mechanisms', *J Neurosci*, 32: 16080-94.

Strasser, G. A., N. A. Rahim, K. E. VanderWaal, F. B. Gertler, and L. M. Lanier. 2004. 'Arp2/3 is a negative regulator of growth cone translocation', *Neuron*, 43: 81-94.

Suarez, C., J. Roland, R. Boujemaa-Paterski, H. Kang, B. R. McCullough, A. C. Reymann, C. Guerin, J. L. Martiel, E. M. De la Cruz, and L. Blanchoin. 2011. 'Cofilin tunes the nucleotide state of actin filaments and severs at bare and decorated segment boundaries', *Curr Biol*, 21: 862-8.

Suter, D. M., and P. Forscher. 2000. 'Substrate-cytoskeletal coupling as a mechanism for the regulation of growth cone motility and guidance', *J Neurobiol*, 44: 97-113.

Sutherland, J. D., and W. Witke. 1999. 'Molecular genetic approaches to understanding the actin cytoskeleton', *Curr Opin Cell Biol*, 11: 142-51.

Takamoto, K., J. K. Kamal, and M. R. Chance. 2007. 'Biochemical implications of a three-dimensional model of monomeric actin bound to magnesium-chelated ATP', *Structure*, 15: 39-51.

Tanaka, E., T. Ho, and M. W. Kirschner. 1995. 'The role of microtubule dynamics in growth cone motility and axonal growth', *J Cell Biol*, 128: 139-55.

Terman, J. R., T. Mao, R. J. Pasterkamp, H. H. Yu, and A. L. Kolodkin. 2002. 'MICALs, a family of conserved flavoprotein oxidoreductases, function in plexin-mediated axonal repulsion', *Cell*, 109: 887-900.

Tessier-Lavigne, M., and C.S. Goodman. 1996. 'The molecular biology of axon guidance.', *Science*, 274: 1123-33.

Tilney, L. G., and D. J. DeRosier. 2005. 'How to make a curved Drosophila bristle using straight actin bundles', *Proc Natl Acad Sci U S A*, 102: 18785-92.

Tochigi, M., K. Iwamoto, M. Bundo, T. Sasaki, N. Kato, and T. Kato. 2008. 'Gene expression profiling of major depression and suicide in the prefrontal cortex of postmortem brains', *Neurosci Res*, 60: 184-91.

Van Battum, E. Y., R. A. Gunput, S. Lemstra, E. J. Groen, K. L. Yu, Y. Adolfs, Y. Zhou, C. C. Hoogenraad, Y. Yoshida, M. Schachner, A. Akhmanova, and R. J. Pasterkamp. 2014. 'The intracellular redox protein MICAL-1 regulates the development of hippocampal mossy fibre connections', *Nat Commun*, 5: 4317.

van Berkel, W.J.H., and F. Muller. 1991. 'Flavin-dependent monooxygenases with special reference to p-hydroxybenzoate hydroxylase.' in F. Muller (ed.), *Chemistry and biochemistry of flavoenzymes* (CRC Press: Boca Raton, FL).

Van Troys, M., L. Huyck, S. Leyman, S. Dhaese, J. Vandekerkhove, and C. Ampe. 2008. 'Ins and outs of ADF/cofilin activity and regulation', *Eur J Cell Biol*, 87: 649-67.
Van Vactor, D., H. Sink, D. Fambrough, R. Tsoo, and C.S. Goodman. 1993. 'Genes that control neuromuscular specificity in Drosophila', *Cell*, 73: 1137-53.
Vanoni, M. A. 2017. 'Structure-function studies of MICAL, the unusual multidomain flavoenzyme involved in actin cytoskeleton dynamics', *Arch Biochem Biophys*, 632: 118-41.
Vanoni, M. A., T. Vitali, and D. Zucchini. 2013. 'MICAL, the Flavoenzyme Participating in Cytoskeleton Dynamics', *Int J Mol Sci*, 14: 6920-59.
Vitali, T., E. Maffioli, G. Tedeschi, and M. A. Vanoni. 2016. 'Properties and catalytic activities of MICAL1, the flavoenzyme involved in cytoskeleton dynamics, and modulation by its CH, LIM and C-terminal domains', *Arch Biochem Biophys*, 593: 24-37.
von der Ecken, J., M. Muller, W. Lehman, D. J. Manstein, P. A. Penczek, and S. Raunser. 2015. 'Structure of the F-actin-tropomyosin complex', *Nature*, 519: 114-7.
Wang, Y., W. Deng, Y. Zhang, S. Sun, S. Zhao, Y. Chen, X. Zhao, L. Liu, and J. Du. 2017. 'MICAL2 Promotes Breast Cancer Cell Migration by Maintaining EGFR Stability and EGFR/P38 Signaling Activation', *Acta Physiol (Oxf)*.
Watabe-Uchida, M., E. E. Govek, and L. Van Aelst. 2006. 'Regulators of Rho GTPases in neuronal development', *J Neurosci*, 26: 10633-5.
Wen, Z., L. Han, J. R. Bamburg, S. Shim, G. L. Ming, and J. Q. Zheng. 2007. 'BMP gradients steer nerve growth cones by a balancing act of LIM kinase and Slingshot phosphatase on ADF/cofilin', *J Cell Biol*, 178: 107-19.
Wierenga, R. K., P. Terpstra, and W. G. Hol. 1986. 'Prediction of the occurrence of the ADP-binding beta alpha beta-fold in proteins, using an amino acid sequence fingerprint', *J Mol Biol*, 187: 101-7.
Williams, J., N. G. Boin, J. M. Valera, and A. N. Johnson. 2015. 'Noncanonical roles for Tropomyosin during myogenesis', *Development*, 142: 3440-52.
Wilson, C., J. R. Terman, C. Gonzalez-Billault, and G. Ahmed. 2016. 'Actin filaments - a target for redox regulation', *Cytoskeleton (Hoboken)*, 73: 577-95.
Winberg, M.L., J.N. Noordermeer, L. Tamagnone, P.M. Comoglio, M.K. Spriggs, M. Tessier-Lavigne, and C.S. Goodman. 1998. 'Plexin A is a neuronal semaphorin receptor that controls axon guidance.', *Cell*, 95: 903-16.
Witherden, D. A., M. Watanabe, O. Garijo, S. E. Rieder, G. Sarkisyan, S. J. Cronin, P. Verdino, I. A. Wilson, A. Kumanogoh, H. Kikutani, L. Teyton, W. H. Fischer, and W. L. Havran. 2012. 'The CD100 receptor interacts with its plexin B2 ligand to regulate epidermal gammadelta T cell function', *Immunity*, 37: 314-25.
Woo, S., and T. M. Gomez. 2006. 'Rac1 and RhoA promote neurite outgrowth through formation and stabilization of growth cone point contacts', *J Neurosci*, 26: 1418-28.
Wu, H., R. J. Hung, and J. R. Terman. 2016. 'A simple and efficient method for generating high-quality recombinant Mical enzyme for in vitro assays', *Protein Expr Purif*, 127: 116-24.

Wu, H., H. G. Yesilyurt, J. Yoon, and J. R. Terman. 2018. 'The MICALs are a Family of F-actin Dismantling Oxidoreductases Conserved from Drosophila to Humans', *Sci Rep*, 8: 937.

Yang, T., and J. R. Terman. 2012. '14-3-3epsilon Couples Protein Kinase A to Semaphorin Signaling and Silences Plexin RasGAP-Mediated Axonal Repulsion', *Neuron*, 74: 108-21.

Yin, H. L., and T. P. Stossel. 1979. 'Control of cytoplasmic actin gel-sol transformation by gelsolin, a calcium-dependent regulatory protein', *Nature*, 281: 583-6.

Yoon, J., R. J. Hung, and J. R. Terman. 2017. 'Characterizing F-actin disassembly induced by the semaphorin-signaling component MICAL', *Methods in Molecular Biology*, 1493: 119-28.

Yoon, J., S. B. Kim, G. Ahmed, J. W. Shay, and J. R. Terman. 2017. 'Amplification of F-Actin Disassembly and Cellular Repulsion by Growth Factor Signaling', *Dev Cell*, 42: 117-29.

Yu, H. H., H. H. Araj, S. A. Ralls, and A. L. Kolodkin. 1998. 'The transmembrane Semaphorin Sema I is required in Drosophila for embryonic motor and CNS axon guidance', *Neuron*, 20: 207-20.

Zhang, X. F., A. W. Schaefer, D. T. Burnette, V. T. Schoonderwoert, and P. Forscher. 2003. 'Rho-dependent contractile responses in the neuronal growth cone are independent of classical peripheral retrograde actin flow', *Neuron*, 40: 931-44.

Zhou, F. Q., and C. S. Cohan. 2004. 'How actin filaments and microtubules steer growth cones to their targets', *J Neurobiol*, 58: 84-91.

Zhou, Y., Y. Adolfs, W. W. Pijnappel, S. J. Fuller, R. C. Van der Schors, K. W. Li, P. H. Sugden, A. B. Smit, A. Hergovich, and R. J. Pasterkamp. 2011. 'MICAL-1 is a Negative Regulator of MST-NDR Kinase Signaling and Apoptosis', *Mol Cell Biol*, 31: 3603-15.

Zhou, Y., R. A. Gunput, Y. Adolfs, and R. J. Pasterkamp. 2011. 'MICALs in control of the cytoskeleton, exocytosis, and cell death', *Cell Mol Life Sci*, 68: 4033-44.

Zucchini, D., G. Caprini, R. J. Pasterkamp, G. Tedeschi, and M. A. Vanoni. 2011. 'Kinetic and spectroscopic characterization of the putative monooxygenase domain of human MICAL-1', *Arch Biochem Biophys*, 515: 1-13.